Mitochondrial DNA gene expression

and consequences of its loss in mammals

Inaugural-Dissertation
zur
Erlangung des Doktorgrades
der Mathematisch-Naturwissenschaftlichen Fakultät
der Universität zu Köln

vorgelegt von
MARIA DEL PILAR MIRANDA VERGARA
aus Bogotá, Kolumbien

Köln, Deutschland
2018

Berichterstatter:
Prof. Dr. Nils-Göran Larsson
Prof. Dr. Aleksandra Trifunovic

Tag der mündlichen Prüfung: 04.09.2018

“The only way to find out what will happen when a complex system is disturbed is to disturb the system, not merely to observe it passively"

– paraphrasing George Box (Mosteller & Tukey 1977)

TABLE OF CONTENTS

ZUSAMMENFASSUNG

Mitochondrien sind intrazelluläre Organellen, die verschiedene essenzielle Funktionen haben wie die Produktion des Hauptanteils zellulärer Energie in Form von Adenosintriphosphat (ATP) durch die oxidative Phosphorylierung (OXPHOS). Mitochondriale Fehlfunktionen treten bei schweren metabolischen Erberkrankungen mit breitem klinischen Spektrum auf, sowie in verschiedenen altersbedingten Erkrankungen, und wurden außerdem mit dem Altersprozess assoziiert. Die mitochondriale Biogenese hängt von der Exprimierung zweier zellulärer Genome ab. Während das mitochondriale Genom (mtDNA) für ein paar wenige essentielle Untereinheiten des OXPHOS Systems, sowie für Transfer- und Ribosomalen-RNAs die zur Translation dieser Untereinheiten in den Mitochondrien notwendig sind, kodiert, ist der Großteil der mitochondrialen Proteine nuklear kodiert (nDNA). Die Mechanismen, die die Expression der mtDNA regulieren, sind größtenteils unbekannt, und wie Störungen dieser Prozesse zu einem pathogenen Erscheinungsbild führen, ist nur unzureichend verstanden.

Das erste Ziel dieser Doktorarbeit war es zu untersuchen welche *in vivo* Rolle die mitochondriale RNA Polymerase (POLRMT) in der Regulation der Exprimierung der mtDNA spielt. Um die Funktion von POLRMT und Spleißvarianten des *Polrmt* Gens in Säugern zu analysieren, haben wir transgene Mausmodelle mit verschiedenen Gendosierungen von *Polrmt* hergestellt und charakterisiert. Zu diesen *Polrmt* Modellen zählten ein homozygoter Ganzkörperknockout sowie ein gewebespezifischer Knockout in Herz- und Skelettmuskel, ein heterozygoter Knockout, und einen überexprimierenden Mausstamm. Unsere Studien ergeben, dass *Polrmt* nur für ein mitochondriales Protein, POLRMT, kodiert, und dass keine andere RNA Polymerase seine Funktion ersetzen kann. Wir zeigen dass POLRMT zwei essenzielle Rollen in Säuger-Mitochondrien hat, i) sie ist die einzige RNA Polymerase die die mtDNA transkribiert, und ii) sie synthetisiert die für die Replikation der mtDNA essentiellen RNA Primer. Desweiteren deuten unsere Daten darauf hin, dass POLRMT Teil eines Prozesses ist, der durch einen promoterspezifischen Transkriptionsstart den Wechsel zwischen mtDNA Replikation und Transkription koordiniert. Abschließend zeigen wir, dass POLRMT der limitierende Faktor für den Transkriptionsstart ist, und dass POLRMT regelmäßig zum Transkriptionsstart an die Promotoren bindet, wohingegen die Synthese von fast genomlanger mitochondrialer RNA (mt-RNA) auf der Ebene der Elongation reguliert ist.

Das zweite Ziel dieser Dissertation war es die zellulären Konsequenzen defekter Gen-Expression der mtDNA und fortschreitender OXPHOS Fehlfunktion zu erforschen. In einer systematischen Studie haben wir das mitochondriale Proteom (Mitoproteom) und das komplette zelluläre Transkriptom vom Herz von fünf Knockout Mausstämmen von denen jeder

defekt für einen essenziellen Faktor für die Regulation der mtDNA Gen-Expression ist, miteinander verglichen. Desweiteren haben wir Veränderungen des Mitoproteoms während der postnatalen Entwicklung des Mausherzens untersucht und Unterschiede im Mitoproteom in einem Mausstamm mit fortschreitender OXPHOS Fehlfunktion verfolgt. Überraschenderweise haben wir entdeckt, dass eine Minderung des intra-mitochondrialen Coenzym Q (Q) Biosynthesestoffwechsels mit fortschreitender OXPHOS Fehlfunktion einher geht. Weiter haben wir gefunden, dass die zelluläre Stressreaktion sehr früh während der fortschreitender OXPHOS Fehlfunktion aktiviert wird, wahrscheinlich durch die Transkriptionsfaktoren myc Protoonkogen Protein (MYC) und zyklischer AMP-abhängiger Transkriptionsfaktor ATF4 (ATF4). Diese zelluläre Antwort umfasst eine Erhöhung der Enzyme des mitochondrialen Kohlenstoffkreislaufes (1C), der Prolinsynthese und der mitochondrialen Proteasen und Chaperone.

Schlussfolgernd lässt sich sagen, dass die hier präsentierte Arbeit fundamentale Mechanismen der Regulation der mtDNA Gen-Exprimierung *in vivo* identifiziert hat, und primäre und sekundäre Konsequenzen defekter Expression der mtDNA genau festlegt. Diese Arbeit ist nicht nur von außerordentlich wichtiger Bedeutung für unser Verständnis der Funktion dieses essentiellen Organells, sondern hat außerdem neue Mechanismen, die in mitochondrialen Krankheitsbildern eine Rolle spielen, identifiziert, was für die Diagnose von Patienten und zukünftigen Behandlungsstrategien bedeutend ist.

ABSTRACT

Mitochondria are intracellular organelles that fulfil multiple essential functions, including the generation of the vast majority of the cellular energy currency adenosine triphosphate (ATP) via the oxidative phosphorylation (OXPHOS) system. Mitochondrial dysfunction is found in severe inherited metabolic disorders with a broad clinical spectrum, in several common age-related diseases, and has been associated with the ageing process itself. Mitochondrial biogenesis depends on the expression of two cellular genomes. While the mitochondrial genome (mtDNA) encodes a few essential subunits of the OXPHOS system and the transfer and ribosomal RNAs required to translate these subunits in mitochondria, most mitochondrial proteins are encoded in the nuclear genome (nDNA). The mechanisms regulating the expression of mtDNA are still largely unknown and how disrupting this process leads to pathogenic phenotypes is poorly understood.

The first aim of this thesis was to elucidate the *in vivo* function of the mitochondrial RNA polymerase (POLRMT) in the regulation mtDNA gene expression. We generated and characterized transgenic mouse models with varying gene dosage of *Polrmt* to investigate the role of POLRMT and the splice variants of the *Polrmt* gene in mammals. These *Polrmt* models included a whole-body knockout, a heart and skeletal muscle knockout, a heterozygous knockout, and an overexpressing mouse strain. Our findings reveal that *Polrmt* only codes for a mitochondrial isoform, POLRMT, and that no other RNA polymerase can replace its function. We show that POLRMT has two essential roles in mammalian mitochondria, i) it is the only RNA polymerase transcribing mtDNA, and ii) it synthesizes the RNA primers required for mtDNA replication. Moreover, our data suggests that POLRMT is part of a mechanism involving promoter-specific transcription initiation that coordinates the switch between mtDNA replication and transcription. Finally, we show that POLRMT is the limiting factor for transcription initiation and that it is frequently loading at the promoters to initiate transcription, whereas productive near-genome length mitochondrial RNA (mt-RNA) synthesis is regulated at the elongation level.

The second aim of this thesis was to investigate the cellular consequences of disrupting mtDNA gene expression and the progression of OXPHOS deficiency. We performed a systematic comparison of the mitoproteome and total cellular transcriptome from heart of five knockout mouse models, each deficient in an essential factor acting at a specific level of gene expression regulation. We also studied the mitoproteome changes during normal post-natal development in mouse heart and followed proteome changes in a model with progressive OXPHOS deficiency in the heart. Surprisingly, we found a decline in the intra-mitochondrial Q

biosynthesis pathway that correlates with the progressive OXPHOS deficiency. Furthermore, we found that cellular stress responses, likely mediated by the myc proto-oncogene protein (MYC) and the cyclic AMP-dependent transcription factor ATF4 (ATF4) transcription factors, are activated very early in the progression of OXPHOS deficiency. These cellular responses include the upregulation of enzymes of the mitochondrial one-carbon (1C) pathway, proline synthesis, and mitochondrial proteases and chaperones.

In conclusion, the work presented in this thesis has identified fundamental mechanisms of regulation of mtDNA gene expression *in vivo* and pinpointed primary and secondary consequences of impaired expression of mtDNA. This work has not only important implications for our understanding of the function of this essential organelle but it has also identified novel mechanisms involved in mitochondrial pathology that can be relevant for patient diagnosis and future treatment strategies.

1. INTRODUCTION

1.1. Mitochondrial origin

According to the endosymbiotic theory, mitochondria are derived from a proteobacterium that was engulfed by an archaeon more than 1.45 billion years ago (Martin & Mentel 2010). This fusion event created the eukaryotic cell. The genome of the engulfed proteobacterium was drastically reduced and the proteobacterium became an integrated organelle – the mitochondrion – that provided the energetic capacity to evolve and express the complex genomes giving rise to the different eukaryotic groups (Lane & Martin 2010). Thus, all eukaryotic organisms studied to date contain an organelle of mitochondrial origin or have secondarily lost this organelle during evolution (Karnkowska et al. 2016). Although it is widely accepted that the precursor of mitochondria had the capacity to convert energy from different sources into ATP (Zimorski et al. 2014), the precise characteristics of mitochondria in the last eukaryotic common ancestor are still a matter of debate. However, several events for the establishment of an integrated organelle must have already occurred: (1) a substantial reduction of the bacterial genome either by gene transfer to the nucleus or loss of redundant and unnecessary genes, (2) the establishment of substrate transport and protein import systems that allowed the biogenesis of the organelle and integration of metabolic reactions with the host organism, and (3) the development of mechanisms for mitochondrial segregation during cell division (Roger et al. 2017). Mitochondria often have diversified functions in different eukaryotic cell types and organisms. Mitochondria and related organelles derived from the mitochondrial ancestor have been classified into five types based on their energy metabolism: aerobic mitochondria, anaerobic mitochondria, hydrogen producing mitochondria, mitosomes, and hydrogenosomes (Müller et al. 2012). Despite the drastic differences in terms of function and composition between these different mitochondrion-related organelles, they all conserve mitochondrial marker proteins like the ones required for iron sulphur (FeS) cluster biosynthesis (Tovar et al. 2003) and some components of the protein import machinery that can be traced back to their ancestral origin (Zimorski et al. 2014). As a remnant from their endosymbiotic origin, mitochondria are surrounded by a double membrane and, remarkably, all aerobic mitochondria have retained a small mtDNA (Stewart & Larsson 2014).

1.2. Mitochondrial functions in mammals

Mitochondria fulfil several functions that are essential for the eukaryotic cell. Mammals contain aerobic mitochondria that harvest electrons from carbon sources and uses the released energy to pump protons necessary for driving ATP synthesis via the OXPHOS system (Nelson & Cox 2009). The mammalian OXPHOS system comprises five multiprotein complexes (I-V) localized in the inner mitochondrial membrane (IMM) (Figure 1.1). Complexes I (reduced nicotinamide adenine dinucleotide (NADH):ubiquinone oxidoreductase), III (ubiquinol-cytochrome c

oxidoreductase), and IV (cytochrome c oxidase) catalyse electron transfer from NADH to oxygen and translocate protons to the intermembrane space. The difference in proton concentration between the mitochondrial matrix (MM) and the intermembrane space (IMS) provides the proton-motive force that is harvested by complex V (F_1F_0-ATP synthase) to convert adenosine diphosphate (ADP) into ATP. Electrons from complex I are transferred to complex III by ubiquinone (coenzyme Q; Q) and from complex III to IV by cytochrome c (Milenkovic et al. 2017). NADH is regenerated during oxidoreduction (redox) reactions and one of the main sources is the tricarboxylic acid (TCA) cycle where reduction of NAD^+ is coupled to the oxidation of carbon sources to carbon dioxide (Nelson & Cox 2009). The enzymes of the TCA cycle are localized in the MM except for the succinate dehydrogenase or OXPHOS complex II that is partly embedded in the IMM and transfers electrons from reduced flavin adenine dinucleotide ($FADH_2$) to the electron carrier Q (Mourier & Larsson 2011).

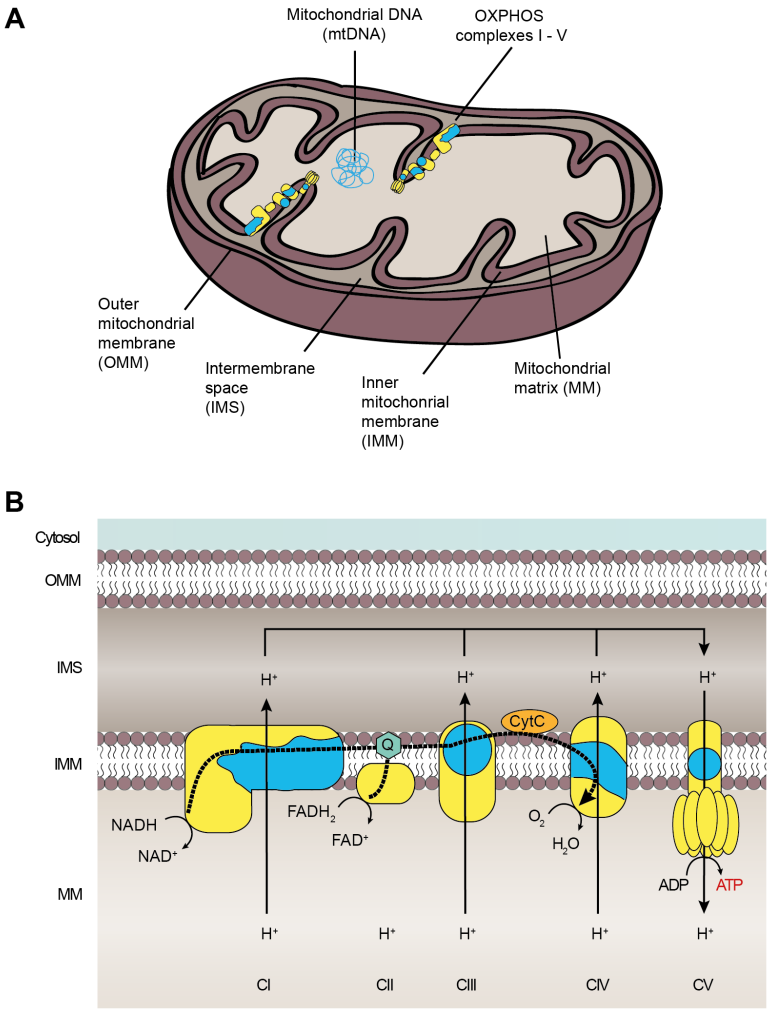

Figure 1.1 | Mitochondrial compartments and OXPHOS system
A) Scheme of mitochondrial compartments, OXPHOS complexes, and mtDNA. (**B**) Scheme of the OXPHOS system. Dotted line represents the electron flow. Yellow represents nDNA-encoded OXPHOS subunits and blue represents mtDNA-encoded subunits. Abbreviations not described in the figure in alphabetic order: ADP, adenosine diphosphate; ATP, adenosine triphosphate; CI - V, OXPHOS complexes I-V; CytC, Cytochrome C; FADH2 and FAD, reduced and oxidized flavine adenine dinucleotide; H^+, hydrogen protons; H_2O, water; NADH and NAD^+, reduced and oxidized nicotinamide adenine dinucleotide; O_2, oxygen; OXPHOS, oxidative phosphorylation; Q, coenzyme Q. Modified from Mourier et al. 2011.

Carbohydrates, lipids, and amino acids are the three carbon sources mammalian cells can use and their metabolism converges in the TCA cycle. Carbohydrates are metabolized via glycolysis to pyruvate that is imported into mitochondria and converted to acetyl-coenzyme A

(CoA). Fatty acids are activated in the cytosol to acyl-CoA esters, imported into mitochondria, and oxidized through several cycles of β-oxidation (FAO) which result in the generation of acetyl-CoA, NADH, and $FADH_2$ (Houten et al. 2016). Several reactions required for amino acid degradation occur in mitochondria and their intermediate products can enter the TCA cycle as acetyl-CoA, α-ketoglutarate, or succinate (Guda et al. 2007). The use of the different carbon sources in mammals depend on the tissue and metabolic state. For example, brain and nerve tissue rely mainly on glucose or ketone body oxidation; heart, skeletal muscle, and kidney mainly use FAO; and enterocytes use energy derived from glutamine oxidation (Vusse & Reneman 1995). Importantly, many of the metabolites, redox cofactors, and ATP generated in these pathways are used to synthesise new macromolecules including non-essential amino acids, carbohydrates, lipids, secondary metabolites, and nucleic acids. Thus, the central carbon metabolism ensures the conversion of energy sources into ATP, redox power, and precursor metabolites required for biosynthesis (Nielsen 2017).

Biosynthesis of Q, FeS clusters, and heme groups partially take place in mitochondria and these compounds are necessary to support OXPHOS. Q is synthesised in the IMM by attaching a tail formed of several isoprenoid units derived from the cytosolic mevalonate pathway to a 4-hydroxybenzoate head, which is subsequently modified by carboxylation, hydroxylation, and methylation reactions (Stefely & Pagliarini 2017). In addition to its role in electron transfer, Q is suggested to be a ubiquitous lipid antioxidant present in all cellular membranes (Wang & Hekimi 2016). FeS clusters are co-factors for several enzymes in the cell, including mitochondrial enzymes of the OXPHOS complexes I-III, TCA cycle and FAO, as well as nuclear enzymes required for DNA replication and repair (Stehling & Lill 2013). Heme groups are also iron-containing essential co-factors. Haemoglobin and myoglobin, for example, use heme-groups to transport oxygen, and cytochrome c is an electron shuttle in OXPHOS (Kranz et al. 2009; Levi & Rovida 2009). Importantly, cytochrome c release to the cytosol is a determining step for the activation of the intrinsic pathway of apoptosis (Galluzzi et al. 2016).

The aforementioned introduction to mitochondrial functions is far from being complete but illustrates the high degree of connectivity and coordination between metabolic reactions and the central role of mitochondria in these processes. Thus, proper mitochondrial biogenesis and function is fundamental to sustain mammalian life.

1.3. Dual genetic control of mitochondrial biogenesis

It is estimated that mammalian mitochondria contain 1000 to 1500 proteins (Pagliarini et al. 2008) from which half of the proteins are core mitochondrial components present in all

mammalian cells whereas the other half are expressed in a tissue-specific manner (Calvo & Mootha 2010).The endeavour of defining the mitoproteome has advanced steadily in recent years but a significant proportion of proteins is still of unknown function in mitochondria (Pagliarini & Rutter 2013).

Mammalian mtDNA encodes only thirteen essential proteins of the OXPHOS complexes I, III, IV, and V. All of the remaining mitochondrial proteins are encoded in the nucleus, translated in the cytosol, and imported into mitochondria (Figure 1.2) (Gustafsson et al. 2016). It is estimated that one quarter of the mitoproteome is dedicated to maintain and express mtDNA (Gonczarowska-Jorge et al. 2017). Furthermore, in mouse, whole-body knockout of different nDNA-encoded proteins involved in mtDNA gene expression lead to embryonic lethality, whereas conditional knockout in heart and skeletal muscle lead to cardiomyopathies and premature death caused by severe mitochondrial dysfunction (Cámara et al. 2011; Larsson et al. 1998; Metodiev et al. 2009; Milenkovic et al. 2013; Ruzzenente et al. 2012; Park et al. 2007). These findings highlight the importance of a concerted expression of both genomes for the mammalian organism.

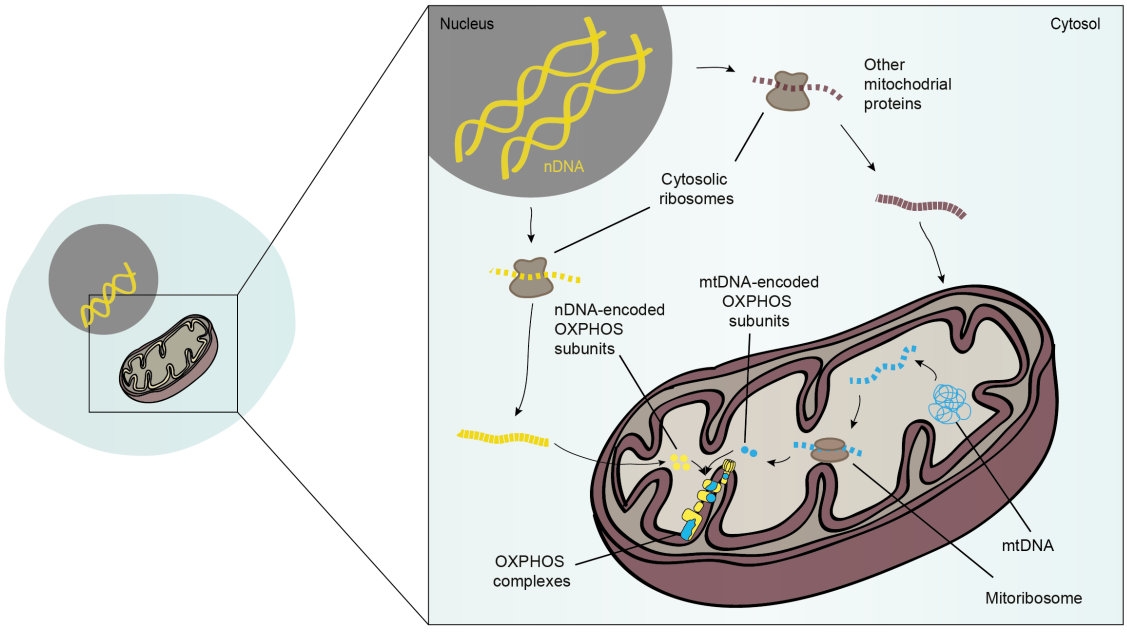

Figure 1.2 | Dual genetic origin of the OXPHOS system
OXPHOS complexes are encoded in two cellular genomes, nDNA and mtDNA. mtDNA encodes 13 subunits of OXPHOS complexes I, III, IV and V that are translated in the mitoribosomes. All other mitochondrial proteins are encoded in the nucleus, translated in the cytosol and imported into mitochondria where they are assembled together with the mtDNA-encoded subunits. Abbreviations in alphabetic order: mtDNA, mitochondrial DNA, nDNA, nuclear DNA; OXPHOS, oxidative phosphorylation. Modified from Larsson 2010.

In terms of energy balance, the maintenance of such an elaborate machinery to express only a few mtDNA-encoded proteins seems counterintuitive and, therefore, different hypotheses have been proposed to explain why mtDNA is still maintained. The first one argues that the process of genome reduction, that accompanied the integration of mitochondria as a

cellular organelle, is still ongoing and, eventually, mtDNA will disappear. The strongest evidence supporting this hypothesis is that the mitochondrial related organelles, hydrogenosomes and mitosomes, do not have mtDNA (Burki 2016; Palmer 1997). However, until now, there is a perfect correlation between maintaining mtDNA and the capacity to perform aerobic respiration. All aerobic mitochondria appear to have retained genes coding for OXPHOS components, at least *mt-Co1, mt-Co3,* and *mt-Cytb*, as well as genes required for mitochondrial translation (Stewart & Larsson 2014). The conservation of such a specific set of mitochondrial genes has been interpreted in two opposite but not mutually exclusive ways. On the one hand, it has been proposed that the complete transfer of these genes to the nucleus is limited by selection constraints. Examples of these constraints are incompatibility in gene expression due to differences in codon usage between nDNA and mtDNA or problems in targeting and importing these proteins into mitochondria due to their high hydrophobicity (Björkholm et al. 2015). The transfer to the nucleus of many of the genes that were once encoded in the genome of the proteobacterium argues that both problems can potentially be circumvented. On the other hand, the co-localization for redox regulation hypothesis postulates that maintaining genes of electron transport chains in the mitochondrial compartment allows rapid regulation of organelle-specific gene expression in response to redox states (Allen 2017).

1.4. Nuclear regulation of mitochondrial biogenesis and stress responses

1.4.1. Mitochondrial biogenesis

Mitochondrial biogenesis is induced in response to developmental and physiological stimuli. To exemplify, cardiomyocytes are the cells with the highest volume density of mitochondria, which provide the energetic reserve capacity that the heart requires (Goffart et al. 2004). The development and maturation of the cardiac mitochondrial system occur largely during the perinatal stages, processes that include a major increase in mitochondrial biogenesis at birth (Piquereau et al. 2010). This increase corresponds to a shift in metabolism from glycolysis to FAO and OXPHOS as mammals adapt to changes in oxygen availability (Finck et al. 2002). Other external stimuli like changes in environmental temperature, exercise, caloric intake, and hormones have also been reported to induce mitochondrial biogenesis (Ryan & Hoogenraad 2007). Furthermore, an increase in mitochondrial mass is a common finding in patients with mitochondrial diseases and transgenic mouse models with mitochondrial dysfunction (Kauppila et al. 2017). Thus, under pathologic or stress conditions, retrograde signalling from the mitochondria to the nucleus activates cellular responses to loss of mitochondrial function that lead to mitochondrial biogenesis.

Several transcription factors acting on the nuclear genome have been implicated in the regulation of expression of mitochondrial proteins in mammals. The nuclear respiratory factors

NRF1 and GABPA (also known as NRF2) function as positive regulators of transcription of nDNA-encoded mitochondrial genes. Binding sites for both transcription factors have been identified in upstream sequences of several mitochondrial genes including genes encoding OXPHOS proteins (Kelly & Scarpulla 2004). In line with this, knockout of *Nrf1* and *Gabpa* in mouse is embryonic lethal with a clear mitochondrial phenotype (Huo and Scarpulla 2001; Ristevski et al. 2004; Yang et al. 2014). Members of the nuclear receptor super family that include the peroxisome proliferated-activated receptors (PPARs) and the estrogen-related receptors (ERRs) regulate the expression of enzymes involved in mitochondrial metabolism (Scarpulla et al. 2012). Finally, several targets of MYC are genes encoding mitochondrial proteins and it has been suggested that this transcription factor coordinates mitochondrial biogenesis during cell cycle and pathologic stress (Ahuja et al. 2010; Morrish & Hockenbery 2014).

The peroxisome-proliferator-activated receptor coactivators (PGC1α, PGC1β, and PPRC1) have been found to interact with NRF1, GABPA, PPARs and ERRs and, therefore, have the potential to induce most aspects involved in mitochondrial biogenesis (Scarpulla et al. 2012). Furthermore, several signalling pathways like the mechanistic target of rapamycin (mTOR) and cyclic adenosine monophosphate (AMP)-activated protein kinase (AMPK) that are activated by changes in the cellular metabolic state (*e.g.* amino-acid concentrations, ADP/ATP or NAD^+/NADH ratios) converge on PGC1α suggesting that it is a master regulator of mitochondrial biogenesis and function (Ryan & Hoogenraad 2007). However, *Pgc1*α knockout mice are viable and only show a mild effect suggesting that other factors, including PGC1β, can compensate for its absence (Kauppila et al. 2017). This finding questions the role of PGC1α as a universal master regulator of mitochondrial biogenesis *in vivo* and suggests that other factors are equally or more important under physiological conditions.

Several of the aforementioned transcription factors have been reported to regulate genes required to express mtDNA and, therefore, have the potential to coordinate the expression of both cellular genomes to promote mitochondrial biogenesis and function. NRF1 has predicted binding sites in the gene coding for the mitochondrial transcription factor A (*Tfam*) and several genes coding for mitochondrial ribosomal (mitoribosomal) proteins. Knockdown of *NRF1* in human cells has been shown to decrease transcript levels of *TFAM* (Cam et al. 2004) and the embryonic lethality in a *Nrf1* knockout mouse correlates with a depletion of mtDNA (Huo & Scarpulla 2001). GABPA was reported to bind the upstream sequences of the genes encoding *POLRMT*, the mitochondrial transcription termination factor 1 (*MTERF1*), and several factors involved in mtDNA replication (Bruni et al. 2010). *TFAM* and *POLRMT* have also been reported to be target genes of MYC and knockdown of *MYC* in

human cancer results in decreased protein levels of both factors (Oran et al. 2016). However, recent studies suggest that coordination of the expression of the two cellular genomes does not have to occur at the transcription level. In baker's yeast, it was shown that transcription of nDNA and mtDNA are not coordinated, whereas translation of the OXPHOS subunits encoded in both genomes is synchronized (Couvillion et al. 2016). This synchronization was shown to be regulated unidirectionally from the cytosolic ribosomal translation which is consistent with the existence of translational activators for most mitochondrial messenger RNAs (mt-mRNAs). In mammals such a mechanism seems less likely as mammalian mt-mRNAs have only very short 5' UTRs and to date only one translational activator for *mt-Co1* called TACO1 has been identified (Richman et al. 2016; Weraarpachai et al. 2009). A recent study on human cells reported that mitochondrial ribosomes (mitoribosomes) translating *mt-Co1* interact with OXPHOS complex assembly factors which can stall mitochondrial translation when the nDNA-encoded subunits are absent (Richter-Dennerlein et al. 2016).

1.4.2. Mitochondrial stress responses

Nuclear genetic programs are activated in response to mitochondrial stress. Impaired coordination of nuclear and mitochondrial gene expression result in the increase of mitochondrial proteases and chaperones. Martinus and collaborators proposed that the accumulation of unfolded proteins in mammalian mitochondria cause activation of a mitochondrial specific stress signalling pathway called the mitochondrial unfolded protein response (mtUPR) (Martinus et al. 1996). This signalling pathway has been extensively studied in *Caenorhabditis elegans* where the current model is that mitochondrial dysfunction reduces import efficiency inhibiting the normal localization of the stress activated transcription factor ATFS-1 to mitochondria. Instead, ATFS-1 translocates to the nucleus where it activates transcription of mitochondrial stress response genes (Nargund et al. 2015). The cleavage of unfolded proteins in mitochondria by the mitochondrial matrix protease ClpP and subsequent release of the resulting peptides has been suggested to be required for the activation of this signalling pathway (Haynes et al. 2007). In mammals, however, there is no consensus with regard to the importance of this stress response pathway. It has been proposed that genes upregulated by mtUPR in mammals contain a binding element for the DNA damage-inducible transcript 3 (DDIT3/CHOP) and CCAT/enhancer-binding protein β (C/EBPβ) flanked by two conserved elements called Mitochondrial Unfolded Protein Response Elements (MURE) 1 and 2 (Aldridge et al. 2007; Martinus et al. 1996; Zhao 2002). However, the proposed CHOP-MURE 1/2 elements are found in several non-mitochondrial genes (Aldridge et al. 2007) arguing against a mitochondrial-specific response mediated only by these regulatory elements. Furthermore, several mouse models deficient in mtDNA gene expression show an increase in mitochondrial proteases and chaperones that do not contain the CHOP-MURE 1/2 elements,

including the AAA^+ LON P protease (LONP1), AFG3-like protein 2 (AFG3L2), and the mitochondrial 75 kDa heat shock protein (TRAP1) (Dogan et al. 2014; Perks et al. 2018). ATF5 was proposed to be the closest homolog of ATFS-1 and to mediate mtUPR via a similar differential translocation mechanism as in *C. elegans* (Fiorese et al. 2016). However, the mitochondrial localization of ATF5 in mammalian mitochondria lacks biochemical support and the proposed translocation to the nucleus upon mitochondrial stress has not been shown. Finally, the requirement of CLPP in mammals has been refuted as a double knockout mouse model deficient in CLPP and the mitochondrial aminoacyl-tRNA synthetase (DARS2) activates mtUPR responsive genes despite the absence of CLPP (Seiferling et al. 2016).

In mammals, mitochondrial dysfunction results in several changes in cellular metabolism regulated at the transcription level. In heart of mice deficient in mtDNA gene expression, a switch in metabolism from FAO to glycolysis mediated by PPARα precedes the increase in mitochondrial biogenesis (Hansson et al. 2004). Several studies in cell culture and mouse have found a strong upregulation of genes that carry a conserved amino acid response element (AARE) in their upstream regulatory region in response to different mitochondrial stresses including impaired mtDNA gene expression as well as loss of membrane potential and OXPHOS function (Bao et al. 2016; Quirós et al. 2017; Tyynismaa et al. 2010). This AARE is recognized by the ATF family of transcription factors, mainly ATF4, and upregulates genes encoding proteins involved in the regulation of lipid and glucose metabolism, anabolic amino acid synthesis, and the 1C pathway (Suomalainen & Battersby 2018). The 1C pathway obtains the 1C units from glycine, sarcosine, and serine and transfers them through different tetrahydrofolate (THF) intermediates to supply 1C units for cellular processes such as methylation, *de novo* purine synthesis, and nicotinamide adenine dinucleotide phosphate (NADPH) synthesis (Ducker & Rabinowitz 2017). Activation of ATF4 correlates with the phosphorylation of the eukaryotic translation initiation factor 2α (eIF2α) in mitochondrial dysfunction (Khan et al. 2017; Quirós et al. 2017), suggesting that the responses to mitochondrial stress converge with the cellular integrated stress response (ISR). However, the kinase phosphorylating eIF2α in response to mitochondrial dysfunction has not been identified (Quirós et al. 2017). A recent study proposed that mTOR complex 1 (mTORC1) upregulates the 1C pathway and purine metabolism independently of eIF2α phosphorylation (Ben-Sahra et al. 2016) and activation of mTORC1 signalling was found in mouse models with mitochondrial dysfunction (Khan et al. 2017; Perks et al. 2018). Furthermore, rapamycin treatment in mice with mitochondrial myopathy reversed the effect of ATF4 indicating that mTORC1 acts upstream of ATF4 in mitochondrial dysfunction (Khan et al. 2017). Finally, one of the target genes of ATF4 is the fibroblast growth factor 21 (*Fgf21*), whose gene product is released into the blood stream and can activate paracrine and endocrine effects resulting in

metabolic remodelling in different tissues (Fisher & Maratos-Flier 2016). FGF21 has been shown to be released by the skeletal muscle and heart in mitochondrial dysfunction mouse models (Dogan et al. 2014; Tyynismaa et al. 2010) and has been proposed as a biomarker of mitochondrial dysfunction in human patients (Lehtonen et al. 2016). Interestingly, mitochondrial stress in cell culture causes a general decrease of mitoribosomal proteins suggesting that mitochondrial gene expression programs respond to mitochondrial stress (Quirós et al. 2017). However, the mechanism leading to this downregulation has not been studied yet.

1.4.3. A nuclear isoform of POLRMT

The *Polrmt* gene has been reported to code for two RNA polymerases acting in the mammalian cells, POLRMT and the fourth nuclear RNA polymerase (spRNAP-IV) (Kravchenko et al. 2005; Kravchenko & Chumakov 2005). In mice and humans, the *Polrmt* gene contains 21 exons. POLRMT is the product of the predominant splice variant and is a ~140 kDa protein that contains an N-terminal mitochondrial targeting sequence (MTS). SpRNAP-IV is an alternative splicing isoform that contains a longer exon 1 producing a premature stop codon. Therefore, translation of spRNAP-IV would initiate from another open reading frame starting at exon 3. Compared to POLRMT, spRNAP-IV lacks the first 262 amino acids resulting in a ~110 kDa protein that does not contain an MTS (Kravchenko et al. 2005; Kravchenko & Chumakov 2005). In the nucleus, spRNAP-IV was reported to transcribe a specific subset of nuclear genes including several muscle actin genes (*ACTC1*, *ACTA1*, *ACTG1*), the zinc-finger BTB domain-containing protein 1 gene (*ZBTB1*), the prenylcysteine oxidase gene (*PCYOX1*) and the *POLRMT* gene itself (Kravchenko et al. 2005; Lee et al. 2011). This observation suggests that transcription of mitochondrial and a subset of nuclear genes could be coupled. However, there are no studies of the mechanism of transcription of spRNAP-IV in the nucleus.

1.5. Mammalian mitochondrial DNA gene expression

1.5.1. The mammalian mitochondrial genome

Mitochondrial DNA is exclusively maternally inherited and the number of copies of mtDNA per cell varies by several orders of magnitude between different tissues (Hällberg & Larsson 2014). Mammalian mtDNA is a double-stranded circular molecule of ~16.5 kb that encodes 37 genes (Figure 1.3A) (Anderson et al. 1981). The two strands of mtDNA have different sedimentation coefficients in alkaline caesium chloride gradients because of differences in guanine content. Consistent with these differences, the two mtDNA strands are designated the heavy (H) and the light (L) strand. The H strand encodes 10 mt-mRNAs, 2 ribosomal RNAs (mt-rRNAs), and 14 transfer RNAs (mt-tRNAs). The L strand encodes one mt-mRNA and 8 mt-tRNAs (Clayton 1991). The 11 mt-mRNAs encoded in the mitochondrial genome are translated into 13 proteins

as two mt-mRNAs, *mt-Atp8/Atp6* and *mt-Nd4l/Nd4*, are bicistronic transcripts (Hällberg & Larsson 2014). Mitochondria use a non-universal codon code that is decoded by the mt-tRNAs (Larsson 2010).

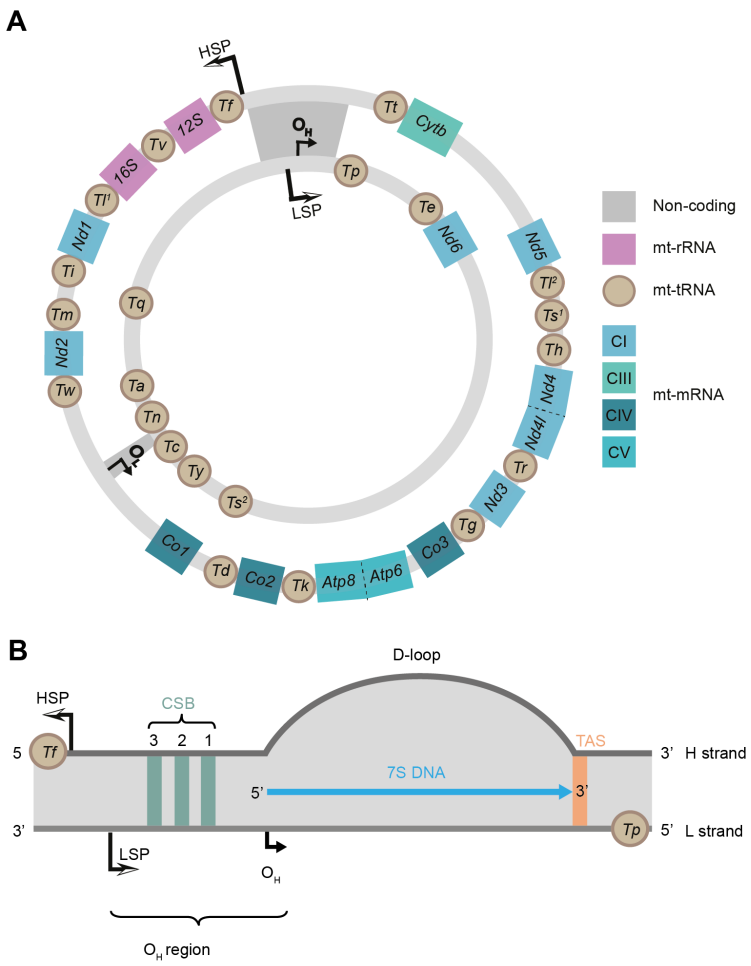

Figure 1.3 | Organisation of the mammalian mitochondrial genome (**A**) Mitochondrial genome illustrating both strands. (**B**) Schematic representation of the NCR with its regulatory elements. Abbreviations in alphabetic order: CI - CV, OXPHOS complex I-V; CSB, conserved sequence blocks; D-loop, displacement loop; H strand, heavy strand; HSP heavy-strand promoter; L strand, light strand; LSP, light-strand promoter; NCR, non-coding control region; TAS, termination associate sequence. Modified from Larsson 2010 and Gustafsson et al. 2016.

The densely packed mammalian mtDNA only contains two non-coding regions. The longer non-coding region (NCR), referred as the control region, is ~1.1 kb and spans from *mt-Tf* to *mt-Tp* (Figure 1.3B). The NCR contains the promoters of transcription for each strand, that is the H-strand promoter (HSP) and the L-strand promoter (LSP), as well as the origin of replication for the H strand (O_H) region. The O_H region comprises the DNA sequence spanning from LSP until the mapped O_H start site. Between LSP and O_H, there are three conserved sequence blocks (CSB1-3) that are important regulatory sequences (Gustafsson et al. 2016). Abortive replication starting at O_H results in a triple-stranded DNA structure as the newly replicated H strand remains bound to mtDNA displacing the non-template H strand. This region is called the displacement loop (D-loop) (Bogenhagen & Clayton 1978). The abortive mtDNA replication product of ~650 nucleotides is called 7S DNA and it ends in the termination-associated sequence (TAS) that contains conserved palindromic motifs in vertebrates (Jemt et al. 2015). Most of the mammalian mtDNA replication events starting from O_H result in 7S

DNA strands that are rapidly turned over (Figure 1.3) (Bogenhagen & Clayton 1978). The precise function and mechanisms regulating the D-loop remain elusive but it has been proposed to be important for the regulation of mtDNA replication and maintenance of mtDNA topology among others (Nicholls & Minczuk 2014).

Mammalian mtDNA is tightly packed in nucleoprotein complexes of ~100 nm called the mitochondrial nucleoids. The main protein component of the mammalian nucleoid is TFAM that binds mtDNA via its two high-mobility group domains resulting in bending and compaction of the mtDNA molecule (Kaufman et al. 2007; Kukat et al. 2011; Kukat et al. 2015). Thus, TFAM is a highly abundant protein and it is estimated that there are ~1000 TFAM molecules per mtDNA. In addition to TFAM, several proteins required for mtDNA replication and transcription transiently interact with the mitochondrial nucleoid (Bonekamp & Larsson 2018; Bogenhagen 2012).

1.5.2. Mitochondrial DNA replication and maintenance

Mitochondrial DNA replication is performed by the phage-derived DNA polymerase γ (POLγ) that is composed of one catalytic subunit (POLγA) and two accessory subunits (POLγB). However, POLγ is unable to use dsDNA as a template on its own and requires the DNA replicative helicase TWINKLE (gene name *TWNK*) that forms a hexameric ring and unwinds mtDNA at the replication fork (Korhonen et al. 2004). Although there are different proposed models for mammalian mtDNA replication, the strand-displacement model has the most robust experimental support (Gustafsson et al. 2016). According to this model, mtDNA replication starts at O_H and DNA synthesis proceeds in one direction generating a new H strand. During the synthesis of the new H strand, the parental H strand is covered by the mitochondrial single-stranded binding proteins (SSBP1). The single-stranded L-strand origin of replication (O_L) forms a stable stem-loop structure that is used as template to generate the primer for L-strand replication. The O_L is activated when the H strand replication has proceeded past this region and thereafter DNA synthesis from both strands proceeds continuously in opposite directions (Clayton 1991). Ligation of the newly replicated mtDNA molecule is performed by DNA ligase III (LIG3) (Lakshmipathy & Campbell 1999) and decatenation is performed by the DNA topoisomerase 3α (Nicholls et al. 2018).

Several transgenic mouse strains have been generated to study mtDNA maintenance and replication *in vivo.* Disruption of *Tfam*, *Twnk*, *Polγ*A, or *Lig3* in mouse is embryonic lethal and leads to mtDNA depletion (Hance et al. 2005; Larsson et al. 1998; Milenkovic et al. 2013; Puebla-Osorio et al. 2006). The levels of TFAM and mtDNA correlate very well in different mouse models and cells, and it has been suggested that they stabilize each other (Ekstrand

et al. 2004; Jiang et al. 2017; Kukat et al. 2015; Larsson et al. 1994). A mechanism proposed to explain the concordance of TFAM and mtDNA levels is that LONP1 degrades TFAM when it is not bound to mtDNA (Lu et al. 2013). Interestingly, *Twnk* overexpression increases mtDNA copy number and a conditional *Tfam* knockout hearts have increased levels of TWINKLE, thus suggesting that TWINKLE is a limiting factor for mtDNA replication (Milenkovic et al. 2013). Super-resolution microscopy of mouse embryonic fibroblasts (MEFs) show a broad distribution of nucleoid sizes, indicating that different levels of compaction are present in mammalian mitochondrial nucleoids (Kukat et al. 2015). Increasing TFAM levels *in vitro* increase the compaction of the mtDNA template, which, in turn, inhibits mtDNA replication and transcription (Farge et al. 2014). Thus, TFAM modulation of nucleoid compaction could be an important mechanism for control of mtDNA replication and transcription *in vivo.*

POLγ requires an RNA primer to initiate replication at O_H and O_L but the mechanism of replication primer formation is still not completely understood. Mapping of RNA and DNA species in the human and mouse D-loop regions has identified RNA species whose 3' ends corresponded to the 5' ends of DNA molecules at O_H. The 5' end of this RNA coincides perfectly with LSP indicating that, in mammals, mtDNA replication uses an RNA primer and that primers are formed by mtDNA transcription (Figure 1.4) (Chang & Clayton 1985; Chang et al. 1985). In support of this hypothesis, *in vitro* studies have shown that transcription from LSP using recombinant human POLRMT results in a stable triple-stranded DNA-RNA hybrid (R-loop) that depends on the G-rich sequence of CSB2 (Lee & Clayton 1996; Xu & Clayton 1996). Furthermore, a reconstituted human mitochondrial transcription system has shown that transcription prematurely terminates at CSB2 because of the formation of a G-quadruplex between CSB2 RNA and the corresponding non-template DNA strand. Since CSB2 is also the major site of RNA-DNA transitions in the complementary D-loop strand, it has been proposed that premature transcription termination at this position generates the RNA primer for H-strand replication (Pham et al. 2006; Wanrooij et al. 2012). However, such an RNA primer cannot support transcription in reconstituted *in vitro* systems suggesting that additional regulatory elements are required (Wanrooij et al. 2012). The 5' ends of non-ligated mtDNA mainly map to O_H, which is located ~100 bp downstream CSB2 (Attardi et al. 1979), suggesting that the nascent H strand is considerably processed at the 5' end to remove the RNA primer and a fragment of DNA (Gustafsson et al. 2016). The ribonuclease H1 (RNASEH1) is thought to degrade the RNA primers on both strands and the mitochondrial genome maintenance exonuclease - 1 (MGME1) is thought to degrade the DNA upstream of O_H (Matic et al. 2018; Uhler & Falkenberg 2015). An additional confounding point is that transcription from LSP also generates a short non-coding RNA transcript of unknown function called the 7S RNA. This transcript extends from LSP to CSB1 (Jemt et al. 2015) and it has been proposed to function

as a primer at O_H. However, 7S RNA is poly-adenylated and does not remain bound to mtDNA (Ojala & Attardi 1974), thus it is not likely the replication RNA primer (Gustafsson et al. 2016).

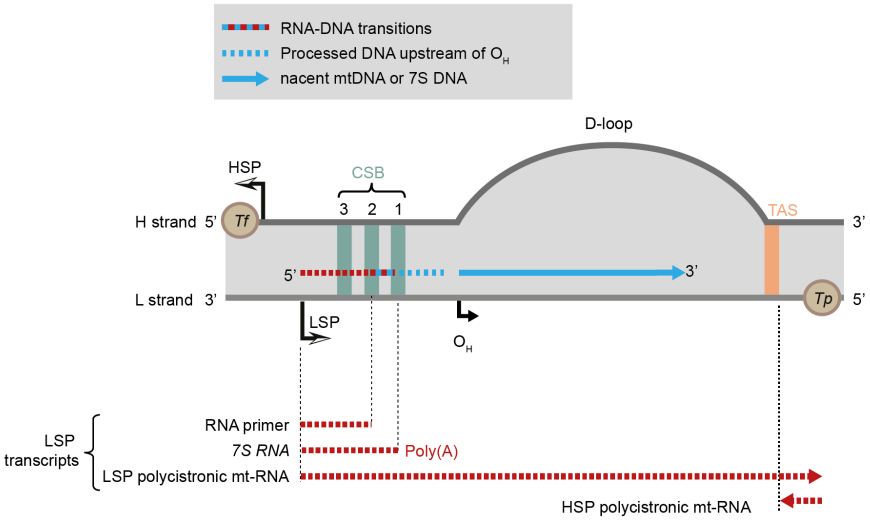

Figure 1.4 | Regulation of transcription in the NCR
Transcription from LSP generates three transcripts: i) the RNA primer that ends at CSB2, ii) 7S RNA that ends at CSB1, and iii) the full-length polycistronic mt-RNA encompassing all of the genes encoded in the L strand. The 7S DNA 5' end maps to O_H. The HSP polycistronic mt-RNA stops at the termination associated sequence (TAS). Abbreviations in alphabetic order: CSB, conserved sequence blocks; H strand, heavy strand; HSP, heavy-strand promoter; L strand, light strand; LSP, light-strand promoter; D loop, displacement loop, O_H, heavy-strand origin of replication; Poly(A), poly-adenine tail; TAS, termination-associated sequence. Modified from Gustafsson et al. 2016

The importance of POLRMT in replication primer formation is debated. In the nucleus primers are generated by specific DNA-dependent RNA polymerases, called DNA primases, distinct from the classical RNA polymerases (Guilliam et al. 2015). Furthermore, early studies identified a mitochondrial primase activity that was thought to generate the primers at the poly-dT stretch in the stem-loop structure of O_L (Ledwith et al. 1986). Phylogenetic analysis suggested that TWINKLE has a primase activity in most eukaryotes but this function is lost in metazoans (Shutt & Gray 2006). The DNA-directed primase/polymerase protein (PRIMPOL) was reported to localize in the nucleus and mitochondria and present primase activity (García-Gómez et al. 2013). However, *Primpol* knockout mice are viable suggesting that it does not have an essential role in mtDNA replication. POLRMT can generate the O_L primer for mtDNA replication *in vitro* (Wanrooij et al. 2008; Fusté et al. 2010) suggesting that POLRMT may be the primase for mtDNA replication at both O_H and O_L, but substantial *in vivo* data are missing to date.

1.5.3. Mitochondrial DNA transcription

POLRMT transcribes mtDNA starting from LSP and HSP and generates two near-genome length polycistronic transcripts encompassing all genes on each strand. Transcription from HSP is terminated in the TAS region of the NCR and transcription from LSP is terminated at *mt-Tl1* (Figure 1.5) (Gustafsson et al. 2016; Jemt et al. 2015).

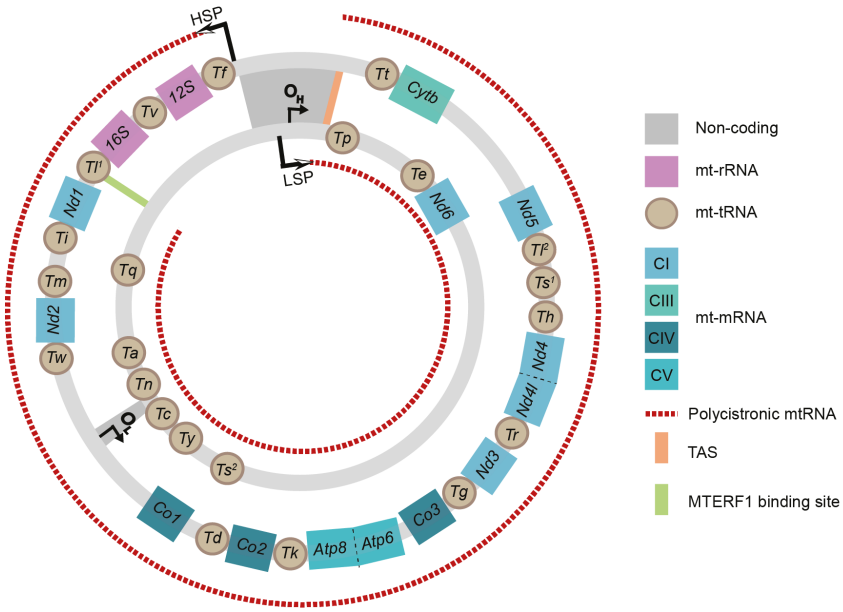

Figure 1.5 | Mammalian mtDNA transcription units mtDNA is transcribed from the two promoters to generate near-genome length polycistronic transcripts. Transcription from LSP is terminated at the *mt-Tl1* where MTERF1 binds. Transcription from LSP is terminated at the TAS region before entering the D-loop in the NCR. Same conventions as Figure 1.3. Modified from Gustafsson et al. 2016

POLRMT requires additional factors for promoter recognition, transcription initiation, transition to elongation, and transcription termination (Morozov et al. 2014; Ringel et al. 2011; Schwinghammer et al. 2013; Shi et al. 2012; Sologub et al. 2009). These factors include TFAM, the mitochondrial transcription factor B2 (TFB2M), the mitochondrial transcription elongation factor (TEFM), and MTERF1. TFAM and TFB2M are required for transcription initiation, TEFM for elongation, and MTERF1 for termination from LSP (Gustafsson et al. 2016). The mechanism of transcription termination from the H strand in the TAS region of the NCR (Jemt et al. 2015) has not been elucidated yet.

Based on biochemical and structural studies of these transcription factors and POLRMT in *in vitro* systems, a sequential model of mitochondrial transcription initiation has been proposed (Agaronyan et al. 2015; Hillen, et al. 2017a; Morozov et al. 2015; Posse et al. 2014; Posse et al. 2015). According to this model, TFAM binds to specific sequences in upstream regions of HSP and LSP inducing conformational changes in the promoter region. These conformational changes allow the binding of POLRMT to TFAM and the promoter DNA forming the pre-initiation complex (pre-IC). Then, TFB2M is required to melt the promoter completing the initiation complex (IC). After transcription initiation, TFAM and TFB2M disengage from the complex and TEFM aids in the processivity of POLRMT to generate the long polycistronic transcripts (Figure 1.6).

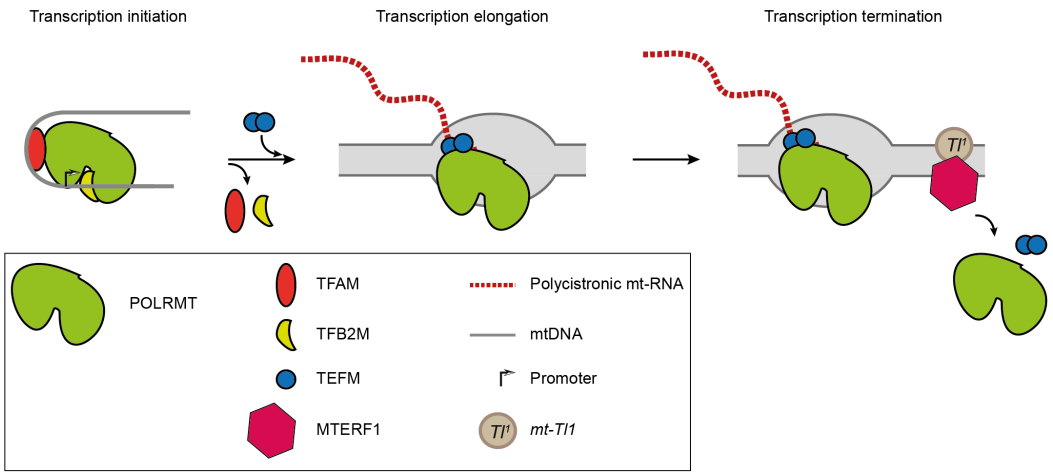

Figure 1.6 | Model of mitochondrial transcription
The initiation complex formed by POLRMT, TFAM and TFB2M assembles in the promoter region. Then, TFAM and TFB2M disengage from the complex and TEFM binds POLRMT forming the elongation complex. Transcription from LSP is terminated by MTERF1 in *mt-Tl1*. Transcription from HSP is terminated in the TAS region (Figure 1.5) but the mechanism is still unknown. Abbreviations in alphabetic order: mtDNA, mitochondrial DNA; MTERF1, mitochondrial transcription termination factor 1; POLRMT, mitochondrial RNA polymerase; TEFM, mitochondrial transcription termination factor 1; TFAM, mitochondrial transcription factor A; TFB2M, mitochondrial transcription factor B2; mt-RNA, mitochondrial RNA.

1.5.3.1. Mitochondrial RNA polymerase

POLRMT is homologous to the T7-phage RNA polymerase (T7-RNAP) (Ringel et al. 2011). It consists of three domains; the C-terminal domain (CTD), the N-terminal domain (NTD), and the N-terminal extension (NTE) that contains the MTS. The CTD is a T7-like catalytic domain that has a conserved mechanism of nucleic acid polymerization dependent on magnesium ions. The structure of the NTD also resembles T7-RNAP and it contains important elements for promoter recognition and melting. The NTE is a unique feature of POLRMT as it is not present in T7-RNAP and contains pentatricopeptide repeat (PPR) motifs (Ringel et al. 2011) that are degenerate 35-amino acid tandem sequence motifs found in proteins involved in RNA metabolism (Lightowlers & Chrzanowska-Lightowlers 2013). During transcription elongation, the nascent transcript emerges towards the PPR motifs of POLRMT (Schwinghammer et al. 2013). Furthermore, a mutant POLRMT enzyme devoid of most of the NTE (Δ320 amino acids) has higher *in vitro* transcription activity than the wild-type polymerase (Posse et al. 2014) indicating that the NTE might have an important regulatory role in POLRMT but the precise function is still unknown.

1.5.3.2. Mitochondrial transcription factor A

In addition to the previously mentioned function of TFAM in mtDNA maintenance, TFAM binds with high affinity to specific regions upstream of HSP and LSP inducing a 180° bend in the promoter (Morozov et al. 2014; Morozov & Temiakov 2016; Ngo et al. 2014; Posse et al. 2014). The specific binding of TFAM to the promoter region is required for mitochondrial transcription initiation (Dairaghi, Shadel & Clayton 1995a; Gaspari et al. 2004; Shi et al. 2012). In this

process, the C-terminal tail of TFAM interacts with the NTE of POLRMT (Hillen et al. 2017a; Morozov et al. 2014; Posse et al. 2014). In agreement with the structural and biochemical data, the transcription factor activity of TFAM is severely impaired in absence of its C-terminal tail (Dairaghi, Shadel & Clayton 1995b). The interaction of TFAM, POLRMT, and promoter DNA is species-specific as human TFAM is a poor activator of mitochondrial transcription in mouse in *in vivo* and *in vitro* systems (Ekstrand et al. 2004; Gaspari et al. 2004). Importantly, the mtDNA maintenance function of TFAM can be dissociated from its function as a transcription factor because expression of human TFAM in a mouse *Tfam* knockout background rescues mtDNA copy number, but not mitochondrial transcription (Ekstrand et al. 2004; Freyer et al. 2010). In addition to promoter specificity, TFAM is also required but not sufficient for promoter melting (Posse & Gustafsson 2017; Ramachandran et al. 2017).

1.5.3.3. Mitochondrial transcription factor B2

TFB2M has structural homology to bacterial rRNA methyltransferases but in mammalian mitochondria it is a *bona fine* transcription initiation factor (Litonin et al. 2010). Consistently, knockout of *Tfb2m* in mouse pancreatic β-cells leads to loss of mt-RNAs (Nicholas et al. 2017). TFB2M interacts with the NTD and CTD of POLRMT as well as with the promoter DNA and priming nucleotide (Morozov et al. 2015). TFB2M induces conformational changes in POLRMT which enables promoter opening and the correct localization of the non-template strand (Hillen et al. 2017a). The sequential model for transcription initiation was founded on crosslinking and footprinting analyses that showed that POLRMT can be recruited to the promoter without the requirement of TFB2M and form a stable pre-IC (Posse et al. 2014; Morozov et al. 2014). However, a recent study has proposed an alternative model where POLRMT and TFB2M can form a complex independently of promoter binding. This model is supported by equilibrium binding analyses that show that POLRMT and TFB2M have a similar dissociation constant as TFAM and LSP (Ramachandran et al. 2017).

1.5.3.4. Mitochondrial transcription elongation factor

TEFM is the most recently described mitochondrial transcription factor. It was identified by homology analyses as a putative human mitochondrial Holliday Junction resolvase. Although this specific activity was not found in recombinant TEFM, silencing of *TEFM* in human cells showed a specific pattern of mt-mRNA abundance whereby promoter-proximal transcripts were increased and promoter-distal transcripts were decreased suggesting a role in transcription elongation (Minczuk et al. 2011). Biochemical characterization of TEFM activity in *in vitro* transcription systems showed that TEFM increases the processivity of POLRMT in longer transcripts by enhancing the affinity of POLRMT to an elongating template and

facilitating the passage over structured or modified DNA sequences like G-quadruplexes or 8-oxo-dG lesions (Agaronyan et al. 2015; Posse et al. 2015; Sultana et al. 2017). The crystal structures of TEFM and POLRMT with TEFM in an elongating complex provided important mechanistic insights that could explain how TEFM promotes transcription elongation (Hillen et al. 2017b). First, TEFM has two domains, an NTD, that contains two globular hairpin-helix-harpin (HhH) domains of unknown function, and a C-terminal dimerization domain that forms the catalytic core. TEFM dimer interacts with POLRMT and the nucleic acids in the transcription bubble. These interactions contribute to the formation of a 'sliding clamp' with the downstream DNA that enhances the processivity of the transcription elongation complex. Second, TEFM binds the single-stranded non-template DNA preventing the collapse of the transcription bubble. Third, TEFM induces conformational changes in POLRMT that contribute to the formation of the RNA channel and prevent the formation of RNA G-quadruplexes during transcription elongation. Since TEFM prevents transcription termination at CSB2, it has been proposed that it is a switch between mtDNA replication and transcription (Agaronyan et al. 2015). However, this function is debated (Posse et al. 2015) as it assumes that the primer for mtDNA replication at O_H would be formed by premature transcription termination at CSB2 and, until now, this prematurely terminated transcript has not been shown to support mtDNA replication *in vitro* suggesting that additional processing is required.

1.5.3.5. Mitochondrial transcription termination factor 1

MTERF1 is the only known factor to date involved in transcription termination. It binds mtDNA in *mt-Tl1* that is located downstream of mt-rRNAs in the H strand (Figure 1.5) (Shang & Clayton 1994; Terzioglu et al. 2013) and was proposed to act as a road block for transcription of LSP and HSP. Termination of HSP-initiated transcription mediated by MTERF1 was suggested to promote the generation of a shorter polycistronic transcript encompassing the mt-rRNAs (Martin et al. 2005). However, *in vitro* and *in vivo* studies demonstrated that MTERF1 mainly terminates the transcription initiated at the LSP preventing the formation of antisense mt-rRNAs and has no effect on the abundance of the H-strand encoded mt-rRNAs (Figure 1.5) (Asin-Cayuela et al. 2005; Terzioglu et al. 2013).

Furthermore, it was recently shown that MTERF1 not only blocks transcription of antisense mt-rRNAs but also directs polar replication fork pausing. This means that MTERF1 acts as a roadblock for the replication machinery in the H strand preventing collisions with the transcription machinery transcribing the mt-rRNAs (Shi et al. 2016). Collisions of replication and transcription machineries can result in replication stalling and genome instability (Merrikh et al. 2012). These collisions can cause either co-directional or heads-on replication-transcription conflicts and different mechanisms to resolve or prevent these conflicts exist in

the nuclear chromosomes and in bacteria with circular genomes (García-Muse & Aguilera 2016; Merrikh et al. 2012). The two different origins of replication are coupled so that initiation at O_H, which depends on LSP transcription, must occur before O_L can be activated. This arrangement may contribute to reduce the possibility of collisions between the replication and transcription machineries in mammalian mitochondria.

Three additional members of the MTERF family of proteins have been found in mammalian mitochondria (MTERF2-MTERF4). MTERF3 was originally reported to be a negative regulator of mitochondrial transcription, but the exact binding site of MTERF3 to mtDNA has not been identified (Park et al. 2007). Then, MTERF3 was shown to bind *mt-16S* rRNA and facilitate assembly of the mitochondrial ribosome but the precise function is still unknown (Wredenberg et al. 2013).

1.5.3.6. Other factors regulating mitochondrial transcription

In addition, several proteins have been described to regulate mitochondrial transcription, including the mitochondrial ribosomal protein L12 (MRPL12) and the mitochondrial DNA topoisomerase 1 (TOP1MT). The role of MRPL12 in regulating mitochondrial transcription is debated. POLRMT was reported to bind a free pool of MRPL12, which was found to stimulate transcription. Here, MRPL12 may act as an allosteric activator of transcription helping in the transition from initiation to elongation (Nouws et al. 2016; Surovtseva et al. 2011; Wang et al. 2007). However, MRPL12 did not stimulate mitochondrial transcription in a reconstituted *in vitro* system (Litonin et al. 2010). TOP1MT was identified as an exclusive mitochondrial protein acting as a negative regulator of transcription through interaction with POLRMT; however, the underlying mechanism is not understood (Sobek et al. 2013).

1.5.4. Mitochondrial RNA processing

Pioneering studies from the Attardi laboratory observed that, in mammals, most mt-mRNAs and mt-rRNAs are flanked by mt-tRNAs (Ojala et al. 1981). They postulated that the polycistronic mitochondrial transcripts were processed into the individual mt-RNAs by precise endonucleolytic cleavage that occurred, in most cases, in the mt-tRNAs. This model is known as the “tRNA punctuation model”. The cleavage of the polycistronic mitochondrial transcripts is performed by the mitochondrial RNase P and the mitochondrial tRNAse Z (Rackham et al. 2012). This endonucleolytic process occurs in a hierarchical manner, that is, the 5’ ends of the mt-tRNAs are cleaved first followed by the 3’ ends (Brzezniak et al. 2011; Rackham et al. 2016). RNase P is formed by three mitochondrial RNAse P proteins (MRPP1, MRPP2, and MRPP3) and processes the 5’ ends of the mt-tRNAs. Furthermore, RNase P also processes the 5’ end of *mt-Co1* that does not contain a delimiting mt-tRNA but the upstream non-coding

sequence forms a tRNA-like structure (Sanchez et al. 2011). Zinc phosphodiesterase ELAC protein 2 (ELAC2) was recently identified as the enzyme processing the 3'ends of mt-tRNAs (Brzezniak et al. 2011).

All mitochondrial transcripts are post-transcriptionally modified to generate the mature, functional transcripts. The proper folding of mt-tRNAs, base pairing, and interaction with the aminoacyl-tRNA synthetases depend on a CCA addition to the 3' end and the modification of specific bases. These modifications include methylations, formylations, and pseudouridylations, among others (Suzuki et al. 2011). Mt-tRNAs are amino-acylated by an almost exclusive set of mitochondrial tRNA synthetases that differs from the cytosolic enzymes (Diodato et al. 2014).

Mammalian mt-mRNAs do not have introns, Shine Dalgarno sequences, conventional 5' and 3' UTRs, 5' 7- methylguanosine caps or base modifications. With the exception of *mt-Nd6*, all mt-mRNAs are polyadenylated in their 3' end and, for several of the transcripts, this process is essential as it completes the termination codon (Rackham et al. 2012). Contrary to the nucleus where polyadenylation promotes RNA degradation, in mitochondria the role of this process remains elusive as loss of the poly(A) tail in mt-mRNAs results in different effects on the abundance of mitochondrial transcripts (Bratic et al. 2016; Rorbach et al. 2011; Wilson et al. 2014). An important factor coordinating mt-mRNA stability and polyadenylation is the leucine-rich PPR motif containing protein (LRPPRC) (Ruzzenente et al. 2012). LRPPRC forms a complex with the mitochondrial SRA stem-loop-interacting RNA-binding protein (SLIRP) (Sasarman et al. 2010). This complex binds throughout the mitochondrial transcriptome and acts as a global RNA chaperone coordinating mt-RNA stability, polyadenylation, and translation (Siira et al. 2017). In line with this, loss of LRPPRC in mouse causes a global decrease of all mt-mRNAs except *mt-Nd6* whereas mt-tRNAs are mostly unchanged and mt-rRNAs are increased in abundance (Ruzzenente et al. 2012). LRPPRC was previously reported to also stimulate mitochondrial transcription by direct interaction with POLRMT (Liu et al. 2011), but *de novo* transcription is not affected by knockout or overexpression of *Lrpprc* (Harmel et al. 2013; Ruzzenente et al. 2011).

In addition to LRPPRC, the Fas-activated serine/threonine kinase (FASTK) family of proteins have recently emerged as key post-transcriptional regulators of mtDNA gene expression. It contains six members, FASTK and the FASTK-domain containing proteins 1 to 5 (FASTKD1 to FASTKD5), all of which localize to mitochondria and interact with specific mitochondrial transcripts. They have been reported to coordinate several processes including mt-RNA processing of *mt-Nd6*, stability of several mt-mRNAs and mt-rRNAs, and translation

of *mt-Co1* (Jourdain et al. 2017). The G-rich sequence factor 1 (GRSF1) was reported to mediate stability of several mt-RNAs and interact with RNase P in the mitochondrial matrix. Importantly, GRSF1 strongly binds to the *mt-Nd6* and silencing of *GRSF1* in human cells leads to the accumulation of pre-processed transcripts containing *mt-Nd6* suggesting an important role for this protein in the processing of this transcript (Antonicka et al. 2013; Jourdain et al. 2013). Importantly, *mt-Nd6* does not contain an mt-tRNA in the junction with the non-coding complementary *mt-Nd5.* A recent study suggested that GRSF1 binds G-rich non-coding RNAs resulting from LSP-initiated transcription promoting their degradation (Pietras et al. 2018). Microscopy analyses of GRSF1 showed that it forms a distinct punctate pattern in the mitochondrial matrix that co-localizes with mt-RNAs and processing enzymes which lead to the proposal that mt-RNA processing occurs in RNA granules (Antonicka et al. 2013; Jourdain et al. 2013). Subsequent co-immunoprecipitation and co-localization studies have identified several additional proteins involved in mt-RNA metabolism to be present in the mitochondrial RNA granules (Antonicka & Shoubridge 2015) including the mitochondrial polyribonucleotide nucleotidyltransferase 1 (PNPT1; PNPase) and the mitochondrial ATP-dependent RNA helicase (SUPV3L1) (Borowski et al. 2013). PNPT1 and SUPV3L1 form a complex that degrades mitochondrial transcripts (Borowski et al. 2013; Chujo et al. 2012; Khidr et al. 2008). The LRPPRC/SLIRP complex has been proposed to prevent the degradation of coding transcripts by maintaining the RNA unfolded (Chujo et al. 2012; Siira et al. 2017). Recently, the β-lactamase metalloprotein LACTB2 was shown to mediate the degradation of mitochondrial transcripts as well (Levy et al. 2016) and the oligoribonuclease REXO2 has been proposed to degrade small RNA oligomers resulting from PNPT1 degradation of mt-RNAs (Bruni et al. 2013; Bruni et al. 2017).

1.5.5. The mammalian mitochondrial ribosome

The mitoribosome contains more than 80 proteins and has a high protein to RNA ratio in comparison to the bacterial ribosomes (Sharma et al. 2003). Mitoribosomes are anchored to the IMM (Liu & Spremulli 2000) and it has been suggested that mtDNA-encoded proteins are inserted co-translationally in the IMM to assemble in the OXPHOS complexes (Gruschke & Ott 2010). The complete mitoribosome (monosome) is formed by two subunits: the small mitoribosomal subunit (28S) containing *mt-12S* rRNA and the large mitoribosomal subunit (39S) containing *mt-16S* rRNA. In addition, cryo-electron microscopy studies of the large ribosomal subunit revealed the presence of an mt-tRNA in the structure which turned out to be either *mt-Tv* or *mt-Tf* in all the mammalian species studied to date (Greber et al. 2014a; Greber et al. 2014b; Rorbach et al. 2016). Assembly of the mitoribosome initiates close to the mitochondrial nucleoids as mt-rRNAs are formed by transcription (Bogenhagen 2014;

Rackham et al. 2016) and it has been suggested that RNA granules are important centres for mt-rRNA post-transcriptional modification (Antonicka & Shoubridge 2015).

The mt-rRNAs are the most abundant mitochondrial transcripts (Mercer et al. 2011) and, to date, ten post-transcriptional modifications have been identified (Pearce et al. 2017). *mt-12S* rRNA has been shown to be methylated by the mitochondrial transcription factor B1 (TFB1M) and the 5-methylcytosine rRNA methyl transferase NSUN4. TFB1M is homologous to TFB2M and it was originally proposed to also act as a transcription factor (Falkenberg et al. 2002). However, knockout of *Tfb1m* in mouse does no repress mitochondrial transcription but results in loss of *mt-12S* rRNA methylation and severely impaired mitochondrial translation (Metodiev et al. 2009). NSUN4 forms a complex with MTERF4 that coordinates the assembly of the monosome (Cámara et al. 2011; Metodiev et al. 2014). *Mt-16S* rRNA is methylated by a group of closely related methyl-transferases that include the mitochondrial rRNA methyl transferases 1 to 3 (MRM1 to 3) (Pearce et al. 2017). Additionally, it has recently been shown that *mt-16S* rRNA is regulated by a protein complex containing a set of RNA binding proteins that include Neugrin (NGRN), RCC1-like G exchanging factor-like protein (RCC1L/WBSCR16), the putative mitochondrial mRNA pseudouridine synthases RPUSD3, RPUSD4 and TRUB2, and FASTKD2 (Arroyo et al. 2016). RPUSD4 was recently shown to pseudourydilate *mt-16S* rRNA (Antonicka et al. 2017; Zaganelli et al. 2017) and the PPR-motif containing protein 2 (PTCD2) was reported to be required for this modification to occur and to interact with FASTKD2 and RPUSD4 (Perks et al. 2018).

1.6. Mitochondrial dysfunction in human health

1.6.1. Mitochondrial genetic diseases

Mitochondrial diseases are one of the most common types of inherited metabolic disorders. They can be caused by mutations in mtDNA or in nuclear genes encoding mitochondrial proteins leading to different patterns of inheritance (Gorman et al. 2016). Since mtDNA is present in multiple copies within each cell, mutations in mtDNA can be present in all the molecules (homoplasmy) or in a fraction of the molecules (heteroplasmy). The levels of heteroplasmic mutations can vary between cells in the same organ or tissue, between organs within the same person, and between individuals in the same family. Moreover, the expression and severity of mitochondrial disease depends on whether mutated mtDNA passes a certain threshold (Stewart & Chinnery 2015). Mitochondrial diseases are clinically heterogenous which means that they can manifest at any time and with a wide variety of clinical symptoms. The severity of mitochondrial diseases can range from asymptomatic or oligosymptomatic carriers to life-threatening multisystemic disorders (Liang et al. 2014). Furthermore, they can manifest in a tissue-specific manner where the same genetic defect can result in different clinical

phenotypes (Nunnari & Suomalainen 2012). In addition to the genetic component, environmental factors can influence the course of mitochondrial diseases (Vafai & Mootha 2012).

Hundreds of different point mutations and re-arrangements in mtDNA have been shown to cause mitochondrial diseases and pathogenic mutations have been reported in in all mt-mRNAs, mt-tRNAs, and mt-rRNAs (Lott et al. 2013). Furthermore, several mutations in nuclear genes required for mtDNA gene expression have also been identified including mutations in *POLγ*, *TWNK*, *MGME1*, *ELAC2, LRPPRC, MTPAP,* several mitochondrial aminoacyl-tRNA synthetases and mitoribosomal proteins (Viscomi & Zeviani 2017). Mutations that affect mitochondrial transcription seem to be rarer. To date, only one pathogenic mutation has been identified in the NCR, specifically in the HSP, causing tubulointerstitial kidney disease (Connor et al. 2017). From the basic transcription machinery, a missense mutation in one of the high-mobility group boxes of *TFAM* was recently found in two siblings born of consanguineous parents of Colombian-Basque descent. This mutation caused neonatal liver failure and the patients died before 4 months of age (Stiles et al. 2016). The multiple genetic causes, different patterns of inheritance, heteroplasmy in the case of mtDNA pathogenic mutations, and heterogeneity of clinical symptoms make the diagnosis of mitochondrial diseases a complex process (Gorman et al. 2016). Furthermore, even when the genetic defect causing mitochondrial disease is identified, the chain of events that lead to the end pathology and the reasons behind the clinical heterogeneity and tissue-specificity of mitochondrial diseases are largely unknown.

Unfortunately, there is still no cure for mitochondrial diseases and, in most cases, clinical management remains largely supportive (Pfeffer et al. 2013). Multiple types of therapies targeting different aspects of mitochondrial dysfunction have been developed. These include therapies aimed at increasing respiratory chain substrate availability, enhancing electron transport transfer within the respiratory chain, bypassing respiratory chain components, increasing antioxidant capacity, improving energy buffering, and inducing adaptations to cope with OXPHOS dysfunction (Pfeffer et al. 2013). Many of these therapies are implemented as dietary supplements that are increasingly used due to their potential benefits and low-risk of developing secondary effects (Camp et al. 2016). An example of a commonly used supplement in patients with mitochondrial disorders is Q_{10} supplementation as it enhances electron transfer in the respiratory chain and is a potent antioxidant. Q_{10} supplementation is an efficient treatment for patients with primary Q deficiency (Emmanuele et al. 2012). However, its efficacy to treat other mitochondrial disorders has been questioned as clinical trials have shown mixed outcomes that can be explained by the experimental design

of the trials, the poor bioavailability of supplemented Q_{10}, and the lack of experimental support to define in which specific mitochondrial diseases would benefit from Q supplementation (Gorman et al. 2016; Pfeffer et al. 2013; Spindler et al. 2009). New treatments are currently being developed that include enhancers of mitochondrial proliferation, rapamycin treatment, hypoxia, and gene therapy approaches to reduce pathogenic heteroplasmic mtDNA mutations and target mutations in nuclear genes (Gorman et al. 2016; Nightingale et al. 2016).

1.6.2. Ageing and age-related diseases

Human ageing strongly correlates with the accumulation of mutated mtDNA molecules in somatic tissues leading to respiratory chain deficiency (Larsson 2010). Although it is not clear whether these mutations drive the ageing process or only correlate with it, there are strong indications that mtDNA mutations can contribute to ageing phenotypes (Kauppila et al. 2017). For a long time, the source of these mutations has been thought to be oxidative damage caused by reactive oxygen species (ROS) that leak from OXPHOS which, in turn, result in a vicious cycle as mutated mtDNA would generate more dysfunctional OXPHOS complexes and ROS (Bandy & Davison 1990). However, this hypothesis has now been extensively challenged as mouse models with increased mtDNA mutations do not have increased ROS (Trifunovic et al. 2005) and as removing ROS scavenging enzymes and mtDNA repair mechanisms does not induce mtDNA mutations (Kauppila et al. 2018). It has therefore been proposed that accumulation of mutations in specific cell types during ageing is driven by shifts in heteroplasmy during cell division, relaxed mtDNA replication, and replication errors (Kauppila et al. 2017; Stewart & Chinnery 2015).

Mitochondrial dysfunction is also found in several age-related diseases including cardiovascular diseases (Brown et al. 2017), neurodegenerative diseases (Golpich et al. 2017), metabolic syndrome (Lowell & Shulman 2005), and cancer (Zong et al. 2016). Hence, targeting mitochondrial dysfunction has developed as a leading therapeutic strategy for many of these common human pathologies. However, similar to the ageing process, distinguishing whether mitochondrial dysfunction causes or correlates with these diseases is an important and challenging endeavour that will greatly improve our understanding of the pathophysiology of these diseases and help to develop targeted therapeutic approaches. In this regard, understanding the fundamental processes that regulate mitochondrial biogenesis, function, homeostasis and how these processes affect cellular metabolism is of great importance from a biological and clinical perspective.

2. RESEARCH AIMS

Elucidating the in vivo function of POLRMT and its nuclear isoform spRNAP-IV *in mammals*

Mammalian mtDNA replication and transcription are intimately related processes as the priming site for H-strand replication coincides with initiation of transcription at LSP (Chang & Clayton 1985; Gillum & Clayton 1979). The primase function of POLRMT continued to be debated as an additional primase activity distinct from POLRMT was identified in mammalian mitochondria (Ledwith et al. 1986), DNA replication in the nucleus relies on specific primases that differ from the RNA polymerases needed for gene transcription (Guilliam et al. 2015), and the process of primer generation and processing is still largely unknown. In addition, the alternative isoform of the *POLRMT* gene, spRNAP-IV, was reported as the fourth eukaryotic nuclear RNA polymerase transcribing a specific set of genes in the nucleus (Kravchenko et al. 2005; Kravchenko & Chumakov 2005; Lee et al. 2011). The relevance of spRNAP-IV for mitochondrial function is unknown, but it was suggested to be involved in the coordination of nuclear and mtDNA gene expression. Thus, the *in vivo* mechanisms coordinating mtDNA replication and transcription and the concerted expression of the two cellular genomes remain significant gaps in our current knowledge of mitochondrial function. Therefore, the first aim of this thesis is to elucidate the *in vivo* function of POLRMT and its nuclear isoform in mammals using the mouse as a model organism.

Identifying the cellular consequences of progressive OXPHOS deficiency caused by loss of mtDNA gene expression

Expression of the mtDNA is essential for the biogenesis of the OXPHOS system. Since metabolism is highly interconnected, OXPHOS dysfunction can result in devastating consequences for the whole cell, organ, or organism. Mitochondrial diseases are the clear example of this, as mutations in mtDNA or nuclear genes encoding mitochondrial proteins can result in a broad spectrum of clinical phenotypes that cannot be explained uniquely by the primary OXPHOS defect (Nunnari & Suomalainen 2012). The pathogenesis of mitochondrial diseases is still far from being understood as distinguishing the direct consequences of OXPHOS dysfunction from the secondary cellular responses is challenging. Therefore, the second aim of this thesis is to systematically study the molecular consequences of progressive OXPHOS deficiency caused by disrupted mtDNA gene expression for protein complexes of dual genetic origin as well as the secondary cellular responses caused by the primary OXPHOS defect at the mitoproteome and cellular transcriptome level.

3. RESULTS

3.1. Elucidating the *in vivo* function of POLRMT and spRNAP-IV in mammals

3.1.1. Mouse strains to study the in vivo function of POLRMT and spRNAP-IV

To study the *in vivo* function of POLRMT and spRNAP-IV we generated several transgenic mouse strains with different gene dosage of *Polrmt*. A conditional knockout allele of *Polrmt* was generated by targeting exon 3 which disrupts the expression of the mitochondrial and nuclear splice variants (Figure 3.1A and B). Heart and skeletal muscle specific knockout (*Polrmt*$^{loxP/loxP}$; *Ckmm-cre*; L/L, cre) and germline heterozygous mice (*Polrmt*$^{+/-}$; +/-) were obtained by breeding mice with a heterozygously floxed *Polrmt* allele (+/Polrmt^{loxP}) to mice expressing the cre recombinase under the control of the creatinine kinase promoter (*Ckmm-cre*) or the ubiquitously expressed β-actin promoter (*β-actin-cre*), respectively. Analysis of complementary DNA (cDNA) by reverse transcription polymerase chain reaction (RT-PCR) verified that sequences corresponding to exon 3 of the *Polrmt* mRNA were lacking in the heart of the conditional *Polrmt* knockout mice (Figure 3.1C). Moreover, western blot analyses showed a drastic reduction of POLRMT in mitochondrial extracts from heart of the conditional *Polrmt* knockout mice (Figure 3.1D) and a 50% decrease in POLRMT levels in heart, skeletal muscle, and liver of *Polrmt*$^{+/-}$ mice (Figure 3.1E).

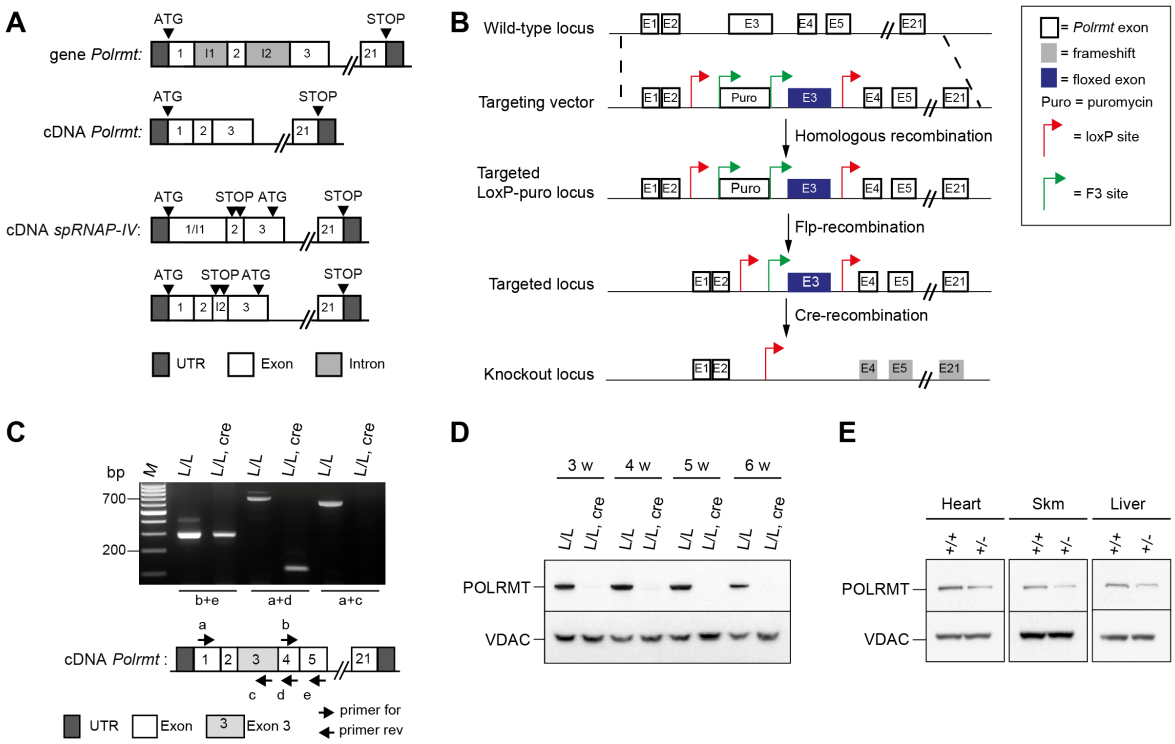

Figure 3.1 | Generation of conditional *Polrmt* knockout mice
(**A**) Schematic depiction of the *Polrmt* gene, *Polrmt* cDNA, and the two alternative splice variants cDNA reported in mouse coding for spRNAP-IV (Kravchenko & Chumakov 2005). (**B**) Targeting strategy for the conditional disruption of *Polrmt*. (**C**) RT-PCR analysis of targeted *Polrmt* transcripts from control (L/L) and tissue-specific knockout mice (L/L, cre). Different primer sets were used as indicated; exon 3: 551 bp. (**D**) Western blot analysis of steady-state POLRMT levels on isolated mitochondria from heart of L/L and L/L, cre mice at different ages. (**E**) Western blot

analysis of steady-state POLRMT levels on heart, skeletal muscle and liver of wild-type (+/+) and heterozygous *Polrmt* knockout (+/-) mice at 26 weeks of age. Loading: VDAC; Skm, skeletal muscle. From Kühl et al. 2014; 2016.

Mice ubiquitously overexpressing *Polrmt* (*Polrmt*$^{+/T}$; +/T) were generated using a bacterial artificial chromosome (BAC) transgenic strategy (Park et al. 2007). This allowed a moderate overexpression of *Polrmt* under the control of its endogenous promoter and surrounding regulatory sequences mimicking physiological expression of endogenous *Polrmt*. A BAC clone containing a fragment of chromosome 10 containing the *Polrmt* gene was modified by introducing a silent point mutation (c420G>T) generating a HindIII site in exon 3 of *Polrmt* (Figure 3.2A and B). The restriction site was used to differentiate the transgene from the endogenous *Polrmt* alleles in the mouse. Germline transmission and expression of the transgene was verified by PCR and subsequent HindIII restriction digest (Figure 3.2C). Quantification of the transgenic allele by pyrosequencing showed that a single copy of the transgene was integrated into the mouse genome (Figure 3.2D), which was consistent with a ~50% increase in *Polrmt* transcript levels (Figure 3.2E) in heart and increased POLRMT protein levels in different mouse tissues (Figure 3.2F).

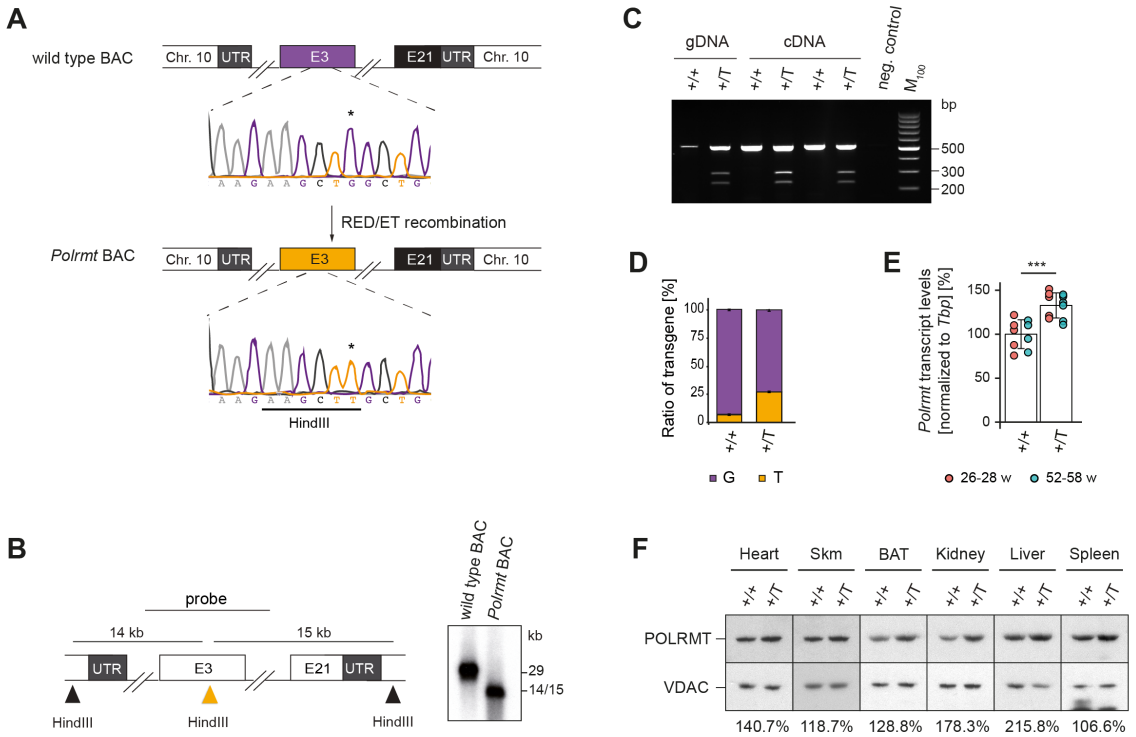

Figure 3.2 | Generation of endogenous *Polrmt* overexpressing mice
(**A**) Scheme of BAC modification strategy. Chr, chromosome; E, exons; asterisk point mutation. The targeted exon is depicted in purple and the modified exon in orange. Sequencing chromatogram is shown. (**B**) Southern blot of BAC construct after HindIII restriction digest. Scheme (left) illustrates location where the probe hybridizes and the size of the fragments. Orange triangle, introduced HindIII site; black triangles, HindIII sites in flanking sequences of *Polrmt* gene. (**C**) PCR and restriction digest analysis of the *Polrmt* BAC transgenic allele in genomic (gDNA) and reverse transcribed DNA (cDNA) from wild-type (+/+) and BAC transgenic *Polrmt* overexpressor (+/T) mice. (**D**) Pyrosequencing analysis of the ratio of wild-type (G) and transgenic (T) alleles in DNA isolated from tail biopsies in +/+ and +/T mice; n: 9 per genotype. (**E**) qRT-PCR analysis of steady-state *Polrmt* transcript levels in +/+ and +/T mouse hearts at different ages. Normalization: tata-binding protein (*Tbp)*; ***p<0.001; ANOVA; n: 5 per genotype and age. (**F**) Western blot of POLRMT levels in +/+ and +/T in mitochondrial extracts from different tissues in 52-week old mice. Loading: VDAC; Skm, skeletal muscle; BAT, brown adipose tissue. Percentage (%) is calculated relative to +/+ levels. Error bars ± sem.

3.1.2. Polrmt only encodes a mitochondrial protein in mammals

We evaluated the expression of the alternative transcripts of *Polrmt* containing intron 1 or intron 2 sequences reported to encode spRNAP-IV (Kravchenko & Chumakov 2005; Kravchenko et al. 2005) in wild-type mice. We performed RT-PCR on cDNA prepared from different mouse tissues but, surprisingly, we did not detect the previously described alternatively spliced *Polrmt* transcripts (Figure 3.1A, 3.3A and B). Next, we performed western blot analyses using an antibody directed against mouse POLRMT. Although we detected a ~140 kDa protein which corresponds to the molecular weight of POLRMT, we did not find a ~110 kDa protein corresponding to the spRNAP-IV in heart, skeletal muscle, kidney, spleen, liver or brain (Figure 3.3C). To further verify that the ~140 kDa protein corresponded to the mitochondrial isoform, we performed subcellular fractionation in wild-type mouse heart and found this protein enriched in the mitochondrial fraction (Figure 3.3D). Finally, we evaluated the steady-state transcript levels of the genes proposed to be transcribed by spRNAP-IV in mouse heart and skeletal muscle of the conditional *Polrmt* knockout. The expression of the sarcoplasmic/endoplasmic reticulum calcium ATPase2 (*Serca2*) was reduced in heart (Figure 3.3E) which is a common finding associated to cardiomyopathy (Arai, Matsui & Periasami 1994). Furthermore, the levels of *mt-16S* rRNA were strongly reduced in skeletal muscle consistent with the loss of mtDNA transcription (Figure 3.3F). However, none of the other nuclear genes reported to be transcribed by spRNAP-IV were reduced in expression.

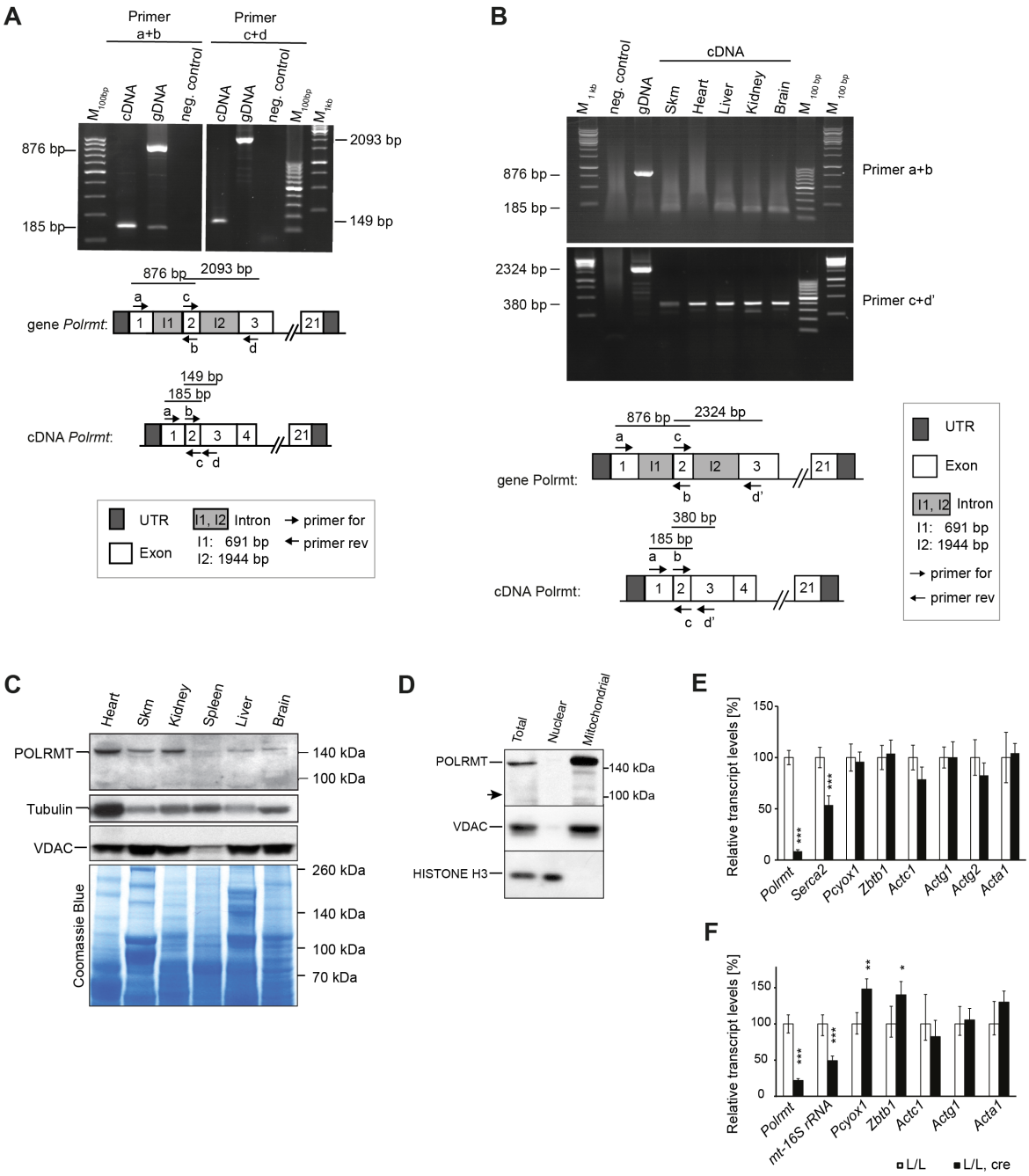

Figure 3.3 | *Polrmt* does not encode a nuclear isoform in mouse
(**A-B**) RT-PCR analysis of *Polrmt* RNA (cDNA) and genomic DNA (gDNA) from control (L/L) mice in heart (**A**) and additional mouse tissues (**B**). Different primer sets were used as indicated. (**C**) Western blot analysis of steady-state POLRMT levels on total protein extracts from different tissues of L/L mice. Loading: VDAC, Tubulin, and Coomassie blue. (**D**) Western blot analysis of subcellular fractions from 4-week old L/L mouse hearts. Loading and purity of fractions: histone H3 and VDAC; arrow indicates ~110 kDa. (**E-F**) qRT-PCR analysis of steady-state transcript levels of nuclear genes in L/L and conditional *Polrmt* knockout (L/L, cre) mouse heart (**E**) and skeletal muscle (**F**). Normalized to beta 2 microglobulin (*B2m*); n: 6 per genotype; *p<0.05, **p<0.01, ***p<0.001; two-tailed Student *t* test. From Kühl et al. 2014.

Since we did not detect spRNAP-IV in the mouse, we proceeded to evaluate whether *POLRMT* codes for spRNAP-IV in human cell lines. First, we verified that the antibody against human POLRMT was specific and recognised both isoforms by silencing *POLRMT* and transiently overexpressing human *POLRMT-EGFP* and *spRNAP-IV-Flag* in human cervix adenocarcinoma HeLa cells followed by western blot analysis (Figure 3.4A and B).

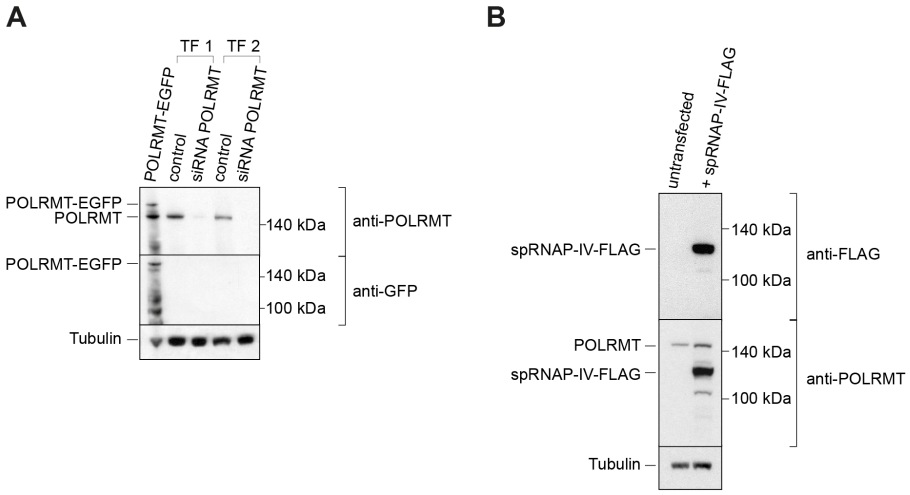

Figure 3.4 | Human POLRMT antibody detects POLRMT and spRNAP-IV in human cells
(**A**) Western blot analysis of total protein extracts isolated from HeLa cells after one (TF1) or two (TF2) transfections with small interfering RNA (siRNA) against human *POLRMT*. The cells were also transfected with a plasmid encoding a POLRMT-EGFP fusion protein. Control, siRNA against GFP. (**B**) Western blot analysis of HeLa cells transfected with a plasmid encoding spRNAP-IV with a Flag tag. Membranes were incubated with antibodies against human POLRMT, GFP, or Flag M2. Loading: tubulin. From Kühl et al. 2014

Next, we performed subcellular fractionation in HeLa cells followed by western blot analysis and only detected a ~140 kDa protein enriched in the mitochondrial fraction consistent with our mouse data (Figure 3.4A). To verify that it was not a cell line specific effect or that the function of POLRMT in mtDNA gene expression masked the expression of spRNAP-IV, we performed the subcellular fractionation in human osteosarcoma 143B cells and 143B cells without mtDNA (143ρ^0) and detected exclusively the ~140 kDa mitochondrial protein (Figure 3.4B). To further corroborate the exclusive mitochondrial localization of the ~140 kDa protein, we performed confocal microscopy using the endogenous POLRMT antibody (Figure 3.4C) and did not find the nuclear spRNAP-IV. As a control, we expressed spRNAP-IV fused to GFP and this construct strongly showed an extra-nuclear localization (Figure 3.4D). Finally, we performed RT-PCR experiments on genomic DNA (gDNA) and cDNA from different human cell lines to identify the alternative spliced *POLRMT* transcript, containing intron 1 sequences using the same primers as the original publication (Kravchenko & Chumakov 2005), but could not verify the existence of the alternative *POLRMT* transcript (Figure 4.3E). Collectively, our data in different human cell lines and mouse tissues conclusively show that *Polrmt* only encodes POLRMT which is exclusively a mitochondrial protein.

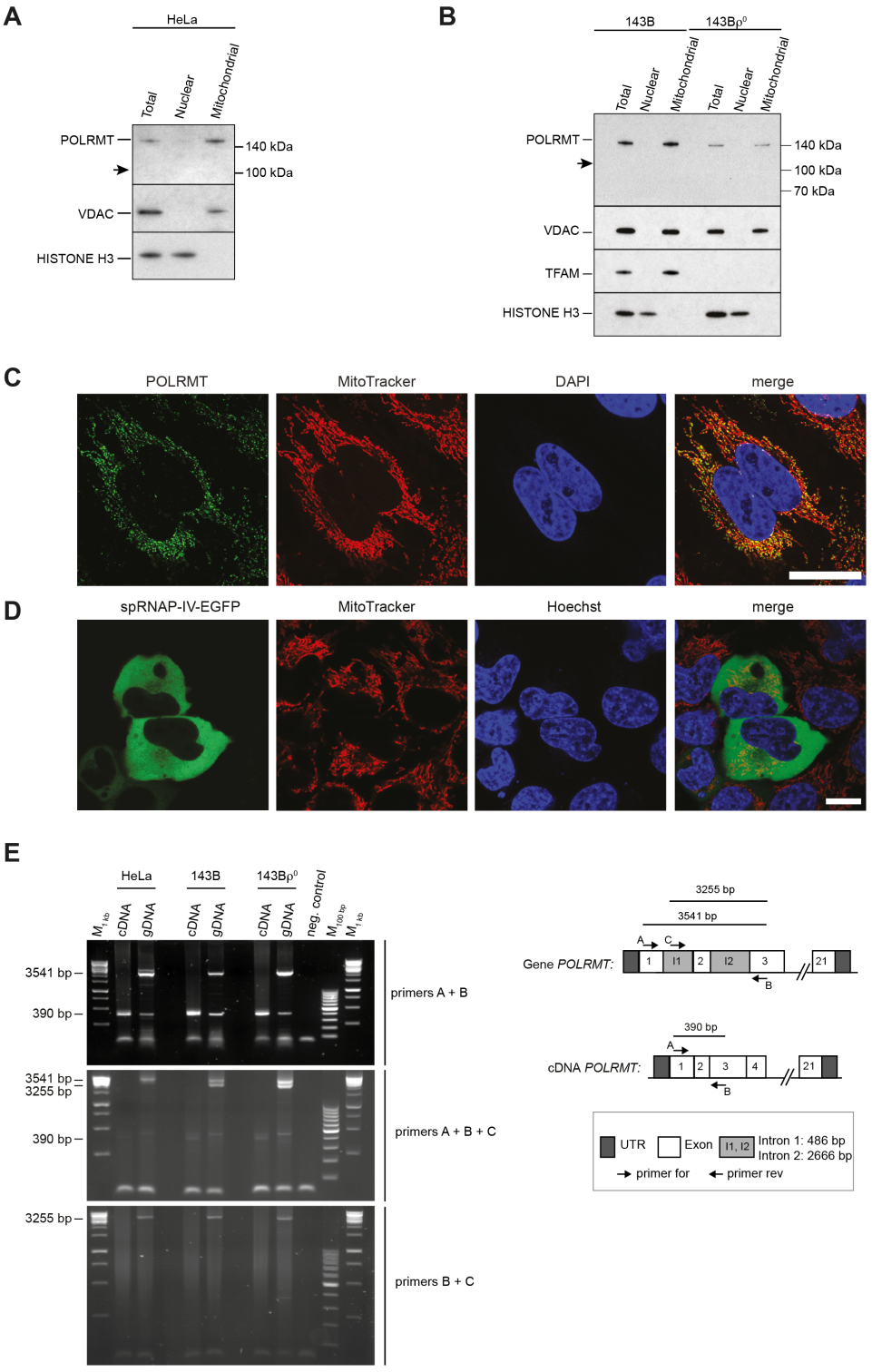

Figure 3.5 | *Polrmt* does not encode a nuclear isoform in human cells
(**A-B**) Western blot analysis of subcellular fractions from HeLa (**A**), 143B and 143Bρ^0 (**B**). Loading and purity of fractions: histone H3 and VDAC; arrow indicates ~110 kDa. (**C**) Immunostaining of endogenous POLRMT in HeLa cells. Scale bar: 25 mm. (**D**) Live-cell imaging of HeLa cells expressing spRNAP-IV fused to EGFP. Scale bar: 10 μm. (**E**) RT-PCR analysis of *Polrmt* RNA (cDNA) and genomic DNA (gDNA) from different human cell lines. Primers are identical to those previously used by (Kravchenko & Chumakov 2005). From Kühl et al. 2014.

3.1.3. Loss of POLRMT in heart causes dilated cardiomyopathy due to severe OXPHOS dysfunction

We proceeded to study the function of POLRMT in mammalian mitochondria. Subsequent intercrosses of *Polrmt*$^{+/-}$ mice did not produce any viable homozygous *Polrmt* knockout mice (*Polrmt*$^{-/-}$) (genotyped offspring, n: 56; *Polrmt*$^{+/-}$: 66%, *Polrmt*$^{+/+}$: 34%, *Polrmt*$^{-/-}$: 0%). We therefore analysed staged embryos at embryonic day (E) 8.5 (n: 47) and found that 23% of the embryos had a mutant appearance and all had the genotype *Polrmt*$^{-/-}$, whereas the normally appearing embryos were either *Polrmt*$^{+/+}$ (28%) or *Polrmt*$^{+/-}$ (49%) (Figure 3.6). Thus, loss of POLRMT leads to embryonic lethality at E8.5.

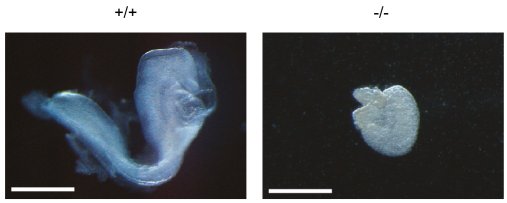

Figure 3.6 | Loss of POLRMT is embryonic lethal
Morphology of +/+ and homozygous *Polrmt* knockout (-/-) embryos at E8.5. Scale bar: 0.5 mm.

The heart and skeletal muscle conditional knockout mice died before 6 weeks of age (Figure 3.7A) and showed a progressive enlargement of the heart with dilation of the left ventricular chamber and no apparent increase in the left ventricular wall thickness (Figure 3.7B). The development of dilated cardiomyopathy was further confirmed by a progressive increase in the heart to body weight ratio during the first weeks of postnatal life (Figure 3.7C).

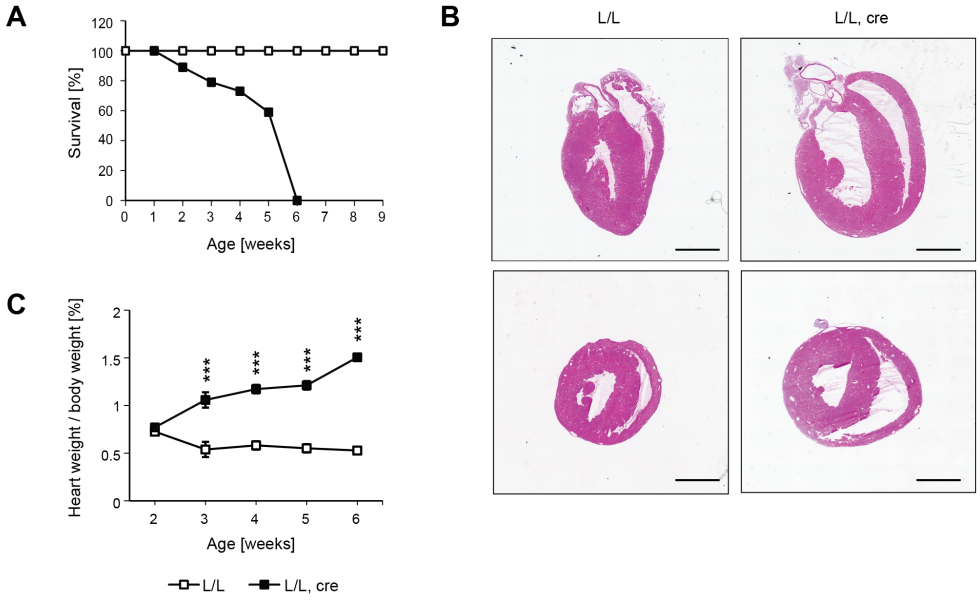

Figure 3.7 | Loss of POLRMT in the heart causes dilated cardiomyopathy
(A) Survival curve of control (L/L; n: 60) and tissue-specific knockout (L/L, cre; n: 37) mice. (**B**) Histological analysis of cardiac phenotype: vertical (upper panels) and transverse (lower panels) sections through the midportion of hearts of L/L and L/L, cre mouse hearts at 4 weeks of age. Scale bars: 2 mm. (**C**) Heart to body weight ratio of L/L (n: 62) and L/L, cre (n: 57) at different time points. Error bars ± sem; ***p<0.001; two-tailed Student's *t*-test. From Kühl et al. 2016.

Transmission electron microscopy of terminal-stage heart tissue revealed a profound disruption in the cardiac tissue ultrastructure where mitochondria had an abnormal appearance with disorganized cristae (Figure 3.8A) suggesting a severe mitochondrial defect. Analysis of OXPHOS capacity in *Polrmt* knockout hearts confirmed that the enzyme activities of complexes I, IV and V were decreased, whereas the activity of the exclusively nucleus-encoded complex II was normal (Figure 3.8B). Moreover, blue native polyacrylamide gel electrophoresis analysis (BN-PAGE) showed reduced levels assembled complexes I, IV, and V (Figure 3.8C). The observed pattern of deficient OXPHOS sparing complex II is typically caused by impaired mtDNA gene expression (Cámara et al. 2011; Milenkovic et al. 2013; Ruzzenente et al. 2012).

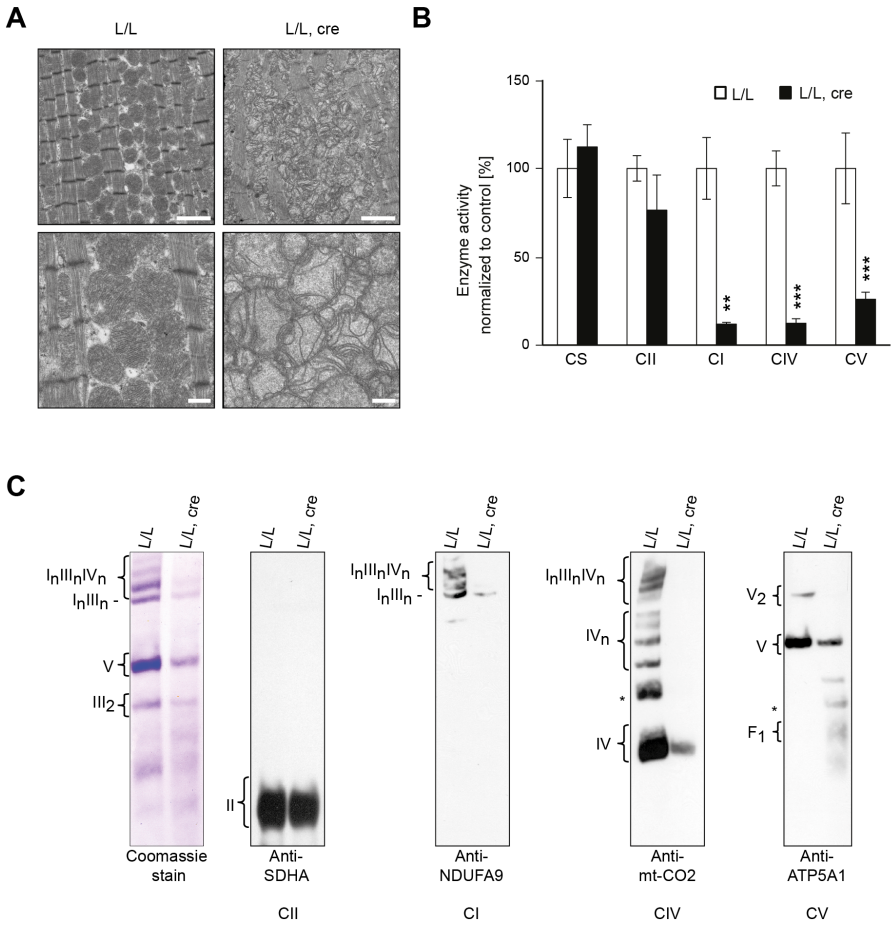

Figure 3.8 | Reduced OXPHOS capacity in *Polrmt* knockout mouse heart
(**A**) Transmission electron micrographs of myocardium of 5-week old control (L/L) and tissue-specific knockout mice (L/L, cre). Scale bar upper panel: 2 μm, lower panel: 0.5 μm; n: 2 per genotype. (**B**) Relative enzyme activities of respiratory chain enzymes measured in heart mitochondrial extracts from L/L and L/L, cre mice at different ages. Citrate synthase was used as an internal control for normalization of the samples. The enzymes measured are: CS, citrate synthase; Complex II (CII), succinate dehydrogenase; Complex I (CI), NADH ubiquinone oxidoreductase; Complex IV (CIV), Cytochrome c oxidase; Complex V (CV), ATPase oligomycin sensitive. **p <0.01, ***p <0.001; two-tailed Student's *t*-test; n: 4 per genotype; error bars ± sem; (**C**) BN-PAGE analyses of isolated mitochondria from 5-week old L/L and L/L, cre hearts. OXPHOS complexes were detected with subunit-specific antibodies or Coomassie Brilliant Blue staining. NDUFA9, CI; SDHA, CII, mt-CO2, CIV, ATP5A, CV. From Kühl et al. 2016.

3.1.4. Moderate alterations in POLRMT do not affect OXPHOS capacity

Contrary to the complete loss of POLRMT, moderate changes on POLRMT levels did not cause any apparent phenotype. Heterozygous *Polrmt* knockout and *Polrmt* overexpressor mice were viable, fertile, and healthy after 1 year of age. *Polrmt* overexpressors had normal body weight until 20 weeks of age, and normal heart to body weight ratios at 13, 26, and 52 weeks (Figure 3.9A-C). We next proceeded to evaluate whether moderately increased levels of POLRMT had an effect OXPHOS capacity. Western blot analyses of respiratory chain subunits showed normal levels of NDUFB8 (complex I), SDHB (complex II), UQCRC2 (complex III), mt-CO1 (Complex IV) and ATP5A1 (complex V) in the *Polrmt* overexpressor mice (Figure 3.9D). Furthermore, there were no differences in the activity of the respiratory chain complexes (Figure 3.9E) and respiration capacity in heart (Figure 3.9F) or liver (data not shown). Taken together, our data show that moderate alterations in POLRMT levels do not affect mitochondrial OXPHOS capacity.

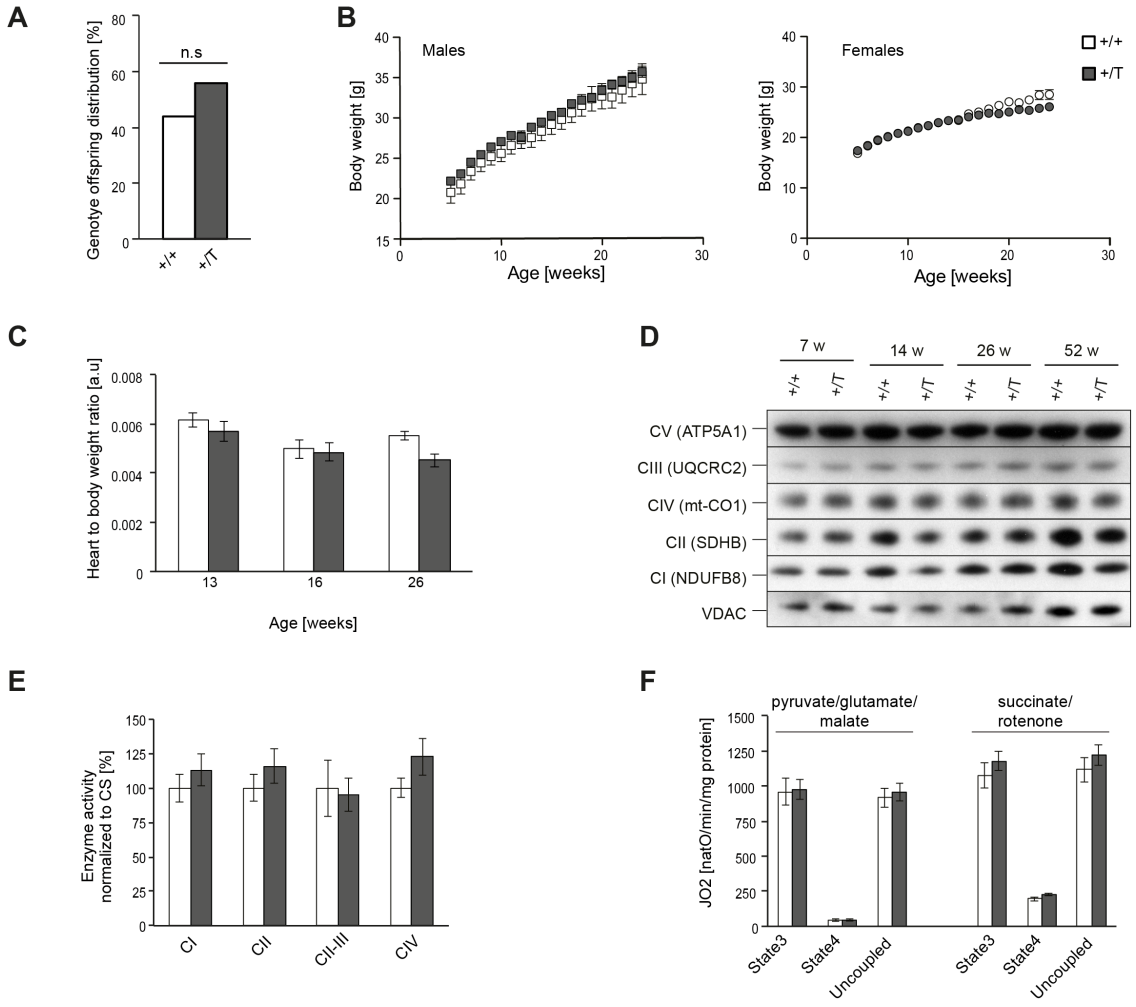

Figure 3.9 | *Polrmt* overexpressor mice does not have any detectable effect on OXPHOS capacity
(**A**) Histogram of genotype distribution of the wild-type (+/+) and *Polrmt* overexpressor (+/T) offspring; n.s: p>0.05; chi-square test. (**B**) Body weight curve of male (left) and female mice (right); n: 8-16 per sex and genotype (**C**) Heart to body weight ratio at different ages; n: 3-5 per age and genotype (**D**) Western blot of OXPHOS subunits levels in isolated mitochondria from heart at different ages; loading: SDHB (complex II; CII) and VDAC. (**E**) Relative enzyme activities of respiratory chain enzymes measured in mitochondria isolated from heart at 13 weeks of age. The

enzymes measured are: citrate synthase (CS); Complex I (CI): NADH ubiquinone oxidoreductase, Complex II (CII): succinate dehydrogenase, Complex II-III: Succinate dehydrogenase - cytochrome c reductase, Complex IV (CIV): Cytochrome c oxidase. CS was used as an internal control for normalization of the samples; n: 3 per genotype. (**F**) Oxygen consumption analysis on isolated mitochondria. Mitochondria were incubated with pyruvate, glutamate, and malate to deliver electrons to CI or with succinate and rotenone to deliver electrons to CII. Permeabilized cell respiration was analyzed in the phosphorylating (state3), non-phosphorylating (state4), and uncoupled states. n: 3 per genotype. Error bars ± sem.

3.1.5. LSP-initiated transcription is favoured at low POLRMT levels

Consistent with the function of POLRMT as the mitochondrial RNA polymerase, loss of POLRMT lead to a profound decrease in *de novo* transcription of mtDNA in the conditional *Polrmt* knockout heart (Figure 3.10A). Furthermore, northern blot and RNA sequencing analyses (RNA-Seq) showed a general reduction in the steady-state levels of all mt-mRNAs, mt-rRNAs and mt-tRNAs (Figure 3.10B-D). Thus, no other protein can compensate for the loss of POLRMT in mammalian mitochondria. Notably, we observed that the steady-state levels of most of the mitochondrial transcripts encoded on the L strand, *i.e*. *mt-Nd6, mt-Tp, mt-Te, mt-Ts2, mt-Tc, mt-Tn,* and *mt-Tq,* were less reduced than transcripts encoded on the H strand, *i.e*. *mt-12S* rRNA, *mt-16S* rRNA, *mt-Nd1, mt-Co1, mt-Co2, mt-Co3, mt-Nd5, mt-Cytb, mt-Tf, mt-Tl1, mt-Tm, mt-Tk, mt-Tl2* and *mt-Tt* (Figure 3.10B-D). To determine whether the difference in mitochondrial steady-state transcript levels was due to promoter-specific transcription initiation effects due to low POLRMT levels, we performed *in vitro* transcription assays (Figure 3.10E and F). We detected a strong reduction of the transcription initiation from an HSP containing construct in comparison to the LSP at POLRMT concentrations below 32 nM (Figure 3.10E and F), indicating that transcription initiation at the LSP is stronger at low POLRMT levels.

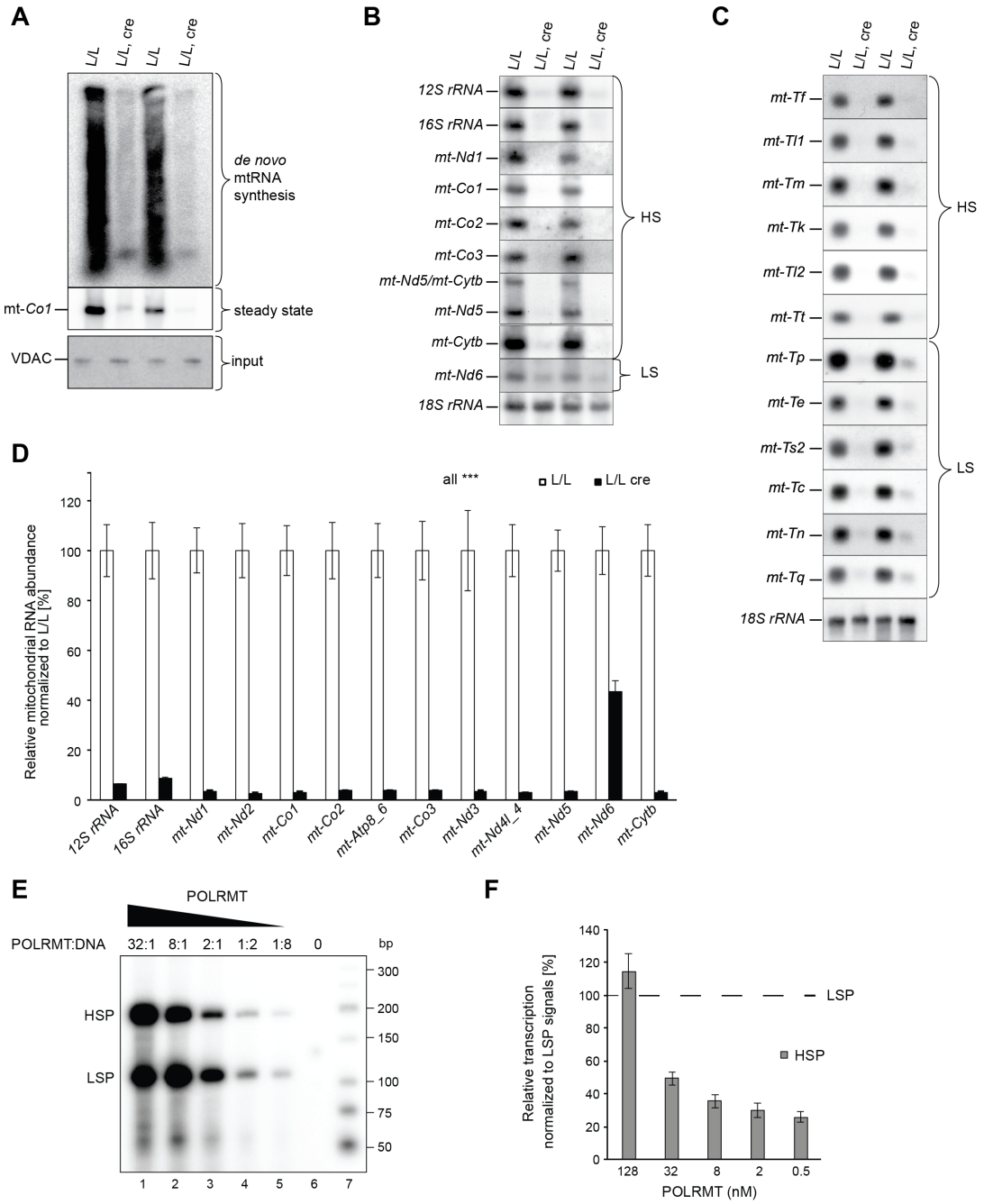

Figure 3.10 | LSP and HSP show different sensitivities at low POLRMT concentrations
(**A**) *De novo* synthesized mitochondrial transcripts from hearts of 4-week old control (L/L) and conditional knockout (L/L, cre) mice. Steady-state levels of individual mitochondrial transcripts were verified with a radiolabelled probe (*mt-Co1*); input: western blot analysis of VDAC on radiolabelled mitochondria. (**B-C**) Northern blot analyses of mt-mRNAs, mt-rRNAs and mt-tRNAs from hearts of 4-week old L/L and L/L, cre mice; loading: *18S* rRNA. (**D**) RNA-Seq of mt-mRNA and mt-rRNA levels in hearts of 4-week old L/L, cre and L/L mice normalized to the upper quartile of the gene count distribution. All mt-RNAs have p≤ 0.0001; n: 3 mice per genotype; error bars: ± sem. (**E**) *In vitro* transcription assay at different POLRMT levels. All reactions contained a cut plasmid template containing the human LSP and HSP promoters giving a run-off product of 101 nt and 180 nt, respectively. POLRMT was added at 128, 32, 8, 2, 0.5 nM in lanes 1-5 respectively; lane 6: control without POLRMT; lane 7: molecular weight marker (New England Biolabs). (**F**) Quantification of the results from D. HSP transcription levels were normalized to LSP for each POLRMT concentration; n: 3 independent experiments; error bars: ± sd; from Kühl et al. 2014, 2016.

3.1.6. POLRMT is essential for mammalian mtDNA replication

Since *in vitro* studies have suggested that transcription initiation from the LSP also forms the primers required to initiate mtDNA replication (Gillum & Clayton 1979), we evaluated the effect of loss of POLRMT in mtDNA replication. *7S* RNA is the most promoter-proximal transcript formed by transcription initiation at the LSP of mtDNA (Gillum & Clayton 1979) and we found this transcript strongly reduced in *Polrmt* knockout hearts (Figure 3.11A). To further investigate this *in vivo,* we evaluated the steady-state levels of 7S DNA and found them also severely reduced pointing to a defect in mtDNA replication (Figure 3.11B). In line with this, there was a strong depletion of mtDNA in the *Polrmt* knockout hearts (Figure 3.11C and D). Next, we performed *in organello* mtDNA replication experiments to determine whether the reduced levels of 7S DNA and mtDNA molecules were due to decreased formation or increased degradation. We found 7S DNA and mtDNA *de novo* synthesis severely reduced (Figure 3.11E) suggesting a defect in initiation of mtDNA replication. Collectively, our data demonstrate that POLRMT is required for mtDNA replication *in vivo*.

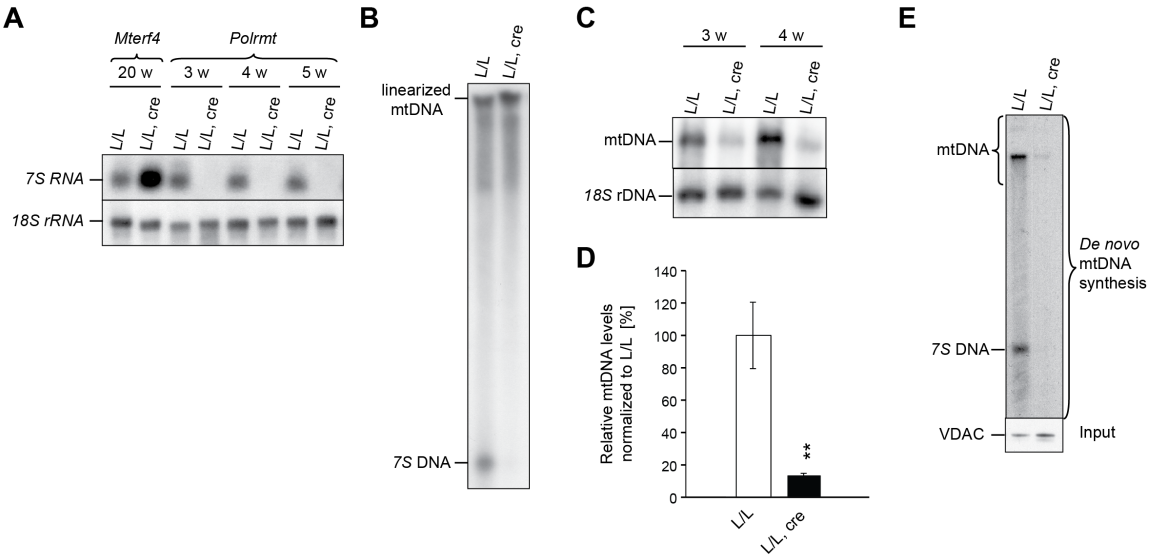

Figure 3.11: Decreased mtDNA replication in *Polrmt* knockout mice
(**A**) Northern blot of *7S* RNA levels of total RNA from control (L/L) and tissue-specific knockout (L/L, cre) hearts at different ages; loading: *18S* rRNA. RNA from hearts of *Mterf4* conditional knockout mice (Cámara et al. 2011) with increased *7S* RNA levels were loaded as controls. (**B**) Southern blot analysis on mtDNA to assess *7S* DNA levels of 4-week old L/L and L/L, cre mice. To allow relative comparison, the loaded amount of mtDNA from knockouts was higher than the amount loaded from control samples. (**C**) Southern blot analyses on total DNA to assess mtDNA levels of L/L and L/L, cre mice at different ages; loading: *18S* rDNA. (**D**) Quantification of Southern blots. mtDNA levels were normalized to *18S* rDNA and presented as the percentage of L/L. Error bars: ± sem; **p <0.01; two-tailed Student's *t*-test. (**E**) *De novo* synthesized mtDNA of isolated heart mitochondria of 4-week old L/L and L/L, cre mice; input: western blot analysis of VDAC after labelling. From Kühl et al. 2016.

3.1.7. Heterozygous Polrmt knockout mice show increased TEFM levels and maintain mitochondrial transcription

To assess the effect of moderate reduction of POLRMT in mtDNA replication and transcription we characterized the heterozygous *Polrmt* knockout mice. There was no significant effect on the steady-state levels of mt-mRNAs, mt-rRNAs and mt-tRNAs in the heterozygous *Polrmt* knockout mice (Figure 3.12A). Consistent with the normal mt-mRNA levels, the steady-state levels of LRPPRC, known to bind and stabilize mt-mRNAs (Ruzzenente et al. 2012), were not changed (Figure 3.12B). RNA-Seq analysis showed that the *mt-Nd6* transcript encoded on the L strand was slightly reduced, whereas all other mt-rRNAs and mt-mRNAs encoded on the H strand showed a tendency to be increased in heterozygous *Polrmt* knockout hearts at 26 weeks of age, however not significant (Figure 3.12C). Interestingly, we observed a strong increase in TEFM protein levels (Figure 3.12B), which may provide a compensatory response to the decreased levels of POLRMT by promoting productive full-length transcription heterozygous *Polrmt* knockout mice. This hypothesis was supported by the slight increase in *de novo* transcription in heart mitochondria (Figure 3.12D). The other components of the basal transcription machinery, TFAM and TFB2M, remained unchanged (Figure 3.12B). Furthermore, the levels of *7S* RNA and mtDNA were normal (Figure 3.12E and F), thus showing that promoter proximal transcription at LSP is sufficient to maintain mtDNA replication and gene expression. Finally, *de novo* formation of 7*S* DNA was not decreased when POLRMT was reduced (Figure 3.12G). Consistent with normal mtDNA levels and replication, TFAM, TWINKLE, POLγA, and SSBP1 protein levels remained unchanged. Thus, a moderate reduction of POLRMT expression does not affect overall mtDNA replication or transcription.

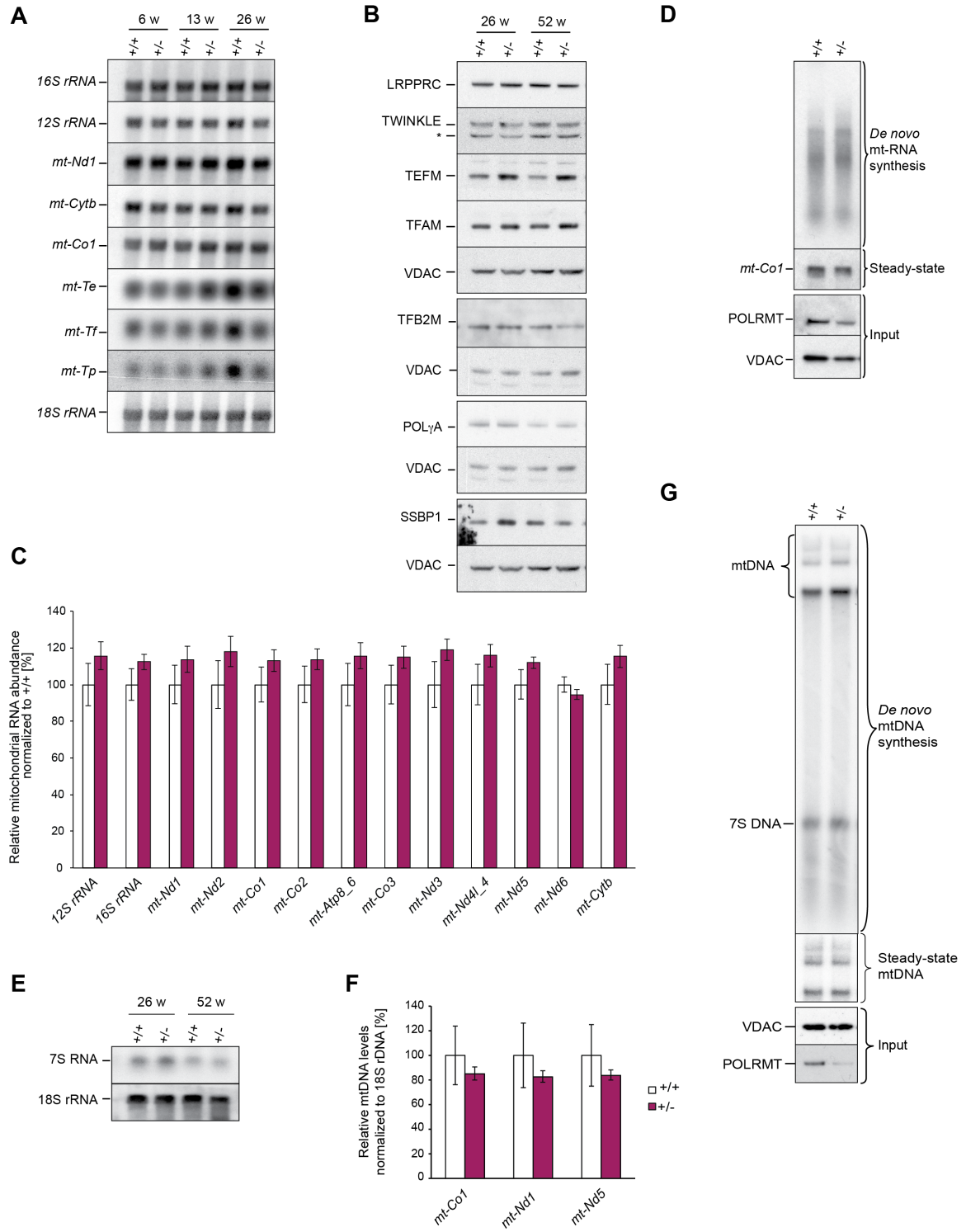

Figure 3.12 | Characterization of heterozygous *Polrmt* knockout mice
(**A**) Northern blot of analysis of mt-mRNAs, mt-rRNAs and mt-tRNAs in wild-type (+/+) and heterozygous knockout (+/-) mice; loading control: *18S* rRNA. (**B**) RNA-Seq on mitochondrial mt-mRNAs and mt-rRNA in heart of 26-week old +/+ and +/- mice; normalized to upper quartile of the gene count distribution; n: 3 per genotype. (**C**) Western blot of levels of nDNA factors of mtDNA gene expression analysed on heart mitochondrial extracts of +/+ and +/- mice; loading: VDAC; asterisk: cross-reacting band. (**D**) *De novo* synthesized mitochondrial transcripts from heart of 52-week old mice in +/+ and +/- mice. Steady-state levels of individual mitochondrial transcripts were verified with a radiolabelled probe (*mt-Co1*); input: western blot analysis of POLRMT and VDAC after labelling. (**D**) Northern blot of *7S* RNA levels in mouse hearts of +/+ and +/- mice; loading: *18S* rRNA. (**E**) qPCR determination of mtDNA levels in +/+ /- mice with *mt-Co1*, *mt-Nd1* and *mt-Nd5* probes on mouse heart. Normalization: *18S* rDNA; n: 3 per genotype. (**F**) *De novo* synthesized mtDNA of isolated mitochondria from hearts of 12-week old +/+ and +/- mice. Radioactively labelled mtDNA was boiled to release newly synthesized *7S* DNA prior Southern blotting; input: western blotting of POLRMT and VDAC after labelling. Error bars ± sem. From Kühl et al. 2016.

3.1.8. POLRMT is a limiting factor for transcription initiation in vivo

We then studied the effect of *Polrmt* overexpression on mtDNA replication and transcription in mouse heart. *7S* RNA levels were significantly increased in different tissues of the *Polrmt* overexpressor mice (Figure 3.13A) and the levels were maintained at different ages (Figure 3.13B and C). To evaluate whether this increased transcription initiation from LSP affected mtDNA replication, we performed Southern blot analysis and found a mild but significant increase in mtDNA levels (~17%) in *Polrmt* overexpressor mouse hearts (Figure 3.13D and E). In line with this, *de novo* mtDNA synthesis had the tendency to be increased (Figure 3.13F and G), suggesting that increased POLRMT levels might have a minor effect on mtDNA replication.

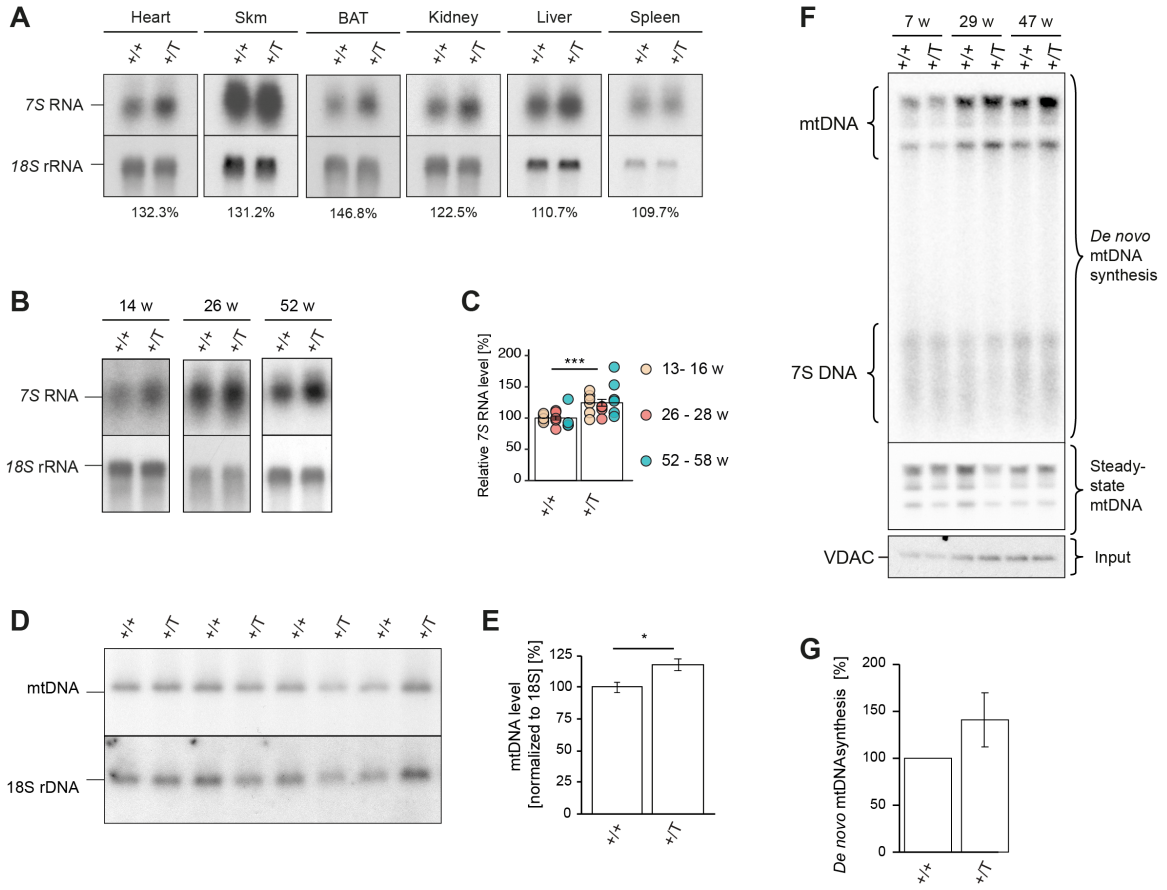

Figure 3.13 | Increased 7S RNA levels in *Polrmt* overexpressor mice
(**A**) Northern blot analysis of *7S* RNA levels in different tissues of a wild-type (+/+) and overexpressor (+/T) 52-week old mice. (**B**) Northern blot analyses of *7S* RNA levels in heart and at different ages. (**C**) Quantification of *7S* RNA levels at different ages. Normalization *18S* rRNA. ***p<0.001; ANOVA; n: 3-6 per age and genotype. (**D-E**) Southern blot analysis and quantification of mtDNA levels in heart of 14-week old mice. Normalization *18S* rDNA. *p<0.05; two-tailed Student's *t*-test; n: 4 per genotype. (**F-G**) *In organello* replication on isolated mitochondria from heart at different ages (**F**) and quantification (**G**). Input: Western blot of VDAC and steady-state mtDNA levels. Normalization: steady-state mtDNA levels; n: 5 per genotype. Error bars ± sem.

Consistent with the increased *7S* RNA steady-state levels, we found a strong increase in *de novo* transcript synthesis in isolated mitochondria from heart of *Polrmt* overexpressor mice (Figure 3.14A and B). There was no accumulation of specific transcription products indicating that the increase in *de novo* transcription is homogeneous and that there is normal

processing of the polycistronic mt-RNAs. Despite the strong increase in *de novo* transcript synthesis, steady-state levels of mt-RNAs were not changed except for the precursor *mt-Nd5/*mt-*Cytb, mt-Cytb,* and *mt-Tf* that were mildly increased (Figure 3.24C-E).

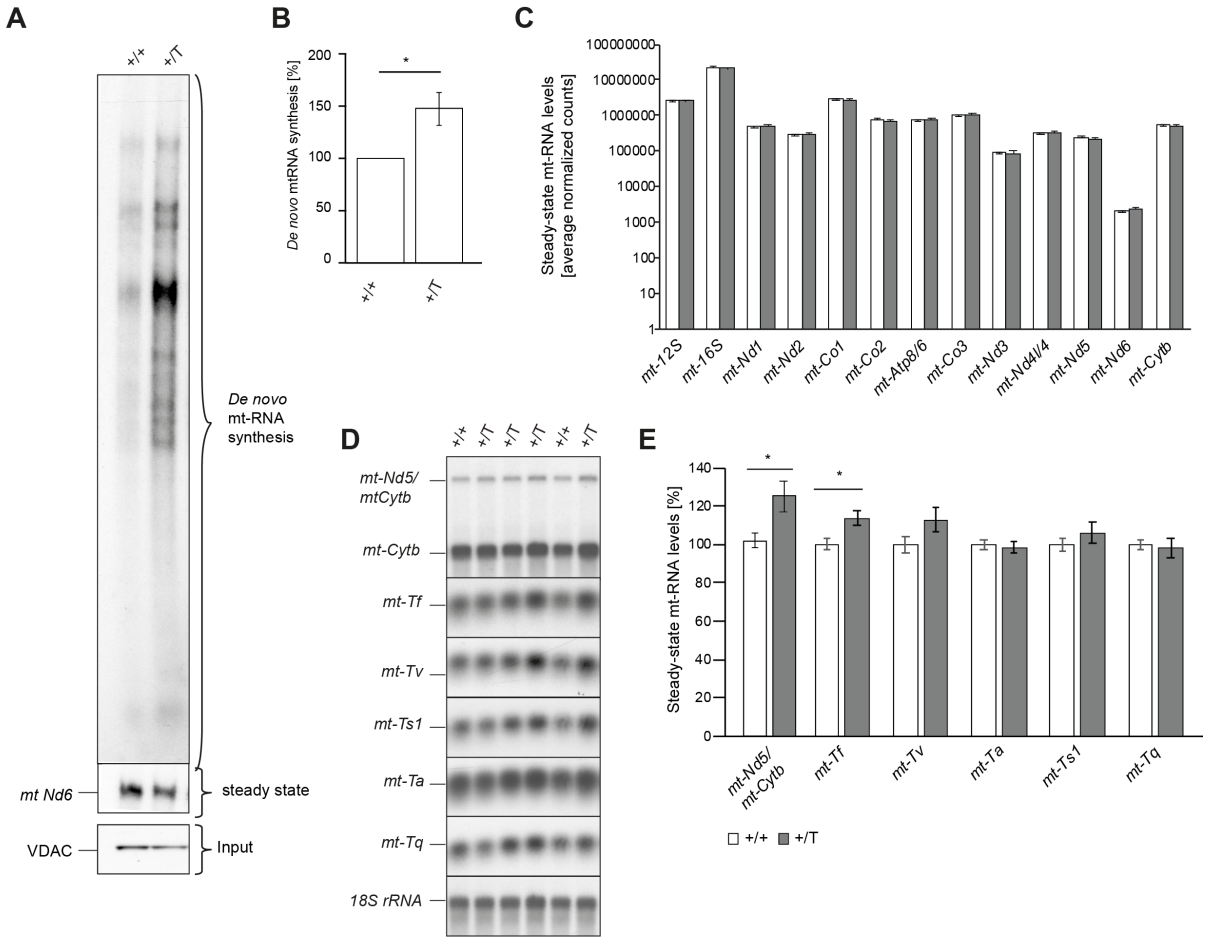

Figure 3.14 | Increased *de novo* transcription in *Polrmt* overexpressor mice
(A) De novo synthesized mitochondrial transcripts from hearts of 14-week old wild-type (+/+) and overexpressor (+/T) mice. Steady-state levels of individual mitochondrial transcripts were verified with a radiolabelled probe (*mt-Nd6*); input: western blot analysis VDAC on radiolabeled mitochondrial extracts. (**B**) Quantification of *de novo* synthesized mitochondrial transcripts of mice at different ages (14 and 26 weeks of age) normalized to VDAC and +/+. *p<0.05; one-sample Student's *t*-test; μ: 100; n: 10 per genotype. (**C**) RNA-Seq of mt-rRNAs and mt-mRNAs on total RNA from heart of 14-week old mice. n: 3 per genotype (**D**) Northern blot analyses of mt-RNA levels in heart of 14-week old mice. (**E**) Quantification of mt-RNA levels; normalization *18S* rRNA; *p<0.05; two-sample Student *t*-test; n: 6 per age and genotype. Error bars ± sem.

Next, we evaluated the protein levels of factors required for mtDNA maintenance (TFAM), replication (TWINKLE, SSBP1, POLRMT), transcription (POLRMT, TFAM, TEFM, TFB2M), RNA processing and stability (GRSF1, ELAC2, LRPPRC, and SLIRP), and translation (MRPL12, MRPL37, and MRPS35) (Figure 3.15A) and found no differences except for POLRMT. To identify if other factors involved in mitochondrial RNA metabolism vary in the *Polrmt* overexpressor mice, we performed a label-free proteomic analysis on purified mitochondria isolated from heart, skeletal muscle, and liver. We did not detect any mitochondrial protein involved in mt-RNA metabolism to be upregulated in any of the tissues; in fact, the majority of significantly changed proteins were downregulated (Figure 3.15B). We

did not identify common proteins with differences in expression in the three tissues except for an isoform of glutaminase (GLS) that was downregulated in heart and liver. In heart, the ATP-dependent RNA helicase SUPV3L1 and TFB1M were ~20 and ~50% decreased, respectively (Figure 3.29B). Interestingly, in the skeletal muscle, the *12S* rRNA chaperone Era G-protein like 1 (ERAL1) was also 50% decreased in the *Polrmt* overexpressor mice (Figure 3.28B). Other proteins involved in mtDNA gene expression such as MRPL22, MRPL57, MRPL12, were changed in heart, and FASTKD2 in skeletal muscle, and MRPS12 in liver. These potential changes still have to be validated by western blot. Since additional factors required for mitochondrial transcription, *i.e.* TFAM, TEFM, and TFB2M, were not changed in *Polrmt* overexpressor mice (Figure 3.15A), our data argues that POLRMT is limiting mitochondrial transcription and, potentially, mtDNA replication. However, the system is very robust and maintains steady-state transcripts at wild-type levels.

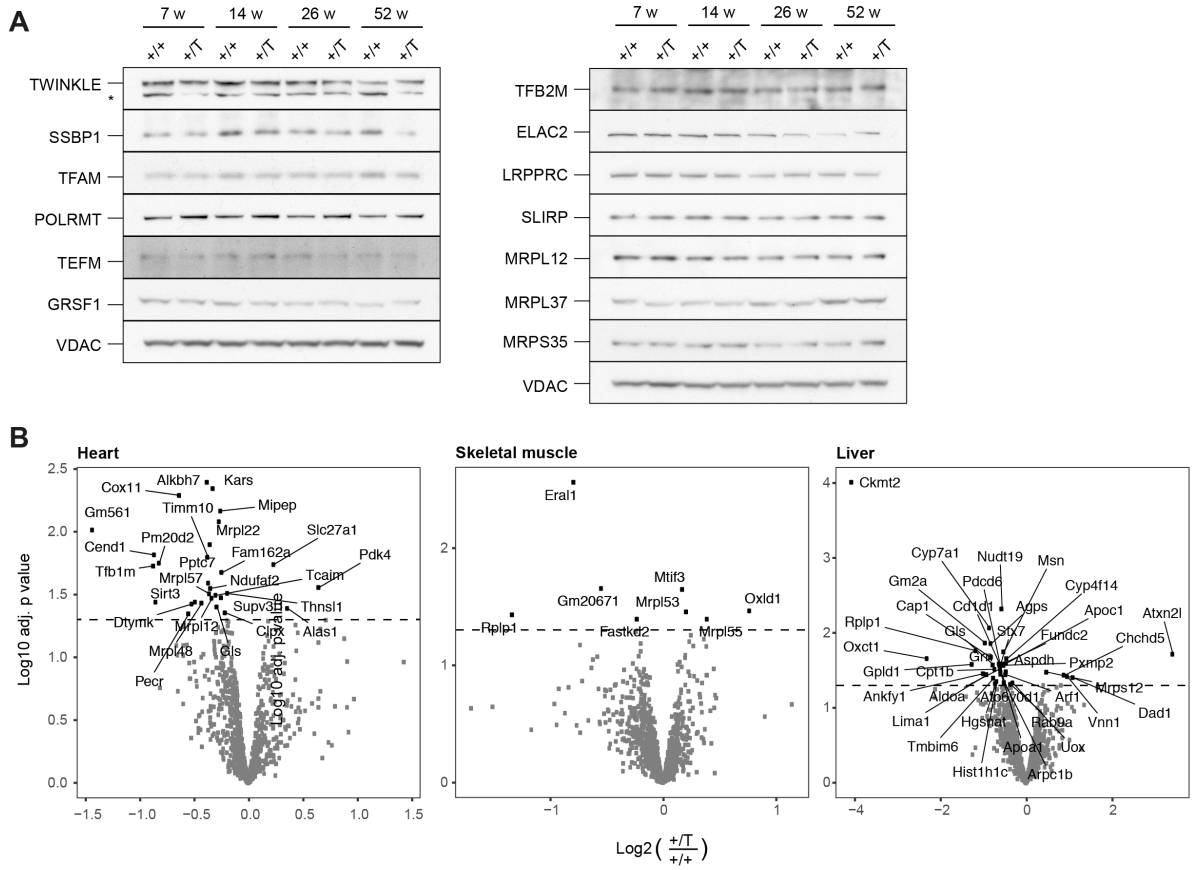

Figure 3.15 | Mitoproteome of *Polrmt* overexpressor mice in different tissues
(**A**) Western blot of factors required for mtDNA gene expression in control (+/+) and *Polrmt* overexpressor (+/T) mice. Loading: VDAC. (**B**) Volcano plots of mitoproteomic analyses of heart, skeletal muscle, and liver in 52-week old mice; adj. p value: Benjamini-Hochberg adjusted p value; n: 5 per genotype; grey dots: p>0.05; black dots: p<0.05; dotted line, p=0.05.

3.1.9. Polrmt overexpression increases transcription capacity

We hypothesized that discrepancy between *de novo* transcription and steady-state transcript levels in the *Polrmt* overexpressor mice was explained by lack of stability due to limiting RNA

binding proteins stabilizing the newly synthesized transcripts. To test this hypothesis, we performed pulse-chase *in organello* transcription labelling experiments but did not find differences in RNA stability between wild-type and *Polrmt* overexpressor mice after 2 h chase (Figure 3.16A and B). Furthermore, we crossed the *Polrmt* overexpressor mice to mice overexpressing *Lrpprc* (Figure 3.16C) (Ruzzenente et al. 2012) to increase the stability of *de novo* synthesized transcripts *in vivo*. Importantly, overexpression of *Lrpprc* alone does not affect *de novo* transcript synthesis or mature steady-state mt-RNAs (Harmel et al. 2013). However, the steady-state transcript levels remained at wild-type levels even when POLRMT and LRPPRC are moderately increased (Figure 3.16D).

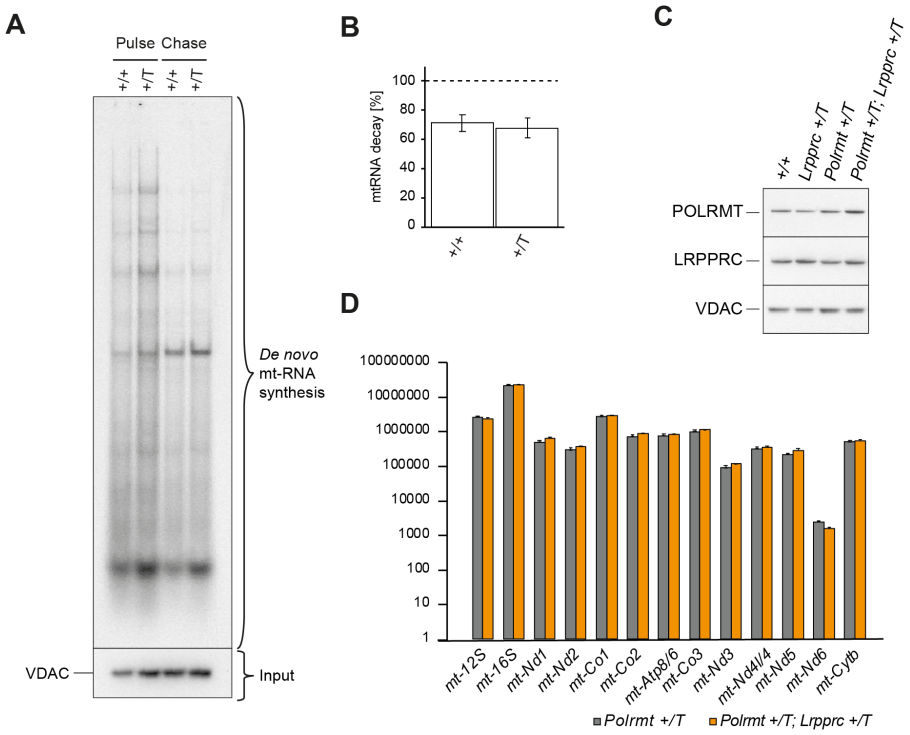

Figure 3.16 | Stability of mt-RNAs is not affected in *Polrmt* overexpressor mice
(**A**) *De novo* synthesized mitochondrial transcripts from hearts of 26-week old wild-type (+/+) and overexpressor (+/T) mice (pulse). The mRNA decay of *de novo* synthesized transcripts was followed after 2h (chase). Input: western blot analysis VDAC on radiolabelled mitochondrial extracts. (**B**) Quantification of *de novo* synthesized mitochondrial transcripts normalized to VDAC and pulse signal; n: 4 per genotype. (**C**) Western blot of steady-state POLRMT and LRPPRC level in mitochondrial extracts from heart. Loading: VDAC. (**D**) RNA-Seq of mt-rRNAs and mt-mRNAs on total RNA from heart of 14-week old *Polrmt* overexpressor or *Polrmt* and *Lrpprc* overexpressor mice. n: 3 per genotype (**D**) Northern blot analyses of mt-RNA levels in heart of 14-week old mice. (**E**) Quantification of mt-RNA levels; normalization *18S* rRNA; n: 6 per age and genotype. *p<0.05; two-sample Student *t*-test; Error bars ± sem.

Interestingly, increased POLRMT levels have been reported as a compensatory response to loss of mtDNA replication in the heart of *Twinkle* conditional knockout mice (Milenkovic et al. 2013). We verified the protein levels of POLRMT in different knockout mouse strains with impaired mtDNA gene expression and found it increased in all the models (Figure 3.17A). However, *Polrmt* transcript levels were slightly decreased or not significantly changed (Figure 3.17B). These data indicate that the increase in POLRMT is not a compensatory response mediated at the transcriptional level and rather suggest that POLRMT is either more

translated or stabilized post-transcriptionally in mtDNA gene expression deficient mice. Thus, our data suggest that increasing POLRMT increases the transcription capacity but under normal physiological conditions this increase is not used further and results in the accumulation of prematurely terminated transcription products. However, under pathological conditions it might be a mechanism to rapidly increase mtDNA gene expression as a compensatory response.

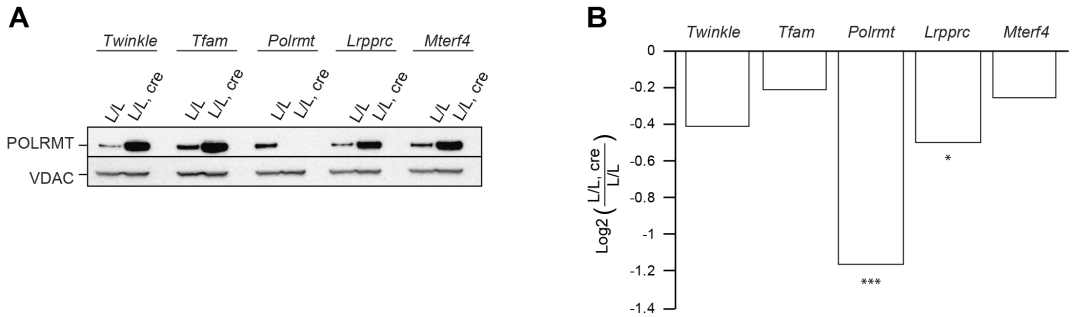

Figure 3.17 | POLRMT is increased in mouse models deficient in mtDNA gene expression
(**A**) Western blot of POLRMT levels in mitochondrial extracts from heart from control (L/L) and knockout (L/L, cre) mice. Loading: VDAC. (**B**) RNA-Seq transcript levels of *Polrmt* from L/L, cre compared to L/L mice. *p<0.05, ***p<0.001. Modified from Kühl, Miranda et al. 2017

3.1.10. Secondary changes in levels of proteins involved in mtDNA gene expression upon loss of POLRMT

To study additional molecular changes associated with loss of mtDNA replication and transcription in the *Polrmt* knockout mouse, we assessed the expression of known nuclear-encoded mitochondrial proteins involved in mtDNA gene expression. Despite the strong reduction in mtDNA replication, the protein levels of TFAM, SSBP1 and POLγA remained unchanged whereas the TWINKLE helicase was strongly upregulated (Figure 3.18A). Transcript levels of *Tfam* were increased by ~50% in *Polrmt* knockout mice suggesting an increase in TFAM synthesis (Figure 3.18B). To determine whether TFAM was stabilized by binding to the remaining mtDNA in the nucleoid, we performed linear density glycerol gradients. Nucleoid-containing fractions were determined by the presence of mtDNA, which was verified by Southern blot and the presence of mtDNA replication factors like TWINKLE and POLγA (Figure 3.18C). Surprisingly, in mitochondria isolated from *Polrmt* knockout hearts there was a clear increase of TFAM in the mtDNA-free fractions (Figure 3.18D and E) that is thus not degraded by LONP1 despite the increased steady-state levels of LONP1 (Figure 3.18A). The other two transcription factors in mitochondria, TFB2M and TEFM, show opposite patters. Steady-state protein levels of TFB2M are drastically reduced the absence of POLRMT suggesting that POLRMT is required for its stability, whereas TEFM is stable or slightly increased in *Polrmt* knockout hearts.

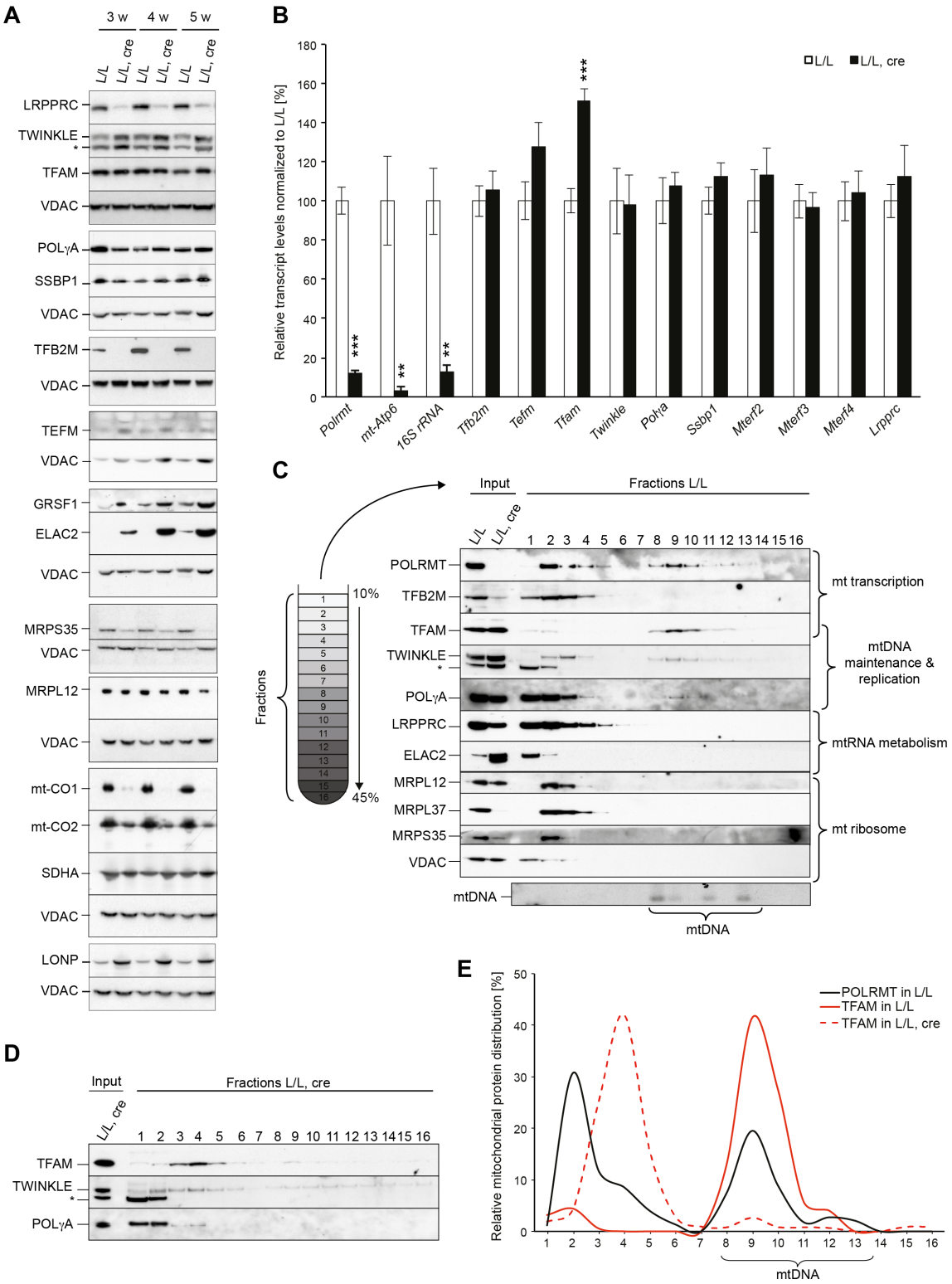

Figure 3.18 | mtDNA-free pool of TFAM increases in *Polrmt* knockout hearts
(**A**) Western blot analysis of steady-state protein levels of nDNA factors required for mtDNA gene expression on mitochondrial extracts from hearts of control (L/L) and tissue-specific knockout (L/L, cre) mice at different ages; loading: VDAC; asterisk: cross-reacting band. (**B**) qRT-PCR of transcript levels of nDNA mitochondrial proteins in L/L and L/L, cre mouse hearts. Normalization: beta 2 microglobulin (*B2m*). *p<0.05, **p<0.005, ***p<0.001; Student's *t*-test; n: 5-21 per genotype; error bars: ± sem. (**C-D**) Linear glycerol density gradient fractionations of mitochondrial lysates from L/L and L/L, cre followed by western blot analysis and Southern blot. Gel numbers (1 to 16) correspond to fractions with increasing density as indicated in the scheme in the left. mtDNA-containing fractions was determined by Southern blotting. (**E**) Relative TFAM and POLRMT protein distribution across the gradient from L/L and L/L, cre mice. From Kühl et al. 2016.

At the RNA processing level, both ELAC2 and GRSF1 were strongly increased in *Polrmt* knockout hearts (Figure 3.18A). On the contrary, LRPPRC is strongly decreased in line with the decreased mt-mRNA levels (Figure 3.18A) (Ruzzenente et al. 2012; Sasarman et al. 2010). Loss of POLRMT also lead to a decrease in proteins of small and large mitoribosomal subunits (MRPS35 and MRPL37), but not of MRPL12 that is suggested to have an additional role in mtDNA transcription (Surovtseva et al. 2011). In agreement with the loss of mtDNA gene expression and OXPHOS capacity (Figure 3.14), levels of mtDNA-encoded cytochrome c oxidase subunits 1 and 2 (mt-CO1 and mt-CO2) are decreased upon loss of POLRMT (Figure 3.18A). Thus, loss of POLRMT affects protein levels of factors in several steps of mtDNA gene expression probably because they depend on the presence of POLRMT, mtDNA, or mt-RNAs for their stability or to compensate for the loss of these essential functions.

3.2. The cellular transcriptome and mitochondrial proteome of OXPHOS deficient mouse heart

3.2.1. An integrated omics approach to study loss of mtDNA gene expression and progressive OXPHOS deficiency

To obtain a comprehensive view of the cellular processes affected by OXPHOS dysfunction, we determined the cellular transcriptome and mitochondrial proteome (mitoproteome) from heart of five conditional knockout mouse strains deficient on genes essential for mtDNA gene expression that had been previously characterized in the laboratory. Mitochondrial DNA gene expression was disrupted at the level of replication (*Twnk*; Milenkovic et al. 2013), maintenance (*Tfam*; Larsson et al. 1998), transcription (*Polrmt*; section 3.1 of this thesis; Kühl et al. 2014; Kühl et al. 2016), RNA processing and stability (*Lrpprc*; Ruzzenente et al. 2012), and translation (*Mterf4*; Cámara et al. 2011). All of these knockouts have a drastically reduced lifespan ranging from <6 – 21 weeks of age due to severe cardiomyopathy caused by progressive OXPHOS dysfunction (Figure 3.19A; Table 3.1).

Table 3.1: Summary of the main characteristics of the tissue-specific mouse strains

Mouse strain	*Twnk*	*Tfam*	*Polrmt*	*Lrpprc*	*Mterf4*
Gene product	Mitochondrial DNA replicative helicase TWINKLE	Mitochondrial transcription factor A	Mitochondrial RNA polymerase	Leucine-rich pentatrico-peptide repeat containing protein	Mitochondrial transcription termination factor 4
Lifespan (weeks)	<19	<10	<6	<16	<21
mtDNA levels	↓	↓	↓	~	↑
mt-RNA levels	↓	↓	↓	↓*	↑
OXPHOS	↓	↓	↓	↓	↓
Reference	Milenkovic et al. 2013	Larsson et al. 1988	This thesis; Kühl et al. 2014; 2016	Ruzzenente et al. 2011	Cámara et al. 2011

* except *mt-12S* rRNA, *mt-16S* rRNA, *mt-Nd6*, and most mt-tRNAs.
Arrows: increase or decrease; ~ not changed.

From Kühl, Miranda et al. 2017

The cellular transcriptome was determined using RNA-Seq on total RNA isolated from heart of all the knockouts at their end-stage and corresponding age-matched controls. In parallel, we determined the mitoproteome of all the knockout strains using label-free mass spectrometry quantification (LFQ) on percoll-purified mitochondria from heart (Figure 3.19B). The transcriptomic and mitoproteomic data was used to generate three datasets. First, we characterized the changes in mitochondrial biogenesis and gene expression in a time-course analysis of wild-type or control mice from infancy (3 weeks) until adulthood (26 weeks). Second, we performed differential expression analysis of each knockout compared to its age-matched control which resulted in a catalogue of expression profiles of genes encoding

mitochondrial proteins affected by loss of mtDNA gene expression at different stages and severe OXPHOS deficiency. Third, we complemented our knockout comparison with a temporal mitoproteomic analysis of heart of *Lrpprc* conditional knockouts and age-matched controls at 2, 3, 5, 7 and 10 weeks of age to study the progression of OXPHOS deficiency (Figure 3.19B and C).

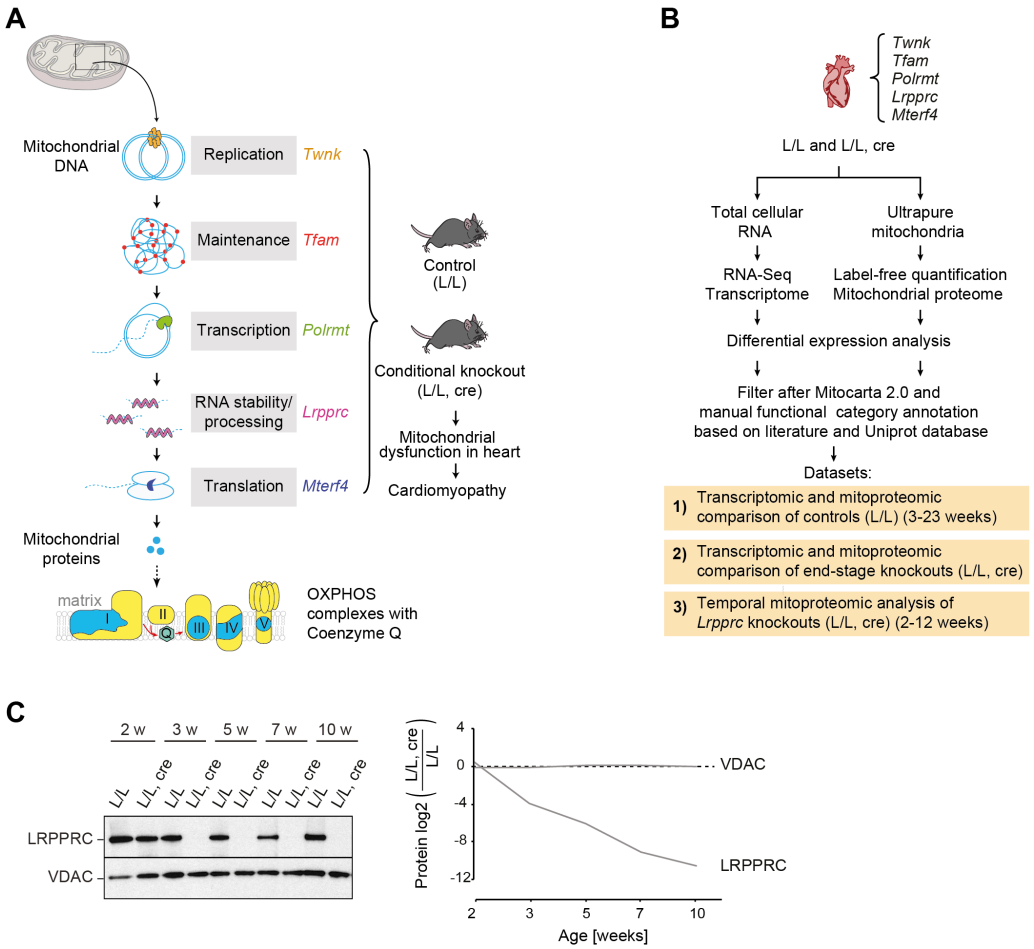

Figure 3.19 | Omics approach to study progressive OXPHOS dysfunction
(**A**) Schematic representation of the tissue-specific knockout (L/L, cre) mouse strains with disrupted mtDNA gene expression and corresponding controls (L/L). mtDNA-encoded proteins are depicted in blue and nDNA mitochondrial proteins in yellow. (**B**) Experimental workflow of data acquisition and analysis of the transcriptome and mitoproteomes from mouse heart generating three datasets (1-3). (**C**) Western blot (left) and LFQ quantification (right) of LRPPRC steady-state levels in time-course analysis of *Lrpprc* knockout strain. Loading: VDAC. From Kühl, Miranda et al. 2017.

Filtering for mitochondrial proteins in all datasets was performed based on MitoCarta 2.0 (Calvo, Clauser & Mootha 2016) and all differentially regulated mitochondrial transcripts or genes were manually classified into 18 functional categories based on annotated functions in Uniprot database (The UniProt Consortium 2017) and literature search (Table 3.2; Figure 3.19B).

Table 3.2: List of manually classified functional categories

Functional category
Apoptosis
Degradation and stress response
Iron sulphur cluster and heme biogenesis
Lipid and acetyl CoA metabolism
Mitochondrial transcription and mt-RNA metabolism
Mitochondrial 1C pathway
Mitochondrial carriers or transport
Mitochondrial import and chaperones
Mitochondrial morphology
Mitochondrial ribosome
mtDNA maintenance and replication
Nucleotide synthesis
Other mitochondrial protein synthesis factors
OXPHOS
OXPHOS assembly and biogenesis
Pyruvate and amino acid metabolism
Ubiquinone biosynthesis
Other

The resulting databases from this study were published as a resource and are available to the scientific community (Kühl et al. 2017).

3.2.2. Technical considerations of transcriptomic and mitoproteomic data acquisition and analysis

The heart is a complex tissue with a high dynamic range in terms of RNA and protein abundance. RNA-Seq techniques have a broad dynamic range which allows the accurate quantification of lowly and highly abundant transcripts simultaneously. This was reflected in the >27000 quantified transcripts in the different knockout strains, from which ~1118 encode mitochondrial proteins. In proteomics, however, the dynamic range is still problematic as highly abundant proteins limit the detection of lowly abundant ones. It was recently shown that mitochondrial contribution to the total heart protein mass in humans ranges from 2 to 21% depending on the heart region (Doll et al. 2017). Therefore, we analysed isolated heart mitochondria that had been purified on percoll gradients to reduce the complexity of the samples and gain more depth in our mitoproteome mass spectrometry analyses. We had a very high enrichment of mitochondrial proteins which accounted for ~99% of the total protein mass quantified. In total, we identified ~1000 proteins in the different knockout strains from which ~750 were quantified and ~650 were mitochondrial (Figure 3.20A). We did not find any significant bias in the detection of proteins based on their charge or hydrophobicity as

evidenced by cumulative distribution plots of the quantified and non-quantified proteins versus isoelectric point or GRAVY score, respectively (Figure 3.20B and C). However, we still had a significant bias against the detection of lowly abundant proteins (Figure 3.20D).

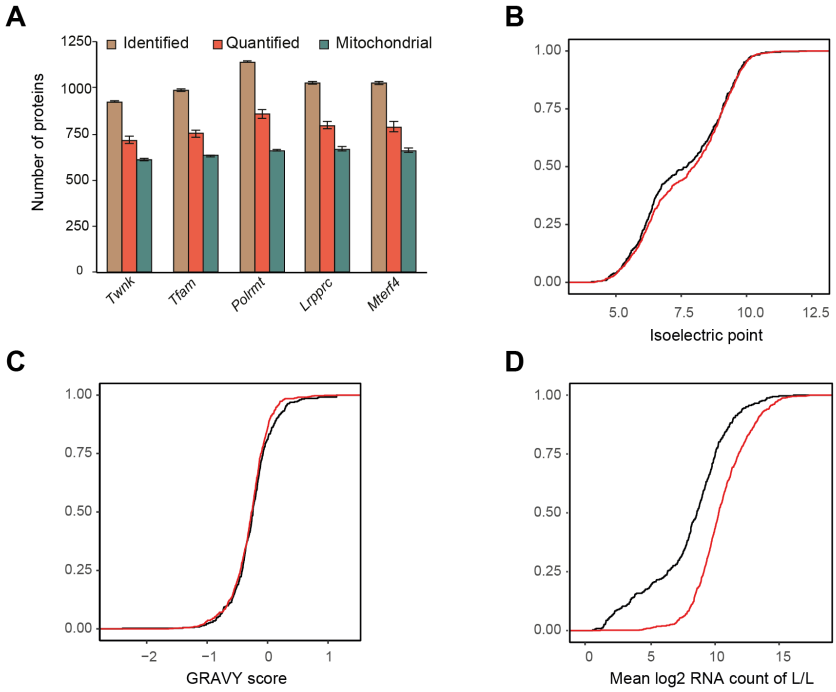

Figure 3.20 | Enrichment of mitochondrial proteins and systematic bias in mitoproteome data acquisition. (**A**) Number of identified, quantified, and mitochondrial proteins in each knockout mouse strain. Error bars: ± sem. (**B-D**) Cumulative distribution of quantified mitochondrial proteins based on isoelectric point as a measure of charge (**B**), GRAVY score as a measure of hydrophobicity (**C**), and mean RNA count of control (L/L) samples across all mouse strains as a measure of protein abundance (**D**). Isoelectric point and GRAVY scores were calculated using the amino-acid sequence of each protein without the first methionine and predicted N-terminus mitochondrial targeting sequence. Black, quantified in at least one knockout strain; red, not quantified. From Kühl, Miranda et al. 2017.

To evaluate the reproducibility in the data acquisition we calculated the Pearson correlation of the normalized counts for transcriptomics and LFQ intensity for proteomics. We had a very high reproducibility with Pearson correlation coefficient > 85% across all samples and > 95% between biological replicates for both, transcriptomics and proteomics (Figure 3.21). The high reproducibility and good number of biological replicates for a mouse omics study (n > 3 for all the analyses) allowed us to have good statistical robustness for subsequent analyses.

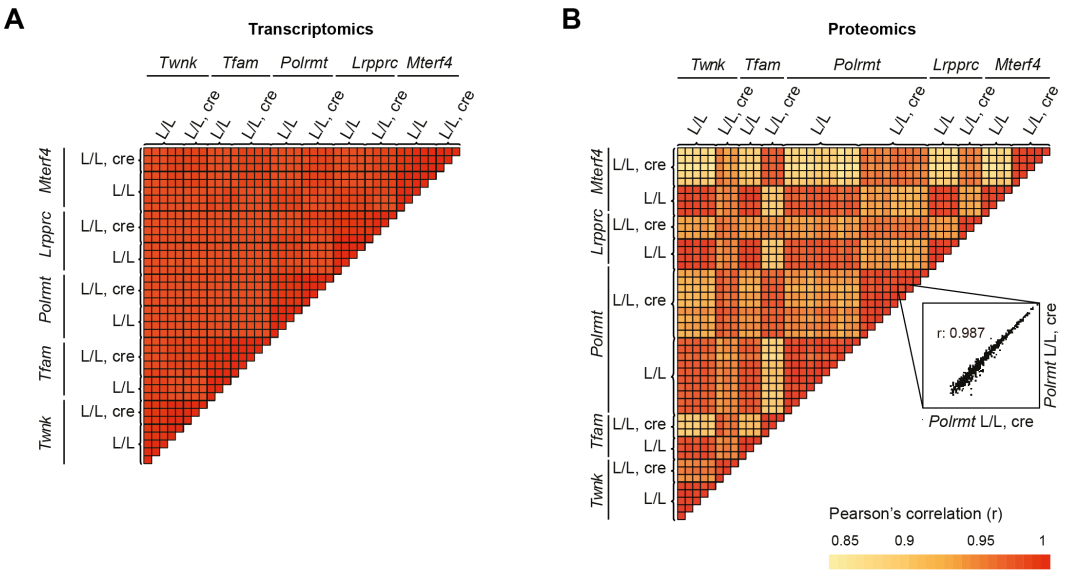

Figure 3.21 | High reproducibility of transcriptomic and mitoproteomic data
(**A-B**) Heatmaps showing the Pearson correlation coefficient (r) for RNA-Seq normalized counts (**A**) and LFQ intensity (**B**) of all the controls (L/L) and knockouts (L/L, cre). As an example, a scatter plot for the LFQ intensity values and r for two *Polrmt* L/L, cre samples is shown. Each square represents the comparison of two biological samples. Heatmaps were generated using the same scale. From Kühl, Miranda et al. 2017.

Standard inclusion criteria for proteomic data analysis filters for proteins that are quantified in at least half of the samples analysed. However, we included all the proteins that were quantified in at least half of the samples of a single genotype in the comparison of the knockouts to identify proteins that are lowly abundant in one genotype (*i.e.* controls or knockouts) but are present at detectable levels in the other genotype. The missing values were imputed following standard procedures which assume that missing values are normally absent because they correspond to lowly abundant proteins and thus imputed values normally fall in the lower quantification range. To assess the effect of the filtering criteria and data imputation we plotted the average LFQ intensity versus the fold-change (knockouts / controls) and found that lowly abundant proteins in controls tend to have high fold-change values whereas lowly abundant proteins in the knockouts tend to have low fold-change values (Figure 3.22). The proteins that presented this pattern have several imputed values indicating that quantification of proteins that are present in one genotype but not the other is largely influenced by imputed values and, therefore, the fold-change estimations are not accurate. Despite this bias in the fold-change estimations of lowly abundant proteins, the filtering criteria used allowed us to gain valuable biologically relevant information such as the previously described loss of SLIRP when LRPPRC is absent (Ruzzenente et al. 2012) or the increase in proteins of the 1C or proline synthesis pathways (discussed in section 3.2.8).

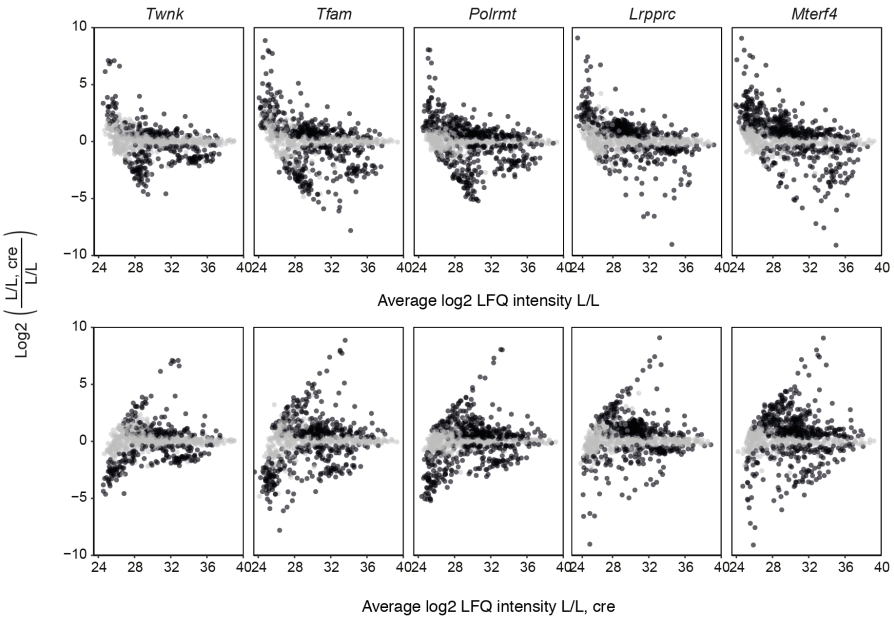

Figure 3.22 | Lowly abundant proteins have broader fold-change distribution
MA plots showing the fold-change distribution in the mitoproteome mice compared to the average LFQ intensity of control (L/L) (top) and knockout (L/L, cre) (bottom) mice per knockout mouse strain. Black, $p < 0.05$, grey, $p > 0.05$ in differential expression analyses of L/L, cre versus L/L. From Kühl, Miranda et al. 2017.

3.2.3. Mitochondrial remodelling during normal post-natal development of mouse heart is mainly regulated at the post-transcriptional level

To get a better understating of the normal post-natal development of mitochondria in mouse heart during the time encompassing the lifespan of the knockout strains used in this study, we compared the mtDNA levels, mitoproteome, and total cellular transcriptome of wild-type or control mice from infancy (2-3 weeks) until adulthood (26 weeks) (Figure 3.19B). Mitochondrial DNA content increases steadily in mouse heart until 6 weeks of age (Figure 3.23A) and protein levels of traditional markers of mitochondrial biogenesis such as TFAM and the voltage dependent anion channel 1 (VDAC) follow this trend (Figure 3.23B). We therefore evaluated the transcript levels of factors regulating mitochondrial biogenesis in heart and did not find differences in gene expression between the different time-points analysed (Figure 3.23C). Furthermore, only 14% of the transcripts of genes encoding mitochondrial proteins were differentially regulated (Figure 3.23D) suggesting that there is not a major shift in the transcriptional regulation of mitochondrial biogenesis after 3 weeks of age in mouse heart. In contrast, differential expression analyses of the mitoproteome showed that 391 out of the 756 mitochondrial proteins quantified in control mice changed during post-natal development (Figure 3.23E).

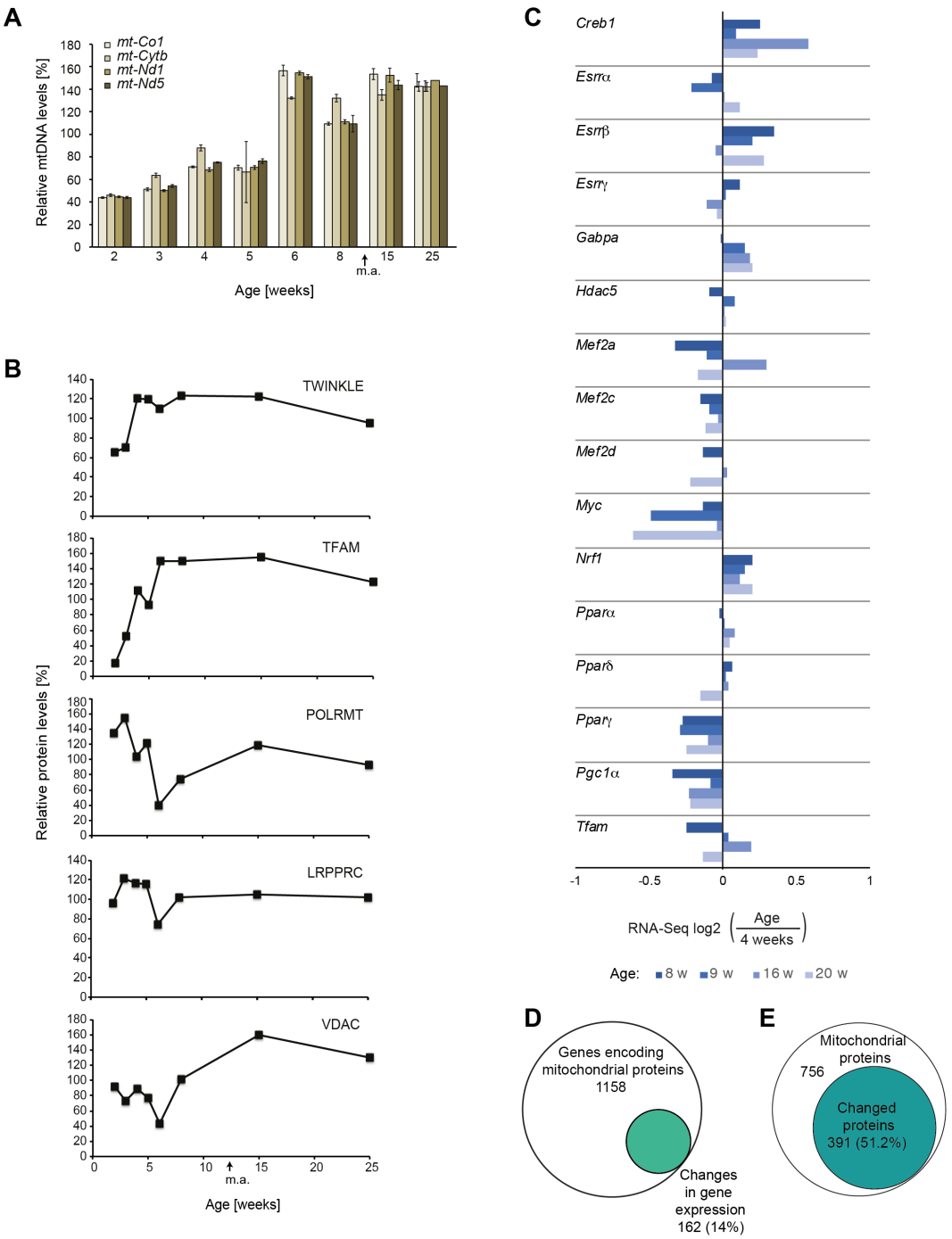

Figure 3.23 | Rapid post-natal increase of mtDNA levels and factors required to express mtDNA in wild-type mouse heart
(**A**) mtDNA levels determined by qPCR on total cellular DNA isolated from heart of wild-type (+/+) mice at different ages. Normalization: *18S* rDNA. Error bars ± sem of technical replicates. (**B**) Western blot quantification of nDNA mitochondrial proteins on heart protein extracts of wild-type mice. Normalization: α-tubulin. Percentage (%) was calculated relative to the average normalized value of all the time-points. (**C**) Expression level of genes encoding transcription factors involved in mitochondrial biogenesis in heart of control (L/L) mice at different ages measured by RNA-Seq. (**D-E**) Venn diagrams illustrating the number genes encoding mitochondrial that are differentially expressed during post-natal development of L/L mouse heart at the transcript (**D**) and protein (**E**) level. m.a. = mature adulthood. Modified from Kühl, Miranda et al. 2017.

To evaluate the changes in protein levels through time we performed hierarchical clustering analysis on the differentially expressed proteins. 91.3% of the proteins were distributed in four main clusters with distinct patterns of protein abundance (Figure 3.24A and B). Clusters 1 and 4 contained most mitochondrial proteins and had opposite patterns of

protein expression; while proteins from cluster 1 increase in abundance until 8 weeks of age, proteins from cluster 4 decrease. Clusters 2 and 3 also showed opposite patterns where proteins from cluster 2 decrease between 4 to 8 weeks and then increase to the original level between 9 and 12 weeks and proteins from cluster 3 increase until 8 weeks of age and then decrease between 9 and 12 weeks (Figure 3.24B). Next, we performed category enrichment analyses on each of the clusters using our manual functional category annotations (Table 3.2). Cluster 1 had an enrichment of proteins involved in pyruvate, amino acid and lipid metabolism (Figure 3.24B). Noteworthy, several proteins required for branched-chain amino acid metabolism and β-oxidation of fatty acids are in this cluster. Cluster 2 contained 50% of the significantly changed OXPHOS proteins and cluster 3 contained proteins involved in mitochondrial transcription, RNA metabolism and protein synthesis. Interestingly, cluster 4 had an enrichment of mitoribosomal proteins containing 93% of the proteins in this category (Figure 3.24B).

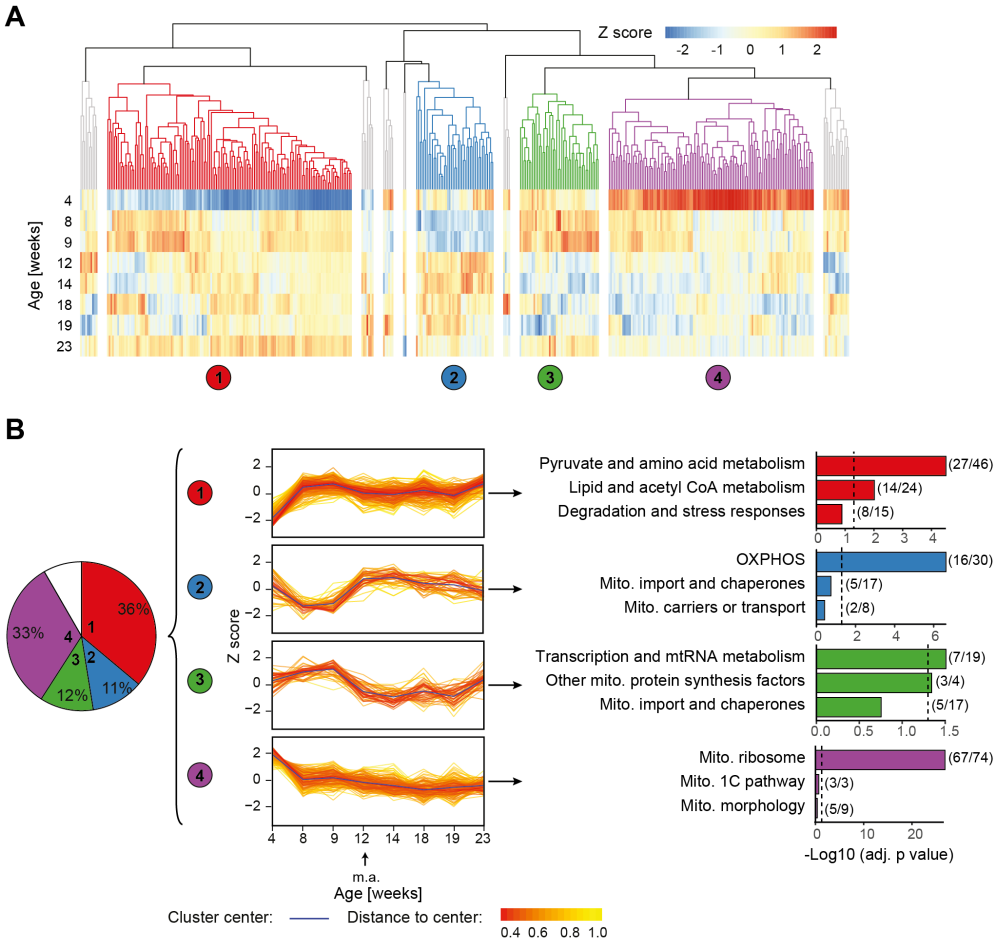

Figure 3.24 | Mitoproteome changes during post-natal development of mouse heart
(**A**) Dendrogram of hierarchical clustering analysis heatmap of mitoproteomes of control (L/L) mice. Fold-changes relative to 3-week-old mice were Z-scored normalized. Proteins in grey (rest) were not classified in the main clusters. (**B**) Cluster analysis. From left to right: pie chart illustrating the distribution in percentage of differentially expressed mitochondrial proteins in each cluster (1-4), in white: not classified; protein distribution patterns through time on each cluster; category enrichment analysis of proteins on each cluster. Top three categories are presented. Dotted line: Benjamini-Hochberg adjusted $p < 0.05$. Parenthesis indicate the number of significantly changed proteins in that category / total number of proteins in that category. m.a = mature adulthood. From Kühl, Miranda et al. 2017.

2D annotation enrichment analysis (Cox & Mann 2012) of the mitochondrial transcripts and proteins at the different time-points showed that the global decrease on the mitoribosomal proteins is most-likely explained by decreased protein stability as the transcript level of most of these proteins is not changed (Figure 3.25A and B). Taken together, the post-natal shift in metabolism seems to extend up to 8 weeks of age where the increased levels of key mitochondrial metabolism proteins and mtDNA levels stabilize but proteins involved in mtDNA expression and maintenance drop.

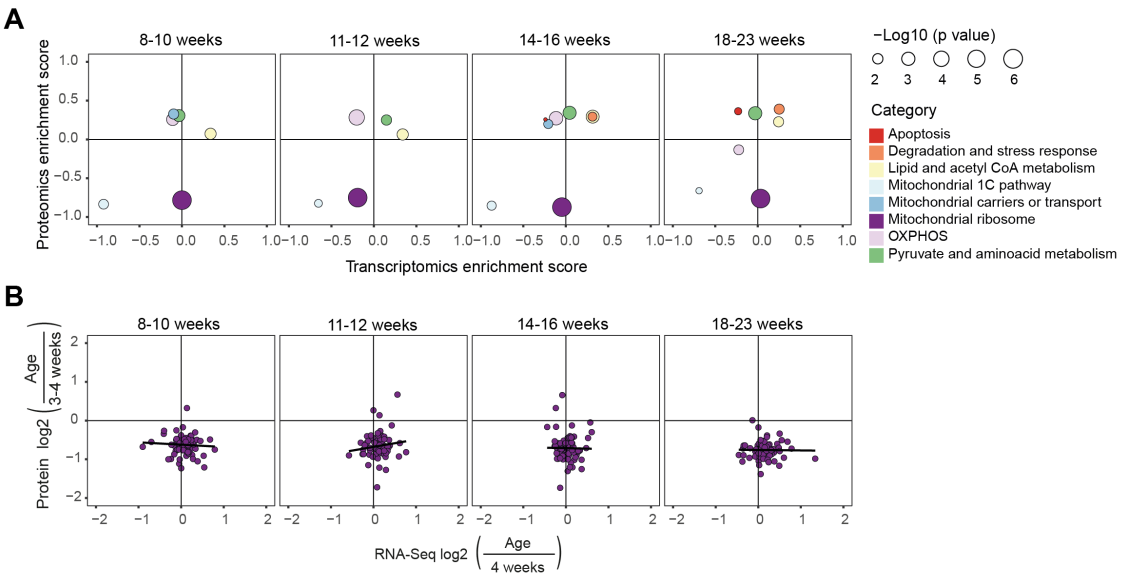

Figure 3.25 | Decrease of mitoribosomal subunits in caused by decreased protein stability
(**A**) Mitochondrial transcriptomic and proteomic 2D-enrichment analysis of functional categories in control (L/L) mice at different ages. Enrichment scores were calculated on the fold-change relative to 3-4-week old mice. (**B**) Scatterplots of fold-changes relative to 3-4-week old mice of mitoribosomal transcript and proteins in L/L mice at different ages. Black line indicates the trend. From Kühl, Miranda et al. 2017.

3.2.4. Loss of mtDNA gene expression profoundly alters the transcript and protein levels of nuclear genes encoding mitochondrial proteins

We compared the transcriptomes and mitoproteomes of the five knockout mouse strains to identify common hallmarks of mitochondrial dysfunction in mouse heart. We found extensive changes in the transcript and protein levels of genes encoding mitochondrial proteins (Figure 3.26A and B). At the transcript level, 38% of the quantified mitochondrial genes were differentially expressed in all knockouts, and most of these transcripts were decreased (Figure 3.26C). At the protein level, ~65% of the quantified proteins were significantly changed and most of these were increased (Figure 3.26D). Furthermore, not only were there many changes in gene expression, but also the range of fold-changes was very high (log2 fold-change between -9 to 9) in both the transcriptomes and mitoproteomes (Figure 3.26A and B). Unless indicated otherwise, further downstream analyses were performed including all the genes that changed significantly in at least one knockout strain. In total, we found 310 genes whose expression changed only at the transcript level, 186 genes at the protein level, and 470 genes

at both, transcript and protein levels (Figure 3.26E). Therefore, severe mitochondrial dysfunction results in a massive remodelling of the expression of genes encoding mitochondrial proteins.

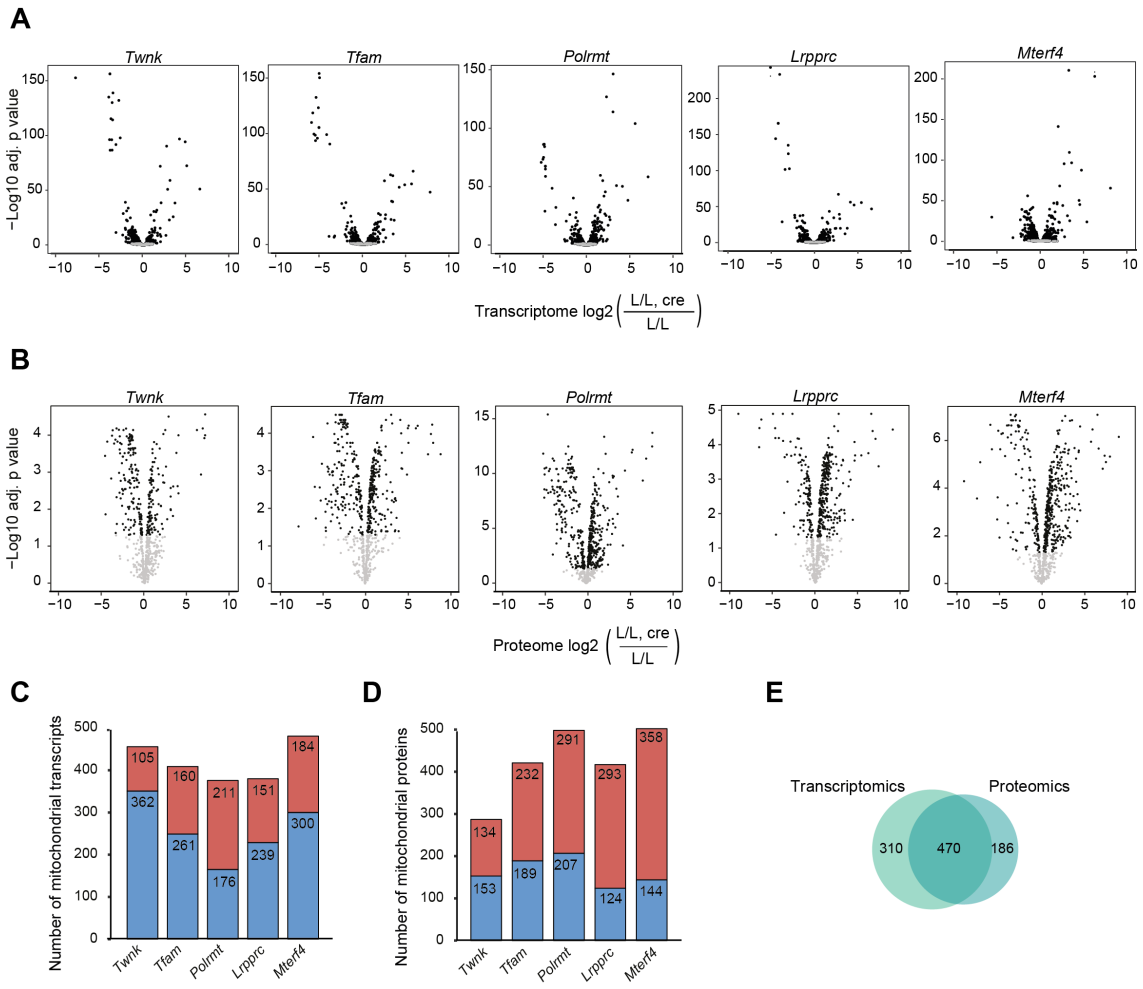

Figure 3.26 | Extensive remodelling of the mitochondrial transcriptome and proteome
(**A-B**) Volcano plots of genes encoding mitochondrial proteins (**A**) and mitoproteomes (**B**) for each knockout strain; black: p<0.05, grey: p>0.05. p values were adjusted using the Benjamini-Hochberg method. (**C-D**) Number of significantly changed mitochondrial transcripts (**C**) and proteins (**D**) from knockouts (L/L, cre) compared to controls (L/L); red: increased, blue: decreased. (**E**) Venn diagram of number of mitochondrial transcripts and proteins quantified and significant in ≥1 knockout strain. Modified from Kühl, Miranda et al. 2017.

To assess to what extent the variation in transcript levels result in corresponding protein abundance changes in the OXPHOS deficient hearts, we determined the Pearson correlation using all the genes for which we had quantification at the transcript and protein level. There was a significant correlation in all knockout strains with adjusted p values below 1.631×10^{-18} and correlation values between 32 – 56% (Figure 3.27A). From all the knockouts, *Polrmt* had the lowest correlation value which could be explained by the early age at which they die (Table 3.1). These data suggest that the composition of the mitoproteome is strongly influenced by post-transcriptional processes. Therefore, we performed 2D annotation enrichment analysis to identify categories of proteins that were regulated at a transcriptional or post-transcriptional

level (Figure 3.27B). There were very few categories of proteins that presented an anti-correlative behaviour such as other mitochondrial protein synthesis factors and lipid and acetyl CoA metabolism. On the contrary the majority of the categories showed a concordant upregulation of transcript and protein levels including apoptosis, degradation and stress response, mitochondrial import and chaperones, and the mitochondrial 1C pathway. Interestingly, the categories of OXPHOS, the mitochondrial ribosome, and ubiquinone (Q) biosynthesis showed a high absolute enrichment scores at the protein level but not at the transcript level suggesting that the protein abundance is mostly defined by post-transcriptional processes. Heatmaps for the individual genes on each category are presented in supplementary material (section 8.1.1).

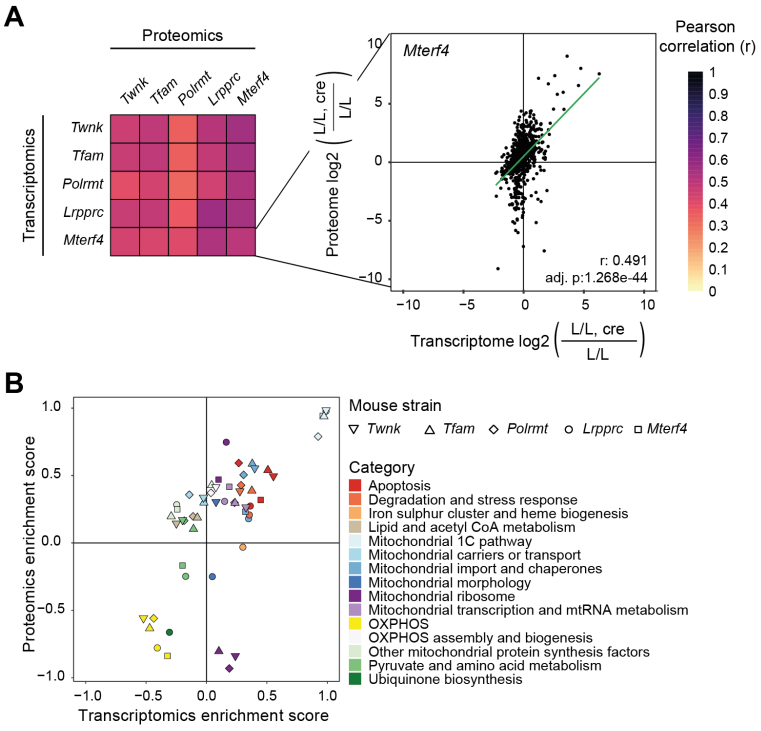

Figure 3.27 | Correlation between the transcriptome and mitoproteome
(**A**) Heatmap showing the Pearson correlation (r) of the changes in transcript and protein level in knockouts (L/L, cre) compared to controls (L/L); as an example, a scatter plot of the transcriptome and proteome fold-changes in the *Mterf4* knockout is shown. adj. p: Benjamini-Hochberg adjusted p value. (**B**) 2D enrichment analysis of the mitochondrial transcriptome and proteome in all knockouts showing the trend and degree of regulation of 15 functional categories that had p<0.05. Modified from Kühl, Miranda et al. 2017.

3.2.5. mtDNA gene expression is required to stabilize the OXPHOS complexes and the mitoribosome

Reduced mtDNA gene expression results in loss of OXPHOS subunits in the five knockout mouse strains (Cámara et al. 2011; Kühl et al. 2016; Milenkovic et al. 2013; Ruzzenente et al. 2012; Wang et al. 1999). To validate our omic approach, we compared the transcript and protein levels of genes encoding OXPHOS subunits in the different knockouts. Transcript levels of mtDNA-encoded subunits were decreased in *Twnk*, *Tfam Polrmt*, and *Lrpprc*

knockouts whereas in *Mterf4* knockout they were increased accurately reflecting the stage at which mtDNA gene expression is disrupted (Figure 3.19A, 3.28A, and Table 3.1). The transcript levels of nuclear genes encoding subunits of complexes I to V were, in general, slightly decreased and did not show a specific pattern of expression in the different knockouts (Figure 3.28A).

Consistent with our analysis of systematic bias (Figure 3.20), we quantified in all the knockout strains the protein levels of 84 out of 95 OXPHOS subunits which, despite being highly hydrophobic, are very abundant. There was a severe decrease in the protein levels of complexes I, III, IV, and V encoded by both, mtDNA and nDNA (Figure 3.28A and B). The exclusively nucleus-encoded complex II and the nucleus-encoded subunits of complex V that can form stable sub-assembled F_1 complex in OXPHOS deficient mitochondria (*i.e.* ATP synthase subunits alpha (ATP5A1), beta (ATP5B), gamma (ATP5C1), delta (ATP5D), and epsilon (ATP5E)) (Mourier et al. 2014), were slightly increased or unaffected in all knockouts. The stronger downregulation of subunits of complex I and IV is consistent with the degree of reduction on the enzyme activity of these complexes in the different knockouts (Cámara et al. 2011; Kühl et al. 2016; Ruzzenente et al. 2012; Wang et al. 1999). Furthermore, we verified the protein levels of some OXPHOS subunits via western blot and obtained consistent results with our mitoproteomic data (Figure 3.28C). Interestingly, the protein levels of the nDNA subunits were homogeneous within each complex, indicating that the stability of the individual subunits depend on the stability of the assembled or sub-assembled complexes. Furthermore, in the case of complexes I, III, IV, and F_0-subunit of complex V, the stability of the complexes depends on the presence of the mtDNA-encoded subunits. Finally, we evaluated the levels of the OXPHOS complexes at different ages in heart of the *Lrpprc* knockout (Figure 3.19B, C and Figure 3.28D) and detected a progressive decline of the different complexes validating our temporal mitoproteomic approach to study the progression of OXPHOS deficiency.

Protein levels of OXPHOS assembly and biogenesis factors were in general increased in the different knockouts, with complex IV assembly factors COX15, COX19 and SCO2 showing the particularly high levels (Figure 3.28E). However, the transcript level of OXPHOS assembly and biogenesis factors were either not changed or slightly decreased suggesting that the increase in proteins is likely a compensatory response to the loss of OXPHOS subunits that occurs at the post-transcriptional level.

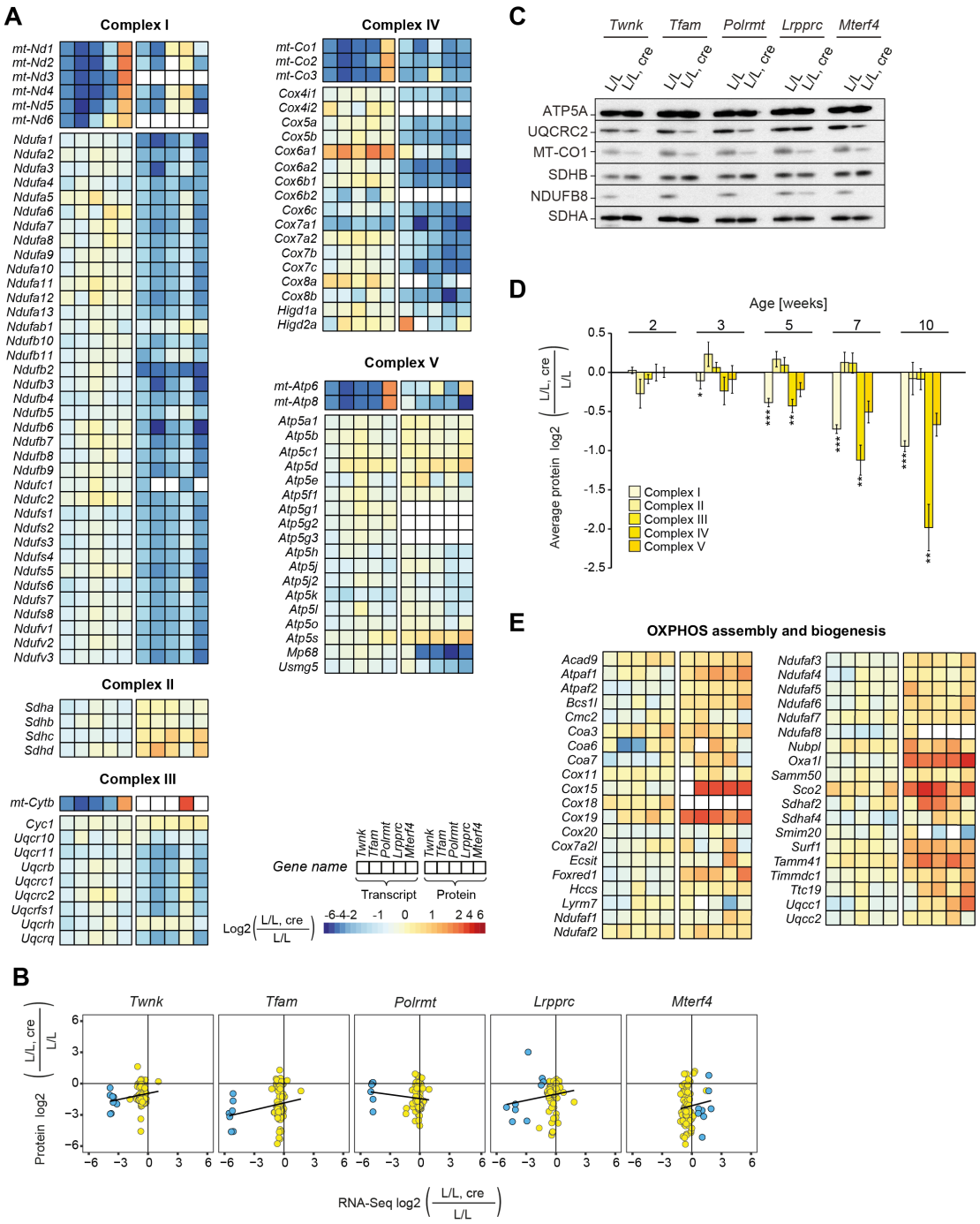

Figure 3.28 | Stability of OXPHOS complexes depend on the presence of the mtDNA-encoded subunits
(**A**) Heatmaps illustrating the fold-change in transcript (left) and protein (right) levels of OXPHOS subunits in heart of knockouts (L/L, cre) compared to controls (L/L). mtDNA-encoded subunits are presented first followed by the nDNA subunits in alphabetic order. (**B**) Scatterplot of fold-changes in transcript and protein levels of OXPHOS subunits; black line indicates the trend; blue: mtDNA-encoded subunits, yellow: nDNA subunits. (**C**) Western blot of OXPHOS subunits on isolated mitochondrial extracts from L/L and L/L, cre mouse hearts; Loading: SDHA. (**D**) Protein levels of OXPHOS complexes at different time points in *Lrpprc* knockout mouse hearts. The graph shows the average fold-change for all the proteins in each complex. *p<0.05, **p<0.01, ***p<0.001; error bars: ± sem. (**E**) Heatmap of OXPHOS assembly and biogenesis factors. Blank boxes: not detected or quantified. Modified from Kühl, Miranda et al. 2017.

Since mtDNA also codes for the two mt-rRNAs, we evaluated the expression of the mitoribosomal protein complexes. The abundance of mitoribosomal proteins clearly depended on the level at which mtDNA gene expression was disrupted. Knockouts with reduced steady-

state levels of mt-rRNAs, such as *Twnk, Tfam* and *Polrmt*, showed massively reduced levels of mitoribosomal proteins, whereas knockouts with increased mt-rRNA levels, such as *Lrpprc* and *Mterf4*, had increased levels of mitoribosomal proteins (Figure 3.29). In contrast, transcript levels of genes encoding mitoribosomal proteins were mildly affected. Our data thus show that the stability of individual mitoribosomal proteins depend on the assembly of the mitoribosomal subunits and strongly support the model that mt-rRNAs stabilize the nucleus-encoded mitoribosomal subunits which are produced and imported into mitochondria in excess.

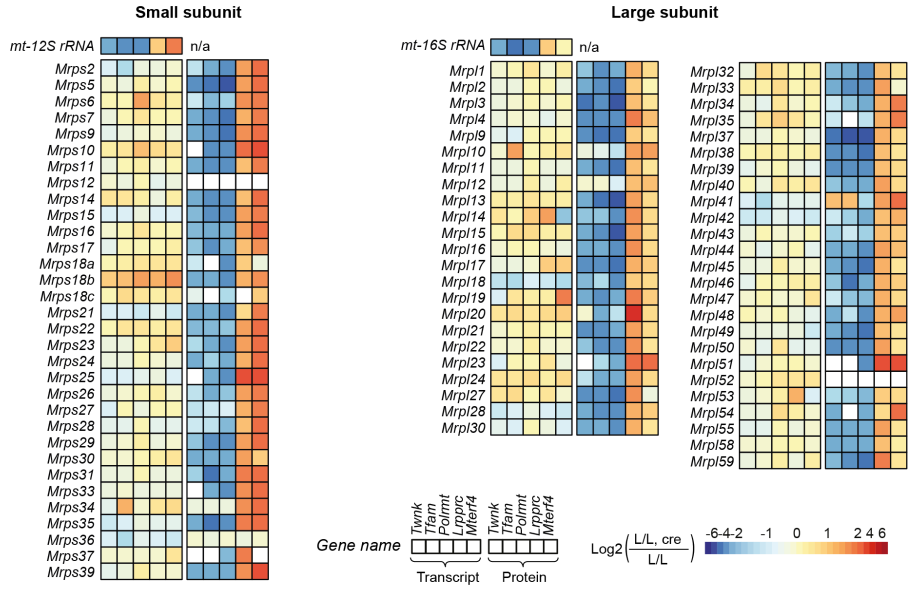

Figure 3.29 | Stability of mitoribosomal protein complexes depend on the abundance of mt-rRNAs
Heatmaps illustrating the fold-change in transcript (left) and protein (right) levels of the small (left) and large (right) mitoribosomal subunits in heart of knockouts (L/L, cre) compared to controls (L/L). Blank boxes: not detected or quantified. From Kühl, Miranda et al. 2017.

In conclusion, our comprehensive transcriptomic and mitoproteomic data not only reproduces the previous molecular characterization of the knockout mouse strains with severe OXPHOS deficiency but also argue that intra-mitochondrial protein level regulation has a predominant role in the biogenesis of the OXPHOS system and the mitoribosome. Furthermore, our findings show that expression of mtDNA-encoded genes determines the abundance of a large proportion of the mitoproteome.

3.2.6. Loss of mtDNA gene expression causes secondary coenzyme Q deficiency

Our 2D annotation enrichment analyses showed that the Q biosynthesis category in *Lrpprc* knockout clustered very closely with the OXPHOS category (Figure 3.28B). We evaluated the expression profiles of the enzymes required for intra-mitochondrial Q biosynthesis in all the knockouts and found them severely reduced at the protein level with the exception of COQ4, COQ8B and PDSS2 (Figure 3.30A and B). PDSS1 and COQ2 were not quantified. The levels of mevalonate pathway enzymes such as HMG-CoA synthase (HMGCS1) and farnesyl

pyrophosphate synthase (FDPS) were normal or slightly increased in all the knockouts (Figure 3.30C). Moreover, the transcript levels of genes encoding cytoplasmic HMGCS1, 3-hydroxy-3-methylglutaryl-CoA reductase (HMGCR) and FDPS were either unaffected or increased (Figure 3.30D). Together with the increased levels of PDSS1 which catalyse the polymerization of the isoprenoid chain, our data suggests that there is no impairment in the mevalonate pathway when mtDNA gene expression is disrupted.

The decrease in the protein levels of COQ3, COQ5, COQ6, COQ8A, COQ9, and COQ10A was apparent at an early stage in the *Lrpprc* knockout strain and decreased further with the progression of OXPHOS deficiency (Figure 3.30E). Although the transcripts encoding Q biosynthesis enzymes were slightly decreased or unchanged, the atypical kinases *Coq8a* and *Coq8b* showed a consistent regulation at the transcriptional level with opposite patterns in all the knockouts. *Coq8a* was downregulated whereas *Coq8b* was upregulated at both the transcript and protein level (Figure 3.30B and D). In this regard, it is worth to note that COQ8B protein levels increased sharply after 5 weeks of age in the *Lrpprc* knockout hearts whereas the other enzymes progressively declined (Figure 3.30E), suggesting that it could be a compensatory mechanism. Interestingly, COQ8A and COQ8B have been recently suggested to interact differentially with the Q biosynthesis complex in mammalian cell lines depending on whether metabolism is adapting to glycolytic or respiratory conditions (Floyd et al. 2016). Finally, we evaluated whether the decreased levels of the intra-mitochondrial Q biosynthesis enzymes affected the cellular steady-state levels of Q. Mice have two forms of Q, Q9 and Q10, from which Q9 is the most abundant (Tang et al. 2004). We therefore measured the levels of both compounds in mouse heart tissue extracts using targeted mass spectrometry and found that, in control mice, Q9 was around tenfold more abundant than Q10 (Figure 3.30F), consistent with previous reports (Tang et al. 2004). In the knockout mice, Q9 was profoundly decreased, consistent with the downregulation of the intra-mitochondrial Q biosynthesis pathway. Taken together, our data show that loss of mtDNA gene expression causes secondary Q deficiency by a progressive loss of intra-mitochondrial Q biosynthesis enzymes.

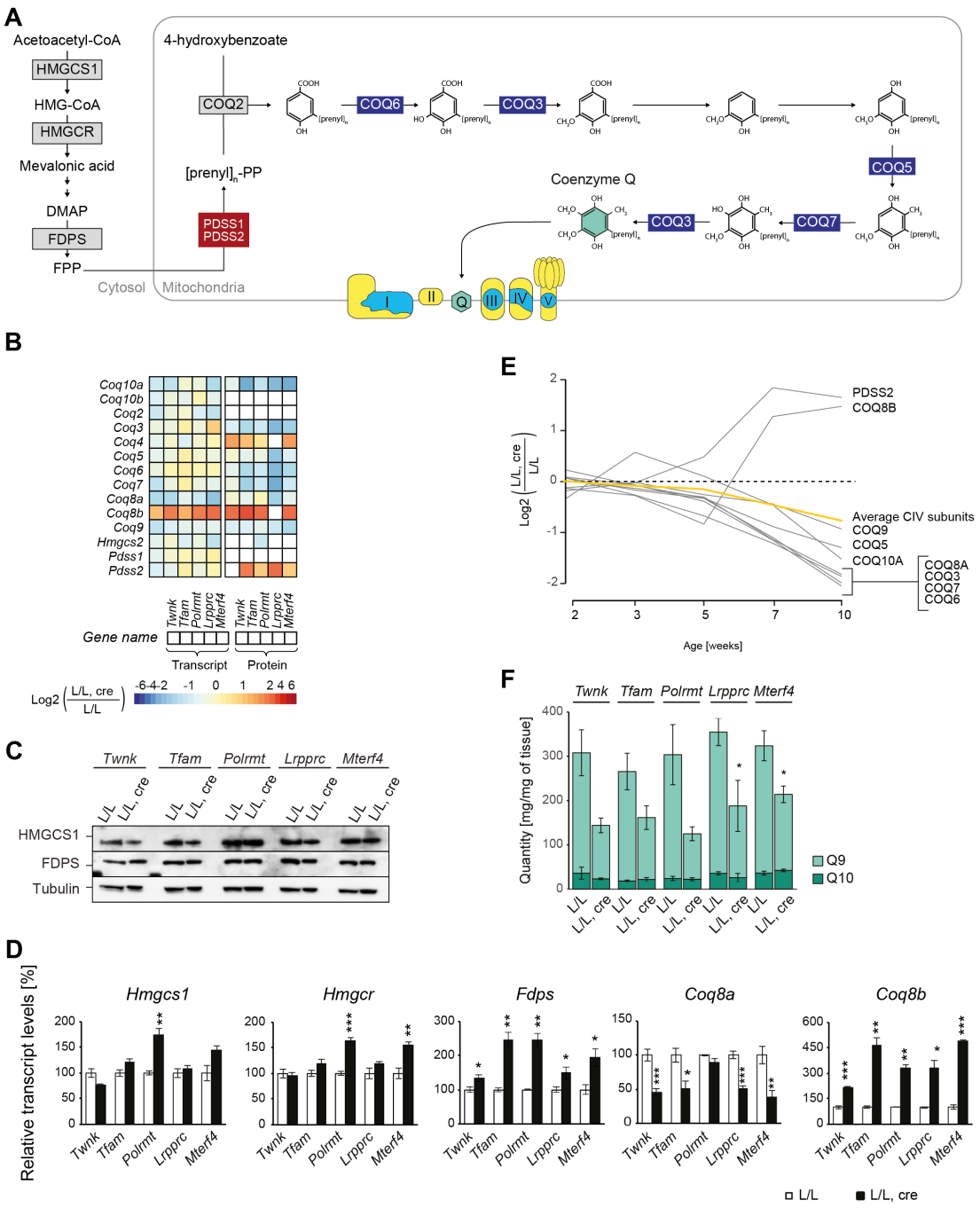

Figure 3.30 | OXPHOS dysfunction leads to secondary Q deficiency caused by a defect in intra-mitochondrial Q biosynthesis

(**A**) Scheme of the mevalonate pathway, intra-mitochondrial Q biosynthesis, and OXPHOS complexes. Coloured boxes: protein levels; red: increased, blue: decreased, grey: not quantified. (**B**) Heatmaps illustrating the fold-change in transcript (left) and protein (right) levels of Q biosynthesis enzymes in heart of knockouts (L/L, cre) compared to controls (L/L). Blank boxes: not quantified. (**C**) Western blot of enzymes of the mevalonate pathway on total protein extracts from L/L and L/L, cre mouse hearts; Loading: tubulin. (**D**) Transcript levels of genes encoding enzymes of the mevalonate and Q biosynthesis pathway in L/L and L/L, cre hearts. Normalization: beta-2-microglobulin (*B2m*). (**E**) Time-course analysis of protein levels of all enzymes of Q biosynthesis quantified in *Lrpprc* L/L, cre compared to L/L. Adjusted p across time <0.05. Yellow line: average value of OXPHOS complex IV (CIV) subunits. (**F**) Quinone quantification (Q9 and Q10) in L/L, cre and L/L mouse hearts. *p<0.05, **p<0.005, ***p<0.001; error bars: ± sem. From Kühl, Miranda et al. 2017.

3.2.7. *Transcriptome-wide analyses indicate that ATF4 and MYC mediate cellular stress responses to loss of OXPHOS function*

We found a general increase in the transcript and protein levels of several genes in the categories of apoptosis, degradation and stress response, and mitochondrial import and chaperones (Figure 3.27B and Figure 3.31) indicating the activation of nuclear stress responses. We found an increase the transcript and protein levels of some reported mtUPR chaperones such as HSPD1, HSPE1, and HSPA9 in all the knockouts (Figure 3.31B and C). However, despite the severe OXPHOS deficiency, several of the reported mammalian mtUPR-regulated factors were not changed such as *Clpp*, mitochondrial DnaJ homolog subfamily A member 3 (*Dnaja3*), endonuclease G (*Endog*), and the ATP-dependent zinc metalloprotease (*Yme1l1*). In agreement with Seiferling and colleagues that report that CLPP is dispensable for the induction of mtUPR in mammals (Seiferling et al. 2016), we did not detect differences in the protein levels of this mammalian matrix protease. Thus, our results indicate that there is a nuclear transcriptional response to mitochondrial stress that differ from the proposed mtUPR mechanism in worms.

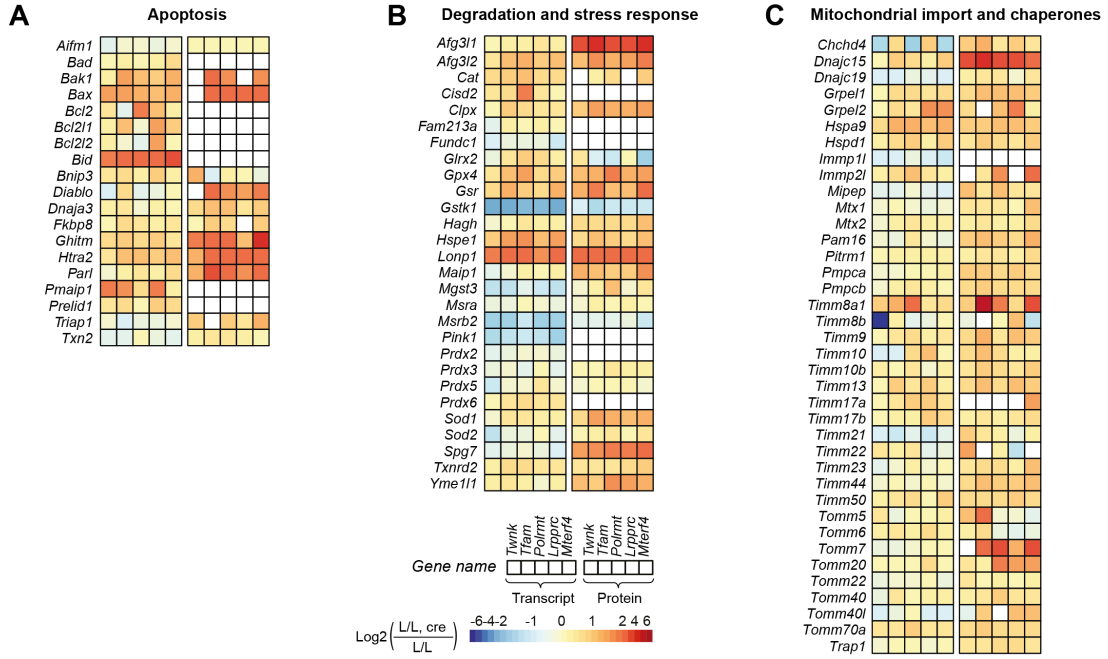

Figure 3.31 | Apoptosis, degradation and stress response, and mitochondrial import and chaperones are upregulated in OXPHOS dysfunction
Heatmaps illustrating the fold-change in transcript (left) and protein (right) levels of apoptosis (**A**), degradation and stress response (**B**), and mitochondrial import and chaperones (**C**) in heart of knockouts (L/L, cre) compared to controls (L/L). Blank boxes: not quantified. From Kühl, Miranda et al. 2017.

To identify factors mediating the nuclear responses to OXPHOS deficiency caused by mtDNA gene expression in mouse heart, we performed transcription factor enrichment analyses using as input the differentially expressed genes in all five knockouts. We identified several transcription factors predicted as the top regulators of the differentially expressed

genes including the nuclear factor NFE2, ATF-4, and MYC (Table 3.3). From the top scored transcription factors, only *Atf4* and *Myc* were upregulated in our transcriptomic data.

Table 3.3: Transcription factor enrichment analysis

Motif or track id	AUC	NES	Transcription factors
swissregulon-NFE2.p2	0.0352041	5.01091	NFE2, NFE2L2, BACH1, MAFK, NFE2L1, MAFG, JUND, JUNB, FOSB, FOSL1, FOS, JUN, FOSL2, BATF, SPI1, BACH2, MAFF, MAFA, MAF, MAFB, NFE2L3
homer-M00001	0.0351042	4.97971	
taipale-NNATGAYGCAATN-ATF4-DBD	0.0346771	4.84631	ATF4, ATF3, CEBPB
wgEncodeSydhTfbsK562CmycStdPk.narrowPeak.gz	0.0431751	4.73114	MYC
taipale-NGGATGATGCAATM-Atf4-DBD	0.0340163	4.6399	ATF4, CEBPB
lcbTfbs_mcf7_p53	0.0426344	4.61952	TP53
yetfasco-966	0.033346	4.43051	JUNB, JUND, JUN, FOSL1, FOS, BATF, FOSL2, BACH2, SPI1, BACH1, FOSB, NFE2, ARNT, TGIF2LY, TGIF2, TGIF2LX, TGIF1, SRF
wgEncodeSydhTfbsK562CmycIfng6hStdPk.narrowPeak.gz	0.040073	4.0908	MYC
wgEncodeSydhTfbsK562CmycIfna30StdPk.narrowPeak.gz	0.0394589	3.96404	MYC
GSM1208654_batch1_chrom1_LoVo_MYC_PassedQC_peaks_hg19	0.0394281	3.95768	MYC

AUC: Area under the cumulative recovery curve; NES: normalized enrichment score

MYC and ATF4 have been implicated in mitochondrial biogenesis and endoplasmic reticulum-stress responses, respectively (Morrish & Hockenbery 2014; Pakos-Zebrucka et al. 2016), and we verified their expression levels via quantitative real time PCR (qRT-PCR). The transcript levels of *Atf4* and *Myc* were strongly induced in all the knockouts in contrast to other transcription factors regulating mitochondrial biogenesis such as *Nrf1*, peroxisome proliferator-*Pgc1a*, and *Gabpa* (Figure 3.32A). Furthermore, canonical pathway enrichment analyses identified several signalling pathways that were enriched from which ATF4 and MYC are important transcription factors including eIF2, calcium, and the mTOR signalling (Figure 3.32B). From the non-mitochondrial transcripts, it is worth to mention that several cytosolic ribosomal proteins, translation initiation factors, and tRNA synthetases were upregulated.

We next evaluated the mitochondrial target genes of MYC and ATF4 that changed at the transcript levels in all the knockouts and found a general increase in ATF4 target genes and differences in gene expression in several MYC target genes (Figure 3.32C and D; supplementary material section 8.1.2). Several chaperones and proteases associated with mitochondrial stress and apoptosis that are target genes of these transcription factors are upregulated such as LONP1, HSPE1, the apoptosis regulator BAX, and the BH3-interacting domain death agonist (BID). Interestingly, genes that presented the strongest upregulation in

transcript and protein levels (*e.g.* mitochondrial bi-functional methylenetetrahydrofolate dehydrogenase/cyclohydrolase (*Mthfd2*), mitochondrial pyrroline-5-carboxylate reductase 1 (*Pycr1*), and delta-pyrroline-5-carboxylate synthase (*Aldh18a1*)), are also target genes of these transcription factors.

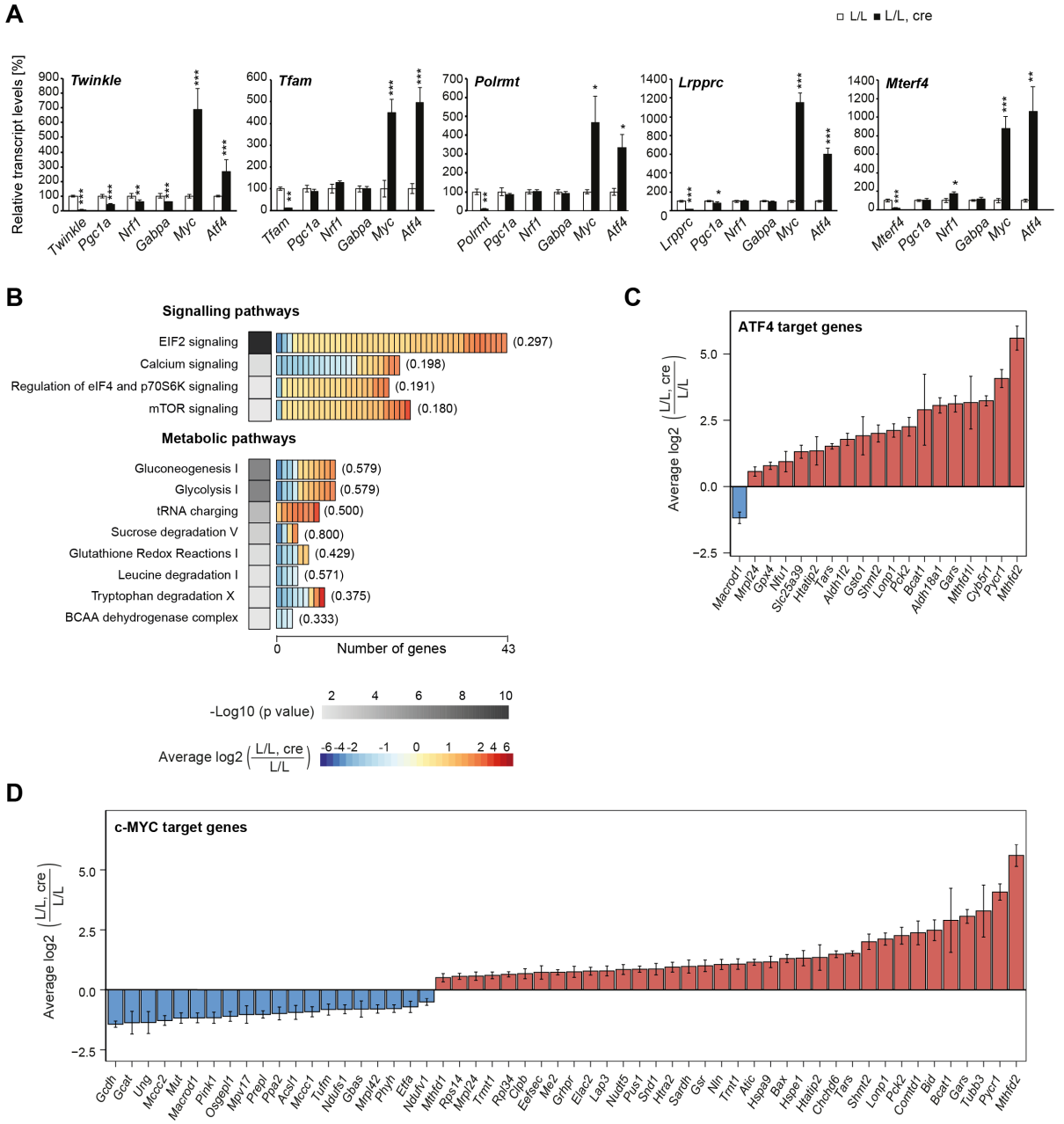

Figure 3.32 | Enrichment of signalling and metabolic pathways in mouse heart with severe OXPHOS dysfunction

(**A**) Transcript levels of genes encoding transcription factors involved in mitochondrial biogenesis in control (L/L) and knockout (L/L, cre) mouse hearts. Normalization: beta-2-microglobulin (*B2m*). *p<0.05, **p<0.005, ***p<0.001; two-tailed Student's *t*-test; error bars: ± sem. (**B**) Canonical pathway enrichment analysis of significantly changed genes in all knockouts. Top 12 categories are shown organized by p value. Fisher's exact test; rectangles in horizontal heatmaps: average expression level in the five knockouts of each gene detected per pathway; parenthesis: fractions of genes detected per pathway. (**C-D**) Average transcript expression levels of target genes of ATF4 (**C**) and MYC (**D**) encoding mitochondrial proteins. p < 0.05 for all genes; error bars ± sd. From Kühl, Miranda et al. 2017.

3.2.8. Identification of early markers of OXPHOS dysfunction in mouse heart

To identify markers of mitochondrial dysfunction, we focused on proteins that were strongly upregulated in all the knockout mouse strains. We found a strong increase on the transcript and protein levels of the enzymes of the mitochondrial 1C cycle (Figure 3.33A and B). In contrast, the cytosolic C-1 tetrahydrofolate synthase (MTHFD1) enzyme was unaltered at the protein level (3.33C). To evaluate the levels of the 1C donors, we performed targeted mass spectrometry metabolomic analysis and found increased levels of glycine, sarcosine, and serine (Figure 3.33D). Consistent with previous studies (Bao et al. 2016), the transcript levels of enzymes required for *de novo* serine synthesis in the cytosol were strongly upregulated in all the knockouts (data not shown). Temporal mitoproteomic analysis of the mitochondrial 1C cycle enzymes in the *Lrpprc* knockout showed that all the central enzymes are increased before there is a decrease in proteins from OXPHOS complex IV (Figure 3.33E), which is the most downregulated complex in *Lrpprc* knockout (Figure 3.28A). Our results support a link between mitochondrial dysfunction and the mitochondrial 1C pathway (Bao et al. 2016; Nikkanen et al. 2016) and show that it is an early event in the progression of OXPHOS dysfunction.

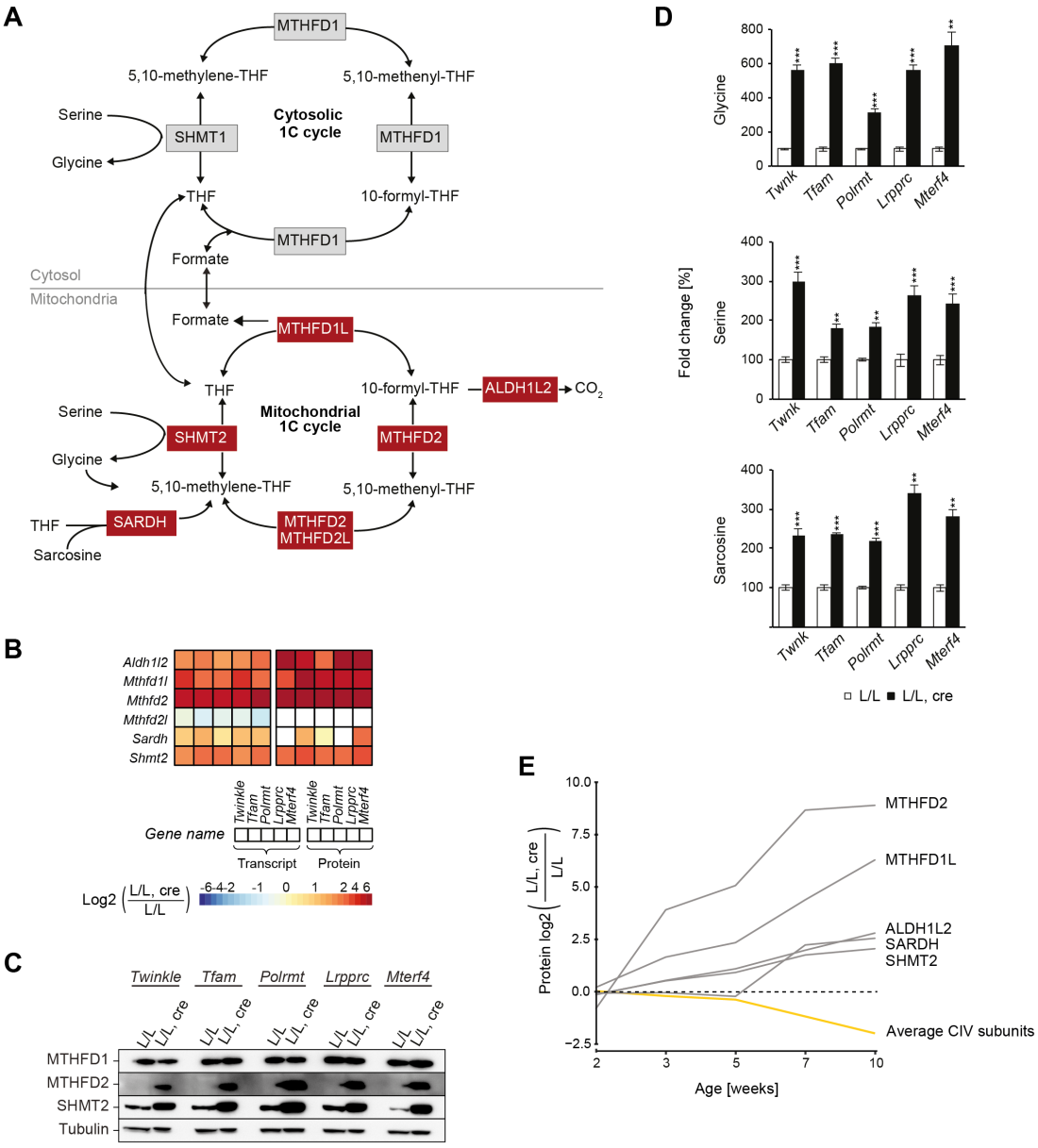

Figure 3.33 | Mitochondrial 1C pathway enzymes are upregulated early in the progression of OXPHOS dysfunction
(**A**) Scheme of 1C pathway. Coloured boxes represent protein levels; red: increased, grey: not quantified. (**B**) Heatmaps illustrating the fold-change in transcript (left) and protein (right) levels of knockouts (L/L, cre) and control (L/L) mouse hearts. (**C**) Western blot of enzymes of the 1C pathway on total protein extracts from L/L and L/L cre hearts. Loading: tubulin. (**D**) Quantification of 1C donor metabolite levels in L/L, cre and L/L. *p < 0.05, **p < 0.01, ***p < 0.001; two-tailed Student's *t*-test; error bars ± sem. (**E**) Time-course analysis of protein levels of enzymes of the 1C pathway quantified in *Lrpprc* L/L, cre compared to L/L. Adjusted p across time <0.05. Yellow line: average value of OXPHOS complex IV subunits. From Kühl, Miranda et al. 2017.

ALDH18A1 was among the most upregulated proteins in most knockout mouse strains (Figure 3.34A and B). Since ALDH18A1 is the first enzyme in the synthesis of proline from glutamate in mitochondria (Pérez-Arellano et al. 2010), we investigated the other enzymes in this pathway. There was a strong increase in the protein levels of PYCR1 and PYCR2, whereas the levels of the delta-1-pyrroline-5-carboxylate dehydrogenase (ALDH4A1) and proline dehydrogenase 1 (PRODH), which catalyse the reverse reaction from proline to glutamate (Pérez-Arellano et al. 2010), were normal (Figure 3.34B). Transcript levels of the genes in this

pathway showed a similar direction as the protein levels with increased levels of *Aldh18a1* and *Pycr1*, and decreased levels of *Aldh4a1*. To assess the effect of this protein imbalance in the metabolic flux, we determined the levels of glutamate and proline by targeted metabolomics and found a drastic increase in the proline to glutamate ratio in the knockout mouse hearts (Figure 3.34C). Similar to the 1C pathway, temporal proteomic analysis in the *Lrpprc* knockout showed a steep increase of ALDH18A1 levels early in the progression of OXPHOS dysfunction (Figure 3.34D)

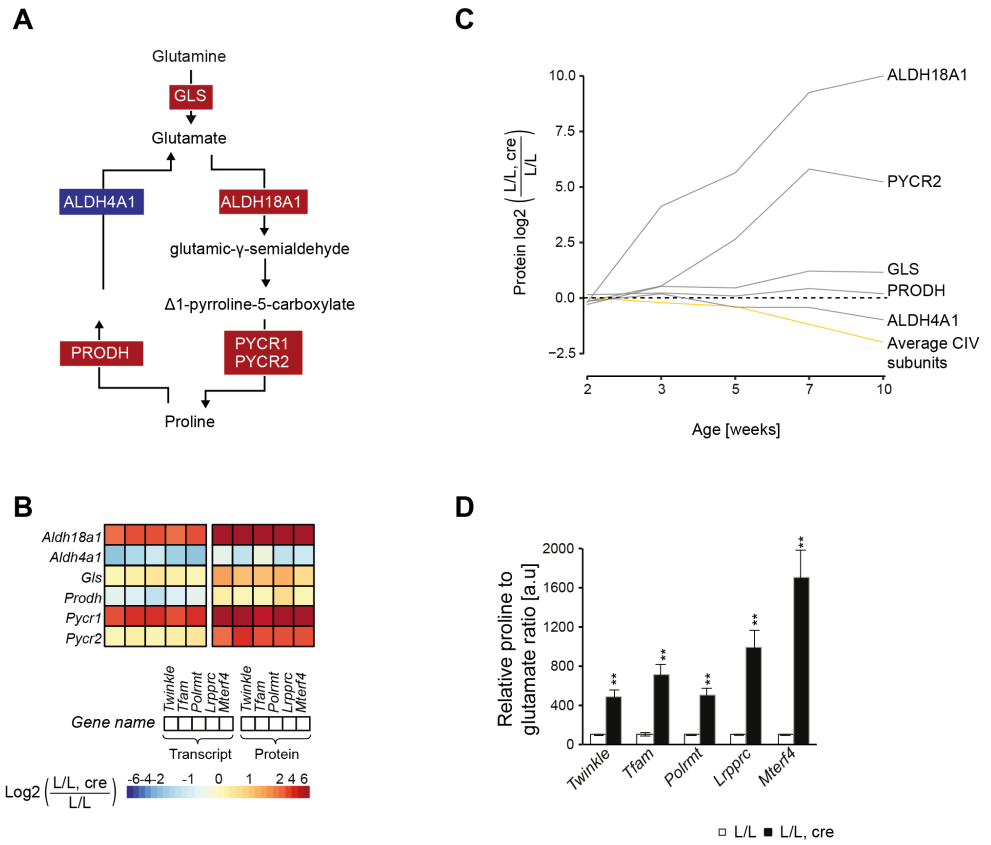

Figure 3.34 | Increased proline synthesis from glutamate upon OXPHOS dysfunction
(**A**) Scheme of glutamate to proline conversion pathway. Coloured boxes represent protein levels; red: increased, blue: decreased. (**B**) Heatmaps illustrating the fold-change in transcript (left) and protein (right) levels of knockouts (L/L, cre) and control (L/L) mouse hearts. (**C**) Time-course analysis of protein levels of enzymes of the glutamate to proline conversion pathway quantified in *Lrpprc* L/L, cre compared to L/L. Adjusted p across time <0.05. Yellow line: average value of OXPHOS complex IV (CIV) subunits. (**D**) Quantification of proline to glutamate ratio in L/L, cre and L/L hearts. **p<0.01; error bars ± sem. From Kühl, Miranda et al. 2017.

To identify additional early markers of OXPHOS deficiency, we performed clustering analysis with the significantly changed proteins in the *Lrpprc* time-course mitoproteome (Figure 3.19B). Two clusters presenting opposite patterns showed marked changes in protein levels at 3 weeks of age (Figure 3.35). The first cluster contained LRPPRC and its interacting partner SLIRP that rapidly decline after birth due to knockout of *Lrpprc* in the heart (Figure 3.19C). The second cluster contained proteins that were strongly upregulated and includes MTHFD2, ALDH18A1, amine oxidase [flavin-containing] A (MAOA), phosho-enol pyruvate carboxykinase (PCK2), MTHFD1L, and PYCR1. The identification of 1C pathway and proline biosynthesis

enzymes in this cluster is a proof of concept that our integrated omics approach comparing different knockout mouse strains deficient of mtDNA gene expression combined with the time-course analysis in the *Lrpprc* knockout can be used to identify early markers of the progression of OXPHOS deficiency.

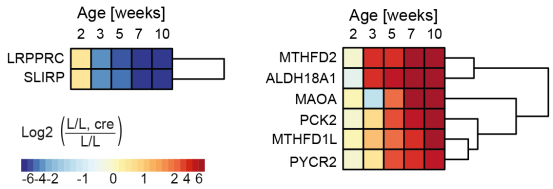

Figure 3.35 | Early markers of OXPHOS dysfunction
Heatmaps illustrating proteins that decrease (left) and increase (right) early in time-course analysis of *Lrpprc* knockouts (L/L, cre) and controls (L/L) mouse hearts at different ages.

4. DISCUSSION

Mammalian mtDNA codes for a handful of genes and the mitoproteome contains a few thousand proteins. The fact that all the components required to express mtDNA are encoded in the nucleus raises the question of how the two cellular genomes coordinate and regulate their expression to build and maintain a functional OXPHOS system. In this thesis we address two aspects of this fundamental question. First, we investigated the *in vivo* function of POLRMT in the regulation of mtDNA replication and transcription as well as its potential role coordinating nDNA and mtDNA gene expression programs via its nuclear isoform spRNAP-IV. Second, we studied the molecular consequences of impaired mtDNA gene expression as well as the secondary cellular responses, both locally at the mitoproteome level but also globally at the cellular gene expression level.

The *POLRMT* gene was reported to code for two different single-subunit RNA polymerases, i) POLRMT that transcribes mtDNA and ii) spRNAP-IV that has been proposed to transcribe a specific subset of nuclear genes. The regulation of gene expression of both cellular genomes under the control of a single gene is an interesting possibility to coordinate the crosstalk between the two genetic systems. However, we did not find the mRNA of the reported nuclear splice variant in mouse tissues or human cell lines using RT-PCR analyses. Furthermore, using an antibody that recognizes both protein isoforms, we only detected a protein of the size of POLRMT (~140 kDa) that exclusively localizes in mitochondria. Finally, knocking out both putative *Polrmt* gene products in mouse had no effect in the transcript levels of the genes reported to be transcribed by spRNAP-IV. Therefore, we conclude that the *POLRMT* gene only encodes a mitochondrial protein with an exclusive function in this organelle in mammals.

Importantly, loss of POLRMT had a severe effect on mtDNA gene expression. Disruption of *Polrmt* in heart caused a global decrease of mt-RNAs and abolished *de novo* transcription, demonstrating that no other RNA polymerase can replace POLRMT in mammalian mitochondria. Although there was a strong decrease in all mt-RNAs in the *Polrmt* knockout hearts, we found that the transcripts encoded on the L strand were less reduced than the transcripts encoded on the H strand. Previous studies have reported the stabilization of L-strand transcripts, in particular *mt-Nd6* when silencing or knocking out the *Lrpprc* gene (Ruzzenente et al. 2012; Wolf & Mootha 2014). LRPPRC levels are strongly reduced in the *Polrmt* knockouts consistent with the previously observed correlation between LRPPRC and mt-mRNA levels (Lagouge et al. 2015). Since LRPPRC binds all mt-mRNAs, the reduced stability in the absence of *Lrpprc* could be explained by loss of polyadenylation which does not affect *mt-Nd6* (Siira et al. 2017). Furthermore, *Polrmt* and *Lrpprc* knockout mice have

increased levels of GRSF1 which has been suggested to interact and regulate *mt-Nd6* and its precursor strand (Antonicka et al. 2013; Jourdain et al. 2013). A compensatory stabilization of mature mt-mRNAs was previously reported upon knockdown of *POLRMT* in human cell lines (Wolf & Mootha 2014). However, it is unlikely that the strand-specific effect observed in the *Polrmt* knockout is explained by differences on the individual transcript stabilities because mt-mRNAs, mt-rRNAs and mt-tRNAs are all stabilized by different mechanisms (Rorbach & Minczuk 2012).

Differences in promoter strength between HSP and LSP have been reported but remain controversial as *in vitro* transcription experiments can be strongly influenced by reaction conditions and the promoter template used (Morozov & Temiakov 2016; Shi et al. 2012). A recent study showed that the pre-IC complex has a similar topology in both promoters based on crosslinking studies between TFAM and promoter sequences. According to this model, transcription machineries can assemble in both promoters and, in that way, be regulated simultaneously (Morozov & Temiakov 2016). On the contrary, previous studies have shown that LSP is a stronger promoter and its activity is strictly dependent on TFAM binding even under permissive conditions that allow promoter breathing like supercoiling or low salt concentrations (Lodeiro et al. 2010; Shi et al. 2012). This suggests that different structural requirements can apply to each promoter. Our *in vitro* transcription data using a single template containing both HSP and LSP show that transcription from LSP is better maintained than transcription from HSP when POLRMT:DNA ratios are low. Importantly, TFAM and TFB2M concentrations were maintained constant in this experiment. Together with the specific mt-RNA abundance pattern, our data indicates that there is a differential regulation of the promoters *in vivo* when POLRMT levels are low.

The defect in mtDNA replication provides conclusive evidence that transcription initiation from LSP forms the primer required for mtDNA replication at O_H and no other primase can compensate for this function in the absence of POLRMT. Differential regulation of LSP compared to HSP could reflect a preference to use LSP-mediated transcription initiation to maintain mtDNA replication. Under normal conditions, most of the replication events are prematurely terminated generating 7S DNA (Bogenhagen & Clayton 1978). When *Polrmt* is depleted 7S DNA is not formed suggesting that most of the residual replication events continue to full length replication. Furthermore, there is a strong increase in the levels of TWINKLE and the levels of TFAM are not changed despite the strong mtDNA depletion. Overexpression of these two factors have been shown to increase mtDNA copy number (Ekstrand et al. 2004; Kukat et al. 2015; Milenkovic et al. 2013). Although the exact mechanism by which TWINKLE regulates mtDNA copy number is unknown, this factor can be loaded at the 3' end of 7S DNA to promote full length replication (Jemt et al. 2015).

The interdependence of TFAM and mtDNA has been shown in different mouse models (Ekstrand et al. 2004; Larsson et al. 1994; Kukat et al. 2015) and it was suggested that mtDNA-free TFAM turnover is mediated by LONP1 (Lu et al. 2013; Matsushima et al. 2010). Remarkably, the *Polrmt* knockout is the first model where TFAM levels are stable despite the strong mtDNA depletion and increased LONP1 levels. Importantly, *Tfam* transcript levels were upregulated suggesting a transcriptional compensatory response to maintain TFAM levels in mitochondria. TFAM stability in the *Polrmt* knockout could be explained by TFAM binding to other proteins or to different post-translational modifications (King et al. 2018). Comparing the post-translational modifications or interaction partners of TFAM in the *Polrmt* knockout to other mouse models where TFAM and mtDNA levels correlate like *Twnk* or *Mterf4* knockouts would provide important insights into the regulation of TFAM and mtDNA copy number.

Finally, we did not detect accumulation of the *7S* RNA transcript in the *Polrmt* knockout further suggesting that when POLRMT levels are low, LSP-transcription initiation is dedicated to maintain productive mtDNA replication. Based on our *in vivo* findings, we propose that promoter-specific transcription initiation can fine-tune the balance between mtDNA replication and transcription and this mechanism is active when POLRMT levels are low as illustrated in Figure 4.1.

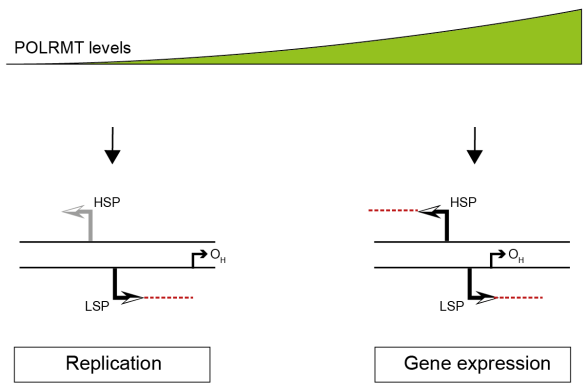

Figure 4.1 | Model of POLRMT regulating replication primer formation and mtDNA gene expression
At low POLRMT levels only LSP is active and generates the RNA primer for mtDNA replication. At high POLRMT levels, transcription initiation is activated from HSP and LSP resulting in mtDNA gene expression. Abbreviations in alphabetical order: HSP, H-strand promoter; LSP, L-strand promoter; O_H, heavy-strand origin of replication; POLRMT, mitochondrial RNA polymerase. Modified from Kühl et al. 2016.

Our data on the heterozygous *Polrmt* knockout and *Polrmt* overexpressor mice verifies that mitochondrial transcription is a very robust process with multiple levels of regulation. Despite the decrease in POLRMT levels, the heterozygous *Polrmt* knockout mice maintain the steady-state mt-RNA levels and have no differences in mtDNA synthesis indicating that one copy of *Polrmt* is sufficient to maintain mtDNA replication and transcription. Interestingly, we found increased TEFM protein levels in these mice suggesting that the decreased POLRMT levels are compensated by promoting transcription elongation. The *Polrmt* overexpressor mouse showed increased *de novo* transcription proportional to the levels of POLRMT. Since the protein levels of the other transcription factors, TFAM, TFB2M and TEFM are not changed in this mouse model, the increase in *de novo* transcripts suggests that a 50% increase of

POLRMT is sufficient to upregulate mtDNA transcription; in other words, POLRMT is a limiting factor for transcription in mammalian mitochondria. The formation of the mitochondrial transcription initiation complex and the transition to elongation are rate-limiting steps in *in vitro* transcription of mtDNA (Lodeiro et al. 2010). In line with this, our *in vivo* findings suggest that engaging more mtDNA molecules in transcription by increasing POLRMT levels or promoting transcription elongation by increasing TEFM are potential mechanisms to regulate mitochondrial transcription *in vivo.* Furthermore, increased POLRMT levels have been found in different mouse models of mitochondrial dysfunction (Milenkovic et al. 2013; Perks et al. 2018; Kauppila et al. 2018), indicating that regulating POLRMT levels is a compensatory mechanism operating when mtDNA gene expression in impaired *in vivo.*

Contrary to the increased *de novo* transcription, steady-state transcript levels in the *Polrmt* overexpressor mice do not reflect a general increase in mitochondrial transcription as only *7S* RNA, precursor *mt-Nd5/mt-Cytb*, and *mt-Tf* are mildly increased. Thus, one possibility is that POLRMT promotes transcription of polycistronic transcripts *in vivo*, but the transcripts are not stabilized. The observed increase in precursor transcripts would support this scenario but it is a very mild effect. Furthermore, we did not find differences in the steady-state transcript levels after parallel overexpression of the mt-mRNA stabilizing factor *Lrpprc* together with *Polrmt.* Although we cannot exclude that other factors in addition to LRPPRC are limiting the stabilization of newly synthesized transcripts in the *Polrmt* overexpressor mice, we did not find differences in the transcript stability in pulse-chase *de novo* transcription experiments. This suggests that isolated mitochondria with increased POLRMT levels in energizing buffer conditions results in increased transcription and normal transcript processing and stability without the requirement of additional factors.

Another possibility is that the *in organello* transcription does not reflect the *in vivo* situation but rather the transcription capacity and that in the mouse heart the additional levels of POLRMT lead to increased mitochondrial transcription initiation but is not continued to generate full-length polycistronic transcripts. The robust accumulation of *7S* RNA transcript is consistent with a strong increase in LSP-initiated transcription in the *Polrmt* overexpressor mice and occurs in most of the tissues evaluated and throughout different ages. Although the function of the *7S* RNA is largely unknown, our findings support the hypothesis that *7S* RNA is an abortive transcription product that accumulates when LSP-initiated transcription is not used to generate mtDNA replication primers or full-length polycistronic transcripts. In line with this and the model presented in Figure 4.1, the effect of *Polrmt* overexpression on mtDNA replication is minor. With the experiments performed so far, we cannot differentiate whether the higher levels of *7S* RNA compared to the HSP-proximal transcript *mt-Tf* reflect differences in the stability of these two transcripts or increased LSP transcription initiation. Interestingly, silencing *TEFM* in human cells results in a gradual decline of the mt-RNAs proportional to the

distance of the promoter, but also in an accumulation of LSP-proximal *mt-Tp* (Minczuk et al. 2011) supporting that POLRMT is constantly reloading at the promoters to initiate transcription. In agreement with our findings, Surovtseva and collaborators reported that overexpression of *POLRMT* in HeLa cells did not affect steady-state mt-mRNA levels; however, they report a mild decrease in respiration and in the steady-state protein levels of the mt-CO2 (Surovtseva & Shadel 2013), that we do not find in our mice. This discrepancy can be explained by the differences in the model organism and the level of overexpression of *POLRMT*.

In the nucleus, protein-coding genes are typically present in two copies per cell and, therefore, activation of a large number of genes is controlled by different combinations of transcription factors binding to the promoter regions. In contrast to the nucleus, mtDNA is present in multiple copies in the cell and all the genes are controlled by only two promoters. This means that mtDNA transcription can be regulated by engaging more mtDNA templates in transcription, increasing transcription from HSP and LSP, or a combination of both. Our *in vivo* data suggests that under normal physiological conditions POLRMT is constantly initiating transcription at available templates but most of this transcription is abortive and results in *7S* RNA products, similar to the *7S* DNA product that is synthesized after mtDNA replication start (Bogenhagen & Clayton 1978). Increasing POLRMT levels either increase transcription initiation from each promoter and/or engage more mtDNA molecules in transcription which would explain the increased transcription capacity in the *Polrmt* overexpressor mice and the accumulation of promoter-proximal transcripts. An increase in TEFM observed in the heterozygous *Polrmt* knockout, would result in the stimulation of productive transcription elongation and evens the transcription rate despite reduced POLRMT levels. However, the balance between mtDNA replication and transcription is not likely mediated by template availability as both machineries require access to the NCR. We thus propose that differential promoter-specific transcription initiation via POLRMT is part of a mechanism mediating this balance as our data suggests that when POLRMT levels are low transcription initiation from LSP is favoured to maintain mtDNA replication (Figure 4.1).

Previous studies from our laboratory have shown that mt-mRNAs are in excess in mammalian mitochondria as mice can tolerate relatively well severe reductions in steady-state transcript levels (Lagouge et al. 2015). This raises the question of why it is important to regulate mitochondrial transcription in the mammalian system. Our multi-omic comparison of hearts from five different knockouts identified that the abundance of nDNA-encoded proteins of complexes of dual genetic origin, *i.e.* the OXPHOS complexes and the mitoribosome, are regulated at the post-transcriptional level. However, the abundance of the complex reflects the expression of mtDNA. On the one hand, the five knockout mouse strains have impaired mtDNA

gene expression and, therefore, the mtDNA-encoded proteins are strongly reduced in all the mouse strains. Consequently, most of the OXPHOS complexes containing mtDNA-encoded proteins decline. On the other hand, disrupting different steps of mtDNA gene expression results in differences in mt-rRNAs levels which are reflected in the abundance of the mitoribosomal proteins. In *Escherichia coli* subunits of multiprotein complexes are produced proportional to their required stoichiometry and synthesis is regulated at the translation level as they are encoded in polycistronic mRNAs (Li et al. 2014). In mammals, a small percentage of the proteins, mainly components of protein complexes, are degraded in a non-exponential manner, which means they are rapidly degraded in the first few hours after synthesis and then stabilized with time (McShane et al. 2016). Our data supports that the few genes encoded by the mtDNA are limiting factors that regulate the protein complex abundance in the complexes of dual genetic origin. In this way, nDNA encoded proteins are produced in excess, imported into mitochondria and assembled into the complexes or degraded. This model is supported by the fact that mtDNA-encoded proteins are required for early steps of assembly of OXPHOS complexes I, III, and IV (Fernandez-Vizarra & Zeviani 2018; Guerrero-Castillo et al. 2017; Stroud et al. 2015) and that the mitoribosome assembly initiates co-transcriptionally (Rackham et al. 2016). On the contrary, in complex V that can form sub-assembled complexes, the mtDNA-encoded subunits are part of the later assembly stages (He et al. 2018). Furthermore, a recent study using SILAC pulse-chase experiments showed that the mitoribosomal proteins are indeed produced in excess and degraded when they are not assembled (Bogenhagen et al. 2018). Although, we show that biogenesis of complexes of dual genetic origin does not result from proportional transcript synthesis in both genomes, the question remains whether there is a coordination at the translational level as it has been proposed in yeast and for *mt-Co2* in mammalian cells (Couvillion et al. 2016; Richter-Dennerlein et al. 2016). We propose that regulating the expression of mtDNA that only encodes a few genes under the control of two promoters is much more efficient than regulating the expression of the ~180 nDNA encoded genes that form the OXPHOS complexes and the mitoribosome. Thus, robust regulation of mtDNA is required to rapidly respond to changes in the cellular energetic demands.

The multi-omics systematic study presented in this thesis revealed a wholesome remodelling of the cellular transcriptome and mitochondrial proteome as a consequence of loss of mtDNA gene expression. This reflects the extent of the secondary cellular responses evoked by the primary OXPHOS defect. Although, some of these secondary responses can be adaptive to maintain mitochondrial function over certain physiological ranges, in a pathogenic situation they are not sufficient to compensate for the primary defect and can further contribute to the disease progression. The latter is supported by the recent successful

reports where the phenotype of mitochondrial disease mouse models is improved after treatment with rapamycin (Felici et al. 2017; Johnson et al. 2013; Khan et al. 2017; Siegmund et al. 2017) or hypoxia (Ferrari et al. 2017; Jain et al. 2016) without fixing the primary defect. However, the mechanisms by which mTORC1 inhibition or activation of hypoxia responses reduce the progression of mitochondrial disease are still unknown and can be explained by the contribution of secondary responses to the pathogenic process, a different modulation of cellular metabolism that partially bypasses the mitochondrial defect, or probably a combination of both. Nevertheless, ascertaining which are the secondary responses, how they contribute to disease progression, and in which settings are they triggered is an important endeavour to understand mitochondrial diseases and develop effective diagnostic and treatment strategies.

We found that impaired mtDNA gene expression in mouse heart results in secondary Q deficiency caused by defective intra-mitochondrial Q biosynthesis that correlates with the progressive OXPHOS deficiency. Q deficiency caused by downregulation of the cytosolic mevalonate pathway was shown to drive respiratory defect in a mitofusin 2 (*Mfn2*) knockout mouse (Mourier et al. 2015). This indicates that the defect of the intra-mitochondrial Q biosynthesis that we report here is specific to loss of mtDNA gene expression and not a common secondary consequence of mitochondrial dysfunction. Although the function of several of the Q biosynthesis enzymes is not known, it has been shown that they form a complex in the inner mitochondrial membrane (Stefely & Pagliarini 2017). Since the abundance of the OXPHOS complexes is not affected in the *Mfn2* knockout and the decline in Q biosynthesis enzymes is not regulated at the transcriptional level, it is possible that the loss of membrane integrity caused by the decreased OXPHOS complexes leads to the instability of the Q biosynthesis complex. As it occurs in the *Mfn2* knockout and in patients with autosomal recessive mutations in genes of the Q biosynthesis pathway (Garrido-Maraver et al. 2014; Wang & Hekimi 2016), Q deficiency can further aggravate the OXPHOS deficiency in these mouse models. Q supplementation is a common treatment for mitochondrial diseases but its efficacy has been questioned due to contradicting clinical trial results (Pfeffer et al. 2013). Our study provides experimental evidence to support that impaired mtDNA gene expression, which is found in a large number of mitochondrial patients, can develop secondary Q deficiency and would benefit from Q supplementation. Patients with inherited autosomal recessive forms of Q deficiency respond well to oral Q supplementation. Therefore, we propose that Q measurements should be performed in all patients with mitochondrial disease and clinical trials of Q supplementation focused in patients with impaired mtDNA gene expression should be performed.

The integration of transcriptomic and proteomic data also allows the identification of mitochondrial processes affected by OXPHOS deficiency that are regulated at the

transcriptional level and, therefore are controlled by nDNA transcription programs. Enrichment analyses combining canonical pathways and transcription factors including the differentially expressed genes in all the knockouts predicted that the ATF family of transcription factors and MYC were enriched in our datasets as well as genes involved in cellular signalling pathways including eIF2, eIF4, calcium and mTOR. We evaluated the expression levels of the target genes of ATF4 and MYC using published chromatin immunoprecipitation sequencing (ChIP-Seq) data sets (Han et al. 2013; Seitz et al. 2011) and found several of them to be mostly upregulated, in particular the ATF4 targets. During the course of this thesis several reports linking mitochondrial dysfunction to the activation of ATF4 transcriptional program via eIF2α and/or mTORC1 were published (Bao et al. 2016; Dogan et al. 2014; Khan et al. 2017; Quirós et al. 2017). Within the ATF4 targets there are several enzymes involved in the mitochondrial 1C pathway and synthesis of proline from glutamate. These pathways included some of the most upregulated genes in transcript and protein levels in the five different knockouts and its miss-regulation shifted the abundances of metabolites involved. Remodelling of the serine synthesis and 1C pathway was also identified in cell lines expressing a dominant negative form of *POLG* (Bao et al. 2016), cell lines treated with different mitochondrial poisons (Quirós et al. 2017), flies expressing *Pink1* mutations leading to mitochondrial dysfunction (Tufi et al. 2014), and a mouse model with mtDNA deletions that results in mitochondrial myopathy (Tyynismaa et al. 2010; Nikkanen et al. 2016), indicating that it is a common effect that occurs in mitochondrial dysfunction.

Today, most of the mitochondrial stress responses are attributed to the activation of ATF4 via the cellular ISR as eIF2α has been shown to be phosphorylated in different model systems of mitochondrial dysfunction (Khan et al. 2017; Quirós et al. 2017). While it remains to be confirmed whether *Myc* is upregulated in other models of mitochondrial dysfunction or only in mouse heart, within the MYC target genes there are several of the target genes reported to be activated by ATF4 and part of the proposed mitochondrial-stress activated ISR including *Gdf15, Lonp1, Mthfd2, Phgdh* and *Psat1.* Furthermore, in addition to *Lonp1,* MYC target genes also include the chaperones *Hspa9* (mtHSP70) and *Hspe1* that are increased in different models of mitochondrial dysfunction and are currently used as makers of mtUPR (Khan et al. 2017; Münch & Harper 2016; Seiferling et al. 2016). Our work underscores that the transcriptional programs activated upon mitochondrial dysfunction result from the synergistic action of different transcription factors *in vivo*. These transcription factors likely include different members of the ATF family of transcription factors, MYC, and potentially factors modulating mitochondrial biogenesis that might not be regulated at the transcript level and, therefore, we did not identify in our analyses. It is important to consider that most of the studies, including the one presented in this thesis, predicted the activation of ATF4 and its target genes based on enrichment of conserved regulatory sequences and/or ChIP-Seq data sets in the

differentially expressed genes. However, to our knowledge, the direct action of ATF4 has only been verified in a handful of genes (~10 different in total in all the studies) in the context of mitochondrial dysfunction (Bao et al. 2016; Quirós et al. 2017).

Comparing the same tissue in five isogenic knockout mouse models with defects in mtDNA gene expression leading to a similar primary OXPHOS defect and housed under the same controlled environmental conditions, identified ~5000 differentially expressed transcripts, from which ~1500 are common for all the knockouts. Since our knockout models have severe mitochondrial dysfunction leading to dilated cardiomyopathy, the transcriptional changes identified in the end-stage reflect the responses to the primary OXPHOS defect, to secondary metabolic alterations, and to the severe cardiomyopathy. Furthermore, our temporal proteomic analysis in the *Lrpprc* knockout revealed that the increase of the 1C pathway and proline synthesis enzymes is detectable early in the progression of OXPHOS deficiency. This finding is consistent with the early expression of *Atf4* and FGF21 in the heart of a *Dars2* knockout mouse (Dogan et al. 2014) and supports that some nuclear transcriptional responses are triggered before measurable OXPHOS deficiency develops in mouse heart. Taking these findings into consideration, during the last years we have advanced substantially identifying miss-regulated processes in mitochondrial dysfunction and some of the upstream factors regulating these processes, but we still cannot differentiate proximal consequences of OXPHOS dysfunction from secondary ripple-effects.

5. CONCLUSION AND FUTURE PERSPECTIVES

The comprehensive analysis presented in this thesis that includes transcriptomics, proteomics and metabolomics in different well-characterized mouse models with impaired mtDNA gene expression show the extent to which mtDNA is determinant in the biogenesis of complexes of dual genetic origin in comparison with nDNA. Therefore, regulation of mtDNA gene expression is fundamental for proper mitochondrial function and allows local and rapid adaptation to changes in the energetic or metabolic demands. The extensive resources generated are a valuable source to generate hypothesis to study unsolved fundamental mitochondrial biology questions, understand pathophysiology of human diseases, identify biomarkers to diagnose mitochondrial diseases, and provide experimental rational for patient treatment.

To exemplify, the specific pattern of mitoribosomal protein abundance can be used to identify core mitoribosomal proteins or proteins whose stability depends on the presence of the mitoribosome. As proof of principle, the mitochondrial 28S ribosomal protein 36 (MRPS36), which is still reported as a mitoribosomal subunit in the Uniprot database, did not show the same profile of gene expression as the other mitoribosomal subunits. MRPS36/KGD4 was reported to have a conserved role in the organization of mitochondrial α-ketoglutarate dehydrogenase complex instead of the mitoribosome in *Saccharomyces cerevisiae* (Heublein et al. 2014) and was not identified in the structure of the human mitoribosome (Amunts et al. 2015). On the contrary, the mitochondrial ribosome associated GTPase 1 (MTG1) and the mitochondrial translation initiation factor 3 (MTIF3) showed the same pattern as the mitoribosomal proteins. Both, MTG1 and MTIF, were reported to interact with the large mitochondrial subunits (Kotani et al. 2013; Koc & Spremulli 2002).

Another interesting example is the changes in the abundance of the mitoribosome in control mice after three weeks of age. This decrease could explain the longer lifespan of knockout models with impaired mitochondrial translation (Cámara et al. 2011; Metodiev et al. 2009; Metodiev et al. 2014; Park et al. 2007). The mouse heart has been established as good model system for the human heart (Wessels & Sedmera 2003). Interestingly, in mitochondrial patients, severe defects in mtDNA translation usually manifest as fatal perinatal or early-infantile rapidly progressive cardiomyopathies. However, the few patients that survive show a spontaneous stabilization of the heart condition at around 6 years of age (Gorman et al. 2016). It is possible that a reduced requirement of mitochondrial translation after a certain time threshold as we report in mice, explains the stabilization in these patients.

The abundance of some enzymes that are strongly upregulated in affected tissues and the metabolic changes caused their altered steady-state levels should be evaluated as early biomarkers of mitochondrial dysfunction and the progression of OXPHOS deficiency. Furthermore, elucidating whether the secondary responses are adaptive or maladaptive can

result in targeted treatment strategies as suggested with the Q supplementation for patients with primary mtDNA gene expression defects.

With regard to the regulation of mtDNA transcription by POLRMT, there are several questions that we are further investigating. First, we want to elucidate whether LSP activity is only increased when POLRMT levels are low or it is a constitutive characteristic of the promoters *in vivo* that is enhanced in the *Polrmt* knockout conditions. This question can be addressed by evaluating whether the accumulation of *7S* RNA in the *Polrmt* overexpressor mice results from increased transcription initiation from LSP in comparison to HSP or increased transcript stability. Second, we are currently performing exercise challenges in the *Polrmt* overexpressor mice to investigate whether the increase in transcription initiation is advantageous when a boost in mitochondrial biogenesis and function is stimulated. Third, we are performing POLRMT pulldowns to identify potential interaction partners or post-translational modifications mediating the function of this enzyme. This could provide valuable information on the regulation of POLRMT binding to the promoter regions, transcription, and the crosstalk between mtDNA replication and transcription. Finally, we are interested in understanding how POLRMT levels are regulated in different models of mitochondrial dysfunction. In the cancer field, it has been proposed that *Polrmt* is regulated by the MYC transcription factor (Oran et al. 2016). However, despite the strong increase in *Myc* transcript levels and several of its target genes, *Polrmt* transcripts are not increased in *Tfam, Twnk, Lrpprc* or *Mterf4* knockouts suggesting that a different mechanism is mediating the increased POLRMT levels.

To understand the pathogenesis of OXPHOS dysfunction, the differentiation of proximal consequences of OXPHOS dysfunction from secondary ripple-effects, is still an important yet challenging venture that requires multidisciplinary approaches to address. Obtaining a better time-resolution early in the progression of OXPHOS deficiency will be important to distinguish early transcriptional responses from later ones. Furthermore, complementation with metabolic measurements (both steady-state and changes in the fluxes) could help identify early changes in mitochondrial function that lead to nuclear transcriptional responses. As the transcription factors identified so far can have broad downstream targets, determining which targets they are binding to in a mitochondrial dysfunction setting would help to define the different transcription programs. Disrupting the activity of these factors *in vivo* would have a profound effect on many cellular aspects and their role in mitochondrial dysfunction would be difficult to differentiate. Therefore, identifying the genes that these transcription factors bind *in vivo* in current models of mitochondrial dysfunction using techniques like ChIP-Seq or DNA affinity purification sequencing (DAP-Seq) would provide

more conclusive experimental evidence of the transcriptional programs they regulate in this specific context.

Studying the effects of each miss-regulated pathway in detail would help to understand the net effect of that pathway to the end pathology. For example, recent studies have knocked out enzymes of the mitochondrial 1C pathway and identified that it is important to maintain mitochondrial translation (Minton et al. 2018; Morscher et al. 2018). However, it has not been studied yet what happens when the enzymes are overexpressed as it occurs in mitochondrial dysfunction and whether the net-effects observed (increased levels of enzymes, THF-intermediates, and decreased formate) result from the upregulation of the enzymes or changes in the redox balance as NAD^+/NADH and $NADP^+$/NADPH are cofactors required for these reactions. The definition and mechanistic study of these processes will be important to understand which nDNA responses contribute to compensate for a primary OXPHOS defect, aggravate the disease progression, or induce gene expression changes reflected in the transcript and protein levels that correlate with mitochondrial dysfunction but are neither beneficial or harmful. Furthermore, it would help explain the end pathology that results from a primary OXPHOS defect and provide valuable information to understand the broad clinical spectrum and pleiotropic tissue manifestations of these diseases.

Finally, understanding how these processes result in mitochondrial diseases can be translated to understand the contribution of mitochondrial dysfunction to other common human pathologies with similar molecular signatures. To exemplify, the 1C pathway enzymes, *Mthfd2* and *Shmt2,* and the enzyme involved in proline synthesis from glutamate, *Pycr1*, have also been identified as highly upregulated in human tumors (Nilsson et al. 2014). Moreover, the same expression pattern that we report for the proline synthesis from glutamate was found in cancer cell models and suggested to be mediated by MYC (Liu et al. 2012). Importantly, the proteomic, transcriptomic, and metabolomic findings we report in mouse should be corroborated in patient samples.

6. MATERIALS AND METHODS

6.1. Experimental models

6.1.1. Mouse strains

The targeting vector to disrupt *Polrmt* in embryonic stem cells (derived from C57Bl/6N mice) was generated using BAC clones from the RPC10-731 BAC library by TaconicArtemis GmbH. Exon 3 of *Polrmt* locus was flanked by loxP sites and a positive selection marker (PuroR) flanked by FRT sites was introduced into intron 2. The puromycin resistance cassette was removed by mating the *Polrmt* $^{+/loxP\text{-}pur}$ mice with transgenic mice ubiquitously expressing *flp* recombinase that recognizes the FRT sites. Next, the resulting *Polrmt*$^{+/loxP}$ mice were mated with transgenic mice ubiquitously expressing the *cre* recombinase under the control of the β-actin promoter (*β-actin cre*) to generate heterozygous knockout *Polrmt*$^{+/-}$ mice. Heart- and skeletal muscle- specific knockouts for *Twnk*, *Tfam*, *Polrmt*, *Lrpprc*, and *Mterf4* were obtained by mating mice containing an exon of the gene of interest flaked by loxP sites with mice expressing the *cre* recombinase from the muscle creatinine kinase promoter (*Ckmm-cre*). The targeting strategy for the generation of *Twnk, Tfam, Lrpprc* and *Mterf4* were published previously (Table S1 in supplementary material section 8.2).

BAC clones containing a fragment of chromosome 10, including *Polrmt*, were purchased from the C57Bl/6N BAC library of DNA Bank, RIKEN BioResource Center. The BAC library was generated in the pBAC3.6 vector. The BAC clone BgN01-092D16 was modified by Red/ET recombination using the counter-selection BAC modification kit (Genebridges). A silent point mutation was introduced into exon 3 leading to a unique HindIII restriction site. Briefly, to modify the BAC, streptomycin-resistant bacteria containing the BAC clone were transformed with a temperature sensitive pRed/ET plasmid that encodes the proteins required for homologous recombination. Then, the bacteria were transformed with a PCR-generated fragment containing *Polrmt* sequences flanking the mutated regions, the mutations, and a cassette that confers resistance to kanamycin and susceptibility to streptomycin. Finally, to replace the antibiotic resistance cassette, bacteria were transformed with a PCR-generated fragment containing the *Polrmt* sequences flanking the mutated regions and the mutations. Positive clones were selected for streptomycin resistance and verified by PCR followed by restriction digest, Sanger sequencing, and Southern blotting (section 6.3.6). All transformations were performed by electroporation at 1350 V and 5 msec. Modified BAC was purified via caesium chloride gradient (section 6.3.2) and injected into the pronucleus of fertilized oocytes. Transgenic BAC lines were maintained as heterozygous. List of transgenic lines used in this thesis is in table S1 and genotyping primers is in table S2.

Animals were housed in individually ventilated cages under specific-pathogen-free conditions with constant temperature (21°C) and humidity (50 - 60%) and a 12 h light/dark cycle. All mice were fed commercial rodent chow and provided with acidified water ad libitum. Mice were sacrificed by cervical dislocation. The health status of the animals is specific pathogen free according to the Federation of the European Laboratory Animal Science Association (FELASA) recommendations. All animal procedures were conducted in accordance with European, national and institutional guidelines and protocols (no.: AZ.: 84-02.05.50.15.004 and AZ.: 84-02.04.2015.A103) were approved by the Landesamt für Natur, Umwelt und Verbraucherschutz, Nordrhein-Westfalen, Germany.

6.1.2. Cell lines

HeLa (ATTC CCL-2) and 143B (CRL8303) cells were maintained at 37°C and 5% CO_2 in Dulbecco's modified eagle medium with high glucose (DMEM GlutaMax, 4.5 g/L glucose, Gibco) and supplemented with 10% foetal bovine serum (Gibco) and 1% Penicillin/Streptomycin (Gibco). 143Bρ^0 (King & Attardi 1989) cell culture media was supplemented with uridine (50μg/mL). All cell lines were tested to be negative for Mycoplasma.

6.2. Methods in cell culture

6.2.1. Cell harvesting and passaging

Cells were passaged when they reached 80 - 100% confluency. To harvest the cells, the culture media was removed and the cells were washed with Dulbecco's modified PBS (DPBS, Gibco) to remove residual traces of the culture medium. Next, 0.05% trypsin/0.02% EDTA (Gibco) was added to the cells followed by a 5 min incubation at 37°C under a 5% CO_2 atmosphere to detach the adherent cells from the culture flasks. The detached cells were resuspended and passaged to a new flask containing fresh culture media.

6.2.2. Cell thawing and freezing

Cells were harvested as described in section 6.2.1 and resuspended in freezing media (DMEM GlutaMax, 4.5 g/L glucose, supplemented with 20% FBS and 10% DMSO). Cells were transferred to a cryo-vial (Nalgene) and placed in a Mr. Frosty Cryo container (Nalgene) with isopropanol, placed at -80°C for 24 h and then transferred to a liquid nitrogen tank for long term storage. To thaw, cells were transferred directly from the cryo-storage liquid nitrogen tank, to a 37 °C water bath. After thawing, the cells were transferred on T175 culture flasks with standard pre-warmed cell culture medium. The medium was changed after 24 h.

6.2.3. Transfection of mammalian cells

Transfection of cell lines to was performed by lipofection using lipofectamine 2000 or 3000 (Invitrogen) for expression vectors and lipofectamine RNAi max (Invitrogen) for small interference RNA (siRNA). For mammalian expression vectors, 70 - 80% confluent cells were transfected according to manufacturer's instructions for 24 - 48 h. For siRNA, 50% confluent cells were transfected and transfections were repeated every 24 h.

6.3. Methods in molecular biology

6.3.1.DNA isolation from mouse tissues and mitochondria

For genotyping and pyrosequencing, tail or ear-clip biopsies DNA was extracted using chloroform and ethanol precipitation. Briefly, samples were lysed overnight in 400 μL TNES buffer (0.5% SDS, 0.1 M NaCl, 50 mM Tris pH 8.0, 2.5 mM EDTA pH 8.0) and 8 μL proteinase K (10 mg/mL) at 56°C. Next, 75 μL potassium acetate was added followed by 500 μL cloroform. The samples were vortexed and centrifuged at maximum speed for 10 minutes. The supernatant was collected and DNA was precipitated with 100% ethanol at -20 or -80°C. After centrifugation, the DNA pellet was washed with 70% ethanol and resuspended in dH_2O. For Southern blotting or qPCR snap frozen tissues were grinded in a cold mortar. 20 - 30 μg of grinded tissue or ~ 9 x 10^6 frozen cells were used to extract DNA using the blood and tissue kit or the Gentra Puregene tissue kit (Qiagen) following manufacturer's instructions. All samples used for Southern blotting and qPCR were treated with RNase (Qiagen). Frozen crude mitochondria were used for mtDNA isolation. Briefly, mitochondria were lysed in 400 μL TNES buffer and 10 μL proteinase K (10 mg/mL) for 2 – 3 h at 56°C. Then, lysates were treated with 3 μL RNase A (4 mg/mL) (Qiagen) and incubated 5 min at room temperature. DNA was extracted using 1 mL Phenol:Chloroform:Isoamyl alcohol (25:24:1 v/v) (ambion), followed by ~400 μL of chloroform. DNA was precipitated overnight with 1/10 v/v 3M NaAc (ambion) and 100% ethanol at -20 °C, washed with 75% ethanol, and resuspended in nuclease-free water.

6.3.2.BAC DNA isolation for pro-nuclear injection

BAC DNA was isolated as previously described (Milenkovic et al. 2013). Bacteria containing the BAC were streaked in LB agar with 18 μg/μL chloramphenicol and 50 μg/μL streptomycin. Single colonies were selected for overnight pre-cultures in 3 mL LB with antibiotics. The following day, 600 μL of the preculture were used to inoculate 1 L LB agar with antibiotics and cultured shaking at 180 rpm overnight. Next, bacterial cultures containing the mutated BACs were pelleted by centrifugation 6000 rcf at room temperature. Bacterial pellets were carefully resuspended in 50 mL buffer P1 (Qiagen) with RNase, followed by alkaline lysis using 50 mL of buffers P2 and P3 (Qiagen) on ice. Lysates were cleared by two sequential centrifugations

at 10000 rpm at 4 °C for 20 min and filtered using a 70 μm cell strainer. DNA was precipitated with isopropanol and pelleted at 10000 rcf for 15 min. The DNA pellet was resuspended in 3.8 mL of nuclease-free water under gentle rotation overnight at 4°C. Then, 3.8 g of $CsCl_2$ were added to the resuspended DNA and dissolved by gentle rotation. 290 μL of ethidium bromide (10 mg/μL; Sigma) were added to the resuspended DNA and homogenized by gentle inversion. Samples were centrifuged at 3000 rcf at room temperature to remove protein precipitates and ultra-centrifuged in a 100Ti rotor (Beckman Coulter) at 70000 rpm for 22 h at 25°C in a Beckman Coulter Optima L-100 XP ultracentrifuge. Supercoiled BAC DNA was visualized under a UV lamp (UVP) and collected. The ethidium bromide was eliminated by organic solvent extraction using 1-butanol. Finally, the DNA was precipitated using ice-cold 95% ethanol, washed with 70% ethanol, and resuspended in embryo-toxic free water. The isolated DNA was quantified using a Qubit Fluorometer and microinjected into the pro-nuclei of one-cell stage mouse embryos.

6.3.3. RNA isolation from cells, mouse tissues, and mitochondria

Total RNA from mouse tissues was extracted from snap-frozen tissues using the ToTALLY RNA™ Kit (Ambion) or miRNAeasy kit (Qiagen) following the manufacturers' instructions. 50-100 mg of grinded mouse tissues were homogenized using lysing matrix D (MPBio) in a fast prep machine with 2x 30 sec pulses at speed 6 (MPBio). The homogenization step was repeated after 5 min incubation at room temperature. Cells pellets were resuspended in Qiazol by pipetting (Qiagen). The isolated RNA was DNase treated using by in-column digestion using RNase-free DNase I (Qiagen) or TURBO DNA-*free*™ kit (Ambion). The RNA concentration was measured with a NanoDrop 2000c spectrophotometer (Peqlab). Concentration, purity, and integrity of RNA for RNA-Seq were confirmed using Bioanalyzer or northern blotting (section 6.4.7). Mitochondrial pellets were either resuspended in Qiazol and extracted using the miRNAeasy kit (Qiagen) or in Trizol LS (Life technologies) and extracted following manufacturer's instructions.

6.3.4. Pyrosequencing

Quantification of *Polrmt* c420G>T was performed on tail DNA using a PyroMark Q24 pyrosequencer (Qiagen). Allele Quantification assay was developed using PyroMark assay design software v. 2.0 (Qiagen). A single PCR reaction was employed to amplify a 192 bp fragment spanning the c.420G>T mutation site, using a biotinylated forward primer and a non-biotinylated reverse primer. PCR products were combined with distilled water, PyroMark binding buffer (Qiagen), and 1μL Streptavidin sepharose TM high performance beads (GE Healthcare). Next, PCR products were purified and denatured using a Pyromakr Q24 vacuum workstation (Qiagen). Sequencing was performed with PyroMark Gold Q24 reagents according

to manufacturer's instructions using the sequencing primer. Primer sequences are listed in Table S2 (supplementary material section 8.2).

6.3.5. RNA sequencing

RNA sequencing was performed on total RNA by the Cologne Genomics Centre (Cologne, Germany) on the Illumina HiSeq platform, according to the Illumina Tru-Seq protocol. Random hexamer primers were used for cDNA library generation and cytoplasmic rRNA depletion using the Ribo-Zero rRNA removal kit was carried out. The alignment to the *Mus musculus* reference genome (GRCm38) was performed using HISAT2 version 2.0.4 (hisat2 -p 8 --dta) (Kim et al. 2015). Alignment files were sorted and indexed with SAMtools version 1.3.1 (samtools sort -@ 8; samtools index -b)(H. Li et al. 2009). The transcript abundances were estimated with StringTie 1.2.4 (stringtie -p 18 -e –B –G) using the Ensembl 81 annotation (Pertea et al. 2016). The raw reads count matrix at gene-level was extracted with prepDE.py script provided at http://ccb.jhu.edu/software/stringtie/dl/prepDE.py on Python version 2.7.6.

Paired-end deep sequencing of the mitochondrial RNAs was performed as previously described (Mercer et al. 2011) on an Illumina MiSeq according to the manufacturer's instructions. Sequenced reads were aligned to the mouse genome (GRCm38) with HISAT 0.1.6 (66) (–fr –rna-strandness RF; total RNA library). Reads that aligned to mtDNA were extracted and subsequently realigned with spliced alignment disabled to reflect the unspliced nature of the mitochondrial transcriptome and prevent the introduction of spurious splice junctions. Gene-specific counts were summarized with featureCounts 1.3.5-p4 (67) (-p -s 2 -Q 10; total RNA library) using the Ensembl 75 gene annotation for nuclear-encoded genes and a modified annotation for mitochondrial genes. The modified annotation contains merged *mt-Atp8/mt-Atp6* and *mt-Nd4l/mt-Nd4* annotations to reflect their bicistronic nature. Initially, genes with a zero count in any sample were filtered from the count table (in addition to mt-tRNAs), followed by loess and upper quartile normalization for guanine/cytosine content and sequencing depth, performed with EDASeq 2.3.2 (68).

6.3.6. Southern blotting

1 - 3 μg of digested DNA were separated in 0.8% agarose gel and transferred to Hybond^{TM}-XL or Hybond N^+ membranes (Amersham Biosciences) by capillary transfer in 20X SSC (3M NaCl, 0.3 M sodium citrate, pH 7.0). Prior transfer, the gels were treated for 10 min with 0.2 M HCl, 15 min in denaturation solution (1.5 M NaCl; 0.5 M NaOH) and 15 min in neutralization solution (1.5 M NaCl, 0.5 M Tris pH 7.4). After ultraviolet (UV) crosslinking, the membranes were successively hybridized with various probes at 65°C in RapidHyb buffer (Amersham) and then washed in 2x and 0.2x SSC/0.1% SDS before exposure. Probes used were gel-purified

restriction fragments labelled with [α -^{32}P]2'-deoxycytidine-5′-triphosphate (dCTP) and the Prime-IT Random Primer Labeling kit random priming kit (Agilent). The *Polrmt* probe was generated by PCR amplification of *Polrmt* cDNA containing exon 2 to exon 4. The PCR product was cloned into pCRII-blunt TOPO vector (Invitrogen), excised by restriction digest using EcoRI, and gel-purified using Qiaquick Gel extraction kit (Qiagen). All other probes were previously generated previously in the laboratory (Table S3 in supplementary material section 8.2). Radioactive signals were detected by autoradiography and the quantifications were performed using the programs ImageJ or MultiGauge with images generated from a Phosphorimager. For the D-loop Southern, samples were heated for 5 min at 95°C prior loading and hybridization was performed at 42 °C. BAC DNA was digested with HindIII and mouse DNA for mtDNA detection was digested with SacI.

6.3.7. Northern blotting

1-3 µg of total RNA was separated in a 1.8% formaldehyde-MOPS [3-(N-morpholino) propanesulfonic acid] agarose gel and transferred to Hybond^{TM}-XL or Hybond N^{+} membranes (Amersham Biosciences) by capillary transfer in 20X SSC. After UV crosslinking, the blots were successively hybridized with various probes at 42 or 65°C in RapidHyb buffer (Amersham) and then washed in 2x and 0.2x SSC/0.1% SDS before exposure. Mitochondrial probes used for visualization of mt-mRNA and mt-rRNA levels were gel-purified restriction fragments labelled with [α -^{32}P]dCTP and the Prime-IT Random Primer Labeling kit random priming kit (Agilent). Mt-tRNAs and 7S RNA were detected using specific end-labelled oligonucleotides with 30 μCi [γ-^{32}P]ATP and the T4 Polynucleotide kinase (New England Biolabs). The membranes were stripped before rehybridization. The images were obtained by autoradiography and the quantifications were performed using the programs ImageJ or MultiGauge with images generated from a Phosphorimager. The list of probes and oligonucleotides is in Table S4 (supplementary material section 8.2).

6.3.8. RT-PCR and qRT PCR

cDNA synthesis was performed on 1-2 μg of DNase treated RNA using the High Capacity cDNA reverse transcription kit (Applied Biosystems). qRT-PCR was performed using the Taqman 2x Universal PCR mastermix, No Amperase UNG (Applied Biosystems) and commercially available assays against mouse from Life technologies on a 7900HT or QuantStudio 6 RealTime PCR System (Applied Biosystems). List of oligonucleotides for RT-PCR and Taqman assays are listed in tables S3 and S4 (supplementary material section 8.2), respectively.

6.3.9. In organello replication and transcription assays

In organello replication and transcription assays were performed on mitochondria isolated from mouse hearts by differential centrifugation as described in section 6.4.1. 0.5-1 mg of freshly isolated mitochondria were resuspended in transcription labelling buffer (25 mM sucrose, 75 mM sorbitol, 100 mM KCl, 10 mM K_2HPO_4, 50 µM EDTA, 5 mM $MgCl_2$, 1 mM ADP, 10 mM glutamate, 2.5 mM malate, 10 mM Tris pH 7.4, 1 mg/ml of bovine serum albumin (BSA), and 1 mM ADP) and incubated with 40 µCi of [α-^{32}P]uridine-5'-triphoshphate (UTP) under rotation for 1 h at 37°C. To reduce the background signal, mitochondria were washed and resuspended in transcription labelling buffer containing 0.2 mM UTP and incubated at 37°C for 10 min. Finally, mitochondria were pelleted and resuspended in washing buffer (10% glycerol, 10 mM Tris-HCl pH 6.8, and 0.15 mM $MgCl_{2)}$. An aliquot of resuspended mitochondria was collected as the input and analysed by western blot (section 6.4.9). Mitochondrial RNA was isolated from the final pellet using the TRIzol LS reagent (Ambion) and resuspended in 10 µl of nuclease-free water to which 10 µL of 2X RNA Sample loading buffer (Sigma) was added. Samples were heated for 10-15 min at 65°C, separated in 1.2% formaldehyde-MOPS horizontal agarose gels at 120 V for 2 h or 1.8% formaldehyde-MOPS vertical agarose gels at 80 V for 1 h and 160 V for 4-5 h. RNA was transferred by northern blotting (section 6.3.7). UV-crosslinked membranes were exposed to autoradiography or decorated with radiolabelled probes.

For *in organello* replication, the same procedure was performed with the following modifications. Labelling buffer was supplemented with 50 mM dCTP, dTTP 2′-deoxythymidine-5′-triphosphate (dTTP), 2′-deoxyguanosine-5′-triphosphate (dGTP), and 20 µCi of [a-^{32}P]deoxyadenosine-5'-triphosphate (dATP) (PerkinElmer or Hartmann analytics). Incubation in labelling buffer was performed for 2 h. mtDNA was isolated by phenol:chloroform:isoamyl alcohol extraction or by Puregene Core Kit A (Qiagen) (section 6.3.1), and radiolabelled replicated DNA was analysed by D-loop Southern blotting and visualized by autoradiography (section 6.3.6). Quantifications of mtDNA and transcript levels were performed using the program MultiGauge with images generated from a PhosphorImager instrument.

6.3.10. In vitro transcription assay

Transcription reactions were performed in 25 µl total volume containing 25 mM Tris pH 8.0, 10 mM $MgCl_2$, 64 mM NaCl, BSA (100 mg/ml), 1 mM dithiothreitol (DTT), 400 µM ATP, 150 µM guanosine-5′- triphosphate (GTP), 150 µM CTP, 10 µM uridine 5′-triphosphate (UTP), 0.02 µM [α-^{32}P]UTP, and 4 U RNase Inhibitor Murine (New England Biolabs). The transcription template was added at 4 nM and consisted of a restriction cut (HindIII/EcoRI), purified (QIAquick PCR Purification Kit) human LSP/HSP plasmid, where a fragment consisting of

positions 325 to 742 of human mtDNA was cloned between the SmaI and HindIII sites of pUC18 (Farge et al. 2014). For each reaction, 128 nM human TFB2M and 320 nM human TFAM (corresponding to 1 TFAM per 40 bp) were added. Human POLRMT was added at five different concentrations: 128, 32, 8, 2, and 0.5 nM. The reactions were incubated at 32°C for 30 min and stopped by the addition of stop buffer (10 mM Tris pH 8.0, 0.2 M NaCl, 1 mM EDTA, and proteinase K (100 mg/ml)) followed by incubation at 42°C for 45 min. The transcription products were ethanol-precipitated, dissolved in 20 ml loading buffer (98% formamide, 10 mM EDTA, 0.025% xylene cyanol FF, and 0.025% bromophenol blue), and analyzed on 4% denaturing polyacrylamide gels (1× tris-borate EDTA and 7 M urea). Quantifications of transcript levels were performed using the program MultiGauge with images generated from a PhosphorImager instrument.

6.3.11. Linear density glycerol gradients

10 to 45% linear density glycerol gradient were modified from previous studies (Lee et al. 2013). Crude mitochondria (1 - 3 mg) from 4 to 5 week-old mouse hearts were isolated by differential centrifugation as described in section 6.4.1, pelleted by centrifugation 15 min at 9.300 rcf and 4°C, and then lysed in a glass potter on ice in lysis buffer (5% glycerol, 20 mM NaCl, 30 mM Hepes pH 8.0, 1 mM EDTA, 2 mM DTT, and 1.2% Triton X-100 supplemented with EDTA-free complete protease inhibitor cocktail and PhosSTOP Tablets (Roche)). After 10 min of incubation, lysates were cleared by centrifugation 5 min at 800 rcf and 4°C and overlaid on top of a 10 to 45% linear glycerol gradient prepared in 20 mM NaCl, 25 mM Hepes pH 8.0, 1 mM EDTA, 1 mM DTT, 0.2% Triton X-100, and EDTA-free complete protease inhibitor cocktail (Roche). Gradients were centrifuged in a SW41 rotor at 21000 rcf at 4°C for 3 hours in a Beckman Coulter Optima L-100 XP ultracentrifuge. Gradients were prepared using Gradient Master (Biocomp Instruments Inc) in 14 mm × 89 mm Ultra-Clear Centrifuge Tubes (Beckman Instruments Inc.). Fractions of 750 ml were collected from the top of the gradients, and 20 μl of each fraction were analysed and western blotting (section 6.4.9). For analysis of mtDNA sedimentation profiles, mtDNA was isolated from two-thirds of each fraction using phenol/chloroform extraction (section 6.3.1), digested with SacI, and subjected to Southern blotting (section 6.3.6).

6.4. Methods in biochemistry

6.4.1. Total protein isolation from mouse tissues

Frozen heart tissue was pulverized with liquid nitrogen and 20-30 mg were resuspended in tissue lysis buffer (25 mM HEPES pH 7.5, 5 mM $MgCl_2$, 0.5 mM EDTA, 1% NP-40, and 140 mM NaCl) containing 1X complete protease inhibitor cocktail (Roche). The tissue homogenate was mixed by pipetting and then sonicated for 10 cycles (30 sec sonication and 30 sec rest).

Finally, the samples were centrifuged at 13000 rpm for 10 min at 4°C to remove cell debris. The supernatant with the total proteins was collected and kept at -20°C. Total proteins were quantified using the Protein DC – Lowry based assay (BioRad).

6.4.2. Isolation of crude mitochondria from mouse tissues

Mouse heart, kidney, liver, brown adipose tissue, and spleen were washed in ice-cold PBS, minced, and homogenized using a Potter S homogenizer (Sartorius) in mitochondrial isolation buffer (320 mM sucrose, 1 mM EDTA, and 10 mM Tris-HCl pH 7.4) containing 1X complete protease inhibitor cocktail (Roche). Then, the homogenized tissue was centrifuged at 1000 rcf for 10 min to pellet cell debris and nuclei and the supernatant was re-centrifuged at 10000 rcf for 15 min to pellet the mitochondria. The mitochondrial pellet was resuspended in mitochondrial isolation buffer and the differential centrifugation was repeated to obtain more pure mitochondria.

Isolation of mitochondria from skeletal muscle was performed as previously described (Frezza et al. 2007). Briefly, skeletal muscle was collected in ice-cold DPBS with 10 mM EDTA, trimmed from visible fat, ligaments and connective tissue, and minced into small pieces. After washing three times in DPBS with 10 mM EDTA, samples were incubated with 0.05% trypsin in DPBS for 30 min, transferred to IB_m1 buffer (67 mM sucrose, 50 mM Tris pH 7.4, 50 mM KCl, 10 mM EDTA, 0.2% BSA) and homogenised using a Potter S homogenizer (Sartorius). Tissue homogenates were centrifuged two times 10 min at 800 rcf, and the supernatant was centrifuged at 8000 rcf for 10 min. The mitochondrial pellet was then resuspended in IB_m2 buffer (250 mM sucrose, 3 mM EGTA/Tris pH 7.4, 10 mM Tris pH 7.4) and centrifuged at 8000 rcf for 10 min.

All the isolation steps were performed on ice and the centrifugations at 4°C. Mitochondria were snap-frozen in liquid nitrogen and kept at -80°C. An aliquot of the isolated mitochondria was quantified using the Bradford reagent. Absorbance at 595 nm was measured using a Tecan 2000 microplate reader. A BSA standard curve was used to determine the protein concentration.

6.4.3. Subcellular fractionation from cells and mouse tissues

Subcellular fractionation of mouse heart was performed as previously described (Cox & Emili 2006). Hearts were minced and washed in ice cold DPBS (Gibco) to remove excess of blood. Then, tissues were rinsed and homogenized using a Potter S homogenizer (Sartorius) in ice cold 250-STMDPS buffer (250 mM sucrose, 50 mM Tris pH 7.4, 5 mM $MgCl_2$, 1 mM DTT, Spermine 25 mg/mL, Sermidine 25 ml/mL) containing 1x complete protease inhibitor cocktail.

An aliquot was collected as the total input fraction. The tissue homogenate was centrifuged 800 rcf for 15 min at 4°C. The supernatant was re-centrifuged and saved for mitochondrial isolation. The pellet from the first centrifugation round was resuspended in buffer 250-STMDPS and re-homogenized using a Potter S homogenizer for 1 min. The homogenized tissue was centrifuged at 800 rcf for 15 min at 4°C. The nuclei were resuspended in 4 volumes of buffer 2 M STMDPS (2M sucrose, 50 mM Tris pH 7.4, 5 mM $MgCl_2$, 1 mM DTT, Spermine 35 mg/mL, Spermidine 25 mg/mL) containing 1x complete protease inhibitor cocktail. The resuspended nuclei were added to a 14 mm × 89 mm Ultra-Clear Centrifuge Tubes (Beckman Instruments Inc.) containing 4 mL of buffer 2 M STMDPS and centrifuged at 80000 rcf for 35 min at 4°C in SW 41Ti rotor using a L-100 XP ultracentrifuge (Beckman Instruments Inc). The pellet containing pure nuclei was saved as the nuclear fraction. The supernatant containing the mitochondria were centrifuged at 6000 rcf for 15 min to pellet the mitochondria and the mitochondrial pellet was resuspended as the mitochondrial fraction. Equal volumes of each fraction were lysed using 2x LDS buffer (Invitrogen) with 50 mM DTT and analysed by western blotting (section 6.4.9).

Subcellular fractionation of cells was performed using the cell fractionation kit (Abcam). 70-90% confluent cells were harvested using 0.05% trypsin (Gibco), washed in cold DPBS and pelleted by centrifugation at 800 rcf for 5 min. 6.6 x 10^6 cells were resuspended in buffer A and an equal volume of buffer B (buffer A + 1:1000 v/v detergent I) was added. An aliquot was collected as the total input fraction. The cell suspension was mixed for 7 min by constant rotation at room temperature followed by centrifugation at 5000 rcf for 1 min at 4°C. The supernatant was then re-centrifuged at 10000 rcf for 1 min at 4°C and the resulting supernatant was collected as the cytoplasmic fraction. The pellets resulting from both centrifugation steps containing nuclei and mitochondria were resuspended in an equal starting volume of buffer A and an equal volume of buffer C (buffer A + 1:25 v/v detergent II) was added. The samples were mixed for 10 min by constant rotation at room temperature followed by centrifugation at 5000 rcf for 1 min at 4°C. The supernatant was then re-centrifuged at 10000 rcf for 1 min at 4°C and the resulting supernatant was collected as the mitochondrial fraction. The pellets resulting from both centrifugation steps were resuspended in two times the original volume of buffer A and corresponded to the nuclear fraction. Equal volumes of each fraction were lysed using 2x LDS buffer (Invitrogen) with 50 mM DTT and analysed by western blotting (section 6.4.9).

6.4.4. Percoll-purification of mitochondria from mouse tissues

Crude mitochondria from mouse tissues were isolated as described in section 6.4.1. Mitochondria isolation buffer was in addition supplemented with PhosStop tablets (Roche).

Mitochondrial pellets were washed in 1x M buffer (220 mM mannitol, 70mM sucrose, 5mM HEPES pH 7.4, 1 mM EGTA pH 7.4; pH was adjusted with potassium hydroxide; supplemented with EDTA-free complete protease inhibitor cocktail and PhosSTOP Tablets (Roche)) and purified on a Percoll density gradient (12%:19%:40% prepared with 2x M buffer) via centrifugation in a SW41 rotor at 15.500 rpm at 4°C for 1 h in a Beckman Coulter Optima L-100 XP ultracentrifuge using 14 mm × 89 mm Ultra-Clear Centrifuge Tubes (Beckman Instruments Inc.). Mitochondria were harvested at the interphase between 19% and 40%, washed three times with buffer 1xM. Mitochondrial pellets were snap-frozen in liquid nitrogen and stored at -80°C.

6.4.5. Peptide digestion and stage-tip peptide clean-up for label-free mass spectrometry

Percoll-purified frozen mitochondria pellets were suspended in lysis buffer (6 M guanidinium chloride, 10 mM Tris(2-carboxyethyl)phosphine hydrochloride, 40 mM chloroacetamide, and 100 mM Tris-HCl) (Kulak et al. 2014). After complete lysis, samples were diluted 1:10 in 20 mM Tris pH 8.0 and quantified a NanoDrop 2000c spectrophotometer (Peqlab). 80 µg of protein were mixed with 3 µg of Trypsin gold (1m/mL)(Promega) and incubated overnight at 37°C to achieve complete digestion. Peptides were cleaned with home-made STAGEtips (Rappsilber et al. 2003) (Empore Octadecyl C18; 3M) and eluted in 60% acetonitrile/0.1% formic acid buffer. Samples were dried in a SpeedVac apparatus (Eppendorf concentrator plus 5305) at 45°C and the peptides were suspended with 0.1% formic acid. Approximately 1.5 µg of peptides were analysed by LC-MS/MS.

6.4.6. LC-MS/MS analysis

For mass spectrometric analysis, peptides were separated on a 25 cm, 75 µm internal diameter PicoFrit analytical column (New Objective, Part No. PF7508250) packed with 1.9 µm ReproSil-Pur 120 C18-AQ media (Dr. Maisch, Mat. No. r119.aq) using an EASY-nLC 1000 or EASY-nLC 1200 (Thermo Fisher Scientific). The column was maintained at 50°C. Peptides were separated on a segmented gradient of buffer A (0.1% formic acid) from 2% to 5% buffer B (0.1% formic acid in acetonitrile) for 10 min, from 5% to 20% buffer B for 100 min, from 20% to 25% buffer B for 10 min, and from 25% to 45% buffer B for 10 min at 200 nl / min (EASY-nLC 1000). Using the EASY-nLC 1200 system, peptides were separated on a segmented gradient of buffer A from 3% to 6% buffer B' (80% acetonitrile, 0.1% formic acid) for 10 min, from 6% to 25% buffer B' for 100 min, from 25% to 31% buffer B' for 10 min, and from 31% to 60% buffer B' for 10 min, at 200 nl / min. Eluting peptides were analysed on a QExactive HF mass spectrometer (Thermo Fisher Scientific). Peptide precursor mass to charge ratio (m/z) measurements (MS1) were carried out at 60000 resolution in the 300 to 1800 *m/z* range. The top ten most intense precursors with charge state from 2 to 7 only were selected for HCD

fragmentation using 25% collision energy. The *m/z* of the peptide fragments (MS2) were measured at 30000 resolution using an AGC target of 2e5 and 80 ms maximum injection time. Upon fragmentation precursors were put on an exclusion list for 45 sec. Peptides from the five knockout strains were analysed in two runs and *Polrmt* knockout was used to control for the variability within runs. The time course analysis on *Lrpprc* knockout was performed in a single run. Peptides from different tissues of the *Polrmt* overexpressor mice were analysed in a single run.

6.4.7. Determination of Coenzyme Q and amino acid content from mouse tissues

Quinones were extracted as previously described (Mourier et al. 2015). 20 mg of pulverized frozen mouse hearts were resuspended in 200 µl 1 mM cupric sulfate ($CuSO_4$) and 200 µl 100% ethanol and then sonicated for 10 cycles (30 sec sonication and 30 sec rest; diagenode Bioruptor plus). Then, 400 µl of hexane were added, the samples were vortexed and sonicated. The upper face was collected and samples were dried in a SpeedVac apparatus (Eppendorf concentrator plus 5305) at 60°C for 25 min. For absolute quantification of Q9 and Q10 in positive ESI multiple reaction monitoring (MRM) mode, an Acquity UPLC system (Waters) was connected to a Xevo TQ (Waters). An Acquity UPLC (Waters). A BEH C18 1.7 µm, 2.1 × 50 mm column was used at 40°C. Solvent A was 90% methanol + 10% propanol + 0.1% FA, and solvent B was 45% acetonitrile/acetone + 10% propanol + 0.1% FA. A linear gradient of solvent A ranging from 100% to 0% in 3.5 min at a low rate of 0.45 ml/min was used. Between 2 and 6 µl of the samples were injected. The sample manager was set to 6°C for the standards and the samples were defrozen and directly injected. The source temperature was set to 150°C, desolvation temperature was 650°C, desolvation gas was set to 800 L/h, and cone gas was set to 50 liter/h. All compounds were freshly prepared daily and dissolved in ethanol/methanol (9:1). Quality control standards of each standard were used during sample analysis and showed between 0.5% and 40% deviation for Q9 and Q10. Standard curve range was 4 – 3500 ng/mL for Q10 and 100-2800 ng/mL for Q9.

Other metabolites analysed in this study were extracted from 20-30 mg grinded frozen mouse hearts in 1 mL sample buffer (methanol:H_2O:chloroform in a 7:2:1 ratio). Samples were mixed, sonicated (10 cycles; 30 sec sonication and 30 sec rest; diagenode Bioruptor plus) and centrifuged at 15000 rcf at 4°C for 5 min. Supernatants were centrifuged through 0.25 µm Centrifugal filters (VWR) and re-centrifuged twice at 15000 rcf for 5 min, placed at -80°C for 2 h and re-centrifuged. Supernatants were dried in a SpeedVac apparatus (Eppendorf concentrator plus 5305) at 45°C for 1h. Next, samples were suspended in 100 µl and diluted 1/20 in 5 mM ammonium formiate + 0.15% formic acid (Sigma), mixed, sonicated for 2 min and filtrated through a 0.2 µm modified nylon centrifugal filter (VWR). For absolute

quantification in positive and negative ESI MRM (multi reaction monitoring) mode an Acquitiy UPLC I-Class System (Waters) was connected to a XevoTM TQ-S (Waters). A Discovery HS F5-3 (Supelco) 3 μm, 2.1 x 100 mm column was used at 25°C. Solvent A was 5 mM ammonium formiate + 0.15% formic acid and B was acetonitrile (VWR). A gradient from 100% A to 80% in 3 min, to 4 min isocrate, to 4,5 min 50%, to 7 min 0%, to 10 min isocrate at a flow rate of 0.35 ml/min was used. An equilibration step of 7 min was performed after each injection. The dilutions were injected twice of each injection volume, 0.1 μL and 8 μL. The sample manager was set to 8°C and the source temperature to 150°C, desolvation temperature was 500°C and desolvation gas was set to 800 L/h, cone gas to 150 L/h. The following MRM transitions were used as quantifier for sarcosine *m/z* 89.84 to 44.02 cone 14 V collision 18 V, glycine *m/z* 75.9 to 30.08 cone 28 V collision 6 V and in a negative mode serine *m/z* 105.9 to 42.09 cone 72 V collision 10 V. All compounds were freshly prepared and dissolved in 5 mM ammonium formiate + 0.15% formic acid. An external standard calibration curve was calculated using 11 concentrations from 100 to 20000 ng/ml (all of them were prepared from stock solutions 100 µg/ml). Correlation coefficient: $r < 0.990$, the peak integrations were corrected manually, if necessary. Quality control standards of each standard were used during sample analysis and showed between 0.5% and 40% deviation respectively. Blanks after the standards, quality control and sample batch proved to be sufficient. No carry over was detected. The MassLynx (Waters) software was used for data management and TargetLynx (Waters) was used for data evaluation and absolute quantification of all metabolite compounds. Two to three technical replicates were performed for each measurement.

6.4.8. Mitochondrial enzyme activity and respiration measurements

To measure mitochondrial respiratory chain complex activities 15 to 50 µg of mitochondria were diluted in phosphate buffer (KH_2PO_4 50 mM, pH 7.4), followed by spectrophotometric analysis of isolated respiratory chain complex activities at 37°C, using a HITACHI UV-3600 spectrophotometer. To follow citrate synthase activity, increase in absorbance at 412 nm (E=13600M-1.cm-1) was recorded after addition of acetyl-CoA (0.1 mM), oxaloacetate (0.5 mM) and DTNB (0.1 mM). Succinate dehydrogenase (SDH) activity was measured at 600 nm (E=21000M-1.cm-1) after the addition of 10 mM succinate, 35 µM dichlorphenolindophenol (DCPIP) and 1 mM KCN. Succinate dehydrogenase - cytochrome c reductase (II-III) activity was measured at 550 nm after the addition of 10 mM succinate, 0.5 mg cytochrome c, and 1 mM KCN. NADH dehydrogenase activity was determined at 340 nm (E=6220M-1.cm-1) after the addition of 0.25 mM NADH, 0.25 mM duroquinone, and 25 mM Azide and controlling for Antimycin A sensitivity. Cytochrome *c* oxidase activity was measured by standard TMPD ascorbate/KCN sensitive assays. Each activity was normalized to mg protein using the Lowry-based BioRad protein DC kit. All chemicals were obtained from Sigma Aldrich.

Mitochondrial oxygen consumption flux was measured at 37°C using 65–125 μg of crude mitochondria diluted in 2.1 ml of mitochondrial respiration buffer (120 mM sucrose, 50 mM KCl, 20 mM Tris-HCl, 4 mM KH_2PO_4, 2 mM $MgCl_2$, 1 mM EGTA, pH 7.2) in an Oxygraph-2k (OROBOROS INSTRUMENTS, Innsbruck, Austria). The oxygen consumption rate was measured using either 10 mM pyruvate, 5 mM glutamate, and 5 mM malate or 10 mM succinate and 10 nM rotenone. Oxygen consumption was assessed in the phosphorylating state with 1 mM ADP or non-phosphorylating state by adding 2.5 μg/ml oligomycin. Respiration was uncoupled by successive addition of carbonyl cyanide m-chlorophenyl hydrazone (CCCP) up to 3 μM to reach maximal respiration.

6.4.9. Western blot

5-50 μg of isolated mitochondria of total protein extracts were resuspended in NuPage LDS sample buffer with 50 mM DTT (Invitrogen). Proteins were separated by SDS-PAGE using either 4-12% or 10% precast gels (Invitrogen) and then transferred onto polyvinylidene difluoride membranes (Hybond™-P from GE Healthcare). Immunodetection was performed according to standard techniques using enhanced chemiluminiscence (Immun-Star HRP Luminol/Enhancer from BioRad). The antibodies used are listed in table S5

6.4.10. BN-PAGE and in gel enzyme activity

100 mg of crude heart mitochondria were solubilized in solubilization buffer (1% (w/v) digitonin (Calbiochem), 20 mM Tris pH 7.4, 0.1 mM EDTA, 50 mM NaCl, 10% (v/v) glycerol) and incubated on ice for 15 min. Non-solubilized material was removed by centrifugation and the supernatant was mixed with loading die (5% (w/v) Coomasie Brilliant Blue G-250 (Serva), 100 mM Tris pH 7.0, 500 mM 5-aminocaproic acid). Samples were resolved on a 4 – 10% (w/v) acrylamide gradient BN- gels (Schägger & Jagow 1991). BN gels were further subjected to western blot (section 6.4.9) or Coomassie Brilliant Blue R staining. The antibodies used are listed in Table S5 (supplementary material section 8.2)

6.4.11. Immunofluorescence

HeLa cells were grown at 37°C, 5% CO2 on coverslips. To detect spRNAP-IV, cells were transfected with a mammalian expression vector encoding spRNAP-IV fused to an EGFP tag using lipofectamine 2000 (Invitrogen). Cells were stained with MitoTracker red CMXRos (Invitrogen) and subsequently fixed with 4% paraformaldehyde. To visualize endogenous POLRMT, cells were incubated with antibodies against human POLRMT and visualized using AlexaFluor 488 goat anti-rabbit secondary antibody. After immunolabelling, samples were stained with 1 g/mL DAPI (AppliChem) and mounted in Prolong Gold (ThermoFisher). The image acquisition was performed with a Leica TCS SP8-X inverted confocal microscope (Leica

Microsystems) using a 100×/1.4 oil objective. The antibodies used are listed in Table S5 (supplementary material section 8.2)

6.4.12. Morphological analyses heart sections

Hematoxylin and eosin stainings were performed on paraformaldehyde (PFA)–fixed cryosections from 4-week old mouse hearts that were immediately embedded in OCT Tissue-Tek in cooled methyl-butan. Images of heart sections were generated by stitching of several images taken with the Nikon Eclipse Ci microscope. For transmission electron microscopy, pieces of the mouse heart apex were fixed in 2% glutaraldehyde and 2% PFA in 0.1 M sodium cacodylate buffer (pH 7.4). Specimens were postfixed in 1% osmium tetroxide [in 0.1 M sodium cacodylate buffer (pH 7.4)]. After thorough washing with water, specimens were dehydrated in ethanol followed by acetone and embedded in medium-grade Agar Low Viscosity Resin (Plano). Ultrathin sections (70 to 80 nm) were cut with a Reichert-Jung Ultracut E Ultramicrotome, stained with 2% uranyl acetate in 70% ethanol, followed by lead citrate, and examined with a Hitachi H-7650 transmission electron microscope operating at 100 kV fitted with a midmounted AMT XR41-M digital camera (Advanced Microscopy Techniques).

6.5. Data and statistical analyses

6.5.1.LC-MS/MS data analysis

The raw data were analysed with MaxQuant version 1.4.1.2 (Cox and Mann, 2008) using the integrated Andromeda search engine (Cox et al. 2011). Peptide fragmentation spectra were searched against the canonical and isoform sequences of the mouse reference proteome (proteome ID UP000000589, August 2015 from UniProt). The database was complemented with 245 sequences of contaminating proteins by MaxQuant. For the analysis methionine oxidation and protein N-terminal acetylation were set as variable modifications. The digestion parameters were set to “specific” and “Trypsin/P,” allowing for cleavage after lysine and arginine also when followed by proline. The minimum number of peptides and razor peptides for protein identification was 1; the minimum number of unique peptides was 0. Protein identification was performed at a peptide spectrum matches and protein false discovery rate (FDR) of 0.01. The “second peptide” option was on to identify co-fragmented peptides. Successful identifications were transferred between the different raw files using the “Match between runs” option, using a match time window of 0.7 min. LFQ (Cox et al. 2014) was performed using a minimum ratio count of 2.

6.5.2. Protein LFQ quantification analysis

Analysis of the LFQ results was done using the Perseus computation platform (Tyanova et al. 2016), version 1.5.0.0 and R, version 3.3.0 (R Development Core Team, 2010). For the analysis, LFQ intensity values were loaded in Perseus and all identified proteins marked as "Reverse", "Only identified by site", and "Potential contaminant" were removed. The corresponding L/L and the L/L, cre genotypes were loaded separately in Perseus, the LFQ intensity values were log2 transformed and all proteins that contained less than two to five missing values in one of the groups (L/L or L/L, cre) were removed. Missing values in the resulting subset of proteins were imputed with a width of 0.3 and down shift of 1.8. Imputed LFQ intensities were loaded into R where a two-sided moderated t-test analysis was performed using limma, version 3.30.13 (Ritchie et al. 2015). Proteins with an adjusted p value ("BH" correction) of less than 0.05 were designated as differentially expressed. Our list of differentially expressed proteins was combined with annotations from MitoCarta2.0 (Calvo, Clauser & Mootha 2016). The first of the semicolon separated entries in the "Gene names" column was used to merge annotations through the "Symbol" or "Synonyms" columns of the Mouse.MitoCarta2.0.txt file. For protein entries that lacked a "Gene names" entry, gene name information was retrieved using UniProt.ws, version 2.14 (Carlson, 2017). Using the principles of the 'Total Protein approach' (Wiśniewski et al. 2014), the LFQ intensity values were used to calculate the contribution of all mitochondrial proteins, according to MitoCarta2.0, to the total protein mass. Log2 transformed LFQ intensity and fold changes were used to generate density ad MA-plots plots. The mean LFQ value of controls was used to generate MA-plots.

Mouse MitoCarta2 protein sequences (Mouse.MitoCarta2.0.fasta) were downloaded from https://www.broadinstitute.org/scientific-community/science/programs/metabolic-disease-program/publications/mitocarta/mitocarta-in-0. The sequences were combined with the Mouse Mitocarta2 protein annotations using the RefSeq ID and the protein length. In cases of multiple matches with identical sequences, a single sequence was randomly selected. The extracted sequences were analyzed using TargetP 1.1 (Emanuelsson et al. 2000). The analysis was performed using "Non-plant" and "no cutoffs" parameters. The "Perform cleavage site predictions" option (Nielsen et al. 1997) was enabled. Protein sequences predicted to localize to the Mitochondrion, indicated by "M" in the Loc column, with reliability class (RC) of one, two, or three, were N-terminally trimmed by the value of predicted mitochondrial target peptide (mTP) presequence length (TPlen columns). The initial methionine was removed from the remaining of sequences. In addition, a second set of sequences was derived by removing the initial methionine only. The seqinr package (Charif and Lobry, 2007) was used to calculate the isoelectric points (pI) and the grand average of hydropathy (GRAVY) scores of the two sets of sequences. The GRAVY scores were computed by calculating the sum of the Hydropathy

index (Kyte and Doolittle, 1982) of all amino acids in the protein sequence and dividing the value by the protein sequence length. The pI and GRAVY score values were combined with the average log2 RNA reads count per L/L, cre genotype and with the number of genotypes that had quantification values in the proteomic analysis. The data was divided into two disjoint sets, namely proteins quantified in zero genotypes and proteins quantified in at least one genotype. The empirical cumulative distributions of the pIs, GRAVY scores and the average log2 RNA counts of the two sets were visualized using the stat_ecdf function of the ggplot2 package.

Mitochondrial proteins were manually placed in functional categories based on literature and Uniprot (The UniProt Consortium 2017). For the L/L comparison across different time points, MaxQuant's proteinGroups.txt file was combined with annotations from MitoCarta2.0 (Calvo, Clauser & Mootha 2016) as described above. The MitoCarta annotated data were imported into Perseus and filtered for at least nine valid LFQ intensity values across all samples (26 in total). Only proteins annotated as mitochondrial, according to the "MitoCarta2_List" column, were kept for analysis. Missing values were imputed as described above. Limma's F-statistic was used to detect proteins with significant differences in protein expression across the time points. Testing was performed after the data were grouped per week (nine week-groups in total). The fold changes of the average LFQ intensity for all time points, relative to week three were calculated, scaled, and z-score normalized in R. Hierarchical clustering of the normalized data was performed with pheatmap, version 1.0.8 (Kolde, 2015), using Euclidean distance as a metric. The rows (proteins) dendrogram was cut into to ten clusters and proteins, which partitioned into the four main clusters. Profiles plots of the normalized fold change values were color-coded using the distance of each profile from the cluster center (mean value).

For the *Lrpprc* knockout time course analysis data were imported into Perseus, filtered for at least 23 valid LFQ intensity values across all samples (46 in total), and missing values were imputed as described above. Limma's F-statistic was used to detect proteins with significant differences in protein expression across the time-points for either the L/L or the L/L, cre genotype. In addition, the F-statistic was used to identify differentially expressed proteins that have a significant difference in the profile across the time-points. To compare complete categories of proteins, Wilcoxon signed-ranked test followed by FDR correction was performed.

6.5.3.RNA-Seq data analysis

Differential expression analyses of total RNA-Seq were performed with DESeq2 package R version 3.3.2 according to the standard DESeq2 tutorial that is part of the package (Love et al.

2014). Mt-RNAs were analysed according to the same protocol except the NUMT regions were masked, filtered to reads in proper pairs and analysed by DESeq2 as described above. Differential expression analysis of PARE sequencing was performed in R 3.2.0 with edgeR 3.11.2 using a generalized linear model approach with tagwise dispersion estimates, and the offsets were generated by EDASeq (Robinson et al. 2010).

RNA-Seq data were analysed through the use of Ingenuity Pathways Analysis (Ingenuity® Systems, www.ingenuity.com). Log2 transformed fold changes and adjusted p values were uploaded to the program. Genes from the data set that met the adjusted p value cutoff of 0.05 in all the knockout strains of this study and were associated with a canonical pathway in Ingenuity's Knowledge Base were considered for the analysis. The significance of the association between the data set and the canonical pathway was measured in 2 ways: 1) A ratio of the number of molecules from the data set that map to the pathway divided by the total number of molecules that map to the canonical pathway is displayed, 2) Fisher's exact test was used to calculate a p value determining the probability that the association between the genes in the dataset and the canonical pathway is explained by chance alone. Genes from the RNA-Seq data sets that had a p value < 0.05 for all the knockout strains were loaded into Cytoscape (version 3.5.0; Shannon et al. 2003) and used as queries to the iRegulon plug-in (Janky et al. 2014). The putative regulatory region was selected to be 20 kb centred on the transcriptional start site (TSS), the normalized enrichment score (NES) threshold was set at 3.0, and the maximum FDR on motif similarity was set at 0.001. Transcription factor enrichment analyses were performed based on motif or ChIP-Seq peaks enrichment using the 10K (9713 PWMs) motif collection and the 1120 ChIP-Seq track collection, respectively. Target genes for MYC and ATF4 were obtained from published ChIP-Seq experiments (Han et al. 2013; Seitz et al. 2011).

6.5.4. 2D annotation enrichment analysis

2D annotation enrichment analysis of the proteomic and transcriptomic data was performed with Perseus (Cox & Mann 2012) using Benjamini-Hochberg FDR for truncation and a threshold value of 0.2. For the evaluation of the protein abundances during the post-natal development, identification of overrepresented functional categories in separate clusters was performed using Fisher exact test in Perseus. Benjamini-Hochberg FDR for truncation with a threshold value of 1. The top three overrepresented categories in each cluster, based on adjusted p value, are shown.

6.5.5. Statistical analyses

Each mouse was considered an independent biological replicate (n) and repeated measurements of the same biological replicate were considered technical replicates. Unless indicated otherwise, ≥3 biological replicates of transgenic mouse strain and their respective age-matched control mice were used for all the experiments presented. Statistical analyses for RNA-Seq and MS protein quantification analyses were performed as described above. For qRT-PCR and metabolomics analyses variance was assessed using an F-test and statistical significance was assessed by a two-sample, two-tailed unpaired Student's *t*-test in Excel. *In organello* experiments were analysed using a one-sample, two-tailed Student's *t*-test with μ: 100. Multiple comparison was corrected using Benjamini-Hochberg or Bonferroni correction as indicated in the figure legends. Statistical analyses were performed in Excel or R Studio version 1.1.383. Data visualization in R was done using ggplot2 version 2.2.1 or pheatmap R packages version 1.08, respectively. The definition of centre and precision measures, and p values are provided in the figure legends. $p < 0.05$ was considered significant.

6.6. Copyright of the main publications included in this thesis

Results figures were reproduced from Kühl et al. 2014, Kühl et al. 2016, and Kühl et al. 2017 from which I am co-author. The authors retain the rights on Kühl et al. 2014 for non-commercial use (https://www.nature.com/reprints/permission-requests.html). Material from Kühl et al. 2016 is reproduced under the Creative Commons Attribution-Non Commercial 4.0 International licence (CC BY-NC 4.0) (https://creativecommons.org/licenses/by-nc/4.0/). Material from Kühl et al. 2017 is reproduced under a Creative Commons Attribution 4.0 International (CC BY 4.0) (https://creativecommons.org/licenses/by/4.0/).

7. REFERENCES

Agaronyan, K. et al., 2015. Mitochondrial biology. Replication-transcription switch in human mitochondria. *Science*, 347(6221), pp.548–551.

Ahuja, P. et al., 2010. Myc controls transcriptional regulation of cardiac metabolism and mitochondrial biogenesis in response to pathological stress in mice. *The Journal of Clinical Investigation*, 120(5), pp.1494–1505.

Aldridge, J.E., Horibe, T. & Hoogenraad, N.J., 2007. Discovery of genes activated by the mitochondrial unfolded protein response (mtUPR) and cognate promoter elements. *PloS One*, 2(9), p.e874.

Allen, J.F., 2017. The CoRR hypothesis for genes in organelles. *Journal of Theoretical Biology*, 434, pp.50–57.

Amunts, A. et al., 2015. Ribosome. The structure of the human mitochondrial ribosome. *Science*, 348(6230), pp.95–98.

Anderson, S. et al., 1981. Sequence and organization of the human mitochondrial genome. *Nature*, 290(5806), pp.457–465.

Antonicka, H. & Shoubridge, E.A., 2015. Mitochondrial RNA granules are centers for posttranscriptional RNA processing and ribosome biogenesis. *Cell Reports*.

Antonicka, H. et al., 2017. A pseudouridine synthase module is essential for mitochondrial protein synthesis and cell viability. *EMBO Reports*, 18(1), pp.28–38.

Antonicka, H. et al., 2013. The mitochondrial RNA-binding protein GRSF1 localizes to RNA granules and is required for posttranscriptional mitochondrial gene expression. *Cell Metabolism*, 17(3), pp.386–398.

Arai, M., Matsui, H. & Periasamy, M., 1994. Sarcoplasmic reticulum gene expression in cardiac hypertrophy and heart failure. *Circulation Research*, 74(4), pp.555–564.

Arroyo, J.D. et al., 2016. A genome-wide CRISPR death screen identifies genes essential for oxidative phosphorylation. *Cell Metabolism*, 24(6), pp.875–885.

Asin-Cayuela, J. et al., 2005. The human mitochondrial transcription termination factor (mTERF) is fully active in vitro in the non-phosphorylated form. *The Journal of Biological Chemistry*, 280(27), pp.25499–25505.

Attardi, G. et al., 1979. Nucleotide sequence of a fragment of HeLa-cell mitochondrial DNA containing the precisely localized origin of replication. *Cold Spring Harbor Symposia on Quantitative Biology*, 43(0), pp.179–192.

Bandy, B. & Davison, A.J., 1990. Mitochondrial mutations may increase oxidative stress: implications for carcinogenesis and aging? *Free Radical Biology & Medicine*, 8(6), pp.523–539.

Bao, X.R. et al., 2016. Mitochondrial dysfunction remodels one-carbon metabolism in human cells. *eLife*, 5, p.1910.

Ben-Sahra, I. et al., 2016. mTORC1 induces purine synthesis through control of the mitochondrial tetrahydrofolate cycle. *Science*, 351(6274), pp.728–733.

Björkholm, P. et al., 2015. Mitochondrial genomes are retained by selective constraints on protein targeting. *Proceedings of the National Academy of Sciences of the United States of America*, 112(33), pp.10154–10161.

Bogenhagen, D. & Clayton, D.A., 1978. Mechanism of mitochondrial DNA replication in mouse L-cells: kinetics of synthesis and turnover of the initiation sequence. *Journal of Molecular Biology*, 119(1), pp.49–68.

Bogenhagen, D.F., 2012. Mitochondrial DNA nucleoid structure. *Biochimica et Biophysica Acta*, 1819(9-10), pp.914–920.

Bogenhagen, D.F., Martin, D.W. & Koller, A., 2014. Initial steps in RNA processing and ribosome assembly occur at mitochondrial DNA nucleoids. *Cell Metabolism*, 19(4), pp.618–629.

Bogenhagen, D.F. et al., 2018. Kinetics and mechanism of mammalian mitochondrial ribosome assembly. *Cell Reports*, 22(7), pp.1935–1944.

Bonekamp, N.A. & Larsson, N.-G., 2018. SnapShot: Mitochondrial Nucleoid. *Cell*, 172(1-2), pp.388–388.e1.

Borowski, L.S. et al., 2013. Human mitochondrial RNA decay mediated by PNPase-hSuv3 complex takes place in distinct foci. *Nucleic Acids Research*, 41(2), pp.1223–1240.

Bratic, A. et al., 2016. Mitochondrial polyadenylation is a one-step process required for mRNA integrity and tRNA maturation. *PLoS Genetics*, 12(5), p.e1006028.

Brown, D.A. et al., 2017. Expert consensus document: Mitochondrial function as a therapeutic target in heart failure. *Nature reviews. Cardiology*, 14(4), pp.238–250.

Bruni, F. et al., 2010. Nuclear respiratory factor 2 induces the expression of many but not all human proteins acting in mitochondrial DNA transcription and replication. *Journal of Biological Chemistry*, 285(6), pp.3939–3948.

Bruni, F. et al., 2013. REXO2 is an oligoribonuclease active in human mitochondria. *PloS One*, 8(5), p.e64670.

Bruni, F., Lightowlers, R.N. & Chrzanowska-Lightowlers, Z.M., 2017. Human mitochondrial nucleases. *The FEBS Journal*, 284(12), pp.1767–1777.

Brzezniak, L.K. et al., 2011. Involvement of human ELAC2 gene product in 3' end processing of mitochondrial tRNAs. *RNA Biology*, 8(4), pp.616–626.

Burki, F., 2016. Mitochondrial Evolution: Going, Going, Gone. *Current Biology*, 26(10), pp.R410–2.

Calvo, S.E. & Mootha, V.K., 2010. The mitochondrial proteome and human disease. *Annual Review of Genomics and Human Genetics*, 11(1), pp.25–44.

Calvo, S.E., Clauser, K.R. & Mootha, V.K., 2016. MitoCarta2.0: an updated inventory of mammalian mitochondrial proteins. *Nucleic Acids Research*, 44(D1), pp.D1251–7.

Cam, H. et al., 2004. A common set of gene regulatory networks links metabolism and growth inhibition. *Molecular Cell*, 16(3), pp.399–411.

Camp, K.M. et al., 2016. Nutritional interventions in primary mitochondrial disorders: Developing an evidence base. *Molecular Genetics and Metabolism*, 119(3), pp.187–206.

Cámara, Y. et al., 2011. MTERF4 regulates translation by targeting the methyltransferase NSUN4 to the mammalian mitochondrial ribosome. *Cell Metabolism*, 13(5), pp.527–539.

Chang, D.D. & Clayton, D.A., 1985. Priming of human mitochondrial DNA replication occurs at the light-strand promoter. *Proceedings of the National Academy of Sciences*, 82(2), pp.351–355.

Chang, D.D., Hauswirth, W.W. & Clayton, D.A., 1985. Replication priming and transcription initiate from precisely the same site in mouse mitochondrial DNA. *The EMBO Journal*, 4(6), pp.1559–1567.

Chujo, T. et al., 2012. LRPPRC/SLIRP suppresses PNPase-mediated mRNA decay and promotes polyadenylation in human mitochondria. *Nucleic Acids Research*, 40(16), pp.8033–8047.

Clayton, D.A., 1991. Replication and transcription of vertebrate mitochondrial DNA. *Annual Review of Cell Biology*, 7, pp.453–478.

Connor, T.M. et al., 2017. Mutations in mitochondrial DNA causing tubulointerstitial kidney disease. *PLoS Genetics*, 13(3), p.e1006620.

Couvillion, M.T. et al., 2016. Synchronized mitochondrial and cytosolic translation programs. *Nature*, 533(7604), pp.499–503.

Cox, B. & Emili, A., 2006. Tissue subcellular fractionation and protein extraction for use in mass-spectrometry-based proteomics. *Nature Protocols*, 1(4), pp.1872–1878.

Cox, J & Mann, M., 2012. 1D and 2D annotation enrichment: a statistical method integrating quantitative proteomics with complementary high-throughput data. *BMC Bioinformatics*, 13 Suppl 16, p.S12.

Cox, J. et al., 2014. Accurate proteome-wide label-free quantification by delayed normalization and maximal peptide ratio extraction, termed MaxLFQ. *Molecular & Cellular Proteomics*, 13(9), pp.2513–2526.

Dairaghi, D.J., Shadel, G.S. & Clayton, D.A., 1995a. Human mitochondrial transcription factor A and promoter spacing integrity are required for transcription initiation. *Biochimica et Biophysica Acta*, 1271(1), pp.127–134.

Dairaghi, D.J., Shadel, G.S. & Clayton, D.A., 1995b. Addition of a 29 residue carboxyl-terminal tail converts a simple HMG box-containing protein into a transcriptional activator. *Journal of Molecular Biology*, 249(1), pp.11–28.

DiMauro, S. & Schon, E.A., 2003. Mitochondrial respiratory-chain diseases. *The New England Journal of Medicine*, 348(26), pp.2656–2668.

Diodato, D., Ghezzi, D. & Tiranti, V., 2014. The Mitochondrial Aminoacyl tRNA Synthetases: Genes and Syndromes. *International Journal of Cell Biology*, 2014(2), pp.787956–11.

Dogan, S.A. et al., 2014. Tissue-specific loss of DARS2 activates stress responses independently of respiratory chain deficiency in the heart. *Cell Metabolism*, 19(3), pp.458–469.

Doll, S. et al., 2017. Region and cell-type resolved quantitative proteomic map of the human heart. *Nature Communications*, 8(1), p.1469.

Ducker, G.S. & Rabinowitz, J.D., 2017. One-carbon metabolism in health and disease. *Cell Metabolism*, 25(1), pp.27–42.

Ekstrand, M.I. et al., 2004. Mitochondrial transcription factor A regulates mtDNA copy number in mammals. *Human Molecular Genetics*, 13(9), pp.935–944.

Emmanuele, V. et al., 2012. Heterogeneity of coenzyme Q10 deficiency: patient study and literature review. *Archives of Neurology*, 69(8), pp.978–983.

Falkenberg, M. et al., 2002. Mitochondrial transcription factors B1 and B2 activate transcription of human mtDNA. *Nature Genetics*, 31(3), pp.289–294.

Farge, G. et al., 2014. In vitro-reconstituted nucleoids can block mitochondrial DNA replication and transcription. *Cell Reports*, 8(1), pp.66–74.

Felici, R. et al., 2017. Post onset, oral rapamycin treatment delays development of mitochondrial encephalopathy only at supramaximal doses. *Neuropharmacology*, 117, pp.74–84.

Fernandez-Vizarra, E. & Zeviani, M., 2018. Mitochondrial complex III Rieske Fe-S protein processing and assembly. *Cell Cycle*, 17(6), pp.681–687.

Ferrari, M. et al., 2017. Hypoxia treatment reverses neurodegenerative disease in a mouse model of Leigh syndrome. *Proceedings of the National Academy of Sciences of the United States of America*, 114(21), pp.E4241–E4250.

Finck, B.N. et al., 2002. Regulatory networks controlling mitochondrial energy production in the developing, hypertrophied, and diabetic heart. *Cold Spring Harbor Symposia on Quantitative Biology*, 67, pp.371–382.

Fiorese, C.J. et al., 2016. The transcription factor ATF5 mediates a mammalian mitochondrial UPR. *Current Biology*, 26(15), pp.2037–2043.

Fisher, F.M. & Maratos-Flier, E., 2016. Understanding the physiology of FGF21. *Annual Review of Physiology*, 78(1), pp.223–241.

Floyd, B.J. et al., 2016. Mitochondrial protein interaction mapping identifies regulators of respiratory chain function. *Molecular Cell*, 63(4), pp.621–632.

Freyer, C. et al., 2010. Maintenance of respiratory chain function in mouse hearts with severely impaired mtDNA transcription. *Nucleic Acids Research*, 38(19), pp.6577–6588.

Frezza, C., Cipolat, S. & Scorrano, L., 2007. Organelle isolation: functional mitochondria from mouse liver, muscle and cultured fibroblasts. *Nature Protocols*, 2(2), pp.287–295.

Fusté, J.M. et al., 2010. Mitochondrial RNA polymerase is needed for activation of the origin of light-strand DNA replication. *Molecular Cell*, 37(1), pp.67–78.

Galluzzi, L., Kepp, O. & Kroemer, G., 2016. Mitochondrial regulation of cell death: a phylogenetically conserved control. *Microbial cell (Graz, Austria)*, 3(3), pp.101–108.

García-Gómez, S. et al., 2013. PrimPol, an archaic primase/polymerase operating in human cells. *Molecular Cell*, 52(4), pp.541–553.

García-Muse, T. & Aguilera, A., 2016. Transcription-replication conflicts: how they occur and how they are resolved. *Nature reviews. Molecular Cell Biology*, 17(9), pp.553–563.

Garrido-Maraver, J. et al., 2014. Coenzyme q10 therapy. *Molecular Syndromology*, 5(3-4), pp.187–197.

Gaspari, M. et al., 2004. The mitochondrial RNA polymerase contributes critically to promoter specificity in mammalian cells. *The EMBO Journal*, 23(23), pp.4606–4614.

Gillum, A.M. & Clayton, D.A., 1979. Mechanism of mitochondrial DNA replication in mouse L-cells: RNA priming during the initiation of heavy-strand synthesis. *Journal of Molecular Biology*, 135(2), pp.353–368.

Goffart, S., Kleist-Retzow, von, J.-C. & Wiesner, R.J., 2004. Regulation of mitochondrial proliferation in the heart: power-plant failure contributes to cardiac failure in hypertrophy. *Cardiovascular Research*, 64(2), pp.198–207.

Golpich, M. et al., 2017. mitochondrial dysfunction and biogenesis in neurodegenerative diseases: pathogenesis and treatment. *CNS Neuroscience & Therapeutics*, 23(1), pp.5–22.

Gonczarowska-Jorge, H., Zahedi, R.P. & Sickmann, A., 2017. The proteome of baker's yeast mitochondria. *Mitochondrion*, 33, pp.15–21.

Gorman, G.S. et al., 2016. Mitochondrial diseases. *Nature Reviews. Disease Primers*, 2, p.16080.

Greber, B.J. et al., 2014a. The complete structure of the large subunit of the mammalian mitochondrial ribosome. *Nature*, 515(7526), pp.283–286.

Greber, B.J. et al., 2014b. Architecture of the large subunit of the mammalian mitochondrial ribosome. *Nature*, 505(7484), pp.515–519.

Gruschke, S. & Ott, M., 2010. The polypeptide tunnel exit of the mitochondrial ribosome is tailored to meet the specific requirements of the organelle. *BioEssays: News and Reviews in Molecular, Cellular and Developmental Biology*, 32(12), pp.1050–1057.

Guda, P., Guda, C. & Subramaniam, S., 2007. Reconstruction of pathways associated with amino acid metabolism in human mitochondria. *Genomics, Proteomics & Bioinformatics*, 5(3-4), pp.166–176.

Guerrero-Castillo, S. et al., 2017. The assembly pathway of mitochondrial respiratory chain complex I. *Cell Metabolism*, 25(1), pp.128–139.

Guilliam, T.A. et al., 2015. Primase-polymerases are a functionally diverse superfamily of replication and repair enzymes. *Nucleic Acids Research*, 43(14), pp.6651–6664.

Gustafsson, C.M., Falkenberg, M. & Larsson, N.-G., 2016. Maintenance and expression of mammalian mitochondrial DNA. *Annual Review of Biochemistry*, 85(1), pp.133–160.

Han, J. et al., 2013. ER-stress-induced transcriptional regulation increases protein synthesis leading to cell death. *Nature Cell Biology*, 15(5), pp.481–490.

Hance, N., Ekstrand, M.I. & Trifunovic, A., 2005. Mitochondrial DNA polymerase gamma is essential for mammalian embryogenesis. *Human Molecular Genetics*, 14(13), pp.1775–1783.

Hansson, A. et al., 2004. A switch in metabolism precedes increased mitochondrial biogenesis in respiratory chain-deficient mouse hearts. *Proceedings of the National Academy of Sciences*, 101(9), pp.3136–3141.

Haynes, C.M. et al., 2007. ClpP mediates activation of a mitochondrial unfolded protein response in C. elegans. *Developmental Cell*, 13(4), pp.467–480.

Hällberg, B.M. & Larsson, N.-G., 2014. Making proteins in the powerhouse. *Cell Metabolism*, 20(2), pp.226–240.

He, J. et al., 2018. Assembly of the membrane domain of ATP synthase in human mitochondria. *Proceedings of the National Academy of Sciences of the United States of America*, 115(12), pp.2988–2993.

Heublein, M. et al., 2014. The novel component Kgd4 recruits the E3 subunit to the mitochondrial α-ketoglutarate dehydrogenase. *Molecular Biology of the Cell*, 25(21), pp.3342–3349.

Hillen, H.S. et al., 2017a. Structural basis of mitochondrial transcription initiation. *Cell*, 171(5), pp.1072–1081.e10.

Hillen, H.S. et al., 2017b. Mechanism of transcription anti-termination in human mitochondria. *Cell*, 171(5), pp.1082–1093.e13.

Houten, S.M. et al., 2016. The biochemistry and physiology of mitochondrial fatty acid β-oxidation and its genetic disorders. *Annual Review of Physiology*, 78(1), pp.23–44.

Huo, L. & Scarpulla, R.C., 2001. Mitochondrial DNA instability and peri-implantation lethality associated with targeted disruption of nuclear respiratory factor 1 in mice. *Molecular and Cellular Biology*, 21(2), pp.644–654.

Jain, I.H. et al., 2016. Hypoxia as a therapy for mitochondrial disease. *Science*, 352(6281), pp.54–61.

Jemt, E. et al., 2015. Regulation of DNA replication at the end of the mitochondrial D-loop involves the helicase TWINKLE and a conserved sequence element. *Nucleic Acids Research*, 43(19), pp.9262–9275.

Jiang, M. et al., 2017. Increased total mtDNA copy number aures male infertility despite unaltered mtDNA mutation load. *Cell Metabolism*, 26(2), pp.429–436.e4.

Johnson, S.C. et al., 2013. mTOR inhibition alleviates mitochondrial disease in a mouse model of Leigh syndrome. *Science*, 342(6165), pp.1524–1528.

Jourdain, A.A. et al., 2013. GRSF1 regulates RNA processing in mitochondrial RNA granules. *Cell Metabolism*, 17(3), pp.399–410.

Jourdain, A.A. et al., 2017. The FASTK family of proteins: emerging regulators of mitochondrial RNA biology. *Nucleic Acids Research*, 45(19), pp.10941–10947.

Karnkowska, A. et al., 2016. A Eukaryote without a Mitochondrial Organelle. *Current biology*, 26(10), pp.1274–1284.

Kaufman, B.A. et al., 2007. The mitochondrial transcription factor TFAM coordinates the assembly of multiple DNA molecules into nucleoid-like structures. *Molecular Biology of the Cell*, 18(9), pp.3225–3236.

Kauppila, J.H.K. et al., 2018. Base-excision repair deficiency alone or combined with increased oxidative stress does not increase mtDNA point mutations in mice. *Nucleic Acids Research*, 29, p.151.

Kauppila, T.E.S., Kauppila, J.H.K. & Larsson, N.-G., 2017. Mammalian mitochondria and aging: an update. *Cell Metabolism*, 25(1), pp.57–71.

Kelly, D.P. & Scarpulla, R.C., 2004. Transcriptional regulatory circuits controlling mitochondrial biogenesis and function. *Genes & Development*, 18(4), pp.357–368.

Khan, N.A. et al., 2017. mTORC1 regulates mitochondrial integrated stress response and mitochondrial myopathy progression. *Cell Metabolism*, 26(2), pp.419–428.e5.

Khidr, L. et al., 2008. Role of SUV3 helicase in maintaining mitochondrial homeostasis in human cells. *The Journal of Biological Chemistry*, 283(40), pp.27064–27073.

Kim, D., Langmead, B. & Salzberg, S.L., 2015. HISAT: a fast spliced aligner with low memory requirements. *Nature Methods*, 12(4), pp.357–360.

King, G.A. et al., 2018. Acetylation and phosphorylation of human TFAM regulate TFAM-DNA interactions via contrasting mechanisms. *Nucleic Acids Research*, 46(7), pp.3633–3642.

King, M. & Attardi, G., 1989. Human cells lacking mtDNA: repopulation with exogenous mitochondria by complementation. Science, 246(4929), pp.500–503.

Koc, E.C. & Spremulli, L.L., 2002. Identification of mammalian mitochondrial translational initiation factor 3 and examination of its role in initiation complex formation with natural mRNAs. *The Journal of Biological Chemistry*, 277(38), pp.35541–35549.

Korhonen, J.A. et al., 2004. Reconstitution of a minimal mtDNA replisome in vitro. *The EMBO Journal*, 23(12), pp.2423–2429.

Kotani, T. et al., 2013. Human G-proteins, ObgH1 and Mtg1, associate with the large mitochondrial ribosome subunit and are involved in translation and assembly of respiratory complexes. *Nucleic Acids Research*, 41(6), pp.3713–3722.

Kranz, R.G. et al., 2009. Cytochrome c biogenesis: mechanisms for covalent modifications and trafficking of heme and for heme-iron redox control. *Microbiology and Molecular Biology Reviews*, 73(3), pp.510–28.

Kravchenko, J.E. et al., 2005. Transcription of mammalian messenger RNAs by a nuclear RNA polymerase of mitochondrial origin. *Nature*, 436(7051), pp.735–739.

Kravchenko, Y.E. & Chumakov, P.M., 2005. Alternative transcripts of *POLRMT* gene coding for nuclear RNA polymerase IV. *Molecular Biology*, 39(1), pp.58–61.

Kukat, C. et al., 2015. Cross-strand binding of TFAM to a single mtDNA molecule forms the mitochondrial nucleoid. *Proceedings of the National Academy of Sciences of the United States of America*, 112(36), pp.11288–11293.

Kukat, C. et al., 2011. Super-resolution microscopy reveals that mammalian mitochondrial nucleoids have a uniform size and frequently contain a single copy of mtDNA. *Proceedings of the National Academy of Sciences of the United States of America*, 108(33), pp.13534–13539.

Kulak, N.A. et al., 2014. Minimal, encapsulated proteomic-sample processing applied to copy-number estimation in eukaryotic cells. *Nature Methods*, 11(3), pp.319–324.

Kühl, I. et al., 2014. POLRMT does not transcribe nuclear genes. *Nature*, 514(7521), pp.E7–11.

Kühl, I. et al., 2016. POLRMT regulates the switch between replication primer formation and gene expression of mammalian mtDNA. *Science Advances*, 2(8), pp.e1600963–e1600963.

Kühl, I. et al., 2017. Transcriptomic and proteomic landscape of mitochondrial dysfunction reveals secondary coenzyme Q deficiency in mammals. *eLife*, 6, p.1494.

Lagouge, M. et al., 2015. SLIRP regulates the rate of mitochondrial protein synthesis and protects LRPPRC from degradation. *PLoS Genetics*, 11(8), p.e1005423.

Lakshmipathy, U. & Campbell, C., 1999. The human DNA ligase III gene encodes nuclear and mitochondrial proteins. *Molecular and Cellular Biology*, 19(5), pp.3869–3876.

Lane, N. & Martin, W., 2010. The energetics of genome complexity. *Nature*, 467(7318), pp.929–934.

Larsson, N.-G., 2010. Somatic mitochondrial DNA mutations in mammalian aging. *Annual Review of Biochemistry*, 79(1), pp.683–706.

Larsson, N.G. et al., 1994. Low levels of mitochondrial transcription factor A in mitochondrial DNA depletion. *Biochemical and Biophysical Research Communications*, 200(3), pp.1374–1381.

Larsson, N.G. et al., 1998. Mitochondrial transcription factor A is necessary for mtDNA maintenance and embryogenesis in mice. *Nature Genetics*, 18(3), pp.231–236.

Ledwith, B.J., Manam, S. & Van Tuyle, G.C., 1986. Characterization of a DNA primase from rat liver mitochondria. *The Journal of Biological Chemistry*, 261(14), pp.6571–6577.

Lee, D.Y. & Clayton, D.A., 1996. Properties of a primer RNA-DNA hybrid at the mouse mitochondrial DNA leading-strand origin of replication. *The Journal of Biological Chemistry*, 271(39), pp.24262–24269.

Lee, K.-W. et al., 2013. Mitochondrial ribosomal RNA (rRNA) methyltransferase family members are positioned to modify nascent rRNA in foci near the mitochondrial DNA nucleoid. *Journal of Biological Chemistry*, 288(43), pp.31386–31399.

Lee, Y.-L., Chiao, C.-H. & Hsu, M.-T., 2011. Transcription of muscle actin genes by a nuclear form of mitochondrial RNA polymerase. *PloS One*, 6(7), p.e22583.

Lehtonen, J.M. et al., 2016. FGF21 is a biomarker for mitochondrial translation and mtDNA maintenance disorders. *Neurology*, 87(22), pp.2290–2299.

Levi, S. & Rovida, E., 2009. The role of iron in mitochondrial function. *Biochimica et Biophysica Acta*, 1790(7), pp.629–636.

Levy, S. et al., 2016. Identification of LACTB2, a metallo-β-lactamase protein, as a human mitochondrial endoribonuclease. *Nucleic Acids Research*, 44(4), pp.1813–1832.

Li, G.-W. et al., 2014. Quantifying absolute protein synthesis rates reveals principles underlying allocation of cellular resources. *Cell*, 157(3), pp.624–635.

Li, H. et al., 2009. The Sequence Alignment/Map format and SAMtools. *Bioinformatics*, 25(16), pp.2078–2079.

Liang, C., Ahmad, K. & Sue, C.M., 2014. The broadening spectrum of mitochondrial disease: shifts in the diagnostic paradigm. *Biochimica et Biophysica Acta*, 1840(4), pp.1360–1367.

Lightowlers, R.N. & Chrzanowska-Lightowlers, Z.M.A., 2013. Human pentatricopeptide proteins: only a few and what do they do? *RNA Biology*, 10(9), pp.1433–1438.

Litonin, D. et al., 2010. Human mitochondrial transcription revisited: only TFAM and TFB2M are required for transcription of the mitochondrial genes in vitro. *Journal of Biological Chemistry*, 285(24), pp.18129–18133.

Liu, L. et al., 2011. LRP130 protein remodels mitochondria and stimulates fatty acid oxidation. *Journal of Biological Chemistry*, 286(48), pp.41253–41264.

Liu, M. & Spremulli, L., 2000. Interaction of mammalian mitochondrial ribosomes with the inner membrane. *The Journal of Biological Chemistry*, 275(38), pp.29400–29406.

Liu, W. et al., 2012. Reprogramming of proline and glutamine metabolism contributes to the proliferative and metabolic responses regulated by oncogenic transcription factor c-MYC. *Proceedings of the National Academy of Sciences of the United States of America*, 109(23), pp.8983–8988.

Lodeiro, M.F. et al., 2010. Identification of multiple rate-limiting steps during the human mitochondrial transcription cycle in vitro. *Journal of Biological Chemistry*, 285(21), pp.16387–16402.

Lott, M.T. et al., 2013. mtDNA variation and analysis using MITOMAP and MITOMASTER. *Current Protocols in Bioinformatics* 1(123):1.23.1-26. URL: http://www.mitomap.org

Love, M.I., Huber, W. & Anders, S., 2014. Moderated estimation of fold change and dispersion for RNA-Seq data with DESeq2. *Genome Biology*, 15(12), p.550.

Lowell, B.B. & Shulman, G.I., 2005. Mitochondrial dysfunction and type 2 diabetes. *Science*, 307(5708), pp.384–387.

Lu, B. et al., 2013. Phosphorylation of human TFAM in mitochondria impairs DNA binding and promotes degradation by the AAA+ Lon protease. *Molecular Cell*, 49(1), pp.121–132.

Martin, M. et al., 2005. Termination factor-mediated DNA loop between termination and initiation sites drives mitochondrial rRNA synthesis. *Cell*, 123(7), pp.1227–1240.

Martin, W.F. & Mentel, M., 2010. The Origin of Mitochondria. *Nature Education*, 3(9), p.58.

Martinus, R.D. et al., 1996. Selective induction of mitochondrial chaperones in response to loss of the mitochondrial genome. *European Journal of Biochemistry*, 240(1), pp.98–103.

Matic, S. et al., 2018. Mice lacking the mitochondrial exonuclease MGME1 accumulate mtDNA deletions without developing progeria. *Nature Communications*, 9(1), p.1202.

Matsushima, Y., Goto, Y.-I. & Kaguni, L.S., 2010. Mitochondrial Lon protease regulates mitochondrial DNA copy number and transcription by selective degradation of mitochondrial transcription factor A (TFAM). *Proceedings of the National Academy of Sciences of the United States of America*, 107(43), pp.18410–18415.

McShane, E. et al., 2016. Kinetic analysis of protein stability reveals age-dependent degradation. *Cell*, 167(3), pp.803–815.e21.

Mercer, T.R. et al., 2011. The human mitochondrial transcriptome. *Cell*, 146(4), pp.645–658.

Merrikh, H. et al., 2012. Replication-transcription conflicts in bacteria. *Nature reviews. Microbiology*, 10(7), pp.449–458.

Metodiev, M.D. et al., 2009. Methylation of 12S rRNA is necessary for in vivo stability of the small subunit of the mammalian mitochondrial ribosome. *Cell Metabolism*, 9(4), pp.386–397.

Metodiev, M.D. et al., 2014. NSUN4 is a dual function mitochondrial protein required for both methylation of 12S rRNA and coordination of mitoribosomal assembly. *PLoS Genetics*, 10(2), p.e1004110.

Milenkovic, D. et al., 2017. The enigma of the respiratory chain supercomplex. *Cell Metabolism*, 25(4), pp.765–776.

Milenkovic, D. et al., 2013. TWINKLE is an essential mitochondrial helicase required for synthesis of nascent D-loop strands and complete mtDNA replication. *Human Molecular Genetics*, 22(10), pp.1983–1993.

Minczuk, M. et al., 2011. TEFM (c17orf42) is necessary for transcription of human mtDNA. *Nucleic Acids Research*, 39(10), pp.4284–4299.

Minton, D.R. et al., 2018. Serine catabolism by SHMT2 is required for proper mitochondrial translation initiation and maintenance of formylmethionyl-tRNAs. *Molecular Cell*, 69(4), pp.610–621.e5.

Morozov, Y.I. & Temiakov, D., 2016. Human mitochondrial transcription initiation complexes have similar topology on the light and heavy strand promoters. *Journal of Biological Chemistry*, 291(26), pp.13432–13435.

Morozov, Y.I. et al., 2015. A model for transcription initiation in human mitochondria. *Nucleic Acids Research*, 43(7), pp.3726–3735.

Morozov, Y.I. et al., 2014. A novel intermediate in transcription initiation by human mitochondrial RNA polymerase. *Nucleic Acids Research*, 42(6), pp.3884–3893.

Morrish, F. & Hockenbery, D., 2014. MYC and mitochondrial biogenesis. *Cold Spring Harbor Perspectives in Medicine*, 4(5), pp.a014225–a014225.

Morscher, R.J. et al., 2018. Mitochondrial translation requires folate-dependent tRNA methylation. *Nature*, 554(7690), pp.128–132.

Mosteller, F. & Tukey, J.W., 1977. *Data analysis and regression: a second course in statistics* 1st ed., Pearson.

Mourier, A. & Larsson, N.-G., 2011. Tracing the trail of protons through complex I of the mitochondrial respiratory chain. *PLoS Biology*, 9(8), p.e1001129.

Mourier, A. et al., 2014. Loss of LRPPRC causes ATP synthase deficiency. *Human Molecular Genetics*, 23(10), pp.2580–2592.

Mourier, A. et al., 2015. Mitofusin 2 is required to maintain mitochondrial coenzyme Q levels. *The Journal of Cell Biology*, 208(4), pp.429–442.

Müller, M. et al., 2012. Biochemistry and evolution of anaerobic energy metabolism in eukaryotes. *Microbiology and Molecular biology Reviews*, 76(2), pp.444–495.

Münch, C. & Harper, J.W., 2016. Mitochondrial unfolded protein response controls matrix pre-RNA processing and translation. *Nature*, 534(7609), pp.710–713.

Nargund, A.M. et al., 2015. Mitochondrial and nuclear accumulation of the transcription factor ATFS-1 promotes OXPHOS recovery during the UPR(mt). *Molecular Cell*, 58(1), pp.123–133.

Nelson, D.L. & Cox, M.M., 2009. *Lehninger Biochemie*

Ngo, H.B. et al., 2014. Distinct structural features of TFAM drive mitochondrial DNA packaging versus transcriptional activation. *Nature Communications*, 5(1), p.3077.

Nicholas, L.M. et al., 2017. Mitochondrial transcription factor B2 is essential for mitochondrial and cellular function in pancreatic β-cells. *Molecular Metabolism*, 6(7), pp.651–663.

Nicholls, T.J. & Minczuk, M., 2014. In D-loop: 40 years of mitochondrial 7S DNA. *Experimental Gerontology*, 56, pp.175–181.

Nicholls, T.J. et al., 2018. Topoisomerase 3α is required for decatenation and segregation of human mtDNA. *Molecular Cell*, 69(1), pp.9–23.e6.

Nielsen, J., 2017. Systems Biology of Metabolism: A driver for developing personalized and precision medicine. *Cell Metabolism*, 25(3), pp.572–579.

Nightingale, H. et al., 2016. Emerging therapies for mitochondrial disorders. *Brain*, 139(Pt 6), pp.1633–1648.

Nikkanen, J. et al., 2016. Mitochondrial DNA replication defects disturb cellular dNTP pools and Remodel One-Carbon Metabolism. *Cell Metabolism*, 23(4), pp.635–648.

Nilsson, R. et al., 2014. Metabolic enzyme expression highlights a key role for MTHFD2 and the mitochondrial folate pathway in cancer. *Nature Communications*, 5, p.3128.

Nouws, J. et al., 2016. Mitochondrial ribosomal protein L12 is required for POLRMT stability and exists as two forms generated by alternative proteolysis during import. *Journal of Biological Chemistry*, 291(2), pp.989–997.

Nunnari, J. & Suomalainen, A., 2012. Mitochondria: in sickness and in health. *Cell*, 148(6), pp.1145–1159.

Ojala, D. & Attardi, G., 1974. Identification of discrete polyadenylate-containing RNA components transcribed from HeLa cell mitochondrial DNA. *Proceedings of the National Academy of Sciences*, 71(2), pp.563–567.

Ojala, D., Montoya, J. & Attardi, G., 1981. tRNA punctuation model of RNA processing in human mitochondria. *Nature*, 290(5806), pp.470–474.

Oran, A.R. et al., 2016. Multi-focal control of mitochondrial gene expression by oncogenic MYC provides potential therapeutic targets in cancer. *Oncotarget*, 7(45), pp.72395–72414.

Pagliarini, D.J. & Rutter, J., 2013. Hallmarks of a new era in mitochondrial biochemistry. *Genes & Development*, 27(24), pp.2615–2627.

Pagliarini, D.J. et al., 2008. A mitochondrial protein compendium elucidates complex I disease biology. *Cell*, 134(1), pp.112–123.

Pakos-Zebrucka, K. et al., 2016. The integrated stress response. *EMBO Reports*, 17(10), pp.1374–1395.

Palmer, J.D., 1997. Organelle genomes: going, going, gone! *Science*, 275(5301), pp.790–791.

Park, C.B. et al., 2007. MTERF3 is a negative regulator of mammalian mtDNA transcription. *Cell*, 130(2), pp.273–285.

Pearce, S.F. et al., 2017. Regulation of mammalian mitochondrial gene expression: recent advances. *Trends in Biochemical Sciences*, 42(8), pp.625–639.

Perks, K.L. et al., 2018. PTCD1 Is required for 16S rRNA maturation complex stability and mitochondrial ribosome assembly. *Cell Reports*, 23(1), pp.127–142.

Pertea, M. et al., 2016. Transcript-level expression analysis of RNA-Seq experiments with HISAT, StringTie and Ballgown. *Nature Protocols*, 11(9), pp.1650–1667.

Pérez-Arellano, I. et al., 2010. Pyrroline-5-carboxylate synthase and proline biosynthesis: from osmotolerance to rare metabolic disease. *Protein Science*, 19(3), pp.372–382.

Pfeffer, G. et al., 2013. New treatments for mitochondrial disease-no time to drop our standards. *Nature Reviews. Neurology*, 9(8), pp.474–481.

Pham, X.H. et al., 2006. Conserved sequence box II directs transcription termination and primer formation in mitochondria. *Journal of Biological Chemistry*, 281(34), pp.24647–24652.

Pietras, Z. et al., 2018. Dedicated surveillance mechanism controls G-quadruplex forming non-coding RNAs in human mitochondria. *Nature Communications*, 9(1), p.2558.

Piquereau, J. et al., 2010. Postnatal development of mouse heart: formation of energetic microdomains. *The Journal of Physiology*, 588(Pt 13), pp.2443–2454.

Posse, V. & Gustafsson, C.M., 2017. Human mitochondrial transcription factor B2 is required for promoter melting during initiation of transcription. *Journal of Biological Chemistry*, 292(7), pp.2637–2645.

Posse, V. et al., 2015. TEFM is a potent stimulator of mitochondrial transcription elongation in vitro. *Nucleic Acids Research*, 43(5), pp.2615–2624.

Posse, V. et al., 2014. The amino terminal extension of mammalian mitochondrial RNA polymerase ensures promoter specific transcription initiation. *Nucleic Acids Research*, 42(6), pp.3638–3647.

Puebla-Osorio, N. et al., 2006. Early embryonic lethality due to targeted inactivation of DNA ligase III. *Molecular and Cellular Biology*, 26(10), pp.3935–3941.

Quirós, P.M. et al., 2017. Multi-omics analysis identifies ATF4 as a key regulator of the mitochondrial stress response in mammals. *The Journal of Cell Biology*, 216(7), pp.2027–2045.

Rackham, O. et al., 2016. Hierarchical RNA processing is required for mitochondrial ribosome assembly. *Cell Reports*, 16(7), pp.1874–1890.

Rackham, O., Mercer, T.R. & Filipovska, A., 2012. The human mitochondrial transcriptome and the RNA-binding proteins that regulate its expression. *Wiley Interdisciplinary Reviews. RNA*, 3(5), pp.675–695.

Ramachandran, A. et al., 2017. Human mitochondrial transcription factors TFAM and TFB2M work synergistically in promoter melting during transcription initiation. *Nucleic Acids Research*, 45(2), pp.861–874.

Rappsilber, J., Ishihama, Y. & Mann, M., 2003. Stop and go extraction tips for matrix-assisted laser desorption/ionization, nanoelectrospray, and LC/MS sample pretreatment in proteomics. *Analytical Chemistry*, 75(3), pp.663–670.

Richman, T.R. et al., 2016. Loss of the RNA-binding protein TACO1 causes late-onset mitochondrial dysfunction in mice. *Nature communications*, 7, p.11884.

Richter-Dennerlein, R. et al., 2016. Mitochondrial protein synthesis adapts to influx of nuclear-encoded protein. *Cell*, 167(2), pp.471–483.e10.

Ringel, R. et al., 2011. Structure of human mitochondrial RNA polymerase. *Nature*, 478(7368), pp.269–273.

Ritchie, M.E. et al., 2015. Limma powers differential expression analyses for RNA-Sequencing and microarray studies. *Nucleic Acids Research*, 43(7), p.e47.

Robinson, M.D., McCarthy, D.J. & Smyth, G.K., 2010. EdgeR: a Bioconductor package for differential expression analysis of digital gene expression data. *Bioinformatics*, 26(1), pp.139–140.

Roger, A.J., Muñoz-Gómez, S.A. & Kamikawa, R., 2017. The origin and diversification of mitochondria. *Current Biology*, 27(21), pp.R1177–R1192.

Rorbach, J. & Minczuk, M., 2012. The post-transcriptional life of mammalian mitochondrial RNA. *Biochemical Journal*, 444(3), pp.357–373.

Rorbach, J. et al., 2016. Human mitochondrial ribosomes can switch their structural RNA composition. *Proceedings of the National Academy of Sciences of the United States of America*, 113(43), pp.12198–12201.

Rorbach, J., Nicholls, T.J.J. & Minczuk, M., 2011. PDE12 removes mitochondrial RNA poly(A) tails and controls translation in human mitochondria. *Nucleic Acids Research*, 39(17), pp.7750–7763.

Ruzzenente, B. et al., 2012. LRPPRC is necessary for polyadenylation and coordination of translation of mitochondrial mRNAs. *The EMBO Journal*, 31(2), pp.443–456.

Ryan, M.T. & Hoogenraad, N.J., 2007. Mitochondrial-nuclear communications. *Annual Review of Biochemistry*, 76(1), pp.701–722.

Sanchez, M.I.G.L. et al., 2011. RNA processing in human mitochondria. *Cell Cycle*, 10(17), pp.2904–2916.

Sasarman, F. et al., 2010. LRPPRC and SLIRP interact in a ribonucleoprotein complex that regulates posttranscriptional gene expression in mitochondria. *Molecular Biology of the Cell*, 21(8), pp.1315–1323.

Scarpulla, R.C., Vega, R.B. & Kelly, D.P., 2012. Transcriptional integration of mitochondrial biogenesis. *Trends in Endocrinology and Metabolism*, 23(9), pp.459–466.

Schägger, H. & Jagow, von, G., 1991. Blue native electrophoresis for isolation of membrane protein complexes in enzymatically active form. *Analytical Biochemistry*, 199(2), pp.223–231.

Schwinghammer, K. et al., 2013. Structure of human mitochondrial RNA polymerase elongation complex. *Nature Structural & Molecular Biology*, 20(11), pp.1298–1303.

Seiferling, D. et al., 2016. Loss of CLPP alleviates mitochondrial cardiomyopathy without affecting the mammalian UPRmt. *EMBO Reports*, 17(7), pp.953–964.

Seitz, V. et al., 2011. Deep sequencing of MYC DNA-binding sites in Burkitt lymphoma. *PloS One*, 6(11), p.e26837.

Shang, J. & Clayton, D.A., 1994. Human mitochondrial transcription termination exhibits RNA polymerase independence and biased bipolarity *in vitro*. *The Journal of Biological Chemistry*, 269(46), pp.29112–29120.

Sharma, M.R. et al., 2003. Structure of the mammalian mitochondrial ribosome reveals an expanded functional role for its component proteins. *Cell*, 115(1), pp.97–108.

Shi, Y. et al., 2012. Mammalian transcription factor A is a core component of the mitochondrial transcription machinery. *Proceedings of the National Academy of Sciences of the United States of America*, 109(41), pp.16510–16515.

Shi, Y. et al., 2016. Mitochondrial transcription termination factor 1 directs polar replication fork pausing. *Nucleic Acids Research*, 44(12), pp.5732–5742.

Shutt, T.E. & Gray, M.W., 2006. Twinkle, the mitochondrial replicative DNA helicase, is widespread in the eukaryotic radiation and may also be the mitochondrial DNA primase in most eukaryotes. *Journal of Molecular Evolution*, 62(5), pp.588–599.

Siegmund, S.E. et al., 2017. Low-dose rapamycin extends lifespan in a mouse model of mtDNA depletion syndrome. *Human Molecular Genetics*, 26(23), pp.4588–4605.

Siira, S.J. et al., 2017. LRPPRC-mediated folding of the mitochondrial transcriptome. *Nature Communications*, 8(1), p.1532.

Sobek, S. et al., 2013. Negative regulation of mitochondrial transcription by mitochondrial topoisomerase I. *Nucleic Acids Research*, 41(21), pp.9848–9857.

Sologub, M. et al., 2009. TFB2 is a transient component of the catalytic site of the human mitochondrial RNA polymerase. *Cell*, 139(5), pp.934–944.

Spindler, M., Beal, M.F. & Henchcliffe, C., 2009. Coenzyme Q10 effects in neurodegenerative disease. *Neuropsychiatric Disease and Treatment*, 5, pp.597–610.

Stefely, J.A. & Pagliarini, D.J., 2017. Biochemistry of mitochondrial coenzyme Q biosynthesis. *Trends in Biochemical Sciences*, 42(10), pp.824–843.

Stehling, O. & Lill, R., 2013. The role of mitochondria in cellular iron-sulfur protein biogenesis: mechanisms, connected processes, and diseases. *Cold Spring Harbor Perspectives in Biology*, 5(8), pp.a011312–a011312.

Stewart, J.B. & Chinnery, P.F., 2015. The dynamics of mitochondrial DNA heteroplasmy: implications for human health and disease. *Nature Reviews Genetics*, 16(9), pp.530–542.

Stewart, J.B. & Larsson, N.-G., 2014. Keeping mtDNA in shape between generations. *PLoS Genetics*, 10(10), p.e1004670.

Stiles, A.R. et al., 2016. Mutations in TFAM, encoding mitochondrial transcription factor A, cause neonatal liver failure associated with mtDNA depletion. *Molecular Genetics and Metabolism*, 119(1-2), pp.91–99.

Stroud, D.A. et al., 2015. COA6 is a mitochondrial complex IV assembly factor critical for biogenesis of mtDNA-encoded COX2. *Human Molecular Genetics*, 24(19), pp.5404–5415.

Sultana, S. et al., 2017. Transcriptional fidelities of human mitochondrial POLRMT, yeast mitochondrial Rpo41, and Phage T7 single-subunit RNA polymerases. *Journal of Biological Chemistry*, p.jbc.M117.797480.

Suomalainen, A. & Battersby, B.J., 2018. Mitochondrial diseases: the contribution of organelle stress responses to pathology. *Nature reviews. Molecular Cell Biology*, 19(2), pp.77–92.

Surovtseva, Y.V. & Shadel, G.S., 2013. Transcription-independent role for human mitochondrial RNA polymerase in mitochondrial ribosome biogenesis. *Nucleic Acids Research*, 41(4), pp.2479–2488.

Surovtseva, Y.V. et al., 2011. Mitochondrial ribosomal protein L12 selectively associates with human mitochondrial RNA polymerase to activate transcription. *Proceedings of the National Academy of Sciences of the United States of America*, 108(44), pp.17921–17926.

Suzuki, T., Nagao, A. & Suzuki, T., 2011. Human mitochondrial tRNAs: biogenesis, function, structural aspects, and diseases. *Annual Review of Genetics*, 45, pp.299–329.

Tang, P.H. et al., 2004. Measurement of reduced and oxidized coenzyme Q9 and coenzyme Q10 levels in mouse tissues by HPLC with coulometric detection. *Clinica Chimica Acta; international Journal of Clinical Chemistry*, 341(1-2), pp.173–184.

Terzioglu, M. et al., 2013. MTERF1 Binds mtDNA to prevent transcriptional interference at the light-strand promoter but is dispensable for rrna gene transcription regulation. *Cell Metabolism*, 17(4), pp.618–626.

The UniProt Consortium, 2017. UniProt: the universal protein knowledgebase. *Nucleic Acids Research*, 45(D1), pp.D158–D169.

Tovar, J. et al., 2003. Mitochondrial remnant organelles of Giardia function in iron-sulphur protein maturation. *Nature*, 426(6963), pp.172–176.

Trifunovic, A. et al., 2005. Somatic mtDNA mutations cause aging phenotypes without affecting reactive oxygen species production. *Proceedings of the National Academy of Sciences*, 102(50), pp.17993–17998.

Tufi, R. et al., 2014. Enhancing nucleotide metabolism protects against mitochondrial dysfunction and neurodegeneration in a PINK1 model of Parkinson's disease. *Nature Cell Biology*, 16(2), pp.157–166.

Tyanova, S. et al., 2016. The Perseus computational platform for comprehensive analysis of (prote)omics data. *Nature Methods*, 13(9), pp.731–740.

Tyynismaa, H. et al., 2010. Mitochondrial myopathy induces a starvation-like response. *Human Molecular Genetics*, 19(20), pp.3948–3958.

Uhler, J.P. & Falkenberg, M., 2015. Primer removal during mammalian mitochondrial DNA replication. *DNA Repair*, 34, pp.28–38.

Vafai, S.B. & Mootha, V.K., 2012. Mitochondrial disorders as windows into an ancient organelle. *Nature*, 491(7424), pp.374–383.

Viscomi, C. & Zeviani, M., 2017. MtDNA-maintenance defects: syndromes and genes. *Journal of Inherited Metabolic Disease*, 40(4), pp.587–599.

Vusse, G.J.V.D. & Reneman, R.S., 1995. Chapter 3 Substrate utilization in mammalian cells. *Principles of Medical Biology*, 4, pp.45–75.

Wang, J. et al., 1999. Dilated cardiomyopathy and atrioventricular conduction blocks induced by heart-specific inactivation of mitochondrial DNA gene expression. *Nature Genetics*, 21(1), pp.133–137.

Wang, Y. & Hekimi, S., 2016. Understanding ubiquinone. *Trends in Cell Biology*, 26(5), pp.367–378.

Wang, Z., Cotney, J. & Shadel, G.S., 2007. Human mitochondrial ribosomal protein MRPL12 interacts directly with mitochondrial RNA polymerase to modulate mitochondrial gene expression. *Journal of Biological Chemistry*, 282(17), pp.12610–12618.

Wanrooij, P.H. et al., 2012. A hybrid G-quadruplex structure formed between RNA and DNA explains the extraordinary stability of the mitochondrial R-loop. *Nucleic Acids Research*, 40(20), pp.10334–10344.

Wanrooij, S. et al., 2008. Human mitochondrial RNA polymerase primes lagging-strand DNA synthesis in vitro. *Proceedings of the National Academy of Sciences of the United States of America*, 105(32), pp.11122–11127.

Weraarpachai, W. et al., 2009. Mutation in TACO1, encoding a translational activator of COX I, results in cytochrome c oxidase deficiency and late-onset Leigh syndrome. *Nature Genetics*, 41(7), pp.833–837.

Wessels, A. & Sedmera, D., 2003. Developmental anatomy of the heart: a tale of mice and man. *Physiological Genomics*, 15(3), pp.165–176.

Wilson, W.C. et al., 2014. A human mitochondrial poly(A) polymerase mutation reveals the complexities of post-transcriptional mitochondrial gene expression. *Human Molecular Genetics*, 23(23), pp.6345–6355.

Wiśniewski, J.R. et al., 2014. A “proteomic ruler” for protein copy number and concentration estimation without spike-in standards. *Molecular & Cellular Proteomics*, 13(12), pp.3497–3506.

Wolf, A.R. & Mootha, V.K., 2014. Functional genomic analysis of human mitochondrial RNA processing. *Cell Reports*, 7(3), pp.918–931.

Wredenberg, A. et al., 2013. MTERF3 regulates mitochondrial ribosome biogenesis in invertebrates and mammals. *PLoS Genetics*, 9(1), p.e1003178.

Xu, B. & Clayton, D.A., 1996. RNA-DNA hybrid formation at the human mitochondrial heavy-strand origin ceases at replication start sites: an implication for RNA-DNA hybrids serving as primers. *The EMBO Journal*, 15(12), pp.3135–3143.

Zaganelli, S. et al., 2017. The pseudouridine synthase RPUSD4 is an essential component of mitochondrial RNA granules. *Journal of Biological Chemistry*, 292(11), pp.4519–4532.

Zhao, Q., 2002. A mitochondrial specific stress response in mammalian cells. *The EMBO Journal*, 21(17), pp.4411–4419.

Zimorski, V. et al., 2014. Endosymbiotic theory for organelle origins. *Current Opinion in Microbiology*, 22, pp.38–48.

Zong, W.-X., Rabinowitz, J.D. & White, E., 2016. Mitochondria and Cancer. *Molecular Cell*, 61(5), pp.667–676.

8. SUPPLEMENTARY MATERIAL

8.1. Heatmaps of gene expression profiles

8.1.1. Transcript and protein expression profiles of genes encoding mitochondrial proteins by category (excluding other and unknown)

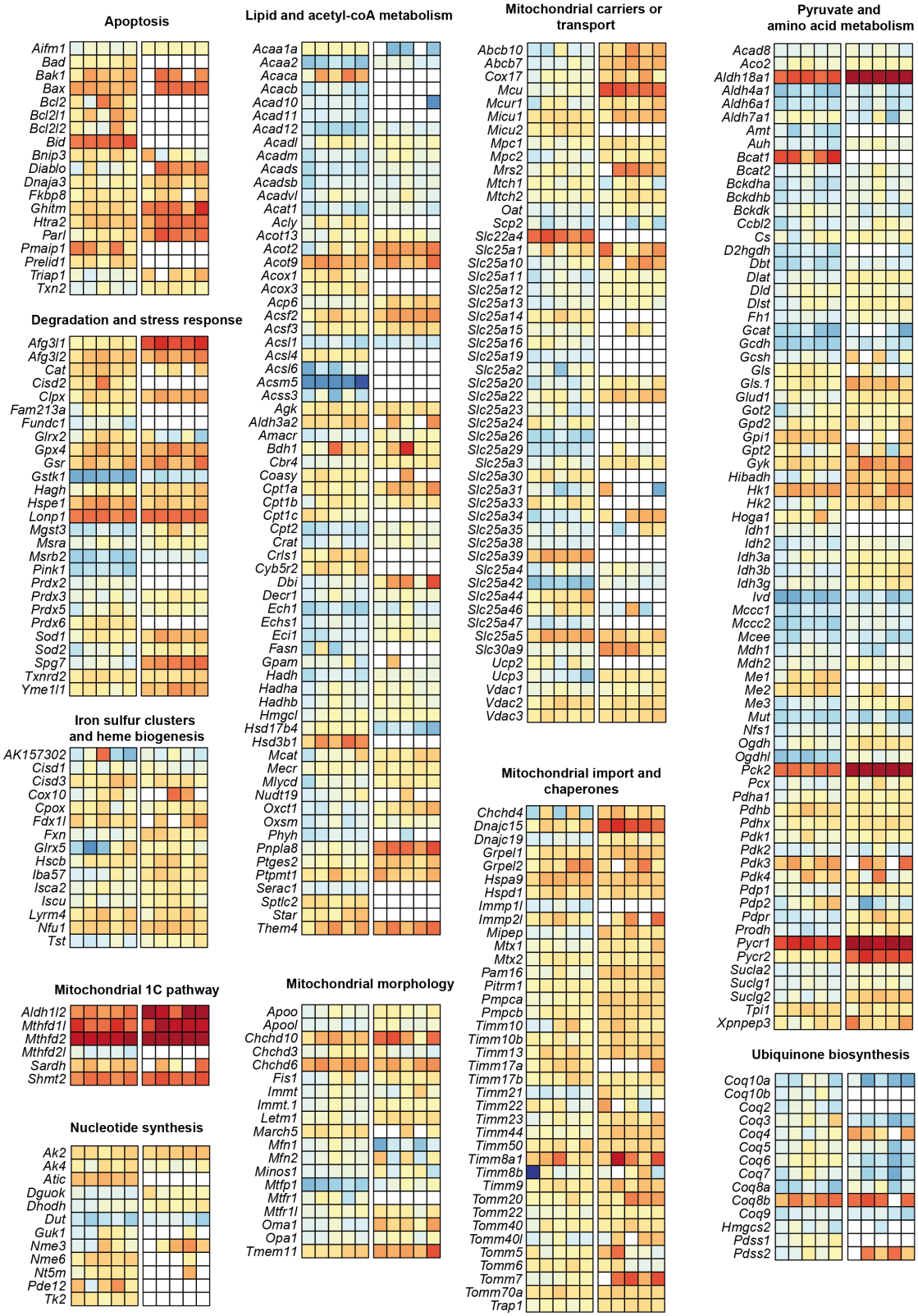

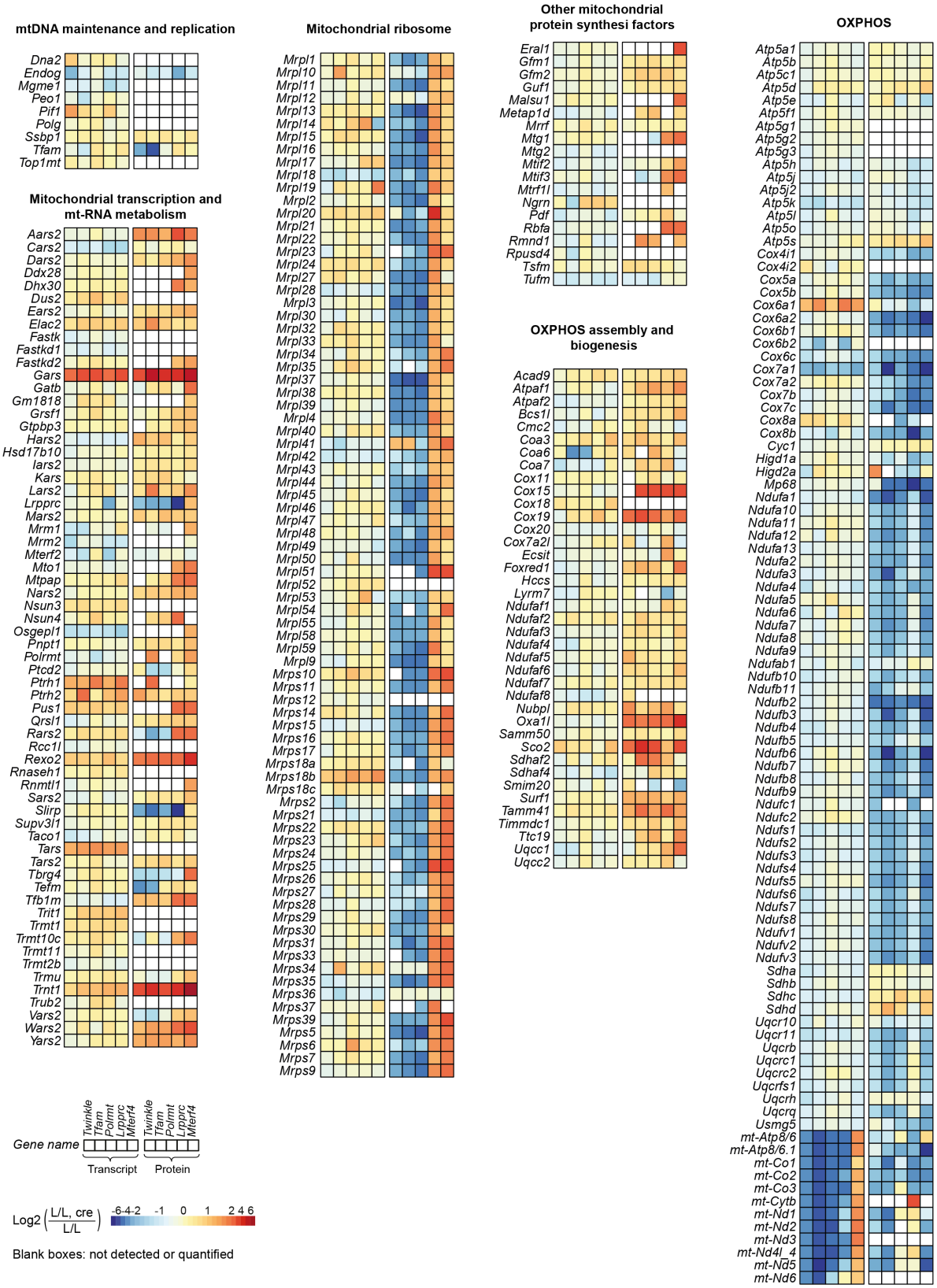
mtDNA maintenance and replication
Dna2
Endog
Mgme1
Peo1
Pif1
Polg
Ssbp1
Tfam
Top1mt
Mitochondrial transcription and mt-RNA metabolism
Aars2
Cars2
Dars2
Ddx28
Dhx30
Dus2
Ears2
Elac2
Fastk
Fastkd1
Fastkd2
Gars
Gatb
Gm1818
Grsf1
Gtpbp3
Hars2
Hsd17b10
Iars2
Kars
Lars2
Lrpprc
Mars2
Mrm1
Mrm2
Mterf2
Mto1
Mtpap
Nars2
Nsun3
Nsun4
Osgepl1
Pnpt1
Polrmt
Ptcd2
Ptrh1
Ptrh2
Pus1
Qrsl1
Rars2
Rcc1l
Rexo2
Rnaseh1
Rnmtl1
Sars2
Slirp
Supv3l1
Taco1
Tars
Tars2
Tbrg4
Tefm
Tfb1m
Trit1
Trmt1
Trmt10c
Trmt11
Trmt2b
Trmu
Trnt1
Trub2
Vars2
Wars2
Yars2
Mitochondrial ribosome
Mrpl1
Mrpl10
Mrpl11
Mrpl12
Mrpl13
Mrpl14
Mrpl15
Mrpl16
Mrpl17
Mrpl18
Mrpl19
Mrpl2
Mrpl20
Mrpl21
Mrpl22
Mrpl23
Mrpl24
Mrpl27
Mrpl28
Mrpl3
Mrpl30
Mrpl32
Mrpl33
Mrpl34
Mrpl35
Mrpl37
Mrpl38
Mrpl39
Mrpl4
Mrpl40
Mrpl41
Mrpl42
Mrpl43
Mrpl44
Mrpl45
Mrpl46
Mrpl47
Mrpl48
Mrpl49
Mrpl50
Mrpl51
Mrpl52
Mrpl53
Mrpl54
Mrpl55
Mrpl58
Mrpl59
Mrpl9
Mrps10
Mrps11
Mrps12
Mrps14
Mrps15
Mrps16
Mrps17
Mrps18a
Mrps18b
Mrps18c
Mrps2
Mrps21
Mrps22
Mrps23
Mrps24
Mrps25
Mrps26
Mrps27
Mrps28
Mrps29
Mrps30
Mrps31
Mrps33
Mrps34
Mrps35
Mrps36
Mrps37
Mrps39
Mrps5
Mrps6
Mrps7
Mrps9
Other mitochondrial protein synthesi factors
Eral1
Gfm1
Gfm2
Guf1
Malsu1
Metap1d
Mrrf
Mtg1
Mtg2
Mtif2
Mtif3
Mtrf1l
Ngrn
Pdf
Rbfa
Rmnd1
Rpusd4
Tsfm
Tufm
OXPHOS assembly and biogenesis
Acad9
Atpaf1
Atpaf2
Bcs1l
Cmc2
Coa3
Coa6
Coa7
Cox11
Cox15
Cox18
Cox19
Cox20
Cox7a2l
Ecsit
Foxred1
Hccs
Lyrm7
Ndufaf1
Ndufaf2
Ndufaf3
Ndufaf4
Ndufaf5
Ndufaf6
Ndufaf7
Ndufaf8
Nubpl
Oxa1l
Samm50
Sco2
Sdhaf2
Sdhaf4
Smim20
Surf1
Tamm41
Timmdc1
Ttc19
Uqcc1
Uqcc2
OXPHOS
Atp5a1
Atp5b
Atp5c1
Atp5d
Atp5e
Atp5f1
Atp5g1
Atp5g2
Atp5g3
Atp5h
Atp5j
Atp5j2
Atp5k
Atp5l
Atp5o
Atp5s
Cox4i1
Cox4i2
Cox5a
Cox5b
Cox6a1
Cox6a2
Cox6b1
Cox6b2
Cox6c
Cox7a1
Cox7a2
Cox7b
Cox7c
Cox8a
Cox8b
Cyc1
Higd1a
Higd2a
Mp68
Ndufa1
Ndufa10
Ndufa11
Ndufa12
Ndufa13
Ndufa2
Ndufa3
Ndufa4
Ndufa5
Ndufa6
Ndufa7
Ndufa8
Ndufa9
Ndufab1
Ndufb10
Ndufb11
Ndufb2
Ndufb3
Ndufb4
Ndufb5
Ndufb6
Ndufb7
Ndufb8
Ndufb9
Ndufc1
Ndufc2
Ndufs1
Ndufs2
Ndufs3
Ndufs4
Ndufs5
Ndufs6
Ndufs7
Ndufs8
Ndufv1
Ndufv2
Ndufv3
Sdha
Sdhb
Sdhc
Sdhd
Uqcr10
Uqcr11
Uqcrb
Uqcrc1
Uqcrc2
Uqcrfs1
Uqcrh
Uqcrq
Usmg5
mt-Atp8/6
mt-Atp8/6.1
mt-Co1
mt-Co2
mt-Co3
mt-Cytb
mt-Nd1
mt-Nd2
mt-Nd3
mt-Nd4l_4
mt-Nd5
mt-Nd6
Twinkle
Tfam
Polrmt
Lrpprc
Mterf4
Gene name
Transcript
Protein
Log2 (L/L, cre / L/L)
-6 -4 -2 -1 0 1 2 4 6
Blank boxes: not detected or quantified

8.1.2. Transcript expression profiles of MYC and ATF4 target genes

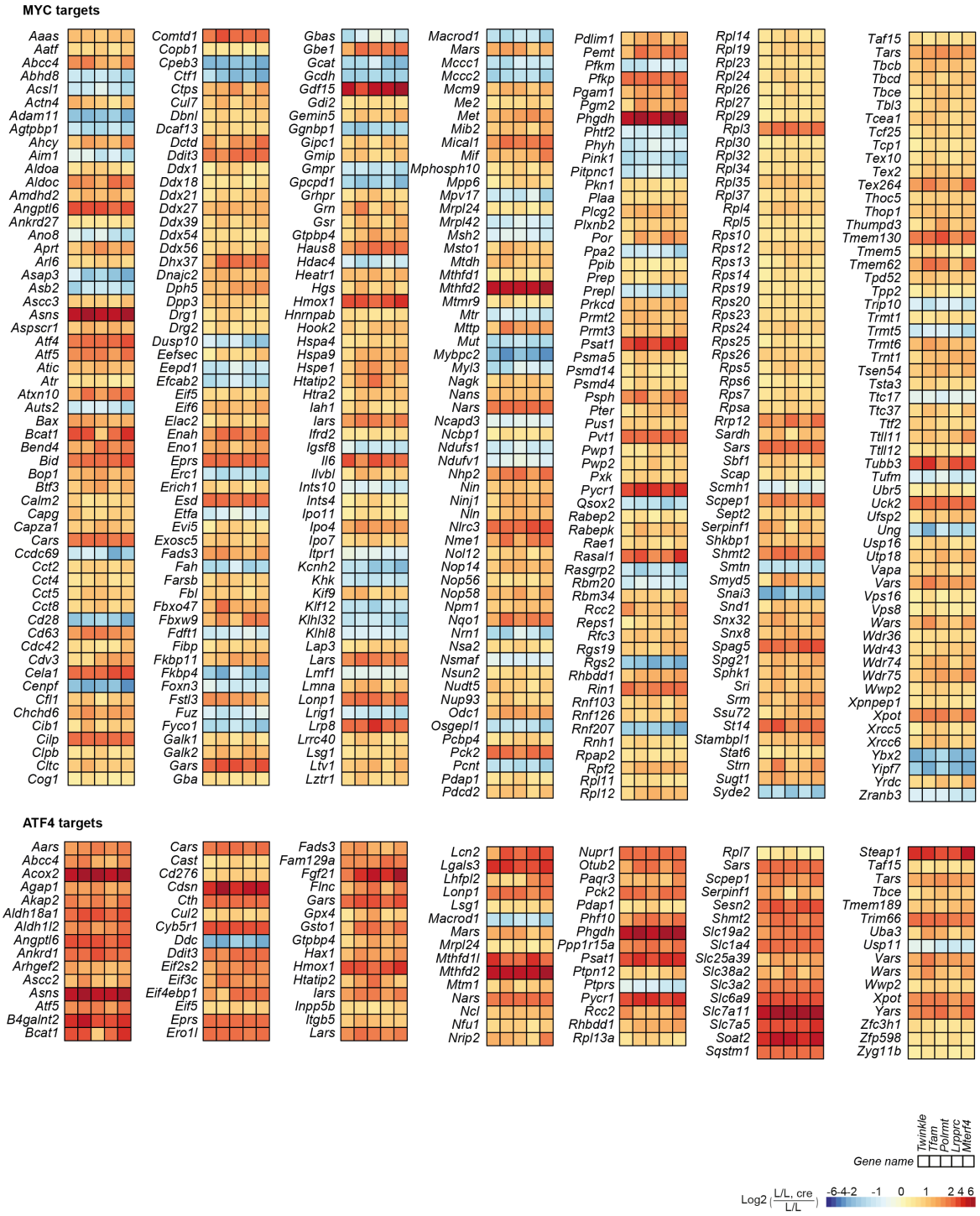

8.2. **Lists of reagents**

Table S1: List of transgenic strains

Mouse strain	Reference	Genotyping primers
Lrpprc$^{loxP/loxP,}$	Ruzzenente et al. 2011	*Lrpprc* F and R
Lrpprc$^{loxP/loxP, +/Ckmm-cre}$	Ruzzenente et al. 2011	*Ckmm c*re F and R
Lrpprc$^{+/T}$	Ruzzenente et al. 2011	*Lrpprc* +/T F and R
Mterf4$^{loxP/loxP,}$	Camara et al. 2011	*Mterf4* loxP F and R
Mterf4$^{loxP/loxP, +/Ckmm-cre}$	Camara et al. 2011	*Ckmm cre* F and R
Polrmt$^{loxP/loxP,}$	This thesis; Kühl et al. 2014; 2016	*Polrmt* loxP F and R
Polrmt$^{loxP/loxP, +/Ckmm-cre}$	This thesis; Kühl et al. 2014; 2016	*Ckmm cre* F and R
Polrmt$^{+/-}$	This thesis; Kühl et al. 2014; 2016	*Polrmt* loxP F and R and *Polrmt* KO R
Polrmt$^{+/T}$	This thesis	*Polrmt* +/T F and R
Polrmt$^{+/T}$; *Lrpprc*$^{+/T}$	This thesis	Same as single transgenic lines
Tfam$^{loxP/loxP,}$	Larsson et al. 1998	*Tfam* loxP F, R1 and R2
Tfam$^{loxP/loxP, +/Ckmm-cre}$	Larsson et al. 1998	*Ckmm cre* F and R
Twnk$^{loxP/loxP,}$	Milenkovic et al. 2013	*Twnk* loxP F and R
Twnk$^{loxP/loxP, +/Ckmm-cre}$	Milenkovic et al. 2013	*Ckmm cre* F and R

Table S2: List of oligonucleotides for genotyping, cloning, RT-PCR, and pyrosequencing

Primer	Sequence
Genotyping *Lrpprc* loxP F	5' GGAGAACAGGCCGCATCACAA 3'
Genotyping *Lrpprc* loxP R	5' TGCCTTCCACCTCAGCTTACCACT 3'
Genotyping *Lrpprc* +/T F	5' GCTGAAAGCTTGGGTACTCG 3'
Genotyping *Lrpprc* +/T R	5' AAAAGGCCCAGCGACTAAAT 3'
Genotyping *Mterf4* loxP F	5' GGGATGTCCAGCCTTTTGATAGTA 3'
Genotyping *Polrmt* loxP F	5' CACTGGAGAGCCCCACCTCCCTTCTCCAGAAGGGT 3'
Genotyping *Polrmt* loxP R	5' CCACTAACCATGGCTGTCTGC 3'
Genotyping *Polrmt* KO R	5' GGCACATACTTGATACAGCTTGG 3'
Genotyping *Polrmt* +/T F	5' GAGGCTCGGGTGCGGCAGCTC 3'
Genotyping *Polrmt* +/T R	5' GTGCAGTGTGAGCACCTGCTGTC 3'
Genotyping *Tfam* loxP F	5' CTGCCTTCCTCTAGCCCGGG 3'
Genotyping *Tfam* loxP R1	5' GTAACAGCAGACAACTTGTG 3'
Genotyping *Tfam* loxP R2	5' CTCTGAAGCACATGGTCAAT 3'
Genotyping *Twnk* loxP F	5' CAGGGATGGTAGTTGGTTCC 3'
Genotyping *Twnk* loxP R	5' CTAGCTGAGACCTTGCATGG 3'
Genotyping *Ckmm cre* F	5' CACGACCAAGTGACAGCAAT 3'
Genotyping *Ckmm cre* R	5' AGAGACGGAAATCCATCGCT 3'
Figure 3.1 primer a	5′ CGGCGCTCCGGTGGACCCGAAGCG 3'
Figure 3.1 primer b	5' GTGGCTTCTGCAGCTCAAGA 3'
Figure 3.1 primer c	5' GCATCACGGTGTTGTACATGTGC 3'
Figure 3.1 primer d	5' TCTTGAGCTGCAGAAGCCAC 3'
Figure 3.1 primer e	5' CGACGAGAAGTGACTGGACCAG 3'
Figure 3.3 primer a	5' CTTGGCCGGGTTCTGCGCTCC 3'
Figure 3.3 primer b	5' TCCAGCAGTTCAGCATGGCC 3'
Figure 3.3 primer c	5' GTGGCTTCTGCAGCTCAAGA 3'
Figure 3.3 primer d	5' TTCACCCTCATCTCAGGTG3'
Figure 3.3 primer d'	5' CTTCACCCTCATCTCAG 3'
Pyrosequencing *Polrmt* +/T F	5' AGAGGCGCCAAAAGGAAGTT 3'
Pyrosequencing *Polrmt* +/T R- biotin	5' TCTTGCTTGGCTGCAGGTAG 3'
Pyrosequencing *Polrmt* +/T Seq	5' CAAGATCTGGAACAAGAA 3'

Table S3: List of probes and oligonucleotides for radioactive labelling

Probe	Sequence
7S DNA	AGTACATAAATTTACATAGTACAACAGTACATTTATGTATATCGTACATTAAACTATTTTCC CCAAGCATATAAGCTAGTACATTAAATCAATGGTTCAGGTCATAAAATAATCATCAACATA AATCAATATATATACCATGAATATTATCTTAAACACATTAAACTAATGTTATAAGGACATATC TGTGTTATCTGACATACACCATACAGTCATAAACTCTTCTCTTCCATATGACTATCCCCTTC CCCATTTGGTCTATTAATCTACCATCCTCCGTGAAACCAACAACCCGCCCACCAATGCCC CTCTTCTCGCTCCGGGCCCATTAAACTTGGGGGTAGCTAAACTGAAACTTTATCAGACAT CTGGTTCTTACTTCAGGGCCATCAAATGCGTTATCGCCCATACGTTCCCCTTAAATAAGAC ATCTCGATGGTATCGGGTCTAATCAGCCCATGACCAACATAACTGTGGTGTCATGCATTT GGTATCTTTTTATTTTGGCCTACTTTCATCAACATAGCCGTCAAGGCATGAAAGGACAGCA CACAGTCTAGACGCACCTACGGTGAAGAATCATTAGTCCGCAAAACCCAATCACCTAAGG CTAATTATTCATGCTTGTTAGACATAAATGCTACTCAATACCAAATTTTAACTCTCCAAACC CCCCACCCCCTCCTCTTAATGCCAAACCCCAAAAACACTAAGAACTTGAAAGACATATAAT ATTAACTATCAAACCCTATGTCCTGATCAATTCTAGTAGTTCCCAAAATATGACTTATATTT TAGTACTTGTAAAAATTTTACAAAATCATGTTCCGTGAACCAAAACTCTAATCATACTCTAT TACGCAATAAACATTAACAA
7S RNA	GACATATAATATTAACTATCAAACCCTATGTCCTGATCAATTCTA
18S rRNA	GGTCTACAAGACGCCACATCCCCTATTATAGAAGAGCTAATAAATTTCCATGATCACACAC TAATAATTGTTTTCCTAATTAGCTCCTTAGTCCTCTATATCATCTCGCTAATATTAACAACA AAACTAACACATACAAGCACAATAGATGCACAAGAAGTTGAAACCATTTGAACTATTCTAC CAGCTGTAATCCTTATCATAATTGCTCTCCCCTCTCTACGCATTCTATATATAATAGACGAA ATCAACAACCCCGTATTAACCGTTAAAACCATAGGGCACCAATGATACTGAAGCTACGAA TATACTGACTATGAAGACCTATGCTTTGATTCATATATAATCCCAACAAACGACCTAAAAC CTGGTGAACTACGACTGCTAGAAGTTGATAACCGAGTCGTTCTGCCAA
mt-12S	TACACATGCAAACCTCCATAGACCGGTGTAAAATCCCTTAAACATTTACTTAAAATTTAAG GAGAGGGTATCAAGCACATTAAAATAGCTTAAGACACCTTGCCTAGCCACACCCCCACGG GACTCAGCAGTGATAAATATTAAGCAATAAACGAAAGTTTGACTAAGTTATACCTCTTAGG GTTGGTAAATTTCGTGCCAGCCACCGCGGTCATACGATTAACCCAAACTAATTATCTTCG GCGTAAAACGTGTCAACTATAAATAAATAAATAGAATTAAAATCCAACTTATATGTGAAAAT TCATTGTTAGGACCTAAACTCAATAACGAAAGTAATTCTAGTCATTTATAATACACGACAG CTAAGACCCAAACTGGGATTAGATACCCCACTATGCTTAGCCATAAACCTAAATAATTAAA TTTAACAAAACTATTTGCCAGAGAACTACTAGCCATAGCTTAAAACTCAAAGGACTTGGCG GTACTTTATATCCATCTAGAGGAGCCTGTTCTATAATCGATAAACCCCGCTCTACCTCACC ATCTCTTGCTAA
mt-16S	ATGCAACACTGTTAGTATGAGTAACAAGAATTCCAATTCTCCAGGCATACGCGTATAACAA CTCGGATAACCATTGTTAGTTAATCAGACTATAGGCAATAATCACACTATAAATAATCCAC CTATAACTTCTCTGTTAACCCAACACCGGAATGCCTAAAGGAAAGATCCAAAAAGATAAAA GGAACTCGGCAAACAAGAACCCCGCCTGTTTACCAAAAACATCACCTCTAGCATTACAAG TATTAGAGGCACTGCCTGCCCAGTGACTAAAGTTTAACGGCCGCGGTATCCTGACCGTG CAAAGGTAGCATAATCACTTGTTCCTTAATTAGGGACTAGCATGAACGGCTAAACGAGGG TCCAACTGTCTCTTATCTTTAATCAGTGAAATTGACCTTTCAGTGAAGAGGCTGAAATATA ATAATAAGACGAGAAGACCCTATGGAG
mt-Co1	GTTCATTATTTTTGGTTGGTTGTCTTGGGTTAGCATTAAAGCCTTCACCTATTTATGGAGG TTTAGGTTTAATTGTTAGTGGGTTTGTTGGTTGTTTAATGGTTTTAGGGTTTGGTGGATCG TTTTTAGGTTTAATAGTTTTTTTAATTTATTTAGGGGGGATGTTGGTTGTGTTTGGATATAC GACTGCTATAGCTACTGAGGAATATCCAGAGACTTGGGGATCTAACTGATTAATTTTGGG TTTTTTAGTATTGGGGGTGATTATAGAGGTTTTTTTAATTTGTGTGCTTAATTATTATGATG AAGTTGGAGTAATTAATCTTGATGGTTTGGGAGATTGGTTGATGTATGAGGTTGATGATGT TGGAGTTATGTTGGAAGGAGGGATTGGGGTAGCGGCAATATATAGTTGTGCTACTTGAAT GATGGTAGTAGCTGGGTGATCTTTGTTTGCGGGTATTTTTATT
mt-Co2	GGTCTACAAGACGCCACATCCCCTATTATAGAAGAGCTAATAAATTTCCATGATCACACAC TAATAATTGTTTTCCTAATTAGCTCCTTAGTCCTCTATATCATCTCGCTAATATTAACAACA AAACTAACACATACAAGCACAATAGATGCACAAGAAGTTGAAACCATTTGAACTATTCTAC CAGCTGTAATCCTTATCATAATTGCTCTCCCCTCTCTACGCATTCTATATATAATAGACGAA ATCAACAACCCCGTATTAACCGTTAAAACCATAGGGCACCAATGATACTGAAGCTACGAA TATACTGACTATGAAGACCTATGCTTTGATTCATATATAATCCCAACAAACGACCTAAAAC CTGGTGAACTACGACTGCTAGAAGTTGATAACCGAGTCGTTCTGCCAA

Probe	Sequence
mt-Cytb	AGTAGACAAAGCCACCTTGACCCGATTCTTCGCTTTCCACTTCATCTTACCATTTATTATC GCGGCCCTAGCAATCGTTCACCTCCTCTTCCTCCACGAAACAGGATCAAACAACCCAACA GGATTAAACTCAGATGCAGATAAAATTCCATTTCACCCCTACTATACAATCAAAGATATCC TAGGTATCCTAATCATATTCTTAATTCTCATAACCCTAGTATTATTTTTCCCAGACATACTA GGAGACCCAGACAACTACATACCAGCTAATCCACTAAACACCCCACCCCATATTAAACCC GAATGATATTTCCTATTTGCATACGCCATTCTACGCTCAATCCCCAATAAACTAGGAGGTG TCCTAGCCTTAATCTTATCTATCCTAATTTTAGCCCTAATACCTTTCCTTCATACCTCAAAG CAACGAAGCCTAATATTCCGCCCAATCACACAAATTTTGTACTGAATCCTAGTAGCCAACC TACTTATCTTAACCTGAATTGGGGGCCAACCAGTAGAACACCCATTT
mt-Nd1	ACGCAAAATCTTAGGGTACATACAACTACGAAAAGGCCCTAACATTGTTGGTCCATACGG CATTTTACAACCATTTGCAGACGCCATAAAATTATTTATAAAAGAACCAATACGCCCTTTAA CAACCTCTATATCCTTATTTATTATTGCACCTACCCTATCACTCACACTAGCATTAAGTCTA TGAGTTCCCCTACCAATACCACACCCATTAATTAATTTAAACCTAGGGATTTTATTTATTTT AGCAACATCTAGCCTATCAGTTTACTCCATTCTATGATCAGGATGAGCCTCAAACTCCAAA TACTCACTATTCGGAGCTTTACGAGCCGTAGCCCAAACAATTTCATATGAAGTAACCATAG CTATTATCCTTTTATCAGTTCTATTAATAAATGGATCCTACTCTCTACAAACACTTATTACAA CCCAAGAACACATATGATTACTTCTGCCAGCCTGACCCATAGCCATAATATGATTTATCTC AACCCTAGCAGAAACAAAC
mt-Nd5	ACAAGACATCCGAAAAATAGGAAACATCACAAAAATCATACCATTCACATCATCATGCCTA GTAATCGGAAGCCTCGCCCTCACAGGAATACCATTCCTAACAGGGTTCTACTCAAAAGAC CTAATTATTGAAGCAATTAATACCTGCAACACCAACGCCTGAGCCCTACTAATTACACTAA TCGCCACTTCTATAACAGCTATGTACAGCATACGAATCATTTACTTCGTAACAATAACAAA ACCGCGTTTTCCCCCCCTAATCTCCATTAACGAAAATGACCCAGACCTCATAAACCCAAT CAAACGCCTAGCATTCGGAAGCATCTTTGCAGGATTTGTCATCTCATATAATATTCCACCA ACCAGCATTCCAGTCCTCACAATACCATGATTTTTAAAAACCACAGCCCTAATTATTTCAG TATTAGGATTCCTAATCGCACTAGAACTAAACAACCTAACCATAAAACTATCAATAAATAAA GCAAATCCATATTCATCCTTCTCAACTTTACTGGGGTTTTTCCCATCTATTATTCACCGCAT TACACC
mt-Nd6	GTTCATTATTTTTGGTTGGTTGTCTTGGGTTAGCATTAAAGCCTTCACCTATTTATGGAGG TTTAGGTTTAATTGTTAGTGGGTTTGTTGGTTGTTTAATGGTTTTAGGGTTTGGTGGATCG TTTTTAGGTTTAATAGTTTTTTTAATTTATTTAGGGGGGATGTTGGTTGTGTTTGGATATAC GACTGCTATAGCTACTGAGGAATATCCAGAGACTTGGGGATCTAACTGATTAATTTTGGG TTTTTTAGTATTGGGGGTGATTATAGAGGTTTTTTTAATTTGTGTGCTTAATTATTATGATG AAGTTGGAGTAATTAATCTTGATGGTTTGGGAGATTGGTTGATGTATGAGGTTGATGATGT TGGAGTTATGTTGGAAGGAGGGATTGGGGTAGCGGCAATATATAGTTGTGCTACTTGAAT GATGGTAGTAGCTGGGTGATCTTTGTTTGCGGGTATTTTTATT
mt-Ta	5’ GACTTCATCCTACATCTATTG
mt-Tc	5’ TCTCTACACCTTCGAATTTG
mt-Te	5 ‘AACTGCGACCAATGACATGAAAAATC
mt-Tf	5’ CATTTTCAGTGCTTTGCTTTGTTATTA
mt-Tk	TCACTATGGAGATTTTAAGGTC
mt-Tl1	AAGTCTTACGCAATTTCCTGGCTCTG
mt-Tl2	GGTTTTTGGTTCCTAAGAC
mt-Tm	CCCGATAGCTTAATTAGCTGACCTTAC
mt-Tn	TACCCTATTACTGGCTTCAA
mt-Tp	TCAAGAAGAAGGAGCTACT
mt-Tq	TTCAAAATTCTCCGTGCTACCTAAACA
mt-Ts2	GCATGAATTAGCAGTTCTTGCAATC
mt-Tt	AAGATCTTCATTTCAGGTTTACAA
mt-Tv	GTGTAGGCCAGATGCTTTAAT

Probe	Sequence
Polrmt E2 – E4	AATTCGCCCTTGTGGGGCCATGCTGAACTGCTGGAAGTGCTGGAGGCTCGGGTGCGGC AGCTCCGGGCAGAGGGCACACCTGAGATGAGGGTGAAGAAGGTGCAGGTGGACCGGC CTCCACAGGGCCACAGCAGCCGCTGGGCGCAAAAGCTAGAGGCTGAGAAAAGGGTGAA GCAGAGGCGCCAAAAGGAAGTTGACCAGCAGAAGCAAGCCCTCACACAGGAGTTCTGG ACCCTTCACAAGGAGCCCAAGATCTGGAACAAGAAGCTGGCTGGCTACCTGCAGCCAAG CAAGAAGGGAACACCCACGAACTCAGAGGAAAAGCAGCTGGCCCAGGCCCTTCAGGCT GCTCTGGGGAGGCTCAGCTCCCGTGAGGCAGAGGCCCTGGCCAGGAAGAAAGCCAAGG CGGTGGAGGCGCAGATCCTGGTCCTCCAGCAGAAGTTCCTGGCTTTCTTTGAGTGCTGC GTCTGCACTGGCCAAGTGCCCCTCGCTCACCACGTGCTGGTCACTCACCATAACAACGG AGACAGACAGCAGGTGCTCACACTGCACATGTACAACACCGTGATGCTTGGCTGGGCCC GCAAGGGCTCCTTCAGAGAGCTGGTCTATGTGAAGGGCG

*All the probes and oligonucleotides were previously generated in the laboratory except *Porlmt* E2 – E4

Table S4: List of Taqman assays

Taqman Assay	Catalog Number
Human 18S rRNA	Hs99999901_s1
Mouse *Acta1*	Mm00808218_g1
Mouse *Actc1*	Mm01333821_m1
Mouse *Actg1*	Mm01963702_s1
Mouse *Actg2*	Mm00656102_m1
Mouse *Adck3*	Mm00469737_m1
Mouse *Adck4*	Mm00505363_m1
Mouse *Atf4*	Mm00515325_m1
Mouse *Coq2*	Mm01203260_g1
Mouse *Coq4*	Mm00618552_m1
Mouse *Coq5*	Mm00518239_m1
Mouse *Coq7*	Mm00501587_m1
Mouse *Fdps*	Mm00836315_g1
Mouse *Gabpa*	Mm00484598_m1
Mouse *Hmgcs1*	Mm01304569_m1
Mouse *Hmgcr*	Mm01282499_m1
Mouse *Lrpprc*	Mm00511512_m1
Mouse *mt-Atp6*	Mm03649417-g1
Mouse *mt-Co1*	Mm04225243_g1
Mouse *mt-Cytb*	Mm04225271_g1
Mouse *mt-Nd1*	Mm04225274_s1
Mouse *mt-Nd5*	Custom-made AIHSNT9
Mouse *mt-Rnr2* (mt-*16S*)	Mm04260181_s1
Mouse *Mterf2*	Mm01233053_m1
Mouse *Mterf3*	Mm00481557_m1
Mouse *Mterf4*	Mm00508298_m1
Mouse *Myc*	Mm00487804_m1
Mouse *Nrf1*	Mm00447996_m1
Mouse *Pdss1*	Mm00450958_m1
Mouse *Pdss2*	Mm01190168_m1
Mouse *Ppargc1(Pgc1a)*	Mm00447183_m1
Mouse *Polrmt*	Mm00553272_m1
Mouse *Polga*	Mm00450527_m1

Taqman Assay	Catalog Number
Mouse *Serca2*	Mm01201431_m1
Mouse *Ssbp1*	Mm01131763_g1
Mouse *Tbp*	Mm00446973_m1
Mouse *Tefm*	Mm01304209_m1
Mouse *Tfam*	Mm00627275_m1
Mouse *Tfb2m*	Mm01620397_s1
Mouse *Peo1*/*Twnk*	Mm00467928_m1
Mouse *Pcyox1*	Mm00482162_m1
Mouse *Zbtb1*	Mm01281881_m1

Table S5: List of primary antibodies

Antibody	Source	Catalog Number
ALDH18A1	Thermofisher Scientific	PA5-19392
CLPP	Sigma-Aldrich	WH0008192M1
COX4	Cell Signaling	4850
CS	Abcam	ab129095
ELAC2	Proteintech	10071-1-AP
FDPS	Abcam	ab189874
FLAG M2	Sigma-Aldrich	F1804
GFP	Millipore	MAB3580
GLS	Abcam	ab93434
GRSF1	Sigma-Aldrich	HPA036985
HISTONE H3	Sigma-Aldrich	H0164
HMGCS1	Abcam	ab194971
HSPA9/mtHSP70/Grp75	Abcam	ab82591
LONP1	Abcam or Lu et al. 2013	ab103809 or self-made polyclonal antisera
LRPPRC mouse	N.-G. Larsson; Ruzzenente et al. 2012	Self-made
MRPL12	Sigma-Aldrich	HPA022853
MRPL37	Sigma-Aldrich	HPA025826
MRLP44	Proteintech	16394-1-AP
MRPS35	Proteintech	16457-1-AP
Mt-CO2	N.-G Larsson; Larsson et al. 1998	Self-made polyclonal antisera
MTHFD1	Abcam	ab103698
MTHFD2	Abcam	ab37840
NDUFA9	Abcam	ab14713
POLRMT mouse	N.-G. Larsson; Kühl et al. 2014	Self-made purified antibody
POLRMT human	Abcam	ab32988
POLγA	Abcam	ab128899
PYCR1	Proteintech	13108-1-AP
SDHA	Thermofisher Scientific	459200
SHMT2	Sigma-Aldrich	HPA020543
SLIRP15C4; rat IgG2a	N.-G Larsson; Lagouge et al. 2015	Self-made polyclonal antisera

Antibody	Source	Catalog Number
SSBP1	Sigma-Aldrich	HPA002866

SDHA	Thermofisher Scientific	459200
SHMT2	Sigma-Aldrich	HPA020543
TFAM	Abcam	ab131607
TEFM	Sigma-Aldrich	HPA023788
TFB2M	N.-G. Larsson, Harmel et al. 2013	Self-made purified antibody
Total OXPHOS Rodent WB Antibody Cocktail	Abcam	ab110413
Tubulin	Cell Signaling	2125
TWINKLE mouse	N.-G. Larsson, Milenkovic et al. 2013	Self-made purified antibody
UQCRFS1	Abcam	ab131152
VDAC1	Millipore	MABN504

8.3. **Lists of figures**

8.4. **Lists of tables**

8.5. **Abbreviations**

1C	One carbon
AARE	Amino acid response element
ACTA1	Actin, alpha skeletal muscle
ACTC1	Actin, alpha cardiac muscle 1
ACTG1	Actin, cytoplasmic 2
ADP	Adenosine diphosphate
AFG3L2	AFG3-like protein 2
ALDH18A1	Delta-1-pyrroline-5-carboxylate synthase
ALDH4A1	Delta-1-pyrroline-5-carboxylate dehydrogenase, mitochondrial
AMP	Adenosine monophosphate
AMPK	AMP-activated protein kinase
ATF	Cyclic AMP-dependent transcription factor
ATFS-1	Stress activated transcription factor atfs-1
ATP	Adenosine triphosphate
ATP5A1	ATP synthase subunit alpha, mitochondrial
ATP5B	ATP synthase subunit beta, mitochondrial
ATP5C1	ATP synthase subunit gamma, mitochondrial
ATP5D	ATP synthase subunit delta, mitochondrial
ATP5E	ATP synthase subunit epsilon, mitochondrial
AUC	Area under the cumulative recovery curve (iRegulon)
B2M	Beta-2-microglobulin
BAC	Bacterial artificial chromosome
BAX	Apoptosis regulator BAX
BID	BH3-interacting domain death agonist
BN-PAGE	Blue-native polyacrylamide gel electrophoresis
C/EBPb	CCAAT enhancer binding protein beta
cDNA	Complementary DNA
ChIP-Seq	Chromatin immunoprecipitation sequencing
CI	OXPHOS complex I - NADH:Q oxidoreductase
CII	OXPHOS complex II - succinate dehydrogenase
CIII	OXPHOS complex III - ubiquinol:cytochrome c oxidoreductase
CIV	OXPHOS complex IV - cytochrome c oxidase
CV	OXPHOS complex V - ATP synthase
Ckmm	Creatinine kinase, muscle
CLPP	ATP-dependent Clp protease proteolytic subunit, mitochondrial

CoA	Coenzyme A
COQ10A	Coenzyme Q-binding protein COQ10 homolog A, mitochondrial
COQ2	4-hydroxybenzoate polyprenyltransferase, mitochondrial
COQ3	Q biosynthesis O-methyltransferase, mitochondrial
COQ4	Q biosynthesis protein COQ4 homolog, mitochondrial
COQ5	2-methoxy-6-polyprenyl-1,4-benzoquinol methylase, mitochondrial
COQ6	Q biosynthesis monooxygenase COQ6, mitochondrial
COQ8A	Atypical kinase COQ8A, mitochondrial
COQ8B	Atypical kinase COQ8B, mitochondrial
COQ9	Q biosynthesis protein COQ9, mitochondrial
COX15	Cytochrome c oxidase assembly protein COX15 homolog
COX19	Cytochrome c oxidase assembly protein COX19
CSB	Conserved sequence block
CTD	C-terminal domain
DAP-Seq	DNA affinity purification sequencing
D-loop	Displacement loop
DARS2	Aspartate-tRNA ligase, mitochondrial
DDIT3/CHOP	DNA damage-inducible transcript 3 protein
DNAJA3	DnaJ homolog subfamily A member 3, mitochondrial
dsDNA	Double-stranded DNA
EGFP	Enhanced green fluorescent protein
eIF2	Eukaryotic translation initiation factor 2
ELAC2	Zinc phosphodiesterase ELAC protein 2
ENDOG	Endonuclease G
ERAL1	Era G-protein like 1
ERR	Estrogen-related receptors
FAD^+	Flavin adenine dinucleotide, oxidized
FADH2	Flavin adenine dinucleotide, reduced
FAO	Fatty acid oxidation
FASTKD1-5	FASTK-domain containing proteins 1-5
FASTK	Fas-activated serine/threonine kinase
FDPS	Farnesyl pyrophosphate synthase
FDR	False discovery rate
FeS	Iron sulfur
FGF21	Fibroblast growth factor 21
GABPA	GA-binding protein alpha chain
GDF15	Growth differentiation factor 15

gDNA	genomic DNA
GRSF1	G-rich sequence factor 1
H	Heavy
HMGCR	3-hydroxy-3-methylglutaryl-CoA reductase
HMGCS1	HMG-CoA synthase
HSP	Heavy-strand promoter
HSPA9/mtHSP70	Stress-70 protein, mitochondrial -
HSPD1/mtHSP60	60 kDa heat shock protein, mitochondrial
HSPE1	10 kDa heat shock protein, mitochondrial
IC	Initiation complex
IMM	Inner mitochondrial membrane
IMS	Inter membrane space
ISR	Integrated stress response
L	Light
LFQ	Label-free quantification
LIG3	DNA ligase 3
LONP1	AAA+ LON P protease
LRPPRC	Leucin-rich PPR motif-containing protein
LSP	Light-strand promoter
m/z	mass/charge ratio
MAOA	Monoamine oxidase A
MEF	Mouse embryonic fibroblast
MGME1	Mitochondrial genome maintenance exonuclease - 1
Mitoproteome	Mitochondrial proteome
MM	Mitochondrial matrix
MRM1-3	mitochondrial rRNA methyl transferases
MRPL	Mitochondrial 39S ribosomal protein
MRPP1-3	Mitochondrial RNAse P protein 1-3
MRPS	Mitochondrial 28S ribosomal protein
mtDNA	Mitochondrial DNA
mt-mRNA	Mitochondrial messenger RNA
mt-RNA	Mitochondrial RNA
mt-rRNA	Mitochondrial ribosomal RNA
mt-tRNA	Mitochondrial transfer RNA
MTERF1-4	Mitochondrial transcription termination factor 1-4
MTG1	Mitochondrial ribosome associated GTPase 1
MTHFD1	C-1 THF synthase, cytosolic

MTHFD2	bi-functional methyleneTHF dehydrogenase/cyclohydrolase, mitochondrial
MTIF3	Mitochondrial translation inititation factor 3
mTOR	Mechanistic target of rapamycin
mTORC1	mTOR complex 1
MTS	Mitochondrial targeting sequence
mtUPR	Mitochondrial unfolded protein response
MURE 1/2	Mitochondrial unfolded protein response elements
MYC	Myc proto-oncogene protein
NAD^+	Nicotinamide adenine dinucleotide, oxidized
NADH	Nicotinamide adenine dinucleotide, reduced
$NADP^+$	Nicotinamide adenine phosphate dinucleotide, oxidized
NADPH	Nicotinamide adenine phosphate dinucleotide, reduced
NCR	Non-coding control region
NES	Normalized enrichment score (iRegulon)
NGRN	Neugrin
NRF1	Nuclear respiratory factor 1
NSUN4	5-methylcytosine rRNA methyl transferase NSUN4
NTD	N-terminal domain
NTE	N-terminal extention
O_H	H-strand origin of replication
O_L	L-strand origin of replication
OMM	Outer mitochondrial membrane
OXPHOS	Oxidative phosphorylation
PCK2	Phosho-enol pyruvate carboxykinase
PCYOX1	Prenylcysteine oxidase gene
PDSS1	Decaprenyl-diphosphate synthase subunit 1
PDSS2	Decaprenyl-diphosphate synthase subunit 1
PGC1	Peroxisome proliferated-activated receptors
PHGDH	D-3-phosphoglycerate dehydrogenase
pI	Isoelectric point
PNPT1	Polyribonucleotide nucleotidyltransferase 1, mitochondrial
POLγ	DNA polymerase gamma
PPAR	Peroxisome proliferated-activated receptors
PPR	Pentatricopeptide repeat
PPRC1	Peroxisome proliferator-activated receptor gamma coactivator-related protein 1

PRIMPOL	DNA-directed primase/polymerase protein
PRODH	Proline dehydrogenase 1
PSAT1	Phosphoserine aminotransferase
PTCD2	PPR-containing protein 2
PYCR1	Pyrroline-5-carboxylate reductase 1, mitochondrial
PYCR2	Pyrroline-5-carboxylate reductase 2
Q	Ubiquinone, Coenzyme Q
qRT-PCR	Quantitative real-time PCR
R-loop	RNA loop
RCC1L/WBSCR16	RCC1-like G exchanging factor-like protein
Redox	Oxido reduction
RNA-Seq	RNA sequencing
RNASEH1	RNase H1
RPUSD3-4	Mitochondrial mRNA pseudouridine synthase RPUSD3-4
RT-PCR	Reverse-transcriptase PCR
SCO2	Protein SCO2 homolog, mitochondrial
siRNA	Small interfering RNA
SLIRP	SRA stem-loop-interacting RNA-binding protein, mitochondrial
spRNAP-IV	Single-polypeptide RNA polymerase IV
SSBP1	Single-stranded binding protein 1
SUPV3L1	ATP-dependent RNA helicase, mitochondrial
T7-RNAP	T7 RNA polymerase
TACO1	Translational activator of cytochrome c oxidase 1
TAS	Termination associated sequences
TBP	TATA binding protein
TCA	Tricarboxylic acid cycle
TEFM	Mitochondrial transcription elongation factor
TFAM	Mitochondrial transcription factor A
TFB1M	Mitochondrial transcription factor B1
TFB2M	Mitochondrial transcription factor B2
THF	Tetrahydrofolate
TOP1MT	DNA topoisomerase I, mitochondrial
TRAP1	Heat shock protein 75 kDa, mitochondrial
TRUB2	Mitochondrial mRNA pseudouridine synthase TRUB2
TSS	Transcription start site
Twnk/TWINKLE	Mitochondrial DNA helicase TWINKLE
UTR	Untranslated region

VDAC	Voltage-dependent anion-selective channel
YME1L1	ATP-dependent zinc metalloprotease YME1L1
ZBTB1	Zinc-finger BTB domain-containing protein 1

Abbreviations one-letter code of amino acids

A	Alanine
R	Arginine
N	Asparagine
D	Aspartic acid
C	Cysteine
E	Glutamic acid
Q	Glutamine
G	Glycine
H	Histidine
I	Isoleucine
L	Leucine
K	Lysine
M	Methionine
F	Phenylalanine
P	Proline
S	Serine
T	Threonine
W	Tryptophan
Y	Tyrosine
V	Valine

ACKNOWLEDGEMENTS

Words fall short to acknowledge so many incredible people that have contributed to my PhD journey. First of all, I would like to express my deepest gratitude to my thesis director *Prof. Nils-Göran Larsson.* Thank you for allowing me to grow scientifically and personally in the stimulating environment of your laboratory at the Max Planck Institute for Biology of Ageing. You have been an incredibly supportive mentor that has taught me to be critical towards science but foremost towards myself. Thank you for the valuable advice and constant support during my PhD and towards building my scientific career, for giving me the trust, freedom, and guidance to develop new ideas, and for opening the doors to so many unique opportunities.

In the NGL laboratory, I had the privilege to work with *Dr. Inge Kühl*, my supervisor, that is greatly responsible for the kind of scientist I am today. Inge, thank you for being so generous with me, for teaching me by example to love research and to do it with the highest standards possible, and for always setting the expectation bar higher with the confidence that I could achieve it. I am eternally grateful for your trust, friendship, and the certainty that you were always (and will continue to be) there to support me, advise me, and be the "dream team" for crazy ventures to come.

Importantly, I would like to acknowledge my advisory and evaluating thesis committee members, *Prof. Aleksandra Trifunovic, Prof. Jan Riemer, Prof. Thomas Langer* and *Dr. Peter Tessarz* for the support, time, and critical evaluation of this thesis.

Furthermore, I would also like to acknowledge all the co-authors of the manuscripts included in this thesis for science is the result of collaborative effort.

I would also like to thank the Max Planck Society, in particular the Max Planck Institute for Biology of Ageing (MPI-Age), that became my scientific home in Germany. Here, I had the privilege (and responsibility) of having my imagination and time as the limiting resource. The *International Max Planck Research School of Ageing* (now called Cologne Graduate School of Ageing), granted me the fellowship that allowed me to do my PhD in this fantastic environment. I thank the coordinators of the Graduate School, in particular *Daniela Morick*, for the constant support to successfully complete my PhD. I would also like to acknowledge the administration of the MPI-Age and everyone who helped with all the required paperwork to live in Germany in particular *Corinna Schwierzy-Krämer, Miriam Krähling, Rosalie Morriset,* and *Andrea Veith.* Moreover, I wish to thank the scientific core facilities that provided constant support throughout my PhD, in particular the transgenic core, comparative biology, phenotyping core, and proteomics core facility. Special thanks go to *Ilian Atanassov* for all the fruitful discussions and

script sharing that helped me navigate and visualize large scale data which is an activity I very much enjoy.

Of course, the NGL lab is the core and the main reason I consider the MPI-Age as my second (or first?) home in Germany. Here I include the past group members (*Inge Kühl, Marie Lagouge, Arnaud Mourier, Benedetta Ruzzenente, Christian Kukat, Jelena Misic* and *Stanka Matic*), the visiting scientists (*Paola Loguercio Polosa, Aleksandra Filipovska,* and *Oliver Rackham*), Jim Stewart's laboratory, and the current members of the NGL lab. I was welcomed in the lab with great kindness from the very beginning and this has been constant throughout my PhD. I do not have the space to properly acknowledge everyone, so I will limit myself here to the people I have closely worked with. I want to specially thank *Nadine Hochhard* and *Magdalena Springer* for their help, patience, and flexibility to work with me. *Nina Bonekamp* and *Dusanka Milenkovic* for their advice, support, and teachings while performing or planning experiments together. *Paola Loguercio Polosa* for always ending up doing one or two experiments with me during her visits to Cologne, teaching me classic techniques that date back to Attardi's laboratory, and, more importantly, for her contagious passion for science. *Aleksandra Filipovska* for being a constant and pivotal collaborator in all our projects. *Arnaud Mourier* for his constant excitement about (pretty much) everything and teaching me mitochondrial metabolism. *Jim Stewart* for including me as a collaborator in some of his projects and constant supply of coffee accompanied with discussions about the politics of science. I have learnt something from each member of the lab and I have always found support when I needed it. José Ortega y Gasset once wrote *"I am I and my circumstance*". The NGL department is a big part of the circumstances of my PhD and for this I can only say THANK YOU to each and every member[1].

My deepest gratitude goes for my linear regression that are my family in Cologne: *Joana, Víctor, Johanna, Timo,* and little *Neea*. Thanks to you I never felt alone in Cologne despite being 10000 km away from Colombia. With you I always found a smile to cheer me up, a coffee to fix the world, or a cookie for desperate (and not so desperate) times. I am extremely lucky to have found so extraordinary friends and certainly your friendship is one of the biggest treasures of my PhD time. I would like to finish by thanking my *Family* and *Camilo* for they are my strongest supporters. Despite the distance you are always cheering up for me, celebrating my successes, and giving me the strength to always go forward. I wouldn't be here without your unconditional support to follow my dreams.

[1] **Current NGL lab members:** Nina Bonekamp, Jakob Busch, Regina Dirksen, Ana Grönke ex Bratic, Nadine Hochhard, Min Jiang, Johanna and Timo Kauppila, Petra Kirschner, Miriam Krähling, Dusanka Milenkovic, Rosalie Morisset, Elisa Motori, Cristina Remes, Lysann Schmitz, Corinna Schwierzy-Krämer, Stefanie Kipschull, Thomas Schöndorf, Eduardo Silva-Ramos, Magdalena Springer, Henrik Spåhr, Avan Taha and Daria Wnuk-Lipinski. **Jim Stewart lab members (former and current):** Sara Albarrán, Marita Isokallio, Marie-Lune Simard, Pamella Sendon, Laila Singh.

ERKLÄRUNG

Ich versichere, dass ich die von mir vorgelegte Dissertation selbständig angefertigt, die benutzen Quellen und Hilfsmittel vollständig angegeben und die Stellen der Arbeit - einschließlich Tabellen, Karten und Abbildungen -, die anderen Werken im Wortlaut oder dem Sinn nach entnommen sind, in jedem Einzelfall als Entlehnung kenntlich gemacht habe; dass diese Dissertation noch keiner anderen Fakultät oder Universität zur Prüfung vorlegen hat, dass sie – abgesehen von unten angegebenen Teilpublikationen – noch nicht veröffentlicht worden ist sowie, dass ich eine solche Veröffentlichung vor Abschluß des Promotionsverfahrens nicht vornehmen werde. Die Bestimmungen dieser Promotionsordnung sind mir bekannt. Die von mir vorgelegte Dissertation ist von Prof. Dr. Nils-Göran Larsson betreut worden.

_____

Köln, 13.07.2018
Maria del Pilar Miranda Vergara

PUBLIKATIONEN

Publikationen dieser Arbeit

Kühl, I.*, **Miranda M*.**, Atanassov, I., Kuznetsova, I., Hinze, Y., Mourier, A., Filipovska, A., Larsson, N-G. 2017. Transcriptomic and proteomic landscape of mitochondrial dysfunction reveals secondary coenzyme Q deficiency in mammals. *eLife*, 6, p.e30952. **(*equal contribution)**.

Kühl, I., **Miranda, M.**, Posse, V., Milenkovic, D., Mourier, A., Siira, SJ., Bonekamp, NA., Neumann, U., Filiposka, A., Logercio-Polosa, P., Gustafsson, CM., Larsson, N-G. 2016. POLRMT regulates the switch between replication primer formation and gene expression of mammalian mtDNA. *Science Advances*, 2(8), p.e1600963.

Kühl, I., Kukat, C., Ruzzenente, B., Milenkovic, D., Mourier A., **Miranda, M.**, Koolmeister, C., Larsson, N-G. 2014. POLRMT does not transcribe nuclear genes. *Nature*, 514(7521), pp.E7–11.

Weitere Publikationen

Bacman, S., Pereira C.S., Williams, S.L., Kauppila, J.H., **Miranda, M.,** Pinto, M., Larsson, N-G., Stewart, J.B., Moraes, C.T. (*In press*). MitoTALEN reduces mutant mtDNA load and restores $tRNA^{Ala}$ levels in a mouse model of heteroplasmic mtDNA mutation. *Nature Medicine.*